COMMUNAUTÉ FRANCAISE DE BELGIQUE
ACADÉMIE UNIVERSITAIRE WALLONIE-EUROPE
UNIVERSITÉ DE LIÈGE - GEMBLOUX AGRO-BIO TECH

Modelling the hygrothermal behaviour of crop-based construction materials

Samuel DUBOIS

A thesis presented for the degree of Doctor of Philosophy in Agronomical Sciences and Biological Engineering

Supervisors: Frédéric Lebeau, Arnaud Evrard

2014

COMMUNAUTÉ FRANCAISE DE BELGIQUE
ACADÉMIE UNIVERSITAIRE WALLONIE-EUROPE
UNIVERSITÉ DE LIÈGE - GEMBLOUX AGRO-BIO TECH

Modelling the hygrothermal behaviour of crop-based construction materials

Samuel DUBOIS

A thesis presented for the degree of Doctor of Philosophy in Agronomical Sciences and Biological Engineering

Supervisors: Frédéric Lebeau, Arnaud Evrard

2014

Dubois Samuel. (2014). *Modelling the hygrothermal behaviour of crop-based construction materials.* Université de Liège — Gembloux Agro-Bio Tech

Abstract: In the context of developing sustainable buildings, crop-based construction materials appear as valuable products given their intrinsic environmental and technical qualities. Their ability to exchange moisture with the surrounding environment and damping humidity peaks in rooms, referred to as *moisture buffering*, is often presented as a way to improve occupants comfort and otentially reduce the operational energy of the building. It is understandable why modelling their hygrothermal behaviour and evaluating the impact on indoor air volumes is essential during the design phases.

This thesis explores the modelling of the hygrothermal behaviour of crop-based materials with a numerical tool. The latter is developed in a widespread general computational environment that brings both modularity and interoperability. Three challenges are addressed: the improvement of mathematical description of crop-based materials in non-standard operating conditions, the improvement of materials properties determination, and the assessment of their impact at room-scale. Several experimental facilities are developed in parallel to validate the proposed approaches, focusing on two materials expected to improve indoor conditions: straw bales and lime-hemp concrete. Results show that the developed model allows improving the understanding and the characterization of these green materials at various scales of study.

Dubois Samuel. (2014). *Modélisation du comportement hygrothermique des matériaux agro-sourcés utilisé en construction.* Université de Liège — Gembloux Agro-Bio Tech

Résumé: Dans le contexte du développement des bâtiments durables, les éco-matériaux issus de l'agriculture (*Crop-Based Materials*) apparaissent comme des produits particulièrement intéressants au regard de leurs qualités environnementales et techniques. Leur capacité d'échanger de l'eau avec l'environnement direct et d'amortir les pics d'humidité, appelée *effet tampon*, est souvent présentée comme un moyen d'améliorer le confort intérieur pour les occupants et, potentiellement, de réduire les dépenses énergétiques du bâtiment en fonctionnement. On comprend pourquoi, au cours de la phase de conception, il est essentiel de pouvoir modéliser le comportement hygrothermique des CBM et de pouvoir évaluer leur rôle dans l'évolution du climat intérieur.

Cette thèse explore la modélisation du comportement hygrothermique des matériaux de construction à base végétale au moyen d'un outil numérique. Ce dernier est développé dans un logiciel de calcul généraliste qui offre modularité et interopérabilité. Trois objectifs sont traités: l'amélioration de la description mathématique des matériaux végétaux dans des conditions de fonctionnement non standard, l'amélioration de la détermination des propriétés de ces matériaux, et la compréhension de leur impact à l'échelle de la pièce. Plusieurs dispositifs expérimentaux sont développés en parallèle pour valider les approches proposées, en se focalisant sur deux matériaux d'origine végétale prometteurs pour la régulation de l'environnement intérieur: les ballots de pailles et les mélanges chaux-chanvre. Les résultats montrent que le modèle proposé permet l'amélioration de la compréhension et la caractérisation des CBM à plusieurs échelles d'étude.

Preface

This dissertation is submitted for the degree of Doctor of Philosophy at the University of Liege. The research described in this document was undertaken at the Department of environmental Sciences and Technologies of the Gembloux Agro-Bio Tech Faculty between October 2010 and October 2014.

Part of this work has been previously presented in the following scientific publications:

- Dubois S., Evrard A. and Lebeau F. (2013). Modelling the hygrothermal behavior of biobased construction materials. *Journal of Building Physics*
- Dubois S. and Lebeau F. (2013). Design, construction and validation of a guarded hot plate apparatus for thermal conductivity measurement of high thickness crop-based specimens. *Materials and Structures*
- Dubois S., Evrard A. and Lebeau F. (2014). Non-isothermal moisture balance equation in porous media: a review of mathematical formulations in Building Physics. *Biotechnologie, Agronomie, Société et Environnement*
- Dubois S., McGregor F., Evrard A., Heath A., and Lebeau F. (2014). An inverse modelling approach to estimate the hygric parameters of clay-based masonry during a Moisture Buffer Value test. *Building and Environment*

Gembloux, October 2014

Samuel Dubois

Acknowledgment

This project actually began in 2010 when Professor Frédéric Lebeau convinced me to get involved in the construction of a prototype straw bale building at the Faculty of Gembloux Agro-Bio Tech. This participatory project was an extremely rewarding experience, both on human and scientific points of view. When he suggested me later to deepen the research in order to understand more fully the interests of bio-based construction materials, it seemed to me that this scientific challenge was of great interest in the context of questioning traditional and modern construction methods. Today, I would like to thank him for the unfailing support he has shown me during these four years of thesis.

I would also like to express my gratitude to Arnaud Evrard, my second supervisor, whose experience in the modelling field was particularly precious and who has always provided me with valuable advices. During my work in *Environmental Sciences and technologies Dept.*, I had the chance to collaborate with many other great people. I want to express my appreciation to Professor Marie-France Destain for her support, to my colleagues for the fruitful discussions and the good moments spent in the office, and to all students for their involvement in the life of the University. For his advices on inverse modelling techniques and DREAM algorithm manipulation, I am sincerely grateful to Benjamin Dumont. I also wish to acknowledge the help provided by Arnaud Louis, who participated greatly in the experimental studies related to straw bales construction. Finally, I would like to offer my special thanks to Rudy Schwartz for his precious help and availability in the laboratory; with his talent and knowledge, every experimental set-up seemed attainable.

This research was funded by the *Fonds National de la Recherche Scientifique* (FNRS) as part of the FRIA program which allows students to prepare theses in domains linked to industry and agriculture. I am sincerely thankful and honoured for having been given the chance of pursuing this scientific research.

I would like to express my gratitude to *Isohemp*, *Prohemp* and *Paille-Tech* companies for their participations in experimental campaigns. I had the pleasure to work with highly motivated people, deeply and truly invested in the promotion of sustainable

construction.

My special thanks are extended to the members of the *Civil engineering and Architecture Dept.* of Bath University for hosting me during summer 2013 and offering me this short but enriching collaboration. I had the honour to work under the supervision of Professor Pete Walker, who apart from being attentive and resourceful, greatly participated in the success of this scientific exchange. I would also like to thank some other very special people I met in Bath University: Fionn, Andrew, Eleana, Neal, Thalia, Michael and Alfonso.

To all my friends, you are an unending source of support and inspiration to me. Time spent with you is always a pure privilege.

To my family, thank you for your encouragement. The moments of laugh and joy we share are particularly enriching. None of this would have been possible without your love and concern.

Summary and Conclusions

In the context of developing sustainable buildings, *Crop-Based Materials* (CBM) appear as valuable products given their intrinsic environmental and technical qualities. Often used in the field of thermal and acoustic insulation, these materials present hygroscopic and capillary properties causing specific physical phenomena related to dynamic phase changes of water within their porous matrix. The resulting ability to exchange moisture with the surrounding environment and to damp indoor humidity peaks, referred to as *moisture buffering*, is often presented as a way to improve occupants' comfort and potentially reduce the operational energy of the building. However, their real participation in the hygrothermal balance at room or building scale is not perfectly understood nor quantifiable with precision. Moreover, the use of CBM may present some risks linked to interstitial and surface condensation, that may potentially cause microbiological decay. In this context, it is understandable why modelling their hygrothermal behaviour and evaluating the impact on indoor air volumes is essential in the design phases, which is a cost-effective approach in comparison to full scale experiments.

The mathematical models used to predict the transient hygrothermal conditions inside porous materials assemblies under imposed interior and exterior climatic conditions are called *Building Element Heat, Air and Moisture* (BEHAM) models. They are central for the study of CBM. Those tools are constantly evolving to account for a larger range of physical phenomena, covering progressively all conditions potentially met in a building envelope under normal or more extreme climatic loads. Similar mathematical models exist in other domains of scientific research, like Soil Physics or Drying Technologies, which are a precious resource for BEHAM tools refinement in the study of highly hygroscopic and capillary materials like CBM.

No matter how good the mathematical description for heat and mass transfer, the efficiency of BEHAM predictions still relies strongly on values assigned to its parameters. Among those, some are used to describe the materials properties (e.g. Thermal conductivity, vapour permeability, etc.). Those properties are actually complex functions which depend on material moisture content and temperature. Moreover, experimental

methods used to measure them are not always easy to apply to CBM.

Whatever the quality of their equations and the accuracy of parameters values, BEHAM tools used alone cannot answer in details to aspects linked to the evaluation of indoor comfort or building energy performance. Because they require data for indoor climate as a boundary condition, the mutual heat and mass exchanges between envelope and indoor air volume cannot be precisely evaluated. This is one of the reasons why much attention has recently been focused on developing hygrothermal model at whole-building scale. One easy way to achieve this level of analysis is to combine a BEHAM model with concepts stemming from *Building Energy Simulation* (BES) tools. The latter model category already offers a whole-building centred vision based on thermal zone balance. However, mass transfers between room air and the envelope are often considered in a very simplified way. Yet, combined with a BEHAM description of envelope it is well promising for solving interrogations linked to large scale impact of CBM use.

Several authors pointed out benefits of using scientific *General Computational Tools* (GCT) for developing and solving BEHAM equations in the perspective of integrating multiple models in a single computational environment. Intrinsically, these numerical tools show a high modularity and their capabilities for tools integration are high. It offers new horizons for whole-building scale hygrothermal modelling but also for novel approaches like inverse modelling.

This thesis explores the modelling of crop-based materials with a BEHAM tool developed in a widespread GCT. Three challenges are addressed: the improvement of mathematical description of CBM in non-standard operating conditions, the improvement of materials properties determination, and the assessment of the hygrothermal exchanges at room scale. Several experimental facilities are developed in parallel to validate the proposed approaches, focusing on two popular CBM materials for improving indoor conditions: straw bales and lime-hemp concrete. Results show that the developed model allows to improve the understanding of CBM at various scales of study. Coupled with an inverse modelling algorithm, it provides a great prospect for parameters determination including materials properties, on the basis of dynamic experiments more representative of the actual behaviour of highly

hygroscopic material. At wall scale, a single-parameter description for the temperature dependence of the material moisture storage is proposed and validated with a thermal shock experiment on a straw bale wall. Based on the same experiment, a room-scale analysis allows to evaluate some practical benefits of the hygrothermal behaviour of CBM.

This document provides guidelines for further exploration since the modelling approaches and simulations results are reproducible and accessible due to the chosen numerical environment.

Résumé et Conclusions

Dans le contexte du développement des bâtiments durables, les éco-matériaux issus de l'agriculture (*Crop-Based Materials - CBM)* apparaissent comme des produits particulièrement intéressants au regard de leurs qualités environnementales et techniques. Souvent utilisés comme isolants thermiques et/ou acoustiques, ces matériaux ont des propriétés hygroscopiques et capillaires à l'origine de phénomènes physiques spécifiques liés aux changements de phases dynamiques de l'eau au sein de leur structure interne poreuse. Leur capacité à échanger de l'eau avec l'environnement direct et à amortir les pics d'humidité intérieure, appelée "effet tampon", est souvent présentée comme un moyen d'améliorer le confort pour les occupants et, potentiellement, de réduire les dépenses énergétiques du bâtiment en fonctionnement. Cependant, leur rôle réel au niveau des bilans hygrothermiques d'une pièce, ou d'un bâtiment, n'est pas compris parfaitement, et n'est pas encore quantifiable précisément. De plus, l'utilisation de tels matériaux peut présenter des risques liés à la condensation superficielle et interstitielle, qui provoquerait une dégradation microbiologique progressive. Dans ce contexte, on comprend pourquoi il est essentiel de pouvoir modéliser leur comportement hygrothermique ainsi que d'évaluer son impact sur le climat intérieur au cours de la phase de conception. La modélisation reste une démarche relativement peu coûteuse face aux expérimentations de grande échelle.

Les modèles mathématiques utilisés pour prévoir les conditions hygrothermiques transitoires au sein de matériaux poreux sont appelés BEHAM, pour *Building Element Heat, Air and Moisture.* Ils sont centraux dans l'étude des éco-matériaux végétaux. Ces outils évoluent sans cesse pour traduire une gamme croissante de phénomènes physiques intervenant dans une enveloppe soumise à diverses sollicitations climatiques, des plus normales aux plus extrêmes. Des modèles similaires existent dans d'autres domaines de la recherche scientifique, comme les Sciences du sol ou l'étude des technologies de séchage, et constituent une source d'inspiration importante pour l'amélioration et la complexification des modèles BEHAM.

Mais peu importe la qualité de la description physique des transferts de chaleur et de

masse, la justesse des prévisions d'un modèle BEHAM dépend toujours fortement des valeurs assignées à ses différents paramètres. Parmi ces derniers, certains servent à la description des propriétés hygrothermiques des matériaux (conductivité thermique, perméabilité à la vapeur, ...). Ces propriétés sont pour la plupart des fonctions complexes qui dépendent de la teneur en eau et de la température du matériau. De plus, les méthodes expérimentales utilisées traditionnellement pour les mesurer ne sont pas toujours adaptées à l'étude des CBM.

Quelle que soit la qualité de leurs formalismes mathématiques ainsi que la pertinence des valeurs attribuées aux paramètres associés, les outils BEHAM utilisés seuls ne peuvent pas répondre en détails aux questions liées au confort intérieur ou à la performance énergétique globale du bâtiment. En effet, les échanges mutuels de chaleur et de masse entre l'enveloppe et les volumes d'air des pièces ne peuvent pas y être évalués avec précision puisque ces modèles requièrent des données pour le climat intérieur, en tant que conditions aux limites. C'est un des facteurs qui expliquent l'intérêt récent pour les modèles hygrothermiques à l'échelle du bâtiment. Une manière facile pour atteindre un tel niveau d'analyse est de combiner les modèles BEHAM aux concepts issus des modèles *BES* pour *Building Energy Simulation*, utilisés pour la caractérisation de l'efficience énergétique d'un bâtiment entier. Cette dernière catégorie de modèles offre déjà une vision à grande échelle basée sur le principe d'un bilan thermique par pièce ou zone intérieure. Les transferts hydriques entre l'air intérieur et l'enveloppe y sont par contre souvent considérés de manière très simplifiée. Combinés aux modèles BEHAM, ils deviennent très prometteurs pour répondre aux interrogations liées à l'impact des CBM à grande échelle.

Plusieurs auteurs ont relevé les bénéfices de l'utilisation d'outils de calcul scientifique de type généraliste, tel que *Matlab*, pour développer et résoudre les équations BEHAM dans l'idée de combiner plusieurs modèles dans un seul et même environnement de simulation. Ces outils numériques montrent intrinsèquement une haute modularité et leurs capacités quant à l'intégration des outils sont grandes. Cela ouvre de nouveaux horizons pour la modélisation des transferts de chaleur et de masse à l'échelle du bâtiment, mais aussi pour des approches innovantes comme la modélisation inverse.

Cette thèse explore la modélisation des CBM au moyen d'un outil BEHAM développé

dans un logiciel de calcul généraliste très répandu. Trois objectifs sont abordés: l'amélioration de la description mathématique des CBM dans des conditions de fonctionnement non standard, l'amélioration de la détermination des propriétés des matériaux, et la compréhension de l'impact du stockage dans les matériaux à l'échelle de la pièce. Plusieurs dispositifs expérimentaux sont développés en parallèle pour valider les approches proposées, en se focalisant sur deux matériaux d'origine végétale prometteurs pour la régulation de l'environnement intérieur: les ballots de paille et les mélanges chaux-chanvre. Les résultats montrent que le modèle proposé permet l'amélioration de la compréhension des CBM à plusieurs échelles d'étude. Couplé à un algorithme de modélisation inverse, il offre de grandes perspectives pour la détermination des paramètres, y compris les propriétés des matériaux, sur base d'expériences dynamiques plus représentatives du comportement réel des matériaux hautement hygroscopiques. A l'échelle du mur, une description mono-paramétrique de la dépendance à la température du stockage d'eau est proposée et validée à l'aide d'une expérience de choc thermique sur un mur en paille. En se basant sur la même expérience, une analyse à l'échelle de la pièce permet d'évaluer les bénéfices pratiques du comportement hygrothermique des CBM.

Ce document fournit des lignes directrices pour des recherches futures; les méthodes de modélisation et les résultats des simulations sont reproductibles et accessibles du fait de la nature de l'environnement de résolution numérique.

Acronyms

BC Boundary conditions

BEHAM Building element heat, air and moisture

BES Building energy simulation

CBM Crop-based materials

CFD Computational fluids dynamics

EMC Equilibrium moisture content

GCT General computational tool

GHP Guarded hot plate

HAM Heat, air and moisture

HVAC Heating, ventilation and air-conditioning

LHC Lime-hemp concrete

MBV Moisture buffer value

MIP Mercury intrusion porometry

ODE Ordinary differential equation

PDE Partial differential equation

RH Relative humidity

Contents

CHAPTER 1

Introduction

1.1 Context

1.1.1 Sustainable building

In this new century, men are faced with a profound questioning of their lifestyle. Human activities are having a huge impact on the environment. It threatens the perspective of keeping our planet the way we know it, with its rich biosphere and a climate to which we were adapted along the millennia. We have reached a turning point where critical decisions have to be made in order to achieve a more responsible economic development, before some irreversible damage occurs.

Buildings are central in our social and economic activities and the construction sector is currently a key energy consumer in our modern societies. It represents the greatest energy savings potential according to the Energy Efficiency Plan (EC, 2011). In Europe, buildings represent about 40% of total final energy requirements (BPIE, 2011), which is more than the transportation sector. A deep metamorphosis of the sector is inescapable in order to ensure the control of greenhouse gases emissions and the security of energy supply. But the energy savings are not the only concerns. Material flows must also be optimized: reduce raw material inputs and control the amount of waste generated, especially when knowing that buildings demolition activities are responsible for around 33% of waste generated annually in the EU (EEA, 2010). The resource-intensive and wasteful traditions must be shaken up. In addition to climate change, waste production and overconsumption of resources, several other issues are indirectly linked to our modern buildings. It includes the loss of biodiversity, the toxification of soil and ground water, the release of synthetic chemicals (including en-

docrine disruptors), etc. (Kibert, 2003).

The views are numerous on what sustainable development should be, and this observation also applies to sustainable buildings definition (Hill and Bowen, 1997). There is no consensus at the international level. Many concepts and terminologies coexist today and try to bring their answers to this relatively recent concern. However, we can say that all are based on similar guidelines, which aim to reduce the impact of buildings on both the environment and the health of occupants. The definition of *green buildings* proposed by Kibert (2003) illustrates this common basis:

" High performance green buildings are facilities designed, built, operated, renovated, and disposed of using ecological principles for the purpose of promoting occupant health and resource efficiency plus minimizing the impacts of the built environment on the natural environment. In the context of green buildings, resource efficiency means high levels of energy and water efficiency, appropriate use of land and landscaping, the use of environmentally friendly materials, and minimizing the life cycle effects of the building's design and operation."

These 'ecological principles' are necessarily subject to a choice. Every movement offers a unique approach by focusing on certain aspects of the building design, based on value choices. However, there is now a large consensus on the fact that the term sustainable building does not only refer to the structure but also to the various processes involved during its entire lifetime, from construction to decommissioning (Hill and Bowen, 1997). New standards, technologies and materials are being constantly introduced in order to meet the need for environmentally-responsible construction, in an innovation perspective.

Nonetheless, while 'sustainable construction' is rapidly becoming more and more popular in the world, legislations often focus mainly on energy issues (EIO, 2011). This is evidenced in some environmental performance evaluation techniques, such as the *Life-Cycle Energy Analysis* (Fay, Treloar et al. 2000). The risk is that too much focusing on improving energy performance may mean that, eventually, other crucial environmental issues mentioned above are not taken into account.

1.1.2 Eco-materials

The choice of materials will always be a crucial step in sustainable building design. Each technical domain of the envelope is characterized by a specific 'catalogue' of products, where the designer can choose to use raw materials as well as highly processed synthetic products. A recent trend is to substitute resource-intensive materials with 'greener' materials, or *eco-materials*, which answer key points of sustainable building definition. The main difficulty is to draw a line between what is green and what is not (EIO, 2011). Designing sustainably means integrating rigorous criteria in the selection of building components. Here we will identify three key criteria in this quest for materials that are more respectful of man and his environment.

- *Environmental impacts*

Every product available on the market hides a more or less complex industrial route during which it is processed in successive steps (Roodman et al., 1995). Each stage of the product processing and each interposed transportation phase induce more or less heavy environmental impacts. The analysis of this course is an essential prerequisite for any reasoned choice. If we want to ensure a more accurate view of the quality of the product, it is in fact the whole cycle of life of the material that must be taken into account, from the extraction of raw materials to disposal or recycling at end-of-life. In that context, the *Life Cycle Assessment* (LCA) tools were developed as mean of comprehensively evaluating the different impacts in this chain and compare materials with quantitative indicators. It acts as an inventory of all energy and primary materials inputs as well as all environmental outputs in a 'from-cradle-to-grave' perspective (Finkbeiner et al., 2006). In the LCA, the renewable and recyclable (or reusable) character of the material is also essential and, ideally, materials that limit intermediate steps in the industrial chain should be promoted. As a concluding remark, a natural material is not necessarily environmentally friendly. For example, cement incorporated in concrete is a natural mineral but requires a lot of energy for its production from raw material (the limestone calcination process is energy intensive and releases considerable CO_2 amounts (Huntzinger and Eatmon, 2009)).

- *Impact on health and occupant comfort*

Another important aspect in the choice of materials is their potential impact on human health. Sustainable building design should aim at producing a comfortable environment for the occupants, in the thermal, acoustic and visual points of view, but also ensure a certain level of air quality in indoor spaces. These aspects are crucial because of the time an individual daily spends inside a building (Moschandreas, 1981). The discovery of the pathologies family referred to as *sick building syndrome* (Redlich et al., 1997; Burge, 2004) made the first concrete link between health problems and the housing environment and its services.

Modern buildings are largely composed of synthetic materials and the rooms are continuously exposed to many contaminants. Health problems related to indoor air quality actually result from a multitude of factors. The combined effects of many sources of volatile compounds, which may also have their origin in the outdoor environment, are still poorly understood. We can identify three types of contaminants within a home: biological, chemical or physical. Building materials are mainly chemical pollution sources and the respiratory tract is the main route of exposure for humans. It is thus important to identify the volatile compounds that are potentially emitted by materials and their potential impact on health.

We could mention many other criteria that fall within the definition of health safety: fumes in case of fire, allergens contaminants, 'breathable' wall property, etc. An even more complete inventory would consider all sanitary impacts related to the stages of the material life cycle.

- *Technical interests and performance*

The third criterion to be taken into account when looking for eco-friendly materials covers a wide amount of data linked to their performance in the chosen application compared to traditional solutions. Each material has an 'identity card' and its own properties make it more or less suitable as a solution to the requirements specifications. These are the basic considerations that any designer takes into account. For example, in the case of insulation materials we may refer to a series of important data such as the thermal properties (thermal inertia, conductivity), the permeance to air

and water vapour, mechanical strength in compression, fire resistance, moisture sensitivity, etc. (Roodman et al., 1995). Some secondary technical interests may be added to those intrinsic properties: ease of implementation, recuperation of several roles in the structure, wear resistance, etc. Finally, the price is another important factor that plays a central role in all decisions.

Many professionals and researchers in the construction industry who show interest in greener buildings put the thermal performance of insulation materials in the foreground. The economic benefits expected from the improved energy efficiency are probably the cause. Yet, an 'operational-centred' vision is not enough to determine the environmental quality of a material. High-performance materials for their insulating properties such as mineral wool, rock or glass, allow substantial energy savings over the life of the building but are extremely energy intensive during production and end of life. Moreover, they draw their raw material from non-renewable sources.

In any case, designing in a sustainable way means finding a right balance of solutions taking into account the defects and qualities of all products faced to the constraints. Roodman (1995) offers a beautiful analogy on the subject by saying that designers should use modern materials in the same way a jeweller uses precious metals - with moderation and sparingly.

1.1.3 Crop-based materials

Crop-based products have been used in construction for a long time. Of course, wood is a widespread product in buildings but other non-food crops applications are traditionally present in many countries, e.g. fibre-reinforced plasters and renders, thatch roofs, and 'wattle and daub' walling (Cripps et al., 2004; Yates, 2006). Recently, there has been a noticeable return to more 'traditional' construction materials in the building sector (EIO, 2011) in order to meet sustainability objectives. *Crop-Based Materials* (CBM) have many interesting features in the quest of green materials. Forgotten for a long time, current circumstances offer them a chance to reargue their intrinsic qualities. Indeed, the (re)mobilization of these eco-materials in housing in region meets sustainable concerns in several ways:

- Reduced carbon footprint that is explained by the low industrial processing needed, the local availability in most regions and the carbon absorbed during the growing phase of the plant
- Reduced use of non-renewable resources
- Abundant availability of crops products considered as agro-waste, offering guidelines for solving the problem of their disposal (Cripps et al., 2004; Madurwar et al., 2013)
- Opportunities for developing the agricultural industry and improving its economic viability (Cripps et al., 2004)
- Low environmental impact at end of life (recycling, composting and reusing)
- Advantages linked to occupants health and reduced emissions of toxic by-products

Nowadays, there are many possible uses of CBM in construction and a growing range of commercialized products is available. It would be difficult to provide here a detailed inventory of all applications and corresponding CBM solutions. However, a succinct overview is provided in the following paragraphs.

Roughly, compressed panels, fibre batts or raw shives are mainly used for thermal or acoustical insulation but never in load-bearing conditions. In practice, thermal and acoustical insulation properties often go in pair. CBM can also serve in light structural wall configuration, where they both ensure thermal insulation and participate in the structure of the wall. Of course, they do not ensure a major role in loads takeover, which is most of the time limited to self-bearing and possibly some participation to bracing efforts (Cripps et al., 2004). In this application category, two main methods of construction can be distinguished (Cripps et al., 2004): block construction (straw bales, prefabricated fibres-earth or fibres-lime blocks) and cast construction (Fibres-lime, fibres-clay). Both methods are usually associated to the will of benefiting from the ability of CBM to exchange moisture with their surrounding environment. This 'breathable structure' paradigm is often presented as a mean of improving occupants comfort and building energy performance. And it is precisely in this area

that the largest number of interrogations persists, as discussed below. Within light structural techniques often associated to breathable qualities, straw bales and lime-hemp concrete construction draw a lot of attention, especially among self-builders (Ronchetti, 2007; Bevan and Woolley, 2008; EIO, 2011).

A direct benefit of straw bale construction is the low embodied energy of the material. It is a renewable resource, often considered as an agricultural waste product, and there is only little processing required in order to use it in construction. In addition, it offers good thermal insulation values given the thickness of the material (Shea et al., 2013). The main drawback of straw bales use is the risk of mould growth that would appear if moisture accumulates in the wall, through capillary rise, plaster defect or vapour condensation. That explains why designers must be particularly precautious in the domain of moisture management.

Many books have discussed the straw bale construction techniques in the two last decades (King, 1996; Lacinski and Bergeron, 2000; Jones, 2002; King and Aschheim, 2006) and have participated in their new popularity among eco-enthusiastic builders. The use of straw bales in building can be divided into two categories, load bearing or non-structural (in-fill) construction. Straw-based construction is still a small sector within the area of eco-innovative construction but in Belgium and other European countries, a growing number of small companies engage in the commercialization of prefabricated straw bale walls, mainly for residential and small office buildings. The requirements of prefabrication as well as standards compliance explain why the in-fill technique is generally chosen by those companies.

Lime-Hemp Concrete (LHC) construction is a typical example of cast construction, the second category of light structural usage of CBM. The technique has recently gained visibility in the domain of green materials in Europe, especially in France and UK. The LHC material consists of hemp stem particles, or *shives*, mixed with the mineral binder in proportions depending on the desired mechanical, acoustic and hygrothermal properties. The binder concentration has a direct impact on thermal and structural performance and light-weight mixes are preferred when a low thermal conductivity is sought for.

Like straw bale construction, the LHC offers a low embodied energy solution that provides an opportunity to reduce the use of highly processed products. Hemp is fast growing and is regarded by farmers as a low-maintenance crop (Rhydwen, 2006; Yates, 2006). Using a lime binder is also compatible with sustainability concerns as its embodied energy is significantly lower than conventional masonry materials (BRE, 2002). Moreover, lime is more vapour permeable than concrete and is thus compatible with breathable properties. Note that recently, research has become interested in other vegetal particles that may offer an alternative to hemp, more adapted to regional constraints.

1.2 Moisture buffering and breathable structure concept

Indoor air humidity is an essential factor of the occupant comfort and perceived air quality (Fang et al., 1998; Toftum and Fanger, 1999). The indoor humidity level depends on many factors: the climate and ventilation scheme, the moisture loads from occupants and their activities, and the effect of envelopes that incorporate hygroscopic materials and allow them to exchange moisture with indoor air. The term 'breathable structure' is not well defined but is generally used to represents a building envelop that interacts with indoor air humidity and pollutants (Imbabi, 2006; Yates, 2006). It is also frequent to specifically express the exchange of moisture between envelope and indoor air as a *moisture buffering* effect (Peuhkuri et al., 2005). The buffering effect provided by hygroscopic materials, like CBM, on the indoor humidity of a building comes from their ability to absorb or release moisture depending on the conditions applied to their surfaces. Their internal structure shows physical and chemical properties that cause water to bind to the solid matrix below the level of saturation of vapour in the air. The resulting ability of the material to store water can be easily observed. In addition, water transport phenomena in liquid and gaseous states often occur and the flows direction follows some thermodynamical laws.

1.2.1 Physical background and involved phenomena

A material is called *hygroscopic* if it can absorb a measurable amount of moisture of the surrounding air. If we place a dry material sample in a thermostatic chamber in which the relative humidity is increased, the sample will gain mass with an amplitude that depends on the nature of the sample and the variation of the relative humidity. The increase in mass corresponds to a fixation of water molecules to the porous matrix by adsorption and capillary condensation phenomena. Inversely, if the relative humidity is decreased in the surrounding air, the sample will tend to lose water.

The sorption isotherm is used to quantify the ability of a material to fix water at a certain temperature. It characterizes the *Equilibrium Moisture Content* (EMC) as a function of *Relative Humidity* (RH) for a given material at a given temperature. For wood and non-food crops it shows a general shape indicated in **Figure 1.1**.

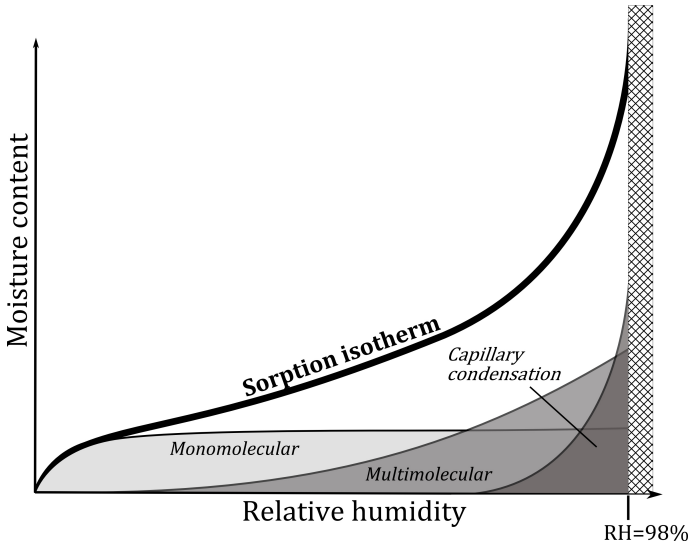

Figure 1.1: The sorption isotherm of a typical CBM

Starting from zero, while the RH is progressively increased, the fixation of water molecules on a porous matrix surface starts with a *monomolecular layer adsorption*. It means that at some point the entire pores surface is covered with a single water molecules layer. This layer is strongly bound to the solid surface, which explains why it is the most difficult to remove. The mono-layered surface corresponds to very low values of RH, around 10-20% (Strømdahl, 2000). While the RH is further increased, several other layers of water molecules tend to fix on the first layer; this is the *plurimolecular adsorption*. As the RH continues to increase, the formation of a liquid

phase can be observed, starting in the smaller pores. This phenomenon, associated to the formation of meniscus, is called capillary condensation. The fact that liquid water appears below 100%RH is due to the lowering of the saturated vapour pressure caused by water surface tension phenomena. And the smaller the pore radius, the smaller is the value of RH that can already cause condensation in this pore. The RH level where capillary condensation starts to have a significant impact on moisture storage depends thus on the porous structure of the material. If it is mainly composed of large pores, surface phenomena will be dominant up to RH values really close to 100%. But because capillary condensation is a volume phenomena, when the structure of the material is composed of many microscopic pores, as for CBM, capillary condensation can have a significant impact on moisture storage capacity simultaneously to adsorption. The sorption isotherm generally shows a steep slope when approaching 100%RH due to the amplification of the capillary condensation phenomenon. The long time required to reach the equilibrium moisture content combined to failures in standard experimental techniques to ensure stable high RH value explain that the sorption isotherm is generally considered valid up to 98%RH. Furthermore, the range for which the sorption isotherm is valid is called the *hygroscopic region* (Time, 1998)

In order to illustrate the potential impact of hygroscopic materials on the surrounding environment, the following example provided by Padfield (1998) is very illustrative. Let us assume that some cotton equilibrated previously at 50%RH and 20°C is put in a sealed container where the air is initially at 50% RH and 20°C. If the temperature is suddenly increased in the box, the cotton will maintain the relative humidity of the air almost constant whereas it would have dropped in the absence of any hygroscopic material. The process is explained as follows: While the temperature of the air starts to rise together with its saturation vapour pressure, the RH in the air tends towards lower values. Almost instantly cotton reacts according to its sorption isotherm and releases water. Because the hygroscopic material stores a much greater volumetric content of water than air, the water lost by the material hardly affects its equilibrium moisture content whereas it strongly affects the vapour pressure of the air. In consequence, the RH drop caused by modification of air temperature is compensated by the water coming out of the material. Ultimately, there is some kind of dampening effect exerted by the material which prevents any steep variation of surrounding RH. However, in a

much larger container, the same cotton sample might not be able to 'fight' against the RH drop of the surrounding air.

It is easily conceivable why this particular effect can contribute to modify the conditions met in the housing environment. Indeed, the capacity to dampen indoor moisture peaks is often presented as an intrinsic benefit of hygroscopic materials (Yates, 2006; Shea et al., 2012). Of course, this is true under the condition that no barrier intervenes, a prerequisite necessary to speak about 'breathable structure'. When humidity rises in the room, the hygroscopic material in direct contact with the indoor air will naturally start to absorb water and slowly transfer it into the depth of the wall. In consequence, the moisture exchange capacity of a porous material does not only depend on its sorption isotherm, but also on its resistance to water diffusion in the porous matrix. If both its moisture storage capacity and vapour permeability are high, as it is the case for CBM, the buffering capacity can potentially act as a passive mean of stabilizing indoor conditions.

In addition, the moisture exchange is coupled to heat transfer through the latent heat involved in the phase change process. When water molecules in suspension in the indoor air penetrate the hygroscopic envelope materials and are adsorbed on his porous matrix, some heat is released. It is important to note that the energy released when a molecule is adsorbed is of the same order of magnitude as the heat of condensation (Strømdahl, 2000). Inversely heat is absorbed from the wall when the latter returns the water to the room.

In the light of all these factes, the moisture buffer effect may have a direct impact on building energy performance: through latent heat effects which may impact heating and cooling needs, through the modification of indoor comfort which impacts the ventilation needs, and through the modification of insulation properties caused by moisture content (Osanyintola and Simonson, 2006). But the experimental evidence of this fact is still limited. A full-scale experimental campaign performed by BRE on LHC houses (2002) is often mentioned in literature as an interesting case study that opens the path to large interrogations concerning breathable structures.

1.2.2 Characterizing the Moisture buffer of materials

Due to the importance of the moisture buffer phenomenon, scientific authors have studied experimentally and analytically the use of hygroscopic materials to dampen indoor humidity. Research at material scale (Padfield, 1998; Svennberg, 2003) led to the definition of the Moisture Buffer Value (MBV), a single parameter that quantify the moisture exchange capacity of a material. It is based on an experimental protocol involving the weighing of a small material sample subject to reference relative humidity cycle. During the test, this sample is allowed to exchange water through one of its faces (Peuhkuri et al., 2005). The experimental MBV can be compared to an ideal value, which is computed from steady-state parameters, *i.e.* moisture capacity and vapour diffusion resistance.

When studying wood, it appeared that its moisture capacity is one of the greatest among 'traditional' construction materials. It means that for a same jump of surrounding RH, wood can theoretically absorb/release a greater amount of moisture compared to most materials. Unfortunately, the moisture diffusion in the radial direction is really slow in that material, which can alter its quality in moisture dampening (Hameury, 2005). In consequence, the moisture buffer value of wood can be either really high or quite low depending on moisture flow orientation. CBM are by nature very similar to wood, but they do not show such a large anisotropy in moisture diffusion. In consequence, among natural materials, they potentially show a great potential for moisture buffering applications and associated benefits.

We must not lose sight of the protocols as MBV are based on strong simplifying assumptions. Although there is currently no real alternative to compare materials with a single value, the parameter gives only few indications on the behaviour and performance of materials under real conditions. First, a permeable wall is almost always composed of several materials, and the CBM are rarely directly exposed to the internal environment. Consequently, they can exercise their regulatory power only through intermediate materials such as finishing boards or plasters. Moreover, while MBV protocol represents the indoor climate by a well-defined relative humidity cycle, in reality, there is a complex mutual interaction between the permeable envelope and indoor humidity.

It appears that understanding more deeply the phenomena linked to the buffering of moisture imposes: (1) to enlarge the mathematical description towards complex material assemblies , room scale and eventually whole-building scale; (2) to establish the potential benefits of incorporating hygroscopic materials in the envelope under various scenarios, characterized by different climatic loads. In order to reach these objectives, numerical modelling approaches are inevitable.

1.3 Modelling the CBM behaviour

1.3.1 Hygrothermal modelling tools

The role of the building envelope is to create a protected indoor environment separated from the outdoor climate (ASHRAE, 2009), where the comfort conditions for the occupants are controlled by active and passive means. Ideally, the climate loads and the environmental parameters of the implementation site must be fully integrated in the building design process in order to minimize the energy and resources demands and improve building sustainability. It is also important to assess how the chosen construction materials and their layout impact the energy balance of the building, occupants' comfort and health, and possibly cause undesirable effects (Viitanen et al., 2010). This last step causes specific challenges when highly hygroscopic materials are involved and are allowed to exchange moisture with the surrounding environment, as shown in **Section 1.2**. For all these issues, computational tools for heat, air and mass transfer modelling play an essential role in early stage of the building design. They constitute one important category of numerical building models, which are dedicated to help practitioners to make decisions when several options are available (Struck et al., 2009) in a cost-effective perspective (Malkawi and Augenbroe, 2004).

A building can be separated into three physical domains, i.e. the heat, air and moisture fields, and three geometrical regions, i.e. the exterior region, the building envelope (including interior space partition walls) and the interior air region (Hens, 2005; Costola, 2011) (**Fig. 1.2**).

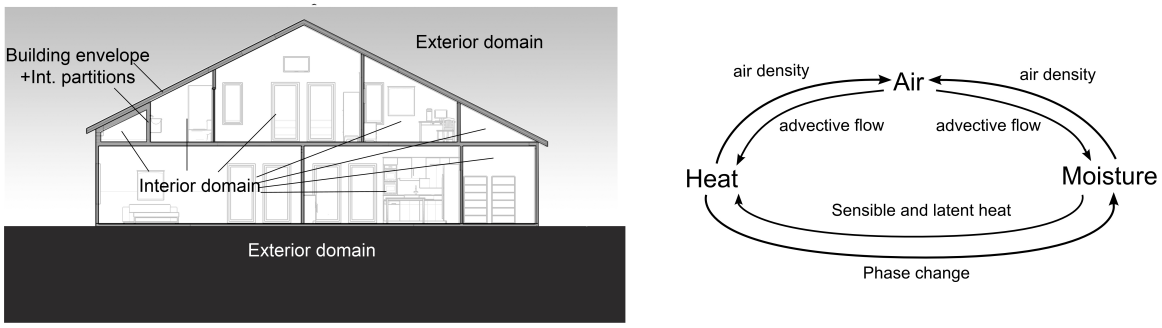

Figure 1.2: Geometrical and physical domains of a building

Various types of hygrothermal models exist and each category generally focuses on some of these domains, while giving simplified assumptions for the others (or simply not considering them). In addition, various time and spatial scales can be used, and various levels of precision are desirable depending on the issue to address. On the basis of the classification proposed by Steeman (Steeman, 2009), most hygrothermal models can be divided into three main categories:

- *Transient energy simulations at building scale*

The first category of tools has been established for more than a decade (Rode and Woloszyn, 2007) and meets the need for the energy performance assessment of whole buildings, central in many green building design standards. Such tools are generally referred to as *Building Energy Simulation* (BES). Most of them are based on the assumption that the air of each room is well mixed and associated with a single temperature value (multi-zone models). Some more simple models only use one thermal zone for the entire building (mono-zone). Each zone is then assigned with a heat balance which includes descriptions for all energy-related loads, *i.e.* gains and losses through building enclosure and between zones, mechanical ventilation systems, heating and cooling devices, etc. In some cases, BES tools also account for air and moisture balance but generally in a very simplified way (Crawley et al., 2008; Janssens et al., 2008).

- *Transient heat, air and moisture simulations in specific envelope parts*

These models focus on the detailed description of transient and coupled hygrothermal transfer in envelope parts. Most of the time they are simply referred

to as *Heat, Air and Moisture* (HAM) models, but we prefer the denomination *Building Element HAM* (BEHAM) simulation tools (Hens, 1996), to avoid confusing with the other types of hygrothermal models. Historically, these tools appeared in Building Physics to assess moisture related damage and evolved from Glaser steady-state method (Glaser, 1959). The simulations outputs are very dependent on the imposed boundary conditions. Moreover, as the indoor climate has to be specified, such models do not allow to directly assess the impact of envelope materials on indoor air. In other words, they lack the description of the mutual link that exists in reality between the interior surfaces of the envelope and the indoor air volume (Rode and Woloszyn, 2007). The variations of the hygrothermal conditions in a room cause some heat and mass transfers towards the surrounding walls. In parallel, such transfers may have a significant impact on indoor conditions. Yet, this second contribution cannot be precisely evaluated by BEHAM models.

- *Airflow simulations*

In this third category, the will is to predict more accurately the air movements occurring in the indoor and outdoor spaces. A first class of airflow models, at room-scale, aims to improve the local representation of air movements by increasing the number of spatial cells used to describe the air volume in computations. Models based on *Computational Fluid Dynamics* (CFD) are the most accurate as they are based on a complete equations set including momentum balance and use a very fine discretization of indoor air volumes. If some include airborne moisture transport, they generally only consider heat exchange with the envelope (Rode and Woloszyn, 2007). *Zonal models* use a coarser space discretization and a simplified mathematical representation but still allow exploring local effects of indoor air movements and outperform the averaged representation found in BES models. At whole-building level, coarser indoor airflow modelling tools are specifically designed to model contaminant dispersion between rooms, and are called multi-zone indoor air quality models (Feustel, 1999; Emmerich, 2001). Outside airflow simulations can offer precious information related to wind loads, driven rain or the infiltration of exterior contaminants.

Of course, each of those typical model categories focuses on different geometric and

physical domains of the building but they basically simulate coexisting phenomena and there are many overlapping areas between them.

1.3.2 CBM numerical studies

Predicting accurately the behaviour of hygroscopic materials under a large variety of imposed solicitations is the prerequisite to answer larger scale interrogations, like the impact of the moisture dampening on the indoor climate or the building energy performance. And the task is not effortless. That explains why, in the actual state of the art, most of numerical studies related to the hygrothermal behaviour of CBM still focus on the description of heat, air and mass transfer in their porous structure with BEHAM tools. Among the researches which include validation data, some were performed at material-scale (Maalouf et al., 2013) and others at wall-scale (Samri, 2008; Bronsema, 2010; Wihan, 2007).

The complexity of the microscopic phenomena involved in heat and mass transfers inside hygroscopic porous media necessary imposes some simplifications in their mathematical translation. Available BEHAM tools, generally oriented to long term evaluation of internal hygrothermal conditions, rely on strong assumptions that do not necessarily hold for all materials nor for all operating conditions. When necessary, models need to be adapted to (re)consider some specific transfer phenomena. For example, much attention is currently addressed to hysteresis phenomena (Time, 2002; Rode and Clorius, 2004; Carmeliet et al., 2005). The dependence of the hygrothermal properties of materials on temperature and moisture content is also critical when large gradients of those variables are met during the simulation. To answer this issue, 'materials models' are more and more frequently used to characterize the materials properties in the form of continuous mathematical functions.

Each proposed improvement for BEHAM models necessarily needs some validation. In order to pursue this validation, the model has to be calibrated by assigning values to its parameters. The parameters linked to materials properties are not always easy to determine experimentally, because of the form of some CBM (bales, non-cohesive particles, etc.) and the natural variability that exists in such bio-based products. It adds another challenge in the numerical prediction of CBM behaviour. Many researches

were entirely dedicated to the experimental determination of CBM properties, like for LHC which has been widely characterized (Collet, 2004; Cerezo, 2005; Evrard, 2008). Beside CBM material parameters, some general experimental parameters are still hard to determine, e.g. parameters linked to the air boundary layer at materials surface.

Having a calibrated and validated BEHAM model is not sufficient to evaluate the impact of materials on building performance and user comfort. Indeed, the BEHAM approach requires an a priori knowledge of the interior and exterior climatic conditions imposed on the studied element. Therefore, it prevents any assessment of real exchanges between the envelope and the indoor environment and prohibits any conclusion concerning the overall performance of materials. On the other hand, BES models, which consider the mutual exchanges between the envelope and the indoor air account for the humidity transfers in a (too?) much simplified manner. Today, there are still only few evaluations of the consequence of the moisture storage in materials on a whole-building perspective and no general strategy to evaluate the impact it might have on building operational energy consumption. Most of room scale studies were essentially experimental and have as an objective to compare various interior wall finishes in term of their moisture exchange potential (Svennberg et al., 2004; Mortensen et al., 2005; Li et al., 2012).

In response to deficiencies of each hygrothermal model category taken separately for predicting both CBM behaviour and its effect on indoor air volumes, the importance of developing whole-building hygrothermal models has recently been raised (Hens, 2005; Rode and Grau, 2008; Woloszyn and Rode, 2008; van Schijndel, 2009). Simple whole-building hygrothermal models can be obtained by combining the central concept from BES tools, i.e. the indoor air volume balance, with a BEHAM tool, able to accurately describe the transient conditions in the materials of the envelope (**Fig. 1.3**).

By integrating those two types of descriptions, it becomes possible to characterize the evolution of the indoor climate of a zone or an entire building while describing the actual participation of envelope materials with coupled heat and mass transfers. In 2005, the Annex 41 of the international Energy Agency (IEA) was a cooperative project on the whole-building heat, air and moisture response, part of the *Energy Conservation in Buildings and Community Systems program* (ECBCS). Several tools were already

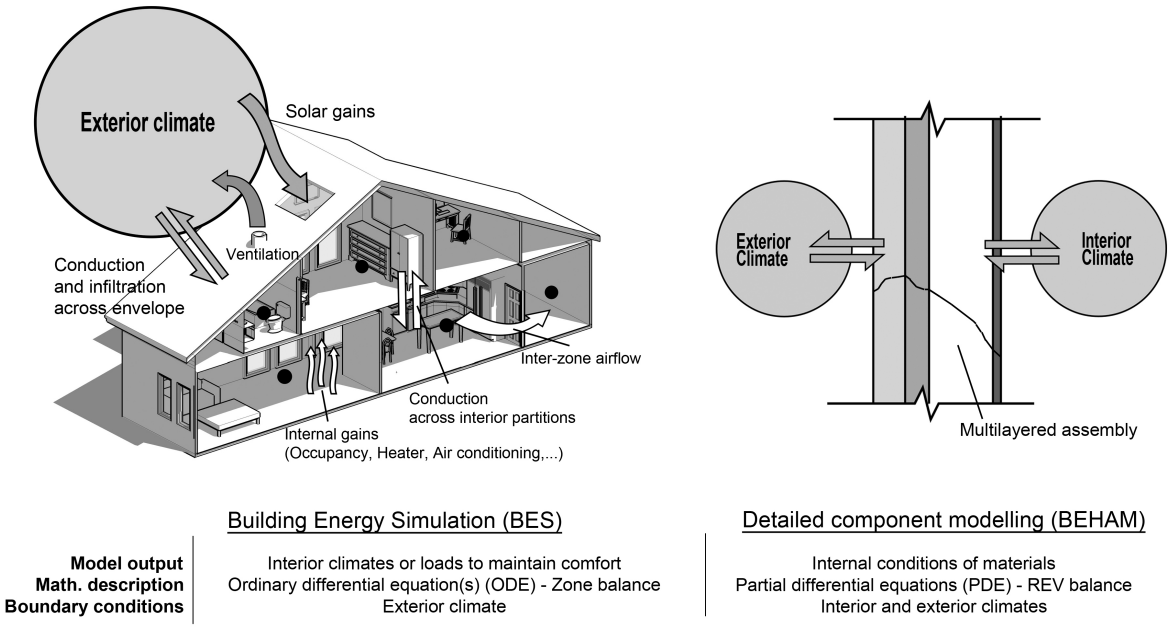

Figure 1.3: Combining BEHAM models with BES concepts

identified as capable of modelling the indoor air of a room including the dynamic interaction with the coupled heat, air and moisture response of the envelope (Rode and Woloszyn, 2007). Although the tools that could account for the impact of CBM-walls at building-scale exist, there is still very few validation studies in real full-scale environments (Salonvaara et al., 2004). One of the very few examples of such validation can be found in (Tran Le et al., 2010), for a room with LHC walls.

1.3.3 The use of general scientific computational tools

In the precedent section, it was observed that many challenges are associated with the modelling of CBM behaviour. The imperatives of research can be divided into two major guidelines: improving the description of heat, air and moisture transfer in hygroscopic materials and scaling up the improved models to eventually reach a whole-building approach. In this context, *General Computational Tools* (GCT), like *Matlab*[1], *SPARK*[2], *Modelica*[3], *Mathematica*[4], etc., offer a valuable solution.

The main benefit of GCT is the flexibility they offer in the coding and resolution of problems. They include of a wide range of powerful modelling tools that can answer

[1] http://www.mathworks.com/products/matlab/
[2] http://gundog.lbl.gov/VS/spark.html
[3] https://modelica.org/
[4] http://www.wolfram.com/mathematica/

the need for improving BEHAM models with evident transparency benefits. As it was shown before, be confined to such wall-scale models does not allow to assess clearly the benefits and drawbacks of CBM usage relatively to occupants' comfort and energy performance. Developing larger scale and validated hygrothermal models is clearly essential. However, a holistic approach, which would combine the most precise techniques to describe all geometric and physical domain of the building, is still far from achievable. Nevertheless, it seems clear that scientists should start defining guidelines to combine validated models efficiently in order to enlarge the level of analysis. For this purpose, the uniqueness of each GCT language allows combining tools in a single computational environment, which offers a maximum level of control on simulated phenomena. In addition, the buoyant user-community of GCT often ensures the immediate availability of some hygrothermal building models in BEHAM, BES or Airflow categories. As it happens, several authors have already used general computational environments to develop whole-building hygrothermal tools (Sasic Kalagasidis, 2004; van Schijndel, 2009; Tariku et al., 2010; Tran Le et al., 2010).

1.4 Objectives

The main purpose of this thesis is to explore the use of a research BEHAM model developed in a GCT as a solution to some of the challenges associated with the hygrothermal modelling of CBM behaviour. This task covers various study scales and two major guidelines described in **Section 1.3**: improving the efficiency of BEHAM models and scaling-up the simulation at room or building scale to evaluate the impact of moisture buffering on indoor air.

Four main objectives are followed in this work:

1. Develop an flexible research BEHAM model based on the state-of-the-art that can easily evolve and combine with other computational tools
2. Improve the prediction efficiency of the BEHAM model by proposing innovative methods for the determination of CBM hygrothermal properties, both experimentally and numerically
3. Improve the prediction efficiency of BEHAM model by proposing new mathematical descriptions for non-standard operating conditions
4. Study the impact of CBM on indoor air climate, by combining the BEHAM model to a zone balance description

In order to achieve these goals, secondary objectives are to be met in the development of multi-scale experimental facilities able to highlight some physical specificities of hygroscopic materials behaviour. Those will allow to implement case studies for validating the proposed modelling approaches.

1.5 Thesis outline

In order to meet the fixed objectives, the document will be presented as follows:

Chapter 2 studies the state-of-the-art related to the modelling of heat and moisture transfer modelling in porous media at microscopic level. Starting from a physically-based approach, the moisture balance equation on a representative material volume

is developed according to various moisture dependent variables. Then all resulting formulations are compared to available models.

Chapter 3 shows how the hygrothermal properties of materials are experimentally obtained and what are the obstacles that remain in this task, especially when studying CBM. An original device designed to measure the thermal conductivity of straw bales is also presented.

Chapter 4 presents a first version of the research model developed in the context of CBM study and the guidelines followed for its creation. It is validated at material scale on the basis of a Moisture Buffer Value test. For this purpose, performance criteria are also defined precisely.

Chapter 5 introduces an innovative inverse modelling technique for parameter estimation which answers the difficulties in measuring the hygrothermal properties of CBM. The technique offers a realistic assessment of storage and transport properties that are optimized on the basis of a dynamic experiment.

Chapter 6 studies the improvement of the BEHAM model in non-isothermal conditions by characterizing the temperature effect on CBM moisture storage. A prefabricated straw bale wall is subject to a 35°C heat shock in a bi-climatic chamber. Various versions of the research BEHAM model are compared in their ability to simulate the internal conditions of straw bales, which are fully monitored.

Chapter 7 introduces a room-scale hygrothermal model, developed in *Simulink* and incorporating the research BEHAM model. Based on an experiment similar to the precedent chapter, this new model is used to assess the effect of moisture buffering on heat and moisture fluxes between the chamber air and the straw bale wall.

It should be noted that the document starts from a theoretical point a view to explore progressively practical aspects of CBM modelling at increasing study scales.

1.6 Working framework and general assumptions

This thesis does not claim to address all issues related to hygrothermal modelling of CBM. It is neither willing to characterize entirely the benefits of CBM use. The magni-

tude of the task necessarily imposes some limitations. In this respect, in all experimental case studies used for validation purpose, the materials solicitations are limited to the hygroscopic moisture content region. In consequence, liquid water transport and hysteresis phenomena descriptions, which are of great interest, are not used during simulations. Additionally, in each study the total air pressure gradients are assumed to be negligible. Finally, in the chapters in which a material assembly is modelled, contact resistances between materials are also neglected.

The studied materials found in the following chapters are straw bales, lime-hemp concrete and clay plaster. They are only representative of some CBM applications. The accent is put on modelling techniques that should be applied to future case studies, with other materials assemblies and operating conditions.

CHAPTER 2

Modelling heat and moisture transfer in porous media

2.1 Introduction

This chapter studies how the hygrothermal transfers in porous media can be transcribed mathematically. Such problems are frequent in many scientific disciplines and rely on coupled *Partial Differential Equations* (PDE) expressing the heat and mass balance on a representative elementary volume (REV).

The appended paper presents a review of mathematical formulations used to describe the moisture balance equation in porous media when the total air pressure gradient is negligible. The heat balance is not treated in details as it depends directly on the moisture flows through latent and sensible heat transport which adds to the well defined heat conduction phenomenon. We chose to start from a physically-based formulation of moisture balance and develop it relatively to each possible couple of dependent variables, *i.e.* temperature and either vapour pressure, relative humidity, capillary pressure or moisture content. The study shows the correspondence between the physically-based approach and many formulations found in Building Physics literature, including frequent simplifications and secondary transport coefficients. It offers a strong basis to develop a flexible BEHAM model in which equations can be adapted to the case study.

2.2 Appended paper

Non-Isothermal Moisture Balance Equation in Porous Media: *A Review of Mathematical Formulations in Building Physics*

Samuel DUBOIS*[1], Arnaud EVRARD[2], Frédéric LEBEAU[1]

[1]Dept. of environmental sciences and technologies, Gembloux Agro-Bio Tech, University of Liege, Belgium

[2]Architecture et Climat, Université Catholique de Louvain, Belgium

*Corresponding author, supported by a F.R.I.A Grant,
Address: Dept. of environmental sciences and technologies, Gembloux Agro-Bio Tech, 2 Passage des déportés, 5030 Gembloux, Belgium (s.dubois@doct.ulg.ac.be)

KEYWORDS

Ham Modelling, Porous media, Adsorption, Capillarity, Diffusivity, Isosteric heat

STATUS

Published in:

Biotechnologie, Agronomie, Société et Environnement (BASE), 2014

ABSTRACT

Understanding heat and mass transfers in porous materials is crucial in many areas of scientific research. Mathematical models have constantly evolved, their differences lying mainly in the choice of the driving potentials used to describe moisture flows, as well as in the complexity of characterizing the physical phenomena involved. Models developed in the field of Building Physics (HAM models) are used to describe the behavior of envelope parts and assess their impact on user comfort and energy performance. The water balance equation can be described in many ways; it is a function of the boundary conditions considered and the fact they induce high or low water content in the porous materials used.

This paper gives an overview of various formulations for this equation that are found in the Building Physics literature. It focuses first on the physically based formulation of moisture balance, drawing on the Representative Elementary Volume (REV) concept, coupled with thermodynamic flow rates description. This is then reformulated in line with various main moisture state variables offering a wide variety of expressions that are compared with available models. This approach provides access to all secondary transport coefficients associated with the process of mathematical transformation. Particular emphasis is placed on the moisture storage function choice and its impact on the final mathematical formulations.

1. INTRODUCTION

Heat, air and moisture (HAM) transfers across envelope elements play a crucial role in building performance and durability as well as in user comfort (Fang et al. 1998; Padfield 1998; Toftum et al. 1999; Adan et al. 2004; Salonvaara et al. 2004; Osanyintola et al. 2006; Mudarri et al. 2007). The ability of porous materials to store and release moisture through capillarity and hygroscopicity effects has an impact on building behavior and can cause damage when not sufficiently controlled. Modeling this complex behavior in multilayered porous walls has become an important research topic in Building Physics and performance analysis.

Moisture flows in porous media have been studied for a long time in various research fields, including ground water hydrology, agricultural, chemical and petroleum engineering, and drying technologies. The first work on drying modeling described moisture transfers via a diffusion-like equation linking the flow rate to the product of a moisture content gradient and a constant transport coefficient (Sherwood 1929). At the same time, soil scientists were discovering the importance of capillary action in moisture movement. Contemporary mathematical models have their roots in the work of Philip and De Vries (1957) and Luikov (1966), who were the first to consider the thermal effect on moisture transfer and to separate liquid and vapor flows. At that point, however, the governing equations remained phenomenological because they were inferred from continuous media descriptions in a rather 'intuitive' way. Whitaker (1977) rationalized the theory by detailing the gap between microscopic and macroscopic description through the *Representative Elementary Volume* (REV) concept. Moisture transfer description was thereafter widely discussed and further investigated (Milly et al. 1982; Nielsen et al. 1986; Milly 1988). The main difficulty remained in accurately describing non-isothermal moisture transfer and determining the transfer coefficients experimentally because of their high dependence on the transfer potentials.

Initially, all these advances in the understanding of porous media had a limited impact on models in the Building Physics field. Other methods had been developed, mainly to characterize the accumulation of water in walls by vapor diffusion in steady-state conditions (Glaser 1959). In this context, some authors showed, prematurely, the potential of incorporating external concepts from soil science into Building Physics (Van Der Kooi 1971; Hall 1977) and the first building-oriented models incorporating transient heat and moisture transfers with capillarity effects appeared in the 1980s. They were all oriented towards envelope part description in 1D. In the 1990s, the first computer models were commercialized (including Rode 1990; Künzel 1995). As the fundamental understanding of the phenomena and computer power have improved, many other models have been developed over the past two decades, with increasing accuracy and capabilities. There is an exhaustive list of available software on the Energy Tools website of the US Department of Energy and in Delgado et al. (2013).

In reality, there is no unique means of describing moisture transfer in porous building materials. The mathematical expression of the moisture balance equation and its complexity depends on the initial definition of driving potentials for moisture flows, the simplification hypothesis, the chosen dependent variables and the consequent secondary transport coefficients. This diversity is related to the wide variety of building materials, the hygrothermal conditions they face and typical cases studied in the laboratory or in the field. It is obvious that the moisture buffering of a homogeneous sample at ambient temperature is not dominated by the same transport mode and would not require the same assumptions for its description as rain absorption in a composite wall. Traditionally, HAM models were first designed to treat unsaturated problems, whereas soil-dedicated tools were first optimized for near-saturation processes. This explains why their sets of preferred variables often differ. Both model types are now trying to broaden moisture content range description, while also addressing non-isothermal case studies. There is an urgent need for standardization of the mathematical formulation.

In this paper, we focus on classic non-isothermal, non-hysteretic moisture transfer in a porous medium. Initially, we look at the moisture balance equation derived from the averaging process over a REV, with all moisture fluxes described according to the actual thermodynamic driving potential. No other balance equation is considered here because the emphasis is on moisture transfer characterization. Linking this balance equation with a physically based description of moisture fluxes, we show how different HAM formulations are obtained by reducing the number of variables and further simplifying the mathematical expressions. Several ways of characterizing moisture storage functions are also presented, including temperature effects, which are seldom discussed in Building Physics. The various mathematical expressions presented in this paper could be used to develop models for general numeric computational tools, such as *COMSOL Multiphysics*. Given their inter-operability, these tools have great potential for solving many HAM building problems (Dubois et al. 2013).

2. PHYSICAL BACKGROUND AND MATHEMATICAL TRANSLATION

2.1 Macroscopic modeling

A porous medium is a heterogeneous system characterized by a complex matter combination: a solid structure whose pores are filled with liquid and gaseous phases. In order to use the traditional continuous *Partial Differential Equations* (PDEs) formulation to describe the structure's hygrothermal behavior, it is necessary to make some simplifications by averaging the phenomena and variables over a REV (Whitaker 1977; Bear 2013). This creates equivalence between the real dispersed environment and a fictitious continuum. At any point of this new mathematical space are assigned values of the variables and parameters that are actually averaged values over a volume around this local point (Bear 2013).

When the porous medium contains multiple fluid phases, as in most cases in Building Physics, it is replaced by the overlap of several fictitious averaged continuums. Each of these continuums is assigned to a phase and fills the entire domain of the porous medium. It can then be described with typical conservation equations for extensive quantities: inner energy and mass. In order to reduce the number of unknowns, some additional information is needed and this is provided by the *constitutive equations*, which are relationships between the flux densities of the conserved quantities and some driving forces expressed as the gradient of a state variable. These equations are also sometime referred as '*phenomenological equations'* (Bear 2013) because of their dependence on experimental observations. Finally, by assigning a reference velocity from the selected Eulerian point of view, all the flux densities of the conserved quantities can be divided into convective and diffusive flows.

2.2 REV conservation equation

2.2.1 General assumptions

It is assumed in the following sections that the porous medium $\Omega \subset R^3$ is a multiphase system consisting of the solid matrix, a liquid water phase and a gaseous phase, comprising dry air and water vapor. The total gas pressure in the porous media is expressed:

$$p_g = p_a + p_v \tag{1}$$

The following additional assumptions are made for the mathematical developments described in this paper: (1) the material is non-deformable and isotropic; for a non-isotropic material, standard transfer coefficients have to be replaced by tensors; (2) the fluid phases do not react chemically with the solid matrix; (3) the moisture content of the material stored as vapor $\rho_v \theta_v$ is considered negligible compared with the correspondent term in the liquid phase; (4) the dry air pressure is constant in the material (no air advection) and the total gas pressure gradient is considered negligible; (5) no solid-liquid phase change is considered; (6) there is a local thermodynamic equilibrium between the different phases, which means that water has the same thermodynamic potential in the gaseous, adsorbed and capillary phases; (7) there are no thermal effects caused by friction or compression; (8) the Soret effect is neglected (Janssen 2011); (9) no hysteresis phenomena are taken into account; and (10) no gravity effect is considered.

The PDE description respects the following general scalar form:

$$d_a \frac{\partial u}{\partial t} = -\nabla \cdot \Gamma + F \tag{2}$$

where u is the dependent variable, F and d_a are scalar coefficients and Γ is the fluxes vector. The different coefficients can be functions of the spatial independent variables, the dependent variable and the space derivatives of the dependent variable.

2.2.2 Moisture balance

Equations 3 and **4** show the equations of mass conservation averaged over the REV for the two water phases present in the porous material. Note that in this paper we omit the averaged notation.

$$\frac{d(\rho_l \theta_l)}{dt} = -\nabla \cdot \boldsymbol{j^{M_l}} - \dot{m} \quad (Liquid) \tag{3}$$

$$\frac{d(\rho_v \theta_v)}{dt} = -\nabla \cdot \boldsymbol{j^{M_v}} + \dot{m} \quad (Vapor) \tag{4}$$

The symbol $\boldsymbol{j^{M_l}}(kg \cdot m^{-2} \cdot s^{-1})$ is the total mass flux density of liquid water, $\boldsymbol{j^{M_v}}$ $(kg \cdot m^{-2} \cdot s^{-1})$ is the total vapor mass flux density and $\dot{m}$ $(kg \cdot m^{-3} \cdot s^{-1})$ is the phase change rate. Since the vapor moisture content is often considered negligible in comparison with liquid moisture content, we can write:

$$\dot{m} = \nabla \cdot \boldsymbol{j^{M_v}} \tag{5}$$

The two balance equations are added to give the total moisture balance:

$$\rho_l \frac{\partial \theta_l}{\partial t} = -\nabla \cdot \left(\boldsymbol{j^{M_v}} + \boldsymbol{j^{M_l}}\right) \tag{6}$$

When assuming negligible total gas pressure gradients in the material, there is no convective vapor flux. **Equation 7** shows the resulting balance equation with detailed transport mechanisms:

$$\rho_l \frac{\partial \theta_l}{\partial t} = -\nabla \cdot \left(\boldsymbol{j_d^{M_v}} + \boldsymbol{j_c^{M_l}} + \boldsymbol{j_{surf}^{M_l}}\right) \tag{7}$$

with the different mass flux densities being $\boldsymbol{j_d^{M_v}}$ the vapor diffusion, $\boldsymbol{j_c^{M_l}}$ the liquid water transport through capillarity and $\boldsymbol{j_{surf}^{M_l}}$ the liquid water transport in the sorbate film (or surface diffusion).

In a porous system containing a binary mixture of dry air and water vapor under constant total gas pressure, the observed diffusive flow of vapor is a combination of Fick's diffusion, Knudsen diffusion and a transition between both modes, depending on the pore size distribution of the material (Descamps 1997). As a result, the total vapor diffusion mass flux density can be expressed as:

$$\boldsymbol{j_d^{M_v}} = -\delta_v \cdot \nabla p_v \tag{8}$$

where p_v (Pa) is the partial vapor pressure and $\delta_v(kg \cdot m^{-1} \cdot s^{-1} \cdot Pa^{-1})$ is the vapor diffusion coefficient of the material, also called vapor permeability. The latter is a complex function of relative humidity and temperature.

In an unsaturated porous building material, the liquid water is subjected to the suction of the medium through capillary forces. In a pore, the capillary pressure $p_c(Pa)$ represents the difference between gas and liquid pressure over the meniscus:

$$p_c = p_g - p_l \tag{9}$$

This variable is always positive for hydrophilic materials and the liquid pressure is necessarily less than the atmospheric pressure. In Soil Physics, it is common to fix the atmospheric pressure to zero, which results in a negative liquid pressure assuring the continuity with the positive water pressure met in saturated regions under a water column. In unsaturated materials, water is thus subject to a pressure deficit and in order to deal with a positive quantity it is common for soil scientists to define the suction ψ as the negative of the liquid pressure:

$$\psi = - \underbrace{(p_l - p_g)}_{\substack{liquid\ pressure \\ in\ Soil\ Science\ referrential}} \tag{10}$$

The suction and the capillary pressure are thus rigorously identical and the use of one or the other term is only a matter of choice or scientific habits. The capillary liquid flow rate is then driven by the capillary pressure or suction gradient following Darcy's law and again assuming a negligible total gas pressure gradient:

$$\boldsymbol{j_c^{M_l}} = -K_l \nabla p_l = K_l \nabla p_c \tag{11}$$

with $K_l\ (s)$ the liquid transfer coefficient (called the 'unsaturated hydraulic permeability'; also referred to as 'liquid conductivity'). It is important to note that moisture transfers due to capillarity go from low suction (high moisture content, high relative humidity) to high suction (low moisture content, low relative humidity), which is shown through the sign of right hand side of **Equation 11**.

The last moisture transport phenomenon to consider is the flow occurring in the liquid film adsorbed on the surface of pores. For building materials under standard operating conditions, multilayer diffusion is expected to prevail because strict monolayer surface diffusion is active only in a very dry state. This transport mode is rather complex and it is particularly difficult to isolate from capillary transport because both phenomena can occur simultaneously in pores of different sizes (Uhlhorn 1990). The transfer occurs from high to low concentration of adsorbed water, which depends on temperature and relative humidity in a homogeneous material. In HAM models, multilayer diffusion is never featured in detail. In this paper, we take this the phenomenon into account through the liquid conductivity function definition, which implies that the temperature effect on multilayer adsorption is not considered. There are more detailed reviews of surface diffusion modeling in Uhlhorn (1990) and Choi et al. (2001).

In consequence, **Equation 12** shows the general moisture conservation equation, with physically based driving potentials:

$$\rho_l \frac{\partial \theta_l}{\partial t} = -\nabla \cdot (K_l \nabla p_c - \delta_v \nabla p_v) \quad (12)$$

2.3 Closing relationships

In order to solve the macroscopic balance equation (**Equation 12**), relationships have to be formulated between the different moisture-related variables (i.e., the moisture content θ_l, the vapor pressure p_v and the capillary pressure p_c) in order to limit the number of unknowns. First, as the local thermodynamic equilibrium hypothesis is assumed to be valid about the meniscus in a pore, Kelvin's equation (Defay et al. 1966) relates the capillary pressure to the vapor pressure through relative humidity:

$$p_c = f(\varphi, T) = -\rho_l R_v T \cdot \ln(\varphi) \quad (13)$$

with the inverse relationship:

$$\varphi = f^{-1}(p_c, T) = \exp\left(\frac{-p_c}{\rho_l R_v T}\right) \quad (14)$$

The *Moisture Storage Curve* (MSC) of the material provides the second necessary relationship. It is a material-dependent continuous function that expresses the equilibrium moisture content present in the REV for a given thermodynamic humidity condition. The storage process can be expressed in relation to either relative humidity or capillary pressure due to local equilibrium hypothesis. The function is complex to characterize on the whole moisture content range because it is determined mainly by physical adsorption at low moisture content and capillary condensation at high moisture content, with a transition point depending on the pore size distribution of the material, as well as on temperature or hysteresis effects, which alter equilibrium moisture content for a given relative humidity/capillary pressure. As the study of building materials behavior takes root in several scientific fields, the moisture storage functions found in the literature on HAM models take many forms, depending on the moisture content range of interest. They always incorporate adjustable parameters that are either physically based or purely empirical.

Scientists studying low moisture content processes or non-capillary materials often use an isothermal function in the form $\theta_l = g_\varphi(\varphi)$. This formulation is common in chemical or food process engineering studies, where the emphasis is on mono- and multilayer adsorption, which are surface phenomena. In this paper we refer to these storage models as *type 1 MSC*. Some of them are semi-empirical g_φ formulations, such as the BET model (Brunauer et al. 1938), whereas others offer a truly empirical g_φ adsorption function, such as the Oswin formulation (Oswin 1946).

In contrast, other scientists emphasize the capillary condensation phenomenon linked to high moisture content. Soil scientists, for example, will often use a storage function that is dependent

on suction. It is then called the *Moisture Retention Curve* and can be easily expressed as $\theta_l = g_p(p_c)$. In this paper, this type of formulation is referred to as *type 2 MSC*. Many of these models evolved from the van Genuchten expression (Van Genuchten 1980) and offer empirical g_p description. Some physically accurate g_p functions are based on pore size distribution models. These may themselves be divided into *Bundle of Tubes Models* (Carmeliet et al. 2002; Grunewald et al. 2003) and *Network Models* (Dullien 1979; Carmeliet et al. 1999). When using a pore-space model, the isothermal moisture retention curve mathematical function is often achievable based on pore-filling theory. There is an example of this approach in Häupl et al. (2003).

For materials showing mono- and multilayer adsorption as well as capillary condensation, type 1 and type 2 MSCs, with a physically based approach, could be combined by choosing relative humidity or capillary pressure as the thermodynamic potential and performing variable transformations of one of the MSCs using Equations 13 or 14.

The temperature effect on moisture storage is still not perfectly understood, nor has it been studied in detail in Building Physics because it is widely expected to have a minor impact. For some products such as wood-based materials, however, it might play a non-negligible role (Rode et al. 2004). There are several approaches for incorporating thermal effects into moisture storage function description. For hygroscopic-oriented models, the temperature effect is sometimes considered by introducing a temperature dependence of the function parameters or by interpolation on the basis of several individual isothermal curves. This typically gives a direct function in the form $\theta_l = g_{\varphi,T}(\varphi, T)$ or *type 3 MSC*. According to Poyet and Charles (2009), temperature affects equilibrium relative humidity through the Clausius-Clapeyron relationship, which describes the heat involved in the adsorption process. The equilibrium relative humidity dependence on temperature and moisture content is then written thus:

$$\varphi(\theta_l, T) = [\varphi]_{T_{ref}} \cdot \exp\left(\frac{q_{st}(\theta_l)}{R_v}\left(\frac{T - T_{ref}}{T \cdot T_{ref}}\right)\right) \tag{15}$$

where q_{st} $(J \cdot kg^{-1})$ is the net isosteric heat and the relative humidity at reference temperature is obtained by the inverse of the isothermal sorption function:

$$[\varphi]_{T_{ref}} = \left[g_{\varphi}^{-1}(\theta_l)\right]_{T_{ref}} \tag{16}$$

Such a $\varphi(\theta_l, T)$ function can be used to obtain different isotherms in order to construct the type 3 MSC interpolation.

In over-hygroscopic and capillary condensation oriented models, it is often assumed that, for a given moisture content, temperature affects equilibrium capillary pressure mainly by modifying water surface tension. **Equation 17** provides an example of this approach, as proposed by Milly et al. (1980).

$$P_c(p_c, T) = p_c \cdot \exp\left(a\left(T - T_{ref}\right)\right) \quad (17)$$

where $a = -\frac{1}{\sigma}\frac{d\sigma}{dT}$ is assumed to be constant. When the temperature-dependent expression of capillary pressure $P_c(p_c, T)$ is incorporated into a type 2 MSC with parameters corresponding to reference temperature, it gives a new function $\theta_l = g_p(P_c) = g_{p,T}(p_c, T)$. In this paper, this is referred to as *type 4 MSC.* Again, it is worth noting here that the representation of physical phenomena varies considerably, depending on the original scientific field. In fact, the effect of temperature on moisture storage is a combination of sorption and capillary condensation equilibrium modification. Currently, there appears to be no model that accounts for both effects, another indication of the need for standardization.

2.4 Material moisture transport coefficients

The liquid conductivity and vapor diffusion coefficient are, in reality, functions of the two chosen dependent variables giving typically non-linear PDEs. In a few particular cases they could be considered as constant parameters, but when large ranges of moisture content or temperature are expected to occur in the material, these simplifications can easily lead to incorrect predictions. As a result, these functions have to be characterized properly when going for so-called 'full-range modeling'. There is an example of such characterization in Grunewald et al. (2003), which illustrates the complexity of defining physically based material water transport functions. We do not go into more detail on this subject here because it is beyond the scope of this paper.

3. FORMULATIONS ACCORDING TO A MAIN MOISTURE DEPENDENT VARIABLE

3.1 Method

We showed how the theoretical moisture balance equation is obtained from a macroscopic description of a porous homogeneous material using the REV concept, with a phase-divided approach. The capillary pressure and vapor pressure emerged as the two physically based driving potentials for the description of water fluxes. The model is based on *pressure-driven flows* (Funk et al. 2008). As shown by Funk and Wakili (2008), the total moisture flux can be described using the combination of the temperature gradient and one of the main moisture variable gradient. Given that moisture variables are linked together during the transfer process through closing relationships ,and assuming local equilibrium, we can perform variable-transformations on each of the constitutive relationships that define liquid or vapor flux (**Equations 8 and 11**). This is done through partial derivative expressions:

$$\begin{cases} \nabla p_v = \left.\frac{\partial p_v}{\partial X_i}\right|_T \nabla X_i + \left.\frac{\partial p_v}{\partial T}\right|_{X_i} \nabla T \\ \nabla p_c = \left.\frac{\partial p_c}{\partial X_i}\right|_T \nabla X_i + \left.\frac{\partial p_c}{\partial T}\right|_{X_i} \nabla T \end{cases} \quad (18)$$

where $\vec{X} = (\varphi, p_v, p_c, \theta_l)$ is the main moisture variables vector. We can see immediately that if the main moisture variable is vapor pressure or capillary pressure, there is no need to reformulate the vapor or liquid flux, respectively. In the final stage, the vapor and liquid fluxes can be expressed in the form:

$$\boldsymbol{j_c^{M_l}} + \boldsymbol{j_d^{M_v}} = D_{X_i X_i} \nabla X_i + D_{X_i T} \nabla T \quad (19)$$

By developing the balance equation in terms of one or other main moisture state variable, new transport coefficients will arise, $D_{X_i X_i}$ and $D_{X_i T}$, called *secondary transport coefficients* associated with the gradient of the main moisture variable X_i and temperature T in the $\mathrm{X_i} - \mathrm{T}$ system, respectively. They are phenomenological functions dependent on the two dependent variables, as well as on primary transport functions. In addition, by choosing a phase-divided approach as a starting point, the vapor and liquid transport sub-functions are easily identified through **Equation 18**.

In this paper, the pressure-driven moisture balance equation is re-formulated using two modeling strategies. The first strategy is to choose one of the thermodynamic variables as the main moisture state variable, $X_i \neq \theta_l$. In this case, the left hand side of **Equation 12** also has to be reformulated through moisture storage functions:

$$\frac{\partial \theta_l}{\partial t} = \underbrace{\left.\frac{\partial \theta_l}{\partial X_i}\right|_T}_{\xi_{X_i X_i}} \frac{\partial X_i}{\partial t} + \underbrace{\left.\frac{\partial \theta_l}{\partial T}\right|_{X_i}}_{\xi_{X_i T}} \frac{\partial T}{\partial t} \quad (20)$$

where $\xi_{X_i X_i}$ is the isothermal moisture capacity of the material (also referred to as specific moisture content in analogy to specific heat) and $\xi_{X_i T}$ is its non-isothermal moisture capacity. The second strategy is to use the moisture content, which is an empirical variable that can be defined only at REV level. It implies usage limitations of the balance equation obtained. Whenever possible in this paper we highlight the links between the obtained formulations and similar or identical approaches found in the literature on Building Physics models. For each variable choice, mathematical developments are provided in the form of a synthesis table. This table contains the partial derivatives needed for the reformulation, as well as the full mathematical developments of secondary transport functions that might be useful when comparing models. For each strategy and main variable choice, the most commonly used MSCs are mentioned and used to develop the connections between moisture content and thermodynamic variables.

3.2 First strategy: thermodynamic variables formulations

3.2.1 Relative humidity

Table 1 shows the mathematical developments for relative humidity as the main moisture variable, with the most frequent expressions of MSC related to this formulation. Here, only type 3 MSC takes account of the influence of temperature on moisture storage.

The expression of moisture balance with respect to relative humidity is very common in Building Physics research. This moisture field formulation is particularly relevant when modeled phenomena are predominantly in the hygroscopic range or have a simplified liquid transfer characterization. In addition, relative humidity is easily measured with widely used and affordable sensors. The sorption isotherm dependence on temperature is rarely taken into account in software based on φ-formulation, which almost always use a type 1 MSC. With this common assumption, the balance equation becomes:

$$\rho_l \xi_{\varphi\varphi} \frac{\partial \varphi}{\partial t} = \nabla \cdot \left[\left(D_{\varphi T}^{l} + D_{\varphi T}^{v} \right) \nabla T + \left(D_{\varphi\varphi}^{l} + D_{\varphi\varphi}^{v} \right) \nabla \varphi \right] \tag{21}$$

which is found in Tariku et al. (2010). Künzel (1995) and Künzel and Kiessl (1996) chose to neglect the effects of temperature on liquid transport, i.e. $D_{\varphi T}^{l} = 0$ and:

$$\boldsymbol{j}_{\boldsymbol{c}}^{\boldsymbol{M_l}} = D_{\varphi\varphi}^{l} \nabla \varphi \tag{22}$$

According to these authors, the transport coefficient $D_{\varphi\varphi}^{l}$ can be derived from wet-cup vapor permeability tests or, more commonly, calculated from the isothermal liquid diffusivity $D_{\theta\theta}^{l}$ $(m^2 \cdot s)$, which is the transport coefficient deriving from the moisture content gradient description for liquid transfer (see the second strategy, **Table 4**). With this second method, the isothermal liquid transport coefficient is expressed as:

$$D_{\varphi\varphi}^{l} = D_{\theta\theta}^{l} \cdot \xi_{\varphi\varphi} \tag{23}$$

Without liquid transport, the equation is further simplified (Roels et al. 1999) and finally, in isothermal conditions, it becomes:

$$\rho_l \xi_{\varphi\varphi} \frac{\partial \varphi}{\partial t} = \nabla \cdot \left[D_{\varphi\varphi}^{v} \nabla \varphi \right] \tag{24}$$

This simplified balance equation is frequently used for studying isothermal behavior in the hygroscopic region, such as during an MBV experiment (Dubois et al. 2013). It should be noted that the notion of isothermal behavior is purely theoretical because any relative humidity change in the material will result in heat transfer through the latent heat involved in the adsorption process (Hens 2012). In some cases, however, the simplification can be judged satisfactory.

Table 1. Moisture balance equation formulated with relative humidity and temperature as the main dependent variables

Relative humidity formulation				
Variables connections				
	$\boldsymbol{\theta_l \leftrightarrow \varphi}$		$\boldsymbol{p_c \leftrightarrow \varphi}$	
Type 1 MSC	$\theta_l = g_\varphi(\varphi)$		$p_c = f(\varphi, T) = -\rho_l R_v T\, ln(\varphi)$	
Type 3 MSC	$\theta_l = g_{\varphi,T}(\varphi, T)$			
Partial derivatives				
	$\left.\frac{\partial \boldsymbol{\theta}}{\partial \boldsymbol{\varphi}}\right\|_T$ **noted** $\boldsymbol{\xi_{\varphi\varphi}}$	$\left.\frac{\partial \boldsymbol{\theta}}{\partial \boldsymbol{T}}\right\|_\varphi$ **noted** $\boldsymbol{\xi_{\varphi T}}$	$\left.\frac{\partial \boldsymbol{p_c}}{\partial \boldsymbol{\varphi}}\right\|_T$	$\left.\frac{\partial \boldsymbol{p_c}}{\partial \boldsymbol{T}}\right\|_\varphi$
Equivalency	-	-	$= \left.\frac{\partial \boldsymbol{f(\varphi, T)}}{\partial \boldsymbol{\varphi}}\right\|_T$	$= \left.\frac{\partial \boldsymbol{f(\varphi, T)}}{\partial \boldsymbol{T}}\right\|_\varphi$
Type 1 MSC	$\frac{dg_\varphi}{d\varphi}$	*0*		
Type 3 MSC	$\left.\frac{\partial g_{\varphi,T}}{\partial \varphi}\right\|_T$	$\left.\frac{\partial g_{\varphi,T}}{\partial T}\right\|_\varphi$	$-\frac{R_v \rho_l T}{\varphi}$	$-\rho_l R_v\, ln(\varphi)$
Balance equation				
$\rho_l \xi_{\varphi\varphi} \frac{\partial \varphi}{\partial t} + \rho_l \xi_{\varphi T} \frac{\partial T}{\partial t} = \nabla \cdot \left[\left(D^l_{\varphi T} + D^v_{\varphi T} \right) \nabla T + \left(D^l_{\varphi\varphi} + D^v_{\varphi\varphi} \right) \nabla \varphi \right]$				
Secondary moisture transport functions				
Vapor transport			**Liquid transport**	
Isothermal	***Non-isothermal***		***Isothermal***	***Non-isothermal***
$D^v_{\varphi\varphi} = \delta_v p_{sat}$	$D^v_{\varphi T} = \delta_v \varphi \frac{\partial p_{sat}}{\partial T}$		$D^l_{\varphi\varphi} = \frac{K_l \rho_l R_v T}{\varphi}$	$D^l_{\varphi T} = K_l \rho_l R_v\, ln(\varphi)$

3.2.2 Vapor pressure

Table 2 shows the development of the moisture balance equation with vapor pressure as the main moisture variable. As the vapor pressure is the thermodynamic variable for vapor diffusion, only the liquid transport and storage terms have to be reformulated. The p_v-based formulation, like the φ-formulation, is more appropriate for describing envelope materials subjected mainly to hygroscopic behavior. The chosen illustration MSC types are therefore the same as for **Table 1**.

After the mathematical transformation, the thermal moisture capacity $\xi_{p_v T} = \left.\frac{\partial \theta}{\partial T}\right|_{p_v}$ consists of two distinct parts. One accounts for moisture storage dependence on temperature, the other for the variation of moisture content with temperature at constant vapor pressure because of the moisture storage equilibrium condition with relative humidity. When the temperature increases, as the saturation pressure increases collaterally, the material releases water molecules in the pore space in order to maintain the equilibrium relative humidity value. As a result, with an

MSC considered to be independent of temperature, the thermal moisture capacity does not disappear and should be expressed as:

$$\xi_{p_v T} = -\xi_{\varphi\varphi} \frac{\varphi}{p_{sat}} \frac{dp_{sat}}{dT} \tag{25}$$

A similar balance equation was proposed by Dos Santos et al. (2009), with the difference that these authors did not provide the complete mathematical developments of the different partial derivatives. Such transformations have been described by Galbraith et al. (2001), providing a detailed expression of secondary transport functions. Only a type 1 MSC, however, is used there. In Qin et al. (2009), the effect of temperature on vapor pressure equilibrium seemed to be considered erroneously in that the authors did not mention any thermal moisture capacity. Nevertheless, these authors presented an original approach for defining the thermal diffusion coefficient $D^l_{p_v T}$ as a proper material function and provided an experimental method in order to measure it.

In isothermal conditions the p_v-balance-equation is reduced to:

$$\rho_l \xi_{p_v p_v} \frac{\partial p_v}{\partial t} = \nabla \cdot \left[\left(D^l_{p_v p_v} + \delta_v \right) \nabla p_v \right] \tag{26}$$

Galbraith (1992) introduced the concept of differential permeability δ^* in order to identify the experimentally liquid and vapor transport function. He wrote:

$$\delta^*(\varphi) = \left(D^l_{p_v p_v} + \delta_v \right) = A + B\varphi^C \tag{27}$$

where A, B and C are constants determined from a set of experiments based on the gravimetric cup test. A review of other mathematical expressions for describing differential permeability is found in (Galbraith et al. 1998).

Table 2. Moisture balance equation formulated with vapor pressure and temperature as the main dependent variables

Vapor pressure formulation				
Variables connections				
	$\boldsymbol{\theta_l \leftrightarrow \varphi}$		$\boldsymbol{p_c \leftrightarrow \varphi}$	$\boldsymbol{\varphi \leftrightarrow p_v}$
Type 1 MSC	$\theta_l = g_\varphi(\varphi)$		$p_c = f(\varphi, T)$ $= -\rho_l R_v T \ln(\varphi)$	$\varphi = \frac{p_v}{p_{sat}}$
Type 3 MSC	$\theta_l = g_{\varphi,T}(\varphi, T)$			
Partial derivatives				
	$\left.\frac{\partial \boldsymbol{\theta}}{\partial \boldsymbol{p_v}}\right\vert_{\boldsymbol{T}}$ $\boldsymbol{noted\ \xi_{p_v p_v}}$	$\left.\frac{\partial \boldsymbol{\theta}}{\partial \boldsymbol{T}}\right\vert_{\boldsymbol{p_v}}$ $\boldsymbol{noted\ \xi_{p_v T}}$	$\left.\frac{\partial \boldsymbol{p_c}}{\partial \boldsymbol{p_v}}\right\vert_{\boldsymbol{T}}$	$\left.\frac{\partial \boldsymbol{p_c}}{\partial \boldsymbol{T}}\right\vert_{\boldsymbol{p_v}}$
Equivalency	$\left(\frac{\partial \boldsymbol{\theta}}{\partial \boldsymbol{\varphi}}\frac{\partial \boldsymbol{\varphi}}{\partial \boldsymbol{p_v}}\right)\Big\vert_{\boldsymbol{T}}$	$\left.\frac{\partial \boldsymbol{\theta}}{\partial \boldsymbol{\varphi}}\right\vert_{\boldsymbol{T}}\left.\frac{\partial \boldsymbol{\varphi}}{\partial \boldsymbol{T}}\right\vert_{\boldsymbol{p_v}} + \left.\frac{\partial \boldsymbol{\theta}}{\partial \boldsymbol{T}}\right\vert_{\boldsymbol{\varphi}}$	$\left(\frac{\partial \boldsymbol{p_c}}{\partial \boldsymbol{\varphi}}\frac{\partial \boldsymbol{\varphi}}{\partial \boldsymbol{p_v}}\right)\Big\vert_{\boldsymbol{T}}$	$\left.\frac{\partial \boldsymbol{p_c}}{\partial \boldsymbol{\varphi}}\right\vert_{\boldsymbol{T}}\left.\frac{\partial \boldsymbol{\varphi}}{\partial \boldsymbol{T}}\right\vert_{\boldsymbol{p_v}} + \left.\frac{\partial \boldsymbol{p_c}}{\partial \boldsymbol{T}}\right\vert_{\boldsymbol{\varphi}}$
Type 1 MSC	$\frac{\xi_{\varphi\varphi}}{p_{sat}}$	$-\xi_{\varphi\varphi}\frac{\varphi}{p_{sat}}\frac{dp_{sat}}{dT}$	$-\frac{R_v \cdot \rho_l \cdot T}{p_v}$	$= \frac{R_v \rho_l T}{p_{sat}} \cdot \frac{dp_{sat}}{dT}$
Type 3 MSC		$-\xi_{\varphi\varphi}\frac{\varphi}{p_{sat}}\frac{dp_{sat}}{dT} + \xi_{\varphi T}$		$-\rho_l R_v \ln(\varphi)$
Balance equation				
$\rho_l \xi_{p_v p_v}\frac{\partial p_v}{\partial t} + \rho_l \xi_{p_v T}\frac{\partial T}{\partial t} = \nabla \cdot \left[D^l_{p_v T}\nabla T + \left(D^l_{p_v p_v} + \delta_v\right)\nabla p_v\right]$				
Secondary moisture transport functions				
Liquid transport				
Isothermal			***Non-isothermal***	
$D^l_{p_v p_v} = \frac{K_l R_v \rho_l T}{p_v}$			$D^l_{p_v T} = K_l R_v \rho_l \left(\ln(\varphi) - \frac{T}{p_{sat}} \cdot \frac{dp_{sat}}{dT}\right)$	

3.2.3 Capillary pressure

The capillary pressure variable is particularly useful when working with capillary materials in case studies where liquid transport is the main transport mechanism. Such a p_c-formulation finds its roots in Soil Physics studies, with Milly and Eagleson (1980) being the first to reformulate the well-known Philip and de Vries equation correctly in terms of capillary pressure head. In Building Physics, capillary-based formulation is fairly unusual and is used by authors who have a particular interest in the near-saturation behavior of materials (e.g., through rain absorption/redistribution or direct soil contact). In this type of research, the hydraulic conductivity and moisture retention functions need to be properly defined in the over-hygroscopic range, which can often be achieved with a pore size distribution model.

Mathematical developments and the final balance equation in terms of temperature and capillary pressure are shown in **Table 3**. A similar balance equation was formulated by Janssen et al.

(2002), who studied the influence of soil moisture on heat losses via the ground. When considering a negligible variation of moisture storage with temperature, the following balance equation is obtained:

$$\rho_l \xi_{p_c p_c} \frac{\partial p_c}{\partial t} = \nabla \cdot \left[\left(D^v_{p_c T} \right) \nabla T + \left(-K_l + D^v_{p_c p_c} \right) \nabla p_c \right] \tag{28}$$

This expression has been reported by Häupl et al. (2003), Janssen et al. (2007) and Li et al. (2009). These models usually incorporate type 2 MSC, which is illustrated in the synthesis table.

Table 3. Moisture balance equation formulated with capillary pressure and temperature as the main dependent variables

Capillary pressure formulation				
Variables connections				
	$\boldsymbol{\theta_l \leftrightarrow p_c}$		$\boldsymbol{\varphi \leftrightarrow p_c}$	
Type 2 MSC	$\theta_l = g_p(p_c)$		$\varphi = f^{-1}(p_c, T) = \exp\left(\frac{-p_c}{\rho_l R_v T}\right)$	
Type 4 MSC	$\theta_l = g_{p,T}(p_c, T)$			
Partial derivatives				
	$\left.\frac{\partial \boldsymbol{\theta}}{\partial \boldsymbol{p_c}}\right\|_T$ $\boldsymbol{noted\ \xi_{p_c p_c}}$	$\left.\frac{\partial \boldsymbol{\theta}}{\partial \boldsymbol{T}}\right\|_{p_c}$ $\boldsymbol{noted\ \xi_{p_c T}}$	$\left.\frac{\partial \boldsymbol{\varphi}}{\partial \boldsymbol{p_c}}\right\|_T$	$\left.\frac{\partial \boldsymbol{\varphi}}{\partial \boldsymbol{T}}\right\|_{p_c}$
Equivalency	-	-	$\left.\frac{\partial \boldsymbol{f^{-1}(p_c, T)}}{\partial \boldsymbol{p_c}}\right\|_T$	$\left.\frac{\partial \boldsymbol{f^{-1}(p_c, T)}}{\partial \boldsymbol{T}}\right\|_{p_c}$
Type 2 MSC	$\frac{dg_p}{dp_c}$	*0*	$\frac{-1}{\rho_l R_v T \cdot \exp\left(\frac{p_c}{\rho_l R_v T}\right)} = -\frac{\varphi}{\rho_l R_v T}$	$\frac{p_c}{\rho_l R_v T^2 \cdot \exp\left(\frac{p_c}{\rho_l R_v T}\right)} = \frac{\varphi}{\rho_l R_v T^2}$
Type 4 MSC	$\left.\frac{\partial g_{p,T}}{\partial p_c}\right\|_T$	$\left.\frac{\partial g_{p,T}}{\partial T}\right\|_{p_c}$		
Balance equation				
$\rho_l \xi_{p_c p_c} \frac{\partial p_c}{\partial t} + \rho_l \xi_{p_c T} \frac{\partial T}{\partial t} = \nabla \cdot \left[\left(D^v_{p_c T} \right) \nabla T + \left(-K_l + D^v_{p_c p_c} \right) \nabla p_c \right]$				
Secondary moisture transport functions				
Vapor transport				
Isothermal			***Non-isothermal***	
$D^v_{p_c p_c} = -\frac{\delta_v p_v}{\rho_l R_v T}$			$D^v_{p_c T} = \delta_v \left(\varphi \frac{\partial p_{sat}}{\partial T} + \frac{p_c p_v}{\rho_l R_v T^2} \right)$	

3.3 Second strategy: moisture content formulation

Philip and de Vries (1957) and Luikov (1966) originally chose to develop moisture fluxes according to moisture content and temperature gradients. Moisture content is only an empirical quantity as it cannot be defined at the microscopic scale. Its value is discontinuous across material interfaces, making it an ‘improper’ driving force (Hens 2012). When studying

assemblies of materials at the wall scale, as is often the case in Building Physics, it is necessary to reformulate the equation using thermodynamic potentials.

Table 4 provides all the mathematical developments related to moisture balance expression, with moisture content as the main dependent variable. We chose to illustrate the case where the moisture storage function is expressed in relation to relative humidity (i.e., type 1 and 3 MSCs). The main difference with the thermodynamic variable strategy can be seen in the presence of moisture capacity terms inside the moisture diffusivity. Because the relationship between the thermodynamic variables and moisture content depends on the porous material and wetting history, this variable choice could lead to complex expressions of moisture diffusivities. If the hysteresis is taken into account, the transport functions would typically depend on the previous state.

A moisture balance equation expressed with temperature and moisture content as dependent variables is rare in Building Physics. For constitutive relationships definition, however, some authors choose a hybrid method, where liquid flux is originally expressed as dependent on the moisture content gradient and vapor flux on vapor pressure (Simonson et al. 2004). The liquid transport coefficient is then called 'liquid diffusivity', for which many authors have proposed empirical expressions (Häupl 1987; Pel 1995; Krus et al. 1999). For more information on diffusivity approaches, Scheffler (2008) provides a pertinent review. From the mathematical developments shown in **Table 4**, it appears that liquid transfer should be assumed to also be linked to temperature gradient through non-isothermal liquid diffusivity, which is equal to zero only when the MSC is independent of temperature.

In isothermal conditions, the equation further simplifies into:

$$\frac{\partial \theta}{\partial t} = \nabla \cdot \left[\left(D_{\theta\theta}^{l} + D_{\theta\theta}^{v} \right) \cdot \nabla \theta_{l} \right] \tag{29}$$

which should be related to the following, still widely used in research papers:

$$\frac{\partial \theta}{\partial t} = \nabla \cdot \left[D \cdot \nabla \theta_{l} \right] \tag{30}$$

The coefficient D $(m^2 \cdot s^{-1})$ is then referred to as 'moisture diffusivity'. In this form, the equation has the great advantage of offering an analytical solution through the Boltzmann transformation. It is worth mentioning here the work of Pel et al. (1996), who used this equation and computed the moisture diffusivity function from isothermal water absorption and drying experiments performed at the material sample scale. Such an expression is not valid when a significant temperature gradient is involved because a complex combination of phenomena can hardly be reduced to one unique transport mechanism.

Table 4. Moisture balance equation formulated with moisture content and temperature as the main dependent variables, where the moisture storage curve is linked to relative humidity

Moisture content formulation				
Variables connections				
	$\boldsymbol{\varphi \leftrightarrow \theta_l}$		$\boldsymbol{p_c \leftrightarrow \theta_l}$	
Type 1 MSC	$\theta_l = g_\varphi(\varphi)$		$\theta_l = g_\varphi\left(f^{-1}(p_c, T)\right)$	
Type 3 MSC	$\theta_l = g_{\varphi,T}(\varphi, T)$		$\theta_l = g_{\varphi,T}\left(f^{-1}(p_c, T), T\right)$	
Partial derivatives				
	$\boldsymbol{\left.\frac{\partial \varphi}{\partial \theta}\right\vert_T}$	$\boldsymbol{\left.\frac{\partial \varphi}{\partial T}\right\vert_\theta}$	$\boldsymbol{\left.\frac{\partial p_c}{\partial \theta}\right\vert_T}$	$\boldsymbol{\left.\frac{\partial p_c}{\partial T}\right\vert_\theta}$
Equivalency	$\left(\left.\frac{\partial \theta}{\partial \varphi}\right\vert_T\right)^{-1} = \frac{1}{\xi_{\varphi\varphi}}$	$-\left.\frac{\partial \varphi}{\partial \theta}\right\vert_T \cdot \left.\frac{\partial \theta}{\partial T}\right\vert_\varphi = -\frac{\xi_{\varphi T}}{\xi_{\varphi\varphi}}$	$\left.\left(\frac{\partial p_c}{\partial \varphi}\frac{\partial \varphi}{\partial \theta}\right)\right\vert_T = \left.\frac{\partial f(\varphi,T)}{\partial \varphi}\right\vert_T \frac{1}{\xi_{\varphi\varphi}}$	$-\left.\frac{\partial p_c}{\partial \theta}\right\vert_T \cdot \left.\frac{\partial \theta}{\partial T}\right\vert_\varphi = -\left.\frac{\partial f(\varphi,T)}{\partial \varphi}\right\vert_T \frac{\xi_{\varphi T}}{\xi_{\varphi\varphi}}$
Type 1 MSC	$\left(\frac{dg_\varphi}{d\varphi}\right)^{-1}$	0		
Type 3 MSC	$\left(\left.\frac{\partial g_{\varphi,T}}{\partial \varphi}\right\vert_T\right)^{-1}$	$-\left.\frac{\partial g_{\varphi,T}}{\partial T}\right\vert_\varphi \cdot \left(\left.\frac{\partial g_{\varphi,T}}{\partial \varphi}\right\vert_T\right)^{-1}$	$-\frac{R_v \rho_l T}{\varphi \xi_{\varphi\varphi}}$	$\frac{R_v \rho_l T \xi_{\varphi T}}{\varphi \xi_{\varphi\varphi}}$
Balance equation				
$\frac{\partial \theta}{\partial t} = \nabla \cdot \left[\left(D_{\theta T}^l + D_{\theta T}^v\right)\nabla T + \left(D_{\theta\theta}^l + D_{\theta\theta}^v\right)\nabla\theta\right]$				
Secondary moisture transport functions				
Vapor transport			**Liquid transport**	
Isothermal	***Non-isothermal***		***Isothermal***	***Non-isothermal***
$D_{\theta\theta}^v = \frac{\delta_v p_{sat}}{\xi_{\varphi\varphi}\rho_l}$	$D_{\theta T}^v = \frac{\delta_v}{\rho_l}\left(\varphi\frac{\partial p_{sat}}{\partial T} - \frac{\xi_{\varphi T} p_{sat}}{\xi_{\varphi\varphi}}\right)$		$D_{\theta\theta}^l = \frac{K_l R_v T}{\varphi \xi_{\varphi\varphi}}$	$D_{\theta T}^l = -\frac{K_l R_v T \xi_{\varphi T}}{\varphi \xi_{\varphi\varphi}}$

4. CONCLUSION

This paper has presented a synthesis of possible moisture balance equation formulations found in coupled heat and moisture transfer models. These tools are intended for the study of porous building materials and can cover a variety of phenomena, sometimes with the focus on the hygroscopic domain and sometimes on the capillary behavior. As a result, they differ in terms of the choice of the main dependent variable and in the levels of simplification that underlie them. All these models are, in fact, rooted in older scientific disciplines that have influenced them in various ways, (e.g., in the choice of moisture storage function expression).

The work presented began with the physically based balance equation, drawing on the REV concept. Assumptions used covered the frequent non-hysteretic and non-isothermal case without convective transfer. It is clear that the moisture balance equation can be reformulated in many ways. By developing the basic equation in terms of each moisture-related variable, including thermodynamic variables and the moisture content pseudo-variable, we provided an exhaustive list of possible final mathematical formulations. We discussed the moisture storage function in detail and proposed a general classification of models. We showed how temperature can affect thermodynamic equilibrium and how thermal moisture capacities can be expressed depending on the main variable choice. All the secondary transport functions, and their relationship to the two primary functions, i.e. the vapor diffusion coefficient and liquid conductivity, are available.

NOMENCLATURE

$\boldsymbol{D_{XT}}$	$(changing)$	Secondary transport coefficient linked to temperature gradient in the equation developed with X as the main moisture variable
$\boldsymbol{D_{XX}}$	$(changing)$	Secondary transport coefficient linked to variable X gradient in the equation developed with X as the main moisture variable
$\vec{\boldsymbol{j}}^{\boldsymbol{M_\alpha}}$	$(kg \cdot m^{-2} \cdot s^{-1})$	Total mass flux density of the α-phase
$\vec{\boldsymbol{j}}_{\boldsymbol{c}}^{\boldsymbol{M_l}}$	$(kg \cdot m^{-2} \cdot s^{-1})$	Mass flux density of liquid water through capillary transport
$\vec{\boldsymbol{j}}_{\boldsymbol{d}}^{\boldsymbol{M_v}}$	$(kg \cdot m^{-2} \cdot s^{-1})$	Mass flux density of vapor through diffusion
$\boldsymbol{K_l}$	(s)	Liquid water conductivity of the porous material
$\dot{\boldsymbol{m}}$	$(kg \cdot m^{-3} \cdot s^{-1})$	Phase change rate
$\boldsymbol{p_c}$	(Pa)	Capillary pressure
$\boldsymbol{p_{sat}}$	(Pa)	Saturation vapor pressure
$\boldsymbol{p_\alpha}$	(Pa)	Pressure of the α-phase
$\boldsymbol{q_{st}}$	$(J \cdot kg^{-1})$	Net isosteric heat
$\boldsymbol{R_v}$	$(J \cdot kg^{-1} \cdot K^{-1})$	Specific gas constant for vapor
$\boldsymbol{T}$	(K)	Temperature
$\boldsymbol{\delta_v}$	$(kg \cdot Pa^{-1} \cdot m^{-1} \cdot s^{-1})$	Vapor diffusion coefficient of the porous material
$\boldsymbol{\delta^*}$	$(kg \cdot Pa^{-1} \cdot m^{-1} \cdot s^{-1})$	Differential permeability (Galbraith 1992)
$\boldsymbol{\varepsilon}$	$(-)$	Total open porosity of the porous material
$\boldsymbol{\theta_\alpha}$	$(m^3 \cdot m^{-3})$	Volumetric fraction of the α-phase
$\boldsymbol{\xi_{XT}}$	$(m^3 \cdot m^{-3} \cdot K^{-1})$	Non-isothermal moisture capacity in the equation developed with X as the main moisture variable
$\boldsymbol{\xi_{XX}}$	$(m^3 \cdot m^{-3})$	Isothermal moisture capacity in the equation developed with X as the main moisture variable
$\boldsymbol{\rho_\alpha}$	$(kg \cdot m^{-3})$	Mass density of the α-phase
$\boldsymbol{\varphi}$	$(-)$	Relative humidity
$\boldsymbol{\psi}$	(Pa)	Suction

Subscripts

l	Related to liquid water
v	Related to water vapor
g	Related to the gaseous mixture of dry air and water vapor
a	Related to dry air

REFERENCES

Adan O. et al., 2004. Determination of liquid water transfer properties of porous building materials and development of numerical assessment methods: introduction to the EC HAMSTAD project. *J. Therm. Envel. Build. Sci.,* **27**(4), 253-260.

Bear J., 2013. Dynamics of fluids in porous media. Dover: DoverPublications.

Brunauer S., Emmett P. H. & Teller E., 1938. Adsorption of gases in multimolecular layers. *J. Am. Chem. Soc.*, **60**, 309-319.

Carmeliet J., Descamps F. & Houvenaghel G., 1999. A multiscale network model for simulating moisture transfer properties of porous media. *Transp. Porous Media*, **35**(1), 67-88.

Carmeliet J. & Roels S., 2002. Determination of the moisture capacity of porous building materials. *J. Build. Phys.*, **25**(3), 209-237.

Choi J.-G., Do D. D., Do H. D., 2001. Surface diffusion of Adsorbed molecules in porous media: monolayer, multilayer, and capillary condensation regimes. *Ind. Eng. Chem. Res.,* **40**, 4005-4031

Defay R. & Prigogine I., 1966. *Surface tension and adsorption*. London: Longmans.

Descamps F., 1997. *Continuum and discrete modelling of isothermal water and air transport in porous media.* PhD Thesis: University of Leuven, Belgium.

Delgado J. M., Barreira E., Ramos N. M. & Freitas V. P., 2013. *Hygrothermal Simulation Tools. Hygrothermal Numerical Simulation Tools Applied to Building Physics*. London: Springer.

Dos Santos G. H. & Mendes N., 2009. Combined heat, air and moisture (HAM) transfer model for porous building materials. *J. Build. Phys*., **32**(3), 203-220.

Dubois S., Evrard A. & Lebeau F., 2013. Modeling the hygrothermal behavior of biobased construction materials. *J. Build. Phys*. http://jen.sagepub.com/content/early/2013/06/12/1744259113489810.abstract (1st July 2013)

Dullien F. L., 1979. *Porous media-fluid transport and pore structure*. New York: Academic Press.

Fang L., Clausen G. & Fanger P. O., 1998. Impact of temperature and humidity on the perception of indoor air quality. *Indoor Air*, **8**(2), 80-90.

Funk M. & Wakili K.G., 2008. Driving potentials of heat and mass transport in porous building materials: a comparison between general linear, thermodynamic and micromechanical derivation schemes. *Transp. Porous Media*, **72**(3), 273-294.

Galbraith G. H., 1992. *Heat and mass transfer through porous building materials.* PhD Thesis: University of Strathclyde, Glasgow, United Kingdom.

Galbraith G. H., McLean R. C., Guo J., 1998. Moisture permeability data: mathematical presentation. *Build. Serv. Eng. Res. Technol.,* **19**(1), 31-36.

Galbraith G. H., Li J. & McLean R. C., 2001. Evaluation of discretized transport properties for numerical modelling of heat and moisture transfer in building structures. *J. Build. Phys.,* **24**(3), 240-260.

Glaser H., 1959. Grafisches verfahren zur Untersuchung von Diffusionvorgänge. *Kältetechnik,* **10**, 345-349.

Grunewald J., Häupl P. & Bomberg M., 2003. Towards an engineering model of material characteristics for input to ham transport simulations - Part 1: an approach. *J. Buil. Phys*., **26**(4), 343-366.

Hall C., 1977. Water movement in porous building materials - I. Unsaturated flow theory and its applications. *Build. Environ*., **12**(2), 117-125.

Häupl P., 1987. *Feuchtetransport in Baustoffen und Bauwerksteilen*. PhD Thesis: Technische Universität Dresden, Germany.

Häupl P. & Fechner H., 2003. Hygric material properties of porous building materials. *J. Therm. Envel. Build*. Sci.,**26**(3), 259-284.

Hens H., 2012. Building Physics - Heat, Air and Moisture: Fundamentals and engineering methods with examples and exercises. Berlin: Ernst & Sohn.

Janssen H., 2011. Thermal diffusion of water vapour in porous materials: Fact or fiction. *Int. J. Heat Mass Transf.,* **54**(7)*,* 1548-1562*.*

Janssen H., Blocken B. & Carmeliet J., 2007. Conservative modelling of the moisture and heat transfer in building components

under atmospheric excitation. *Int. J. Heat Mass Transf.*, **50**(5), 1128-1140.

Janssen H., Carmeliet J. & Hens H., 2002. The influence of soil moisture in the unsaturated zone on the heat loss from buildings via the ground. *J. Build. Phys*., **25**(4), 275-298.

Krus M. & Holm A., 1999. *Approximationsverfahren für die Bestimmung feuchtetechnischer Materialkennwerte*. http://www.hoki.ibp.fraunhofer.de/ibp/publikationen/konferenzbeitraege/pub1_15.pdf (7 May 2013)

Künzel H. M., 1995. *Simultaneous heat and moisture transport in building components*. PhD Thesis: IRB-Verlag Stuttgart, Germany.

Künzel H. M. & Kiessl K., 1996. Calculation of heat and moisture transfer in exposed building components. *Int. J. Heat Mass Transf.,* **40**(1), 159-167.

Li Q., Rao J. & Fazio P., 2009. Development of HAM tool for building envelope analysis. *Build. Environ*., **44**(5), 1065-1073.

Luikov A., 1966. Heat and mass transfer in capillary-porous colloïdal bodies. *Colloque International sur les Phénomènes de Transport avec Changement de Phase dans les Milieux poreux ou Colloïdaux, 1966, Paris, France*.

Milly P., 1988. Advances in modeling of water in the unsaturated zone. *Transp. Porous Media*, **3**(5), 491-514.

Milly P. & Christopher D., 1982. Moisture and heat transport in hysteretic, inhomogeneous porous media: A matric head-based formulation and a numerical model. *Water Resour. Res*., **18**(3), 489-498.

Milly, P. & Eagleson P. S., 1980. *The coupled transport of water and heat in a vertical soil column under atmospheric excitation*. Report: Department of Civil Engineering, Massachusetts Institute of Technology, USA.

Mudarri D. & Fisk W. J., 2007. Public health and economic impact of dampness and mold. *Indoor Air*, **17**(3), 226-235.

Nielsen D. & Biggar J., 1986. Water flow and solute transport processes in the unsaturated zone. *Water Resour. Res*., **22**(9), 89-108.

Osanyintola O. F. & Simonson C. J., 2006. Moisture buffering capacity of hygroscopic building materials: Experimental facilities and energy impact. *Energy Build*., **38**(10), 1270-1282.

Oswin C., 1946. The kinetics of package life. III. The isotherm. *J. Soc. Chem. Ind*., **65**(12), 419-421.

Padfield, T. (1998). The role of absorbent building materials in moderating changes of relative humidity. Department of Structural Engineering and Materials, Lyngby, Technical University of Denmark **150**.

Pel L., 1995. *Moisture transport in building materials*. PhD Thesis: Technische Universiteit Eindhoven, The Netherlands.

Pel L., Kopinga K. & Brocken H., 1996. Moisture transport in porous building materials. *HERON*, **41**(2), 95-105.

Philip J. & De Vries D., 1957. Moisture movement in porous materials under temperature gradients. *Trans. Am. Geophys. Union*, **38**, 222-232.

Poyet S. & Charles S., 2009. Temperature dependence of the sorption isotherms of cement-based materials: Heat of sorption and Clausius–Clapeyron formula. *Cem. Concr. Res*., **39**(11), 1060-1067.

Qin M., Belarbi R. & Ait-Mokhtar A., 2009. Coupled heat and moisture transfer in multi-layer building materials. *Constr. Build. Mat*., **23**(2), 967-975.

Rode C. (1990). *Combined heat and moisture transfer in building constructions*. PhD Thesis: Technical University of Denmark, Lyngby, Denmark.

Rode C. & Clorius C. O., 2004. Modeling of moisture transport in wood with hysteresis and temperature-dependent sorption characteristics. *Proceedings of Buildings IX, 2004, Clearwater, Florida*.

Roels S., Depraetere W., Carmeliet J. & Hens H., 1999. Simulating non-isothermal water vapour transfer: an experimental validation on multi-layered building components. *J. Build. Phys*., **23**(1), 17-40.

Salonvaara M. et al., 2004. Moisture buffering effects on indoor air quality-experimental and simulation results. *Proceedings of Buildings IX, 2004, Clearwater, Florida*.

Sheffler G. A., 2008. *Validation of hygrothermal material modelling under consideration of the hysteresis of moisture storage.* PhD thesis: Dresden University of Technology, Germany.

Sherwood T., 1929. The drying of solids – I. *Ind. Eng. Chem*., **21**(1), 12-16.

Simonson C. J., Salaonvaara M. & Ojanen T., 2004. Heat and mass transfer between indoor air and a permeable and hygroscopic building envelope: part II– verification and numerical studies. *J. Therm. Envel. Build. Sci.*, **28**(2), 161-185.

Tariku F., Kumaran K. & Fazio P., 2010. Transient model for coupled heat, air and moisture transfer through multilayered porous media. *Int. J. Heat Mass Transf*., **53**(15), 3035-3044.

Toftum J. & Fanger P., 1999. *Air humidity requirements for human comfort*. PhD Thesis: Technical University of Denmark, Denmark.

Uhlhorn R. J. R., 1990. *Ceramic membranes for gas separation: synthesis and transport properties.* PhD thesis: Universiteit Twente, Enschede, The Netherlands.

Van Der Kooi J., 1971. *Moisture transport in cellular concrete roofs*. PhD Thesis: Technische Hogeschool, Eindhoven, The Netherlands.

Van Genuchten M. T., 1980. A closed-form equation for predicting the hydraulic conductivity of unsaturated soils. *Soil Sci. Soc. Am. J.,* **44**(5), 892-898.

Whitaker S., 1977. A Theory of drying. *Adv. Heat Tranf*., **13**, 119-203.

CHAPTER 3

Measuring crop-based materials properties

3.1 Introduction

In **Chapter 2**, the materials properties required to simulate the hygrothermal behaviour of a porous material were described. There are the heat and moisture storage properties (moisture capacities, specific heat) and the primary transport properties (vapour permeability, liquid conductivity, and thermal conductivity). Those can possibly be combined to form secondary transport properties. Often, the term *material function* is used to account for the dependence of the hygrothermal properties on temperature and moisture content. Empirical or physically based models can be used to describe those functions in which case some parameters need to be determined. These models offer a continuous expression of the transfer properties and allow a better interpolation of properties between the local points that are measurable experimentally. For products showing a high moisture storage capacity, like CBM, the effect of moisture content on the transport functions needs to be investigated with attention. However, depending on the modelling case study, some properties can often be simplified into single constant values as shown in **Chapter 4**.

An important experimental task bound to the modelling procedure is to assign values to material properties, or to parameters used to describe these properties with some mathematical functions. Most of the time, measurements are gathered in steady-state conditions with well defined experimental protocols transcribed into international and national standards. In the next chapter, such steady-state properties taken from

literature are used to simulate the behaviour of a LHC bloc, which results in a good simulation efficiency. As BEHAM models rely on the local thermodynamics equilibrium assumption (Baggio et al., 1997), these steady-state properties are assumed to be representative of the material behaviour in transient conditions.

In comparison to widespread and industrialized construction materials, e.g. extruded polystyrene, manufactured bricks, plywood, etc., some CBM are difficult to characterize with standard experimental techniques or show some product variability that stands against a precise consensus on standard properties values. This chapter deals with some challenges encountered when measuring properties of crop-based materials, with emphasis on typical CBM used in light structural applications (see **Chapter 1**). First a brief overview of the most standard techniques for hygrothermal properties evaluation is provided. In a synthetic way, each class of material property is studied with the applicability of standard characterization methods to LHC and straw bales materials. Straw bales are typically characterized by large dimensions, an un-cohesive nature and anisotropy in hygrothermal properties due to main fibres orientation. It causes particular issues in the properties evaluation task whereas LHC is more compliant with standard methods. The appended paper shows how to overcome some limitations of standard techniques in the context of straw bales properties assessment. More specifically, it deals with the development of a prototype apparatus for thermal conductivity measurement on high thickness materials. This work is presented as an illustration of the heavy experimental effort that is associated with the determination of materials properties, an essential input in BEHAM models, with additional challenges for some CBM. In **Chapter 5**, a numerical method is presented to estimate materials properties through inverse modelling. This technique offers a valuable alternative to the application of standard experimental methods for the characterization of construction materials, which can require important experimental efforts.

3.2 Porous matrix morphology

3.2.1 Pore size distribution

Knowing the actual solid matrix morphology of the material is not strictly needed in order to solve heat and moisture transfer problems. As we showed in **Chapter 2**, the REV concept (Bear, 1988) allows to average the micro-physical phenomena and reduce the description complexity. However, experimental methods that give access to the pore size distribution of the material can provide useful information to interpret the behaviour of the material or underlying properties, which necessarily results from its microscopic structure. Additionally, such data can serve as a basis to calibrate pore space models, which translate the complexity of the inner structure into simplified representations and generally allow inferring material storage and transport functions. Such pore space models can be divided into bundle of tubes models and network models. A good review of such approaches can be found in (Scheffler, 2008).

Several pore filling/emptying techniques exist to characterize the pore size distribution and total pore volume of materials. Usually, only the open porosity can be decribed. These methods include the extrusion porometry, the intrusion porometry and gas adsorption (Jena and Gupta 2002). They are all based on surface tension and pressure relationship to extrapolate information about internal structure. The most frequently used technique is *Mercury Intrusion Porometry* (MIP), a method originally conceived by Washburn (Washburn, 1921) and applied later by Ritter and Drake (1945), and many others. MIP analysis results for LHC can be found in (Collet, 2004; Collet et al., 2008) but such measurements have not yet been reported for raw vegetal stem. Each technique provides slightly different information and requires specific precautions in the interpretation of results. For example, several issues are associated with MIP: the ink-bottle effect (Moro and Böhni, 2002), the presence of residual water, and the chosen value for the contact angle between the mercury and the pores walls. The assumed integrity of internal porous structure subject to the high level of imposed pressure is also questionable (Landry, 2005).

The thermoporometry offers an alternative to the widespread techniques based on

pore filling theory. It relies on the analysis of liquid-solid phase transformations in the porous space knowing that the surface curvature of the water meniscus in a pore influences the phase transition free energy (Brun et al., 1977; Landry, 2005). Although promising, this relatively new technique requires a complex calibration (Landry, 2005). So far, CBM have not been studied intensively with this technique.

In complement, image analysis tools can also provide useful qualitative and quantitative information concerning the internal structure of the material at microscopic level, taking benefits of recent improvements in high resolution microscopy and tomography techniques. It is always useful in determining the relationships between the measured structural parameters and the real configuration and characteristics of pores in the material.

3.2.2 Dry density

The only physical property linked to porous matrix morphology which is strictly needed to solve the REV balance equations is the dry density of the material. The density is the weight of $1m^3$ of material. The term 'dry' is a standardized concept, characterizing materials dried at 105°C until the decrease in weight between two successive daily measurements remains below 1% relatively to the initial weight (IEA, 1991). The main difficulty for CBM is sometimes to determine the volume of the tested sample. Whereas some CBM allow to be easily divided into smaller samples of known volumes, like LHC (Evrard, 2008), for oversized, irregularly shaped and hardly divisible materials, like straw bales, it is more difficult to get a standardized and repeatable measurement.

3.3 Moisture transfer properties

3.3.1 Moisture storage curves

The moisture storage curve of the materials, defined precisely in **Chapter 2**, can be divided into two main regions. In the hygroscopic region, where capillary condensation does not play a major role, the moisture storage curve is referred to as

the sorption isotherm (see **Chapter 1**). The measuring principle consists in bringing dry samples (adsorption isotherms), or humid samples (desorption isotherms), in equilibrium with an atmosphere controlled in temperature and relative humidity and measure the equilibrium weight. The most frequent methods used to control the RH precisely are the salt solutions method (also referred to as dessicator method) and the climatic chamber method. Both methods are normalized in ISO 12571 (2000). Alternatively, automated gravimetric devices, called *Dynamic Vapour Sorption* (DVS) apparatus, provide an efficient way to determine sorption and desorption isotherms with chosen RH steps without sample manipulation during the test. However, such apparatus require small test samples, which in the context of CBM study can cause representativeness issues. In constrast, the two 'traditional' measurement techniques are not difficult to apply to CBM because they do not impose much restriction on test specimen. Sorption isotherms of LHC can be found in various recent works (Evrard, 2008; Collet et al., 2013; Samri, 2008). For straw bales, the first measurements were performed by Hedlin (1967) for frequent crops; such measurements were repeated later in various works (JTI, 1985; Duggal and Muir, 1981; Nilsson et al., 2005)

The moisture storage in the overhygroscopic water region (generally above 95%RH), referred to as moisture retention curve, is impossible to determine with the methods dedicated to sorption isotherm characterization. This is caused by difficulties in artificially maintaining a constant high RH. In soil study, where the high moisture content region is of primary importance, the moisture retention curve is characterized with the pressure plate apparatus, a method that is normalized in ASTM C1699 (2009). In Building Physics, due to a lower interest in the nearly saturated condition, the pressure plate is not very common. However, Evrard (2008) used such a method for LHC characterization. The straw material is not compatible with the experimental set-up that requires a good planarity of the test specimen. In consequence, other techniques would have to be considered if the moisture retention curve of straw bales has to be determined.

3.3.2 Vapour and liquid transport functions

In conditions where both phenomena are of equal importance, evaluating vapour and liquid flows separately is almost impossible. In consequence, the vapour permeability

and liquid conductivity functions are only precisely measurable on either dry or saturated samples, where one mechanism completely overcomes the other. The widespread experimental method used to measure the material resistance to vapour transport in dry conditions is called the 'dry cup' method. The principle of this method involves placing a sample between two atmospheres with controlled RH. Silica gel is placed in a cup that is sealed with the material sample, which causes a dry atmosphere inside the recipient. The cup is then placed in an isothermal atmosphere controlled at 50%RH. The gradient of vapour pressure which is created in this way induces a vapour flow across the sample. After a transient phase where the sample equilibrates with surrounding conditions, the steady-state transfer is reached. The constant vapour flux across the material layer is then easily measured with a scale, and the vapour permeability is assessed on the basis of the sample thickness. This method is frequently used for the characterization of construction products and is normalized in ISO 12572 (2001). However, it requires to work on cohesive samples like LHC (Evrard, 2008; Collet et al., 2013). When operating on non-cohesive materials such as straw, it is necessary to adjust the experimental device (Hansen et al., 2001, see). The saturated liquid conductivity, *i.e.* the liquid conductivity when all pores of the materials are filled with water, can be experimentally assessed based on the Darcy's Law with techniques common in soil studies (ASTM, 2006, 2011b, 2003).

Between the dry and the saturated states, the vapour permeability and liquid conductivity show a complex evolution with moisture content which depends on the characteristics of the porous matrix. This dependence on moisture content is a key issue in material modelling. Again, in the current state-of-the-art, it is impossible to isolate liquid and vapour flows in that moisture content range. In consequence, the evaluation of vapour permeability and liquid conductivity separately is tricky and the most frequent approach is to evaluate secondary transport coefficients, which combine the two functions in a single property (see **Chapter 2**). In that context, the 'wet cup' method is often used to gather the steady-state moisture transfer at several averaged RH in the sample, in isothermal conditions. Such an approach is illustrated for LHC in (Collet et al., 2013). The non-cohesive nature of straw bales imposes to choose another experimental protocol or transient approaches, like dynamic moisture profiles measurement.

3.4 Heat transfer properties

3.4.1 Dry thermal capacity

The dry thermal capacity is the heat needed to change the temperature of 1kg of dry material with $1°C$. The most common method used to evaluate this property is the differential scanning calorimetry. The method is normalized in ISO 11357-4 (2013) and ASTM E1269 (2011a). A more accessible method consists in performing thermodifferential analysis with an adiabatic can. The method is illustrated in Evrard's Thesis (2008) for LHC samples.

3.4.2 Thermal conductivity

Due to the need for building energy performance assessment and the concomitant emergence of BES models, the steady-state thermal conductivity measurement methods have been widely normalized in the past two decades. The *Guarded Hot Plate* (GHP) method, normalized in ISO 8302 (1991b), aims to reproduce a heat flux density across a material sample which is unidirectional, uniform in space and constant in time. In addition, it is an absolute method which means that the device does not require to be calibrated with known samples. In contrast, the heat flow meter method, described in ISO 8301 (1991a), provides relative measurements and need a precise calibration. Beside steady-state methods, transient measurement methods offer better perspective for evaluating the thermal conductivity with humid samples. The goal of this section is not to give a complete overview of available techniques with their advantages and drawbacks. Such analysis can be found in (De Ponte and Klarsfeld, 2002).

The LHC material is compliant with standard methods as shown in (Evrard, 2008; Collet, 2004). The thermal conductivity measurement of straw bales, with the associated challenges, is widely discussed in the appended paper.

3.5 Appended paper

Design, Construction and Validation of a Guarded Hot Plate Apparatus for Thermal Conductivity Measurement of High Thickness Crop-Based Specimens

Samuel DUBOIS*[1], Frédéric LEBEAU[1]

[1]Dept. STE, Gembloux Agro-Bio Tech, University of Liege, Belgium

*Corresponding author, supported by a F.R.I.A Grant,
Address: Dept. of environmental sciences and technologies, Gembloux Agro-Bio Tech, 2 Passage des déportés, 5030 Gembloux, Belgium (s.dubois@doct.ulg.ac.be)

KEYWORDS

Thermal Conductivity, Guarded Hot Plate, Crop-based materials, Straw bale

STATUS

Published in:

Materials and structures, 2013

ABSTRACT

The search for sustainability achievement in the building sector led to the use of crop-based insulation materials. Among these, raw products like plant straws bales can present elementary representative volumes (REVs) in the size order of several square centimeters. Fibers orientation may play an important role on material thermal behavior. Measuring their thermal conductivities with standard steady-state equipment can thus lead to some inaccuracies due to the necessity of resetting lower thickness samples. This paper presents a Guarded Hot Plate (GHP) apparatus designed to test high thickness samples, up to 40cm, with an accuracy of 2%. The different parts of the machine are described in details along with design process and challenges encountered. Temperature and heat flux measurements in the device represent critical design stages where optimal accuracy is needed in order to optimize the resulting global error. Regarding this, necessary numerical and experimental analyzes were conducted emphasizing on intrinsic systematic error assessment. To complete the study, some validations tests are performed on a reference material and other widely-spread polystyrene slabs. These tests take into account the optimal computation parameters resulting from the numerical analysis and the apparatus proved to be in accordance with accuracy requirements.

1. INTRODUCTION

The determination of the thermal conductivity of building materials is fundamental for solving problems related to building performance and user comfort. A variety of organic insulation products have been recently promoted for their sustainability, which includes crop-based materials [1, 2]. Among these some require a great thickness of implementation, either because their very nature requires it, like for straw bales construction [3-5], or to compensate for their lower thermal conductivity relatively to high performance inorganic insulation materials. There are many methods for measuring the thermal conductivity of materials, both in steady state and transient conditions. The stationary methods such as the so-called 'guarded hot plate technique' require thermal equilibrium and thus a significant measurement time. The boundary conditions imposed on the sample need also to be controlled precisely. However, if these boundary conditions are met, the results obtained by these methods are often very accurate [6]. The transient methods provide generally faster results and can be used on smaller samples but at the cost of lower accuracy.

The work presented here was directed towards the conception of an apparatus for thermal conductivity measurement in steady state, capable of performing over a wide range of thickness. More specifically it's expected to provide reliable results on an entire straw bale. This would be particularly useful to assess the effect of actual straws particles orientation in the bale on final thermal conductivity. This information might be particularly relevant for producers targeting the construction sector.

Much research has already been conducted on the thermal conductivity of straw bales. The effect of the direction of heat flow relatively to fibers orientation has already been highlighted [7-9]. It is accepted that the more the flow is parallel to the fibers, the greater the thermal conductivity. It is important to note however that most of available data drives either from transient methods [10], from steady-state methods performed on lower thickness re-built bales [11] or from compressed loose material [12, 13]. Absolute thermal conductivity measurements on an entire two-wired straw bale are thus still missing. The rearrangement of the samples often observed in literature for steady-state measurement is required by the low thickness generally imposed by commercial guarded-hot plate or heat flow meter apparatus. As the straw particle length can generally extend to 50cm [14], resetting lower thickness samples from original bale could lead to changes in structure the impact of which is hard to quantify.

The guarded hot plate prototype presented here allows measurements on thick specimens and offers the possibility to assess the thermal conductivity of non-altered straw bales samples. The approach is thus complementary to existing data. It offers the possibility of direct and easy comparison of bales from different origins or manufacturing. The original device is described in this paper along with particular design details and challenges encountered. Its performance will be assessed by performing the necessary numerical and experimental tests.

2. GUARDED HOT PLATE METHOD

2.1 General principle

The guarded hot plate (GHP) apparatus is traditionally recognized as the only absolute method for thermal conductivity measurement in steady-state of homogeneous materials able to achieve a global measurement uncertainty below 2% [6]. Its principle is to reproduce the uniform, unidirectional and constant thermal flux density existing through an infinite homogeneous slab-shaped specimen caught between two infinite isothermal planes. The method is defined in an international standard under the designation 'Thermal insulation - Determination of steady-state thermal resistance and related properties - Guarded hot plate apparatus' [15].

The device developed in this research is based on the 'single specimen apparatus' (**Fig. 1**). Their principle is the following: the analyzed specimen is sandwiched between an electrically-heated hot plate maintained at temperature T_h and a cold plate maintained at a lower temperature T_c. The heat dissipated by the Joule effect in the hot plate would travel to the cold plate through the sample, but also backwards and laterally on the edges of the hot plate. Back and lateral 'guard zones' are then necessary to neutralize these leaks. By maintaining the different guard zones at the same temperature T_h with precise control, all unwanted thermal transfers are indeed canceled. The hot plate is thus separated in two parts: a heater zone (or measurement zone) of known area and heated electrically and an adjacent guard ring heated with a different circuit. A small gap separates the two zones and a thermopile is often used to control the temperature difference between these. The back face of the hot plate is provided with an additional guard plate with identical dimensions providing protection from backwards thermal fluxes. This back guard plate also has its own heating system and is associated with appropriate temperature differential control as in lateral gap.

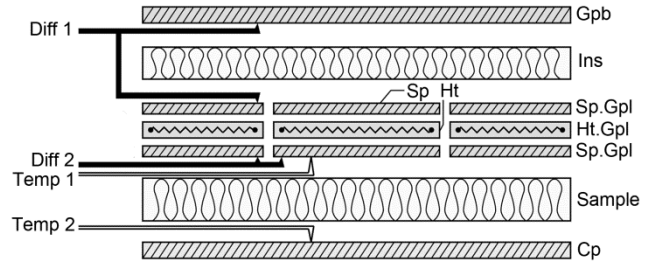

Cp : Cold plate
Diff 1 : Imbalance sensing element 1
Diff 2 : Imbalance sensing element 2
Gpb : Back guard plate
Ht : Measurement zone heating element
Ht.Gpl : Lateral guard heatin element
Ins : Thermal insulation
Sp : Measurement zone surface plate
Sp.Gpl : Lateral guard surface plate
Temp 1 : Temperature sensor 1
Temp 2 : Temperature sensor 2

Fig. 1. Single specimen GHP

When working well, with all three elements at exactly the same temperature T_h, the heat produced in the measurement plate will flow unidirectionally towards the cold plate. All the

others heat fluxes are supposed to be eliminated. With such device, the thermal conductivity is obtained by the one-dimensional Fourier equation:

$$\lambda = \frac{\Phi e}{A(T_h - T_c)} \tag{1}$$

Where Φ (W) is the heat flow-rate that in an ideal unidirectional condition would traverse the specimen through an area A (m^2) called measurement area. The variable e (m) is the thickness of the specimen. It's important to notice that the thermal flux Φ is equal to the electric power injected in the heater plate only if the instrument is perfect. For low thicknesses of samples the measurement area is considered approaching the surface bounded by the edge of the measurement plate. When using thick samples this area tends to the surface delimited by the line passing through the center of the gap. Generally the thermal conductivity value deduced is related to the average temperature of the tests T_m (**Equation 2**).

$$T_m = (T_h + T_c) / 2 \tag{2}$$

2.2 Chosen measurement approach

Figure 2 shows the schematic diagram of the GHP prototype presented here and highlights the differences in measurement strategy in comparison to a typical single specimen apparatus (**Fig. 1**). We will used what is referred as a 'hybrid method' [16] to obtain the heat flux Φ crossing the specimen, similarly to the device developed in [17]. The lateral and back guard plates are combined into a single massive metallic piece, called simply the guard (or hot) plate, and circulating water passing through tubes and thermal diffusers is used to maintain it at the temperature T_h. The measurement plate is incorporated in the center of this guard plate and electrically-heated. A heat flux meter (HFM) is sandwiched between the unique guard plate and the heater and allows to control precisely the temperature difference between the two pieces. **Figure 3** presents more precisely the principle of the hybrid method with the different heat fluxes involved.

At steady state the heat balance on the heater plate gives:

$$P_e = \Phi + \underbrace{\Phi_{gb} + \sum_{i=1}^{4} \Phi_{gl,i} + \sum_{i=1}^{4} \Phi_{edge,i}}_{\text{Parasite heat fluxes}} \tag{3}$$

$$P_e = \Phi + \Phi' \tag{4}$$

Where P_e is the electric power dissipated in the electric resistive circuit, Φ is the heat flux actually passing through the sample, $\sum_{i=1}^{4} \Phi_{gl,i}$ the heat flow passing to the guard plate laterally through the gap, Φ_{gb} the back heat flux going to the guard plate through the HFM and

$\sum_{i=1}^{4} \Phi_{edge,i}$ the edge loss, i.e. the heat produced by the heater that derives from the ideal vertical flow orientation and leave the sample through its edges. All these 'leak' fluxes depend on the temperature difference between the guard plate and the heater plate as well as the temperature of the edge of the sample during the test. When the temperature is the same in the guard and measurement plate and the edge of the sample is well insulated or far enough from the heater plate, it can be assumed that all the electrical power dissipated in the heater flows vertically through the sample, i.e. $P_e \cong \Phi$. In appropriate designs, Φ' is typically less than 0.5% of Φ [15].

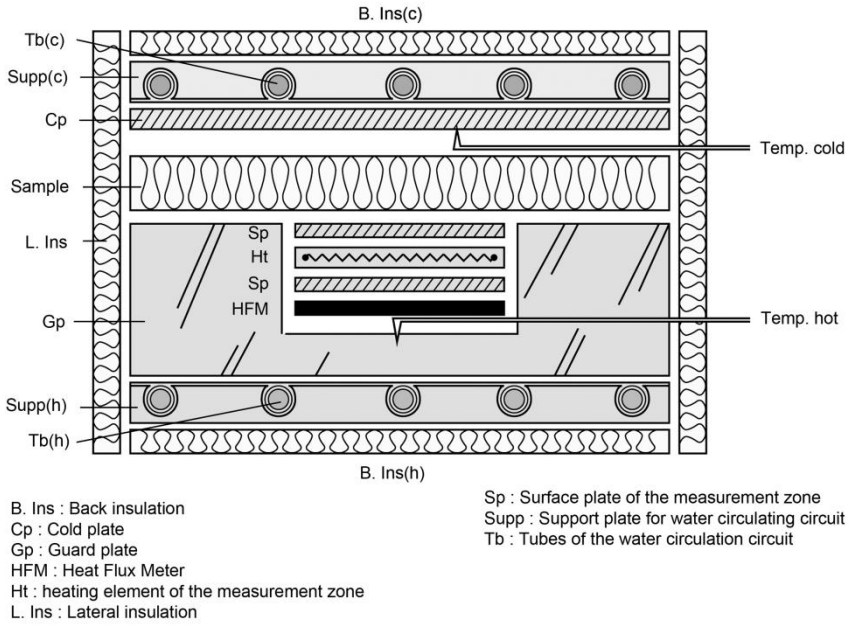

Fig. 2. Measurement principle

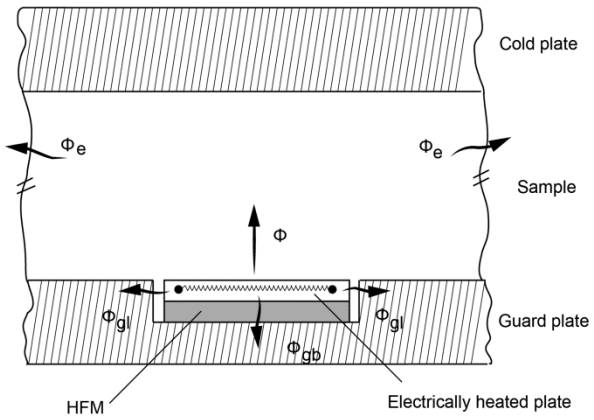

Fig. 3. The hybrid method and associates heater fluxes

3. OVERVIEW OF THE GHP APPARATUS

3.1 General specifications

The conception of the GHP presented in this research was made in accordance with ISO 8302 recommendations [15], in order to guarantee an accuracy of 2% for mean test temperature around the ambient temperature and a repeatability of 0.5% with two successive measurements on the same sample. The proposed final design for the apparatus is shown on **Figure 4** which gives a general section view. The slab square-shaped specimen with thickness e is placed between a hot plate assembly and an upper cold plate assembly, mounted horizontally on a support frame. A rail system allows to displace the cold plate assembly vertically, to adjust the GHP to the thickness of the sample. On its lateral faces, the sample is surrounded by lateral (or edge) insulation.

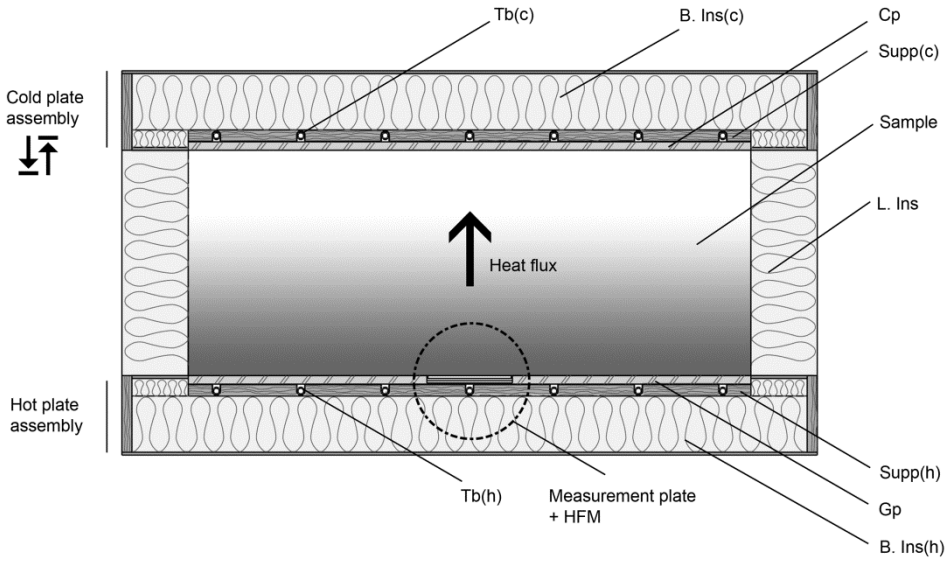

Fig. 4. Proposed design for the GHP apparatus

Table 1 shows the general performance specifications of the GHP apparatus, presented similarly to [18]. The GHP device was designed to measure thermal conductivity on building construction materials with thermal resistance ranging from 0.1 to 15 $m^2 \cdot K \cdot W^{-1}$. In practice, the principal limitation is the maximum power that the heater plate is able to give, i.e. 1 W. For a temperature difference of 10°C between the hot and cold plate, the thermal resistance of the specimen is limited in the lower range to 0.225 $m^2 \cdot K \cdot W^{-1}$. In parallel, the thermal resistance is limited in the upper range by the noise level of the acquisition system for the heater dissipated power. Small temperature difference between the hot and cold plate induces small power dissipation in the heater plate. The limit is thus fixed as before by the acquisition system. Two circulating baths are controlled independently in temperature to maintain the guard plate and the cold plate respectively at the temperature T_h and T_c . The upper limit of temperature difference

is fixed by the power capacity of these circuits. It should be noted that most of the tests will be conducted with a temperature difference of 10 or 20°C, as they will be performed on insulation materials.

In order to test materials with thickness up to 400mm with acceptable edge heat loss errors the guard area was extended to 425mm laterally all around the measurement plate. The lower limit of the samples thickness is fixed to ten times the size of the gap, i.e. 20mm.

Table 1. General specifications

Parameter	Value		Comment
	Minimum	Maximum	
Operational mode	1 sided		
Orientation	Vertical heat flow		Upward heat flow
Specimen			
○ Conductivity ($mW \cdot m^{-1} \cdot K^{-1}$)	0.03	0.2	
○ Thickness (m)	0.02	0.40	
○ Thermal resistance ($m^2 \cdot K \cdot W^{-1}$)	0.1	15	
Test conditions			
○ Ambient temperature ($°C$)	~20		
○ Hot plate temperature ($°C$)	15	35	
○ Heater plate max power (W)	1		
○ Hot water circuit power (W)	300		
○ Cold plate temperature ($°C$)	5	20	
○ Cold water circuit power (W)	~90W (at 20°C)		
○ Temperature difference ($°C$)	5	30	
Hot plate			
1. Total dimensions (mm)	1000 x 1000 x 15		Square form
2. Heater plate dimensions (mm)	150 x 150 x 3.6		Square form. Real dimensions
3. Gap wide (mm)	2		Mid gap area = 152 x 152 mm
4. Gap area/Measurement plate area (%)	2.7		

3.2 Cold and hot plates assemblies

The hot plate assembly is based on a square aluminum plate with dimensions 1000x1000x15mm giving the necessary width to limit the edge loss error. Aluminum was chosen for its high thermal conductivity and the alloy (6082 T651) for milling workability. A square recess cut with a side of 154mm and depth of 10mm is made in the center of the aluminum plate to host the measurement plate. The cold plate assembly is almost identical, except that there is no measurement bloc and its thickness is limited to 5mm. In both plates assemblies, water circulating channels are used to maintain the isothermal conditions of plates. Each circulating circuit is connected to an independent thermostatic bath through a low discharge pump. The

temperature of the baths is controlled over a temperature range of 5-40°C using Proportional-Integral (PI) regulation with the temperature of the linked plate as feedback. In fact, the PI controller acts on heating elements immersed in the bath that balance the continuous cooling effect of a compressor chiller. Water circulates then through plastic tubes that show a serpentine shape with 7 crossings spaced by 150mm. Tightly attached to them come linear aluminum thermal diffusers that are in direct contact with the main metal plates. The system composed by the tube and the diffusers is supported by a specific wood particle board. The validity of the system in terms of temperature homogeneity at the surfaces of the plates will be assessed by implementation of several temperature sensors at different locations in the plates.

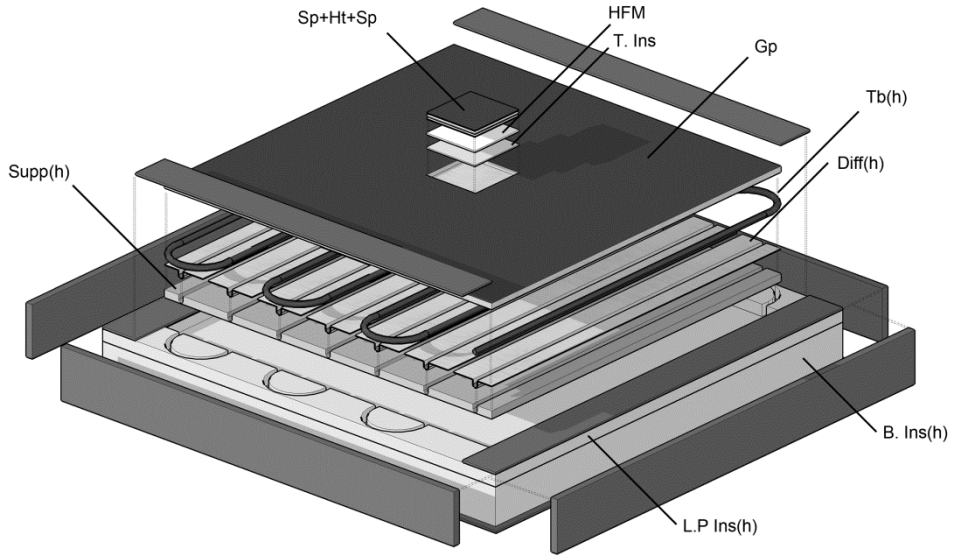

B. Ins(h) : Back insulation of the guard plate (XPS, 1200 x 1200 mm)
Diff(h) : Thermal diffusers (Aluminum fins)
Gp : Guard plate
HFM : Heat Flux Meter (Serial thermoelectric elements)
L.P. Ins(h) : Lateral insulation of the guard plate (XPS)
Sp+Ht+Sp : The heater plate composed of Heater circuit board and 2 surface plates
Supp(h) : Support of the water circuit (Particle board)
Tb(h) : Water circuit tube
T. Ins : Thin thermal insulation

Fig. 5. Hot plate assembly

Figure 5 shows a detailed isometric view of the hot plate assembly, with the central measurement plate, the large guard plate, the water circulating circuit and a case with back and lateral thermal insulation.

3.3 Temperature measurement

3.3.1 Temperature sensors

In order to obtain the thermal conductivity data of the tested material, it is necessary to measure accurately the temperature at different locations, and most particularly at the surface of the plate on either side of the specimen. Most guarded hot plates use thermocouples at this purpose. Here

DS18b20 (*Dallas*) numeric sensors are used instead. They convert temperature in 12-bit mode which offers a resolution of 0.0625°C. In order to obtain the necessary accuracy, 18 sensors (named T1 to T18) are properly calibrated using a certified thermometer (*Testo* 950 with sensor 06280016) and a thermally controlled stirred liquid bath (*Haake* C40 with F8 circulator). The sensors are mounted on an electrical plate and are placed in de-ionized water in the bath together with the tip of the reference thermometer. The digital sensors calibration is done at 7 temperature plateaus, from 10 to 40°C with 5°C steps. For each temperature plateau, the water bath was kept at a constant temperature for at least 15 minutes with a thermal precision of 0.01°C. The sampling rate and duration of the sensors measurement are fixed respectively to 10 seconds and 10 minutes, giving a total of 60 measurements per plateau. It was observed to the standard deviation of these measurements is typically less than the resolution of the sensors, which can be considered in consequence the main precision error of our numeric temperature sensors.

The reference thermometer shows a precision of 0.021°C. Its bias error was given at 3 temperature points by a calibration certificate. **Figure 6** shows the bias error regression on the interest zone, which will be used to correct measured data. At each calibration temperature, the true temperature value is given by the average of the reference thermometer readings, corrected by the bias error regression. This true value is then compared to the average of the DS18b20 measurements. Their bias is always less than 0.1°C and properly taken into account in the forms of individual correction formulas based on linear regressions.

Once calibrated, the nine chosen temperature sensors are implemented in the cold and guard plates to monitor the temperature at different locations (**Fig. 7**). Sensors T5, T6 and T7 are used to determine the hot side temperature whereas sensor T12 gives the cold side temperature. The other sensors are complementary and will give information about the temperature homogeneity of the plates and eventually to detect fault behavior. Their placement was chosen after completing some numerical thermal simulations. To implement the different sensors, holes with 4.8mm diameter were drilled to within 2mm of the front surface of the plates (13mm deep) for all sensors except T6 and T7. For these last two sensors, additional holes were drilled in the center of the plate to 1mm of the surface. Finally, additional recess tracks are made to host the leads of the different sensors, so that they come in close contact to the plates, in order to minimize thermal conduction from ambient temperature.

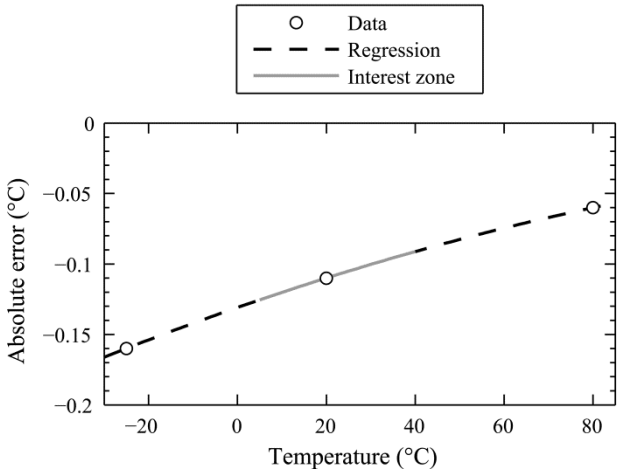

Fig. 6. Absolute error of the reference thermometer

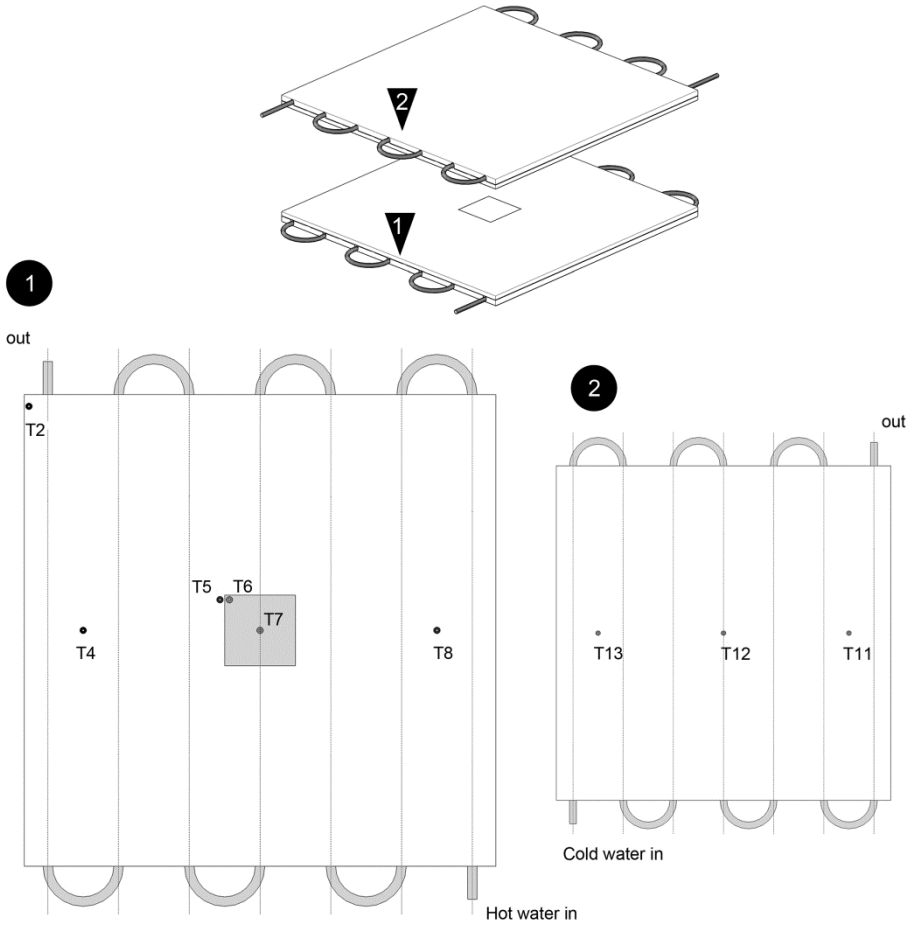

Fig. 7. Temperature sensors location

3.3.2 Temperature stability and homogeneity

In order to test temperature homogeneity and stability of the plates an experimental study was performed. The water circuits of the GHP were turned on with a 5cm polystyrene slab between the two plates and the different sensors were continuously monitored. The cold plate temperature was set to 5°C and the hot plate to 15°C, which will be the most frequent test temperatures. There is first the stabilization phase, where plates slowly approach their respective temperature threshold, followed by the steady-state phase. During the test, the room temperature is kept at 20°C, to simulate non-ideal test conditions.

Table 2 shows the average temperature and its standard deviation for all nine implemented sensors during one hour in steady state conditions. With these test conditions, the stability and homogeneity of the hot plate temperature stays below the recommended 0.2°C [9]. This criterion represents actually 2% of the temperature difference between hot and cold plate. For the cold plate, it seems that the apparatus homogeneity is barely respected, with temperature at the center of the plate (T12) a bit lower than on its side (T11 and T13). It can be explained by the position of the central sensor, which lies just under the water circulating tube. **Figure 8** shows the temperatures of T4, T7 and T8 for 10 minutes in steady state conditions as illustration purposes. The numeric nature of the sensors can be clearly seen by the specific jumps of temperature readings.

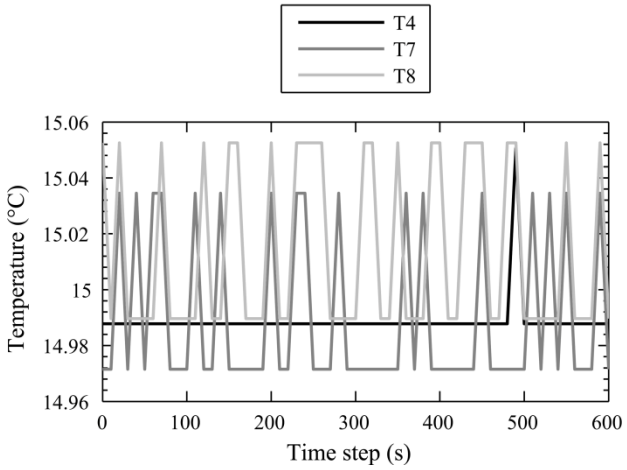

Fig. 8. Hot plate temperature distribution in steady-state

Table 2. Temperature readings during steady-state

Sensor	Average temperature ($°C$)	Standard deviation ($°C$)
T2	15.03	<E-5
T4	14.99	9.3E-3
T5	15.00	3.2E-2
T6	14.97	4.7E-3
T7	14.99	3.0E-2
T8	15.01	3.0E-2
T11	5.04	2.4E-2
T12	4.91	3.3E-3
T13	5.09	3.2E-2

3.4 Measuring the heat flow-rate through the specimen

3.4.1 Measurement plate

The measurement plate is formed of several layers. The heating part strictly speaking is a printed circuit board with dimensions 150x150mm and 1.6mm thick. It consists of a layer of glass fibers sandwiched between two thin 35µm copper layers. A resistive circuit is etched on both copper sides giving a total electric resistance of 33.63 Ω at 20°C. The linear temperature dependence of the resistance is given by $0.136 \cdot T + 30.908$, obtained after measuring the total resistance of the heater at several temperature between 5 and 40°C. This circuit board is in turn sandwiched between two 1mm aluminum platelets to enhance the temperature distribution (**Fig. 9**). These platelets are electrically insulated from the electric circuit by a thin layer of thermal adhesive.

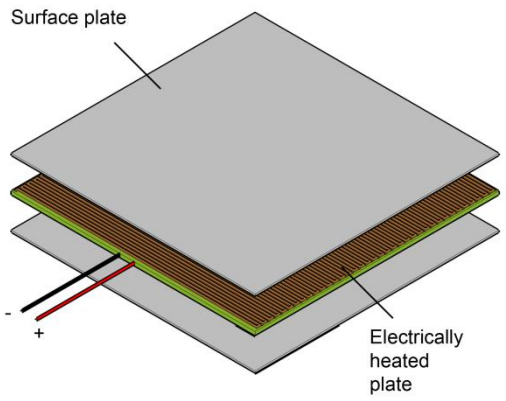

Fig. 9. Measurement plate assembly

The heating copper resistor is subjected to a pulse-square signal generated by a micro-controller and width-modulated according to the necessary electrical power. In serial with the heater, a 47 Ω reference resistor calibrated with an accuracy of 0.1% is inserted in the circuit. A high precision voltmeter (± 52 µV) is used to measure the voltage drop across this reference. Knowing this value, the current passing through the circuit is then easily computed. Finally, the power dissipated in the heater is obtained by combining this electrical current, the electrical resistance of the heater plate adjusted with hot plate temperature and the pulse width-modulated signal information.

3.4.2 Heat Flux Meter

The heat flux meter (HFM) is made by serial assembly of several thermoelectric (TE) modules (**Fig. 10** and **11**) that are inserted between the guard plate and the heater plate. Such TE modules are acting to like heat pump devices when a DC current passes through them i.e. heat will be moved through the module from one of its face to the other. However they can be used in

reverse mode, acting like power generator or heat flow detectors [19]. In the hybrid method of heat flux measurement implemented here, such elements are thus really convenient to use as HFM in an open circuit configuration. They allow controlling the flow of heat that goes from the measurement plate area to the guard zone and vice versa. Any heat exchange between the two elements will automatically create an output voltage. In fact under an open thermo-electrical circuit the relation can be written as follow:

$$\Phi_{gb} = \frac{\lambda_{te}}{\beta_{te}} \cdot V \tag{5}$$

Where Φ_{gb} (W) is the heat flux between the measurement plate and the guard plate, through the HFM, λ_{te} is the thermal conductivity of the thermoelectric module, β_{te} (V/K) is the Seebeck coefficient of the thermoelectric assembly and V the output voltage. Depending on the sign of the output voltage, the measurement plate is either cooler or hotter than the guard plate. Knowing this, the parasite heat flow can be cancelled by adapting the pulse-width-modulated signal that directs energy supply to the heater plate. In practice, 9 thermoelectric blocs with dimension 50x50x4mm are arranged in a tight square shape, giving the exact same area as the measurement plate and are fixed with thermal adhesive on the surface plate of the latter (**Fig. 10**). Having the entire back area of the measurement plate covered with the HFM is really important in order to take into account local variations of the temperature on the surface of the recess cut of the guard plate. It's the only way to ensure that the thermal imbalance is accurately taken into account for heater plate input power adjustment.

Finally, a thin insulation layer of 2.44mm thick is fixed on the free side of the HFM and will come in contact with the guard plate. The role of this layer is to filter the small temperature heterogeneities of the guard plate.

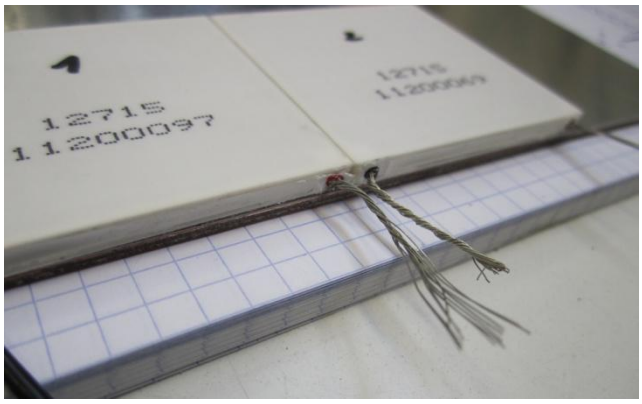

Fig. 10. Tight assembly of thermoelectric modules used as HFM

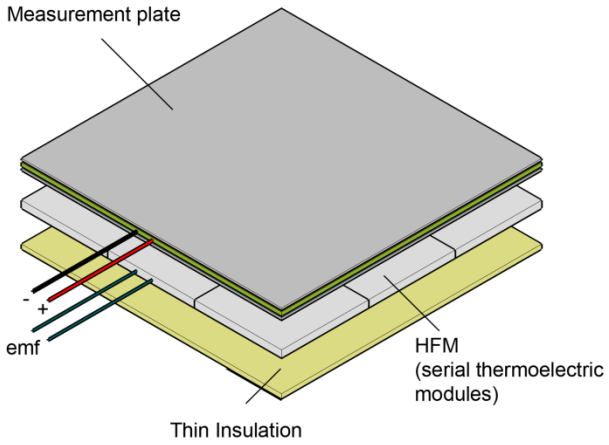

Fig. 11. HFM assembly

4. DEVICE PERFORMANCE EVALUATIONS

4.1 Intrinsic systematic error on heat flow-rate measurement

As mentioned before, in an ideal case, the measured electric power P_e is equal to the heat flow-rate Φ that in a unidirectional condition would traverse the sample. In reality, some parasite fluxes cause difference between the ideal heat flux and the measured electrical power of the heater (**Eq. 3**). The fact that high thickness samples will be tested with the device calls for particular caution in thermal conductivity results interpretation as well as a great knowledge of potential errors. The total intrinsic error in heat flow measurement is:

$$E_\Phi = \frac{\Phi'}{\Phi} \tag{6}$$

$$E_\Phi = \frac{(P_e - \Phi)}{\Phi} \tag{7}$$

Where Φ' is the sum of the edge and unbalance parasite heat fluxes. The total error E_Φ should always remain below 0.5% in order to respect the criteria fixed by the international standard [15]. This criterion is expected to be particularly difficult to respect when testing high thickness samples, mainly due to edge losses.

The first numerical analysis was carried out to estimate the total heat flow error for different material case studies in normal use conditions. The entire GHP apparatus was modeled precisely in COMSOL Multiphysics in two-dimensions (**Fig. 12**). A precise model in 3 dimensions stays difficult to handle especially given the required computational power. The actual geometry and materials layout were modeled with the specimen considered as square-shaped with a side of 1000mm. The heat conservation equation was solved in steady-state with a heat source term in the heater plate.

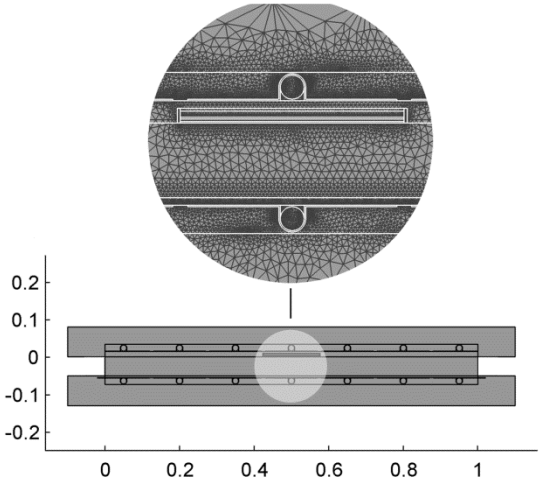

Fig.12. Modeling the GHP in COMSOL with dimensions in meters - zoom on the FEM mesh

The three considered materials studies are shown in **Table 3**. Study 3, which represents straw bales, covers several thicknesses from 0.1 to 0.45m. The hot and cold plate temperatures are applied on the internal surface of the modeled circulating tubes and are called target temperatures. The room temperature is noted T_{env} and kept at mean test temperature as in normal use.

Table 3. Material studies for intrinsic error numerical simulations

Material studies	$Type$	e (m)	λ_D $(mW \cdot m^{-1} \cdot K^{-1})$
1	Polystyrene	0.05	35
2	Vegetal fibers loose	0.2	50
3	Straw bale	0.1; 0.2; 0.3; 0.4; 0.45	80

The choice was made to link the right choice of the measurement area A to this error estimation (**Eq. 1**). The measurement area is used to compute the thermal conductivity and is traditionally fixed to the square delimited by the middle of the gap (here a square with a side of 152mm). Since the device proposed is different than traditional single-specimen model, by its unique guard plate and particular HFM system, it's important to confirm that the standard measurement area gives the best results i.e. minimize the total heat flow error E_Φ. If it's not the case, an optimal measurement area will be defined which may possibly vary according to the thickness of the sample.

The error estimation procedure is repeated for each of the material studies and goes as follows: the approximated heat flux across the specimen $\Phi_{152,app}$ is computed using **Equation 1** with the material data, $T_{h,targ} = 15°C$, $T_{c,targ} = 5°C$ (**Table 3**) and the traditional mid-gap measurement area (152x152mm). This first value gives an approximation of the power to inject in the heater plate $P_{e,app}$. After that, a parametric thermal simulation is run with various heater

power values around $P_{e,app}$. The integral of the heat flux passing through the HFM is recorded for the different power values explored. Like in the real operation of the device, when this flux is equal to zero, the corresponding power injected in the heater is gathered and gives P_e. Another simulation is run with this heater power value and the hot and cold plates temperature are taken at the location of actual temperature sensors, giving $T_{h,sens}$ and $T_{c,sens}$. Two theoretical values of the heat flux Φ_{152} and Φ_{150} are finally computed using actual plate temperatures and two different values for the measurement area 0.150x0.150mm and 0.152x0.152mm (which are respectively the exact area of the heater plate and the area at the center of the gap). These two theoretical values give two total errors, $E_{\Phi,152}$ and $E_{\Phi,150}$.

A second numerical analysis was performed to assess the effect of room temperature on the intrinsic error E_Φ for the straw bale material study. This parameter may indeed have a strong effect on heat edge-loss, especially for high thickness samples. The room temperature was incrementally increased above mean test temperature with the following steps: $(T_{env} - T_m)$ = 0.5, 1, 2.5, 5 and 10°C. The errors sign is thus expected to be negative. In addition, two scenarios are examined: with or without side insulation of the sample. The side insulation is considered 0.1m wide extruded polystyrene with $\lambda = 35\, mW \cdot m^{-1} \cdot K^{-1}$ and may reduce the edge losses.

4.2 Validations tests

Once the device fully operational, some validation tests were performed to analyze its performance and also confirm the predicted systematic error. The first series of tests will be conducted on a reference Expanded Polystyrene (EPS) slab. The specimen shows a square shape of 0.6x0.6m and was tested beforehand by the Belgian *Centre Scientifique et Technique de la Construction* (CSTC) with a certified apparatus (accuracy <1.5%). Its thermal conductivity was there evaluated at $34.16\, mW \cdot m^{-1} \cdot K^{-1}$ for a mean temperature of 10°C and a thickness of 0.0486m. When tested for validation of the apparatus, the specimen is placed in the center of the plates, with additional 0.3m wide thermal insulation on its four lateral edges. Three repetitions are performed at a mean temperature of 10, 15 and 20°C. For each repetition, the device was switched off, the sample removed from the apparatus, upturned and placed again between the plates before starting a new test.

A second series of tests is performed on two commercial Extruded Polystyrene slabs (Specimens A and B). For each test, the effective thickness of the slab is measured precisely with a caliper and reported in the thermal conductivity computation formula. After that, the slabs are cut and assembled in order to get a final square shape of 1.2 x 1.2m with no joint covering the measurement zone. **Table 4** gives the data of the two materials, the nominal and measured thickness along with the declared thermal conductivities at 10°C. Four tests are conducted on each specimen, for mean temperatures of 10, 15, 17.5 and 20°C.

Table 4. Commercial materials data

	e_n (m)	e (m)	λ_D $(mW \cdot m^{-1} \cdot K^{-1})$
Specimen A	0.05	0.0507	33
Specimen B	0.08	0.0824	35

As the measurement principle lay on steady state conditions, it is necessary to let the device and the sample sufficient time to reach such conditions and to fix a criterion to end the measurement. First, the thermal conductivity is computed for each time step using **Equation 1**. The measurement area used has a side of 150.4mm, which corresponds to the optimal area obtain by numerical simulation in the previous section for 5 cm sample. This experimental validation will thus also confirm this area choice. The moving averaged thermal conductivity $\bar{\lambda}_{720}(t_i)$ is then evaluated as in Equation 8, with $t_i > 720$. At each time step t_i, it corresponds to the mean of the thermal conductivity measured during the 2 preceding hours.

$$\bar{\lambda}_{720}(t_i) = \sum_{t=t_i-720}^{t_i-1} \frac{\lambda(t)}{720} \tag{8}$$

The moving standard deviation of the thermal conductivity is defined by **Equation 9**. At each time step t_i, it describes the variations of measured thermal conductivity around the average on the time interval $[t_{(i-720)}, t_i]$.

$$\sigma_{\bar{\lambda}}(t_i) = \sqrt{\sum_{t=t_i-720}^{t_i-1} \frac{\left(\lambda(t) - \bar{\lambda}_{720}(t_i)\right)^2}{720}} \tag{9}$$

Finally, the moving variation coefficient at time t_i is the ratio of the moving standard deviation of thermal conductivity on its moving average and will serve to fix the steady-state threshold. The measurement stops when the moving variation coefficient falls below 0.4%, which is defined as the stability threshold. The final thermal conductivity is the first moving average value that respects the criterion.

5. RESULTS

5.1 Numerical study

Table 5 gives the results of the error analysis for the three simulated materials studies. The first thing to observe is that if the room is well controlled around mean test temperature, the apparatus error stays in the same range for all the specimen thicknesses.

The second important observation is the impact of the measurement area choice on the resulting total error. With this device, it seems that using the mid-gap area to compute thermal conductivity always gives a negative total error whose amplitude is larger than the recommended 0.5%. **Figure 13** shows the optimal dimension of the measurement area as a

function of thermal resistance of modeled samples. Each time, the optimal side dimension of the measurement area is the value that minimizes the total error in the 2D model. Of course, this information depends strongly on the model complexity and underlying hypothesis. The two-dimensional nature of the model leads to imperfections in the error estimation. It's possible anyway to gain confidence in the fact that using standard mid-gap measurement area could lead to non-negligible systematic errors. A simplified 3D model gives the same trend. But the only way to confirm these error estimations is to perform experimental tests, as in the following section.

Table 5. Error analysis in normal use conditions ($T_m = T_{env}$)

Material study	λ $(mW \cdot m^2 \cdot K^{-1})$	e (m)	$T_{h,sens}$ $(°C)$	$T_{c,sens}$ $(°C)$	P_e (W)	Φ_{152} (W)	Φ_{150} (W)	$E_{\Phi,152}$ (%)	$E_{\Phi,150}$ (%)
1	35	0.05	14.98	5.03	0.1577	0.1611	0.1569	-2.09	0.54
2	50	0.20	14.99	5.02	0.0566	0.0576	0.0561	-1.58	1.06
3a	80	0.10	14.98	5.01	0.1799	0.1839	0.1791	-2.16	0.47
3b	80	0.20	14.99	5.02	0.0904	0.0921	0.0897	-1.92	0.70
3c	80	0.30	14.99	5.02	0.0604	0.0614	0.0598	-1.71	0.93
3d	80	0.40	14.99	5.02	0.0454	0.0461	0.0449	-1.46	1.18
3e	80	0.45	14.99	5.01	0.0405	0.0410	0.0399	-1.18	1.47

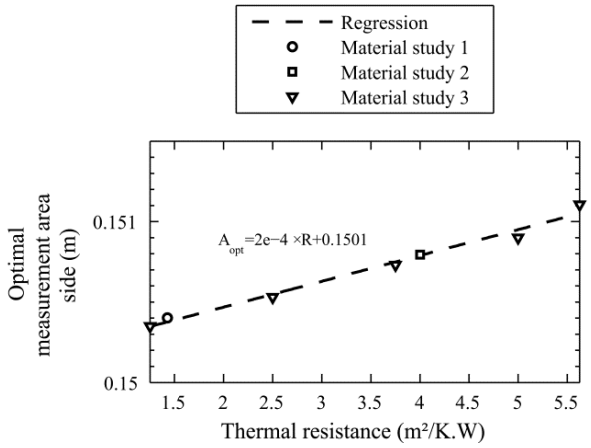

Fig. 13. The optimal measurement area expressed by its side dimension as a function of thickness or thermal resistance of the sample

The sensitivity analysis results are given in **Figure 14**. It shows that for materials with thickness greater than 10cm, a particular attention should be given to room temperature control in order to guarantee an error inferior to 0.5%. A control of $T_m \pm 5°C$ is enough for samples up to 20cm without any edge insulation where it should be reduce to 1°C for 40cm samples with edge insulation. Although the 45cm sample is theoretically beyond the limits of the machine the error threshold can be respected as long as the room temperature is precisely controlled.

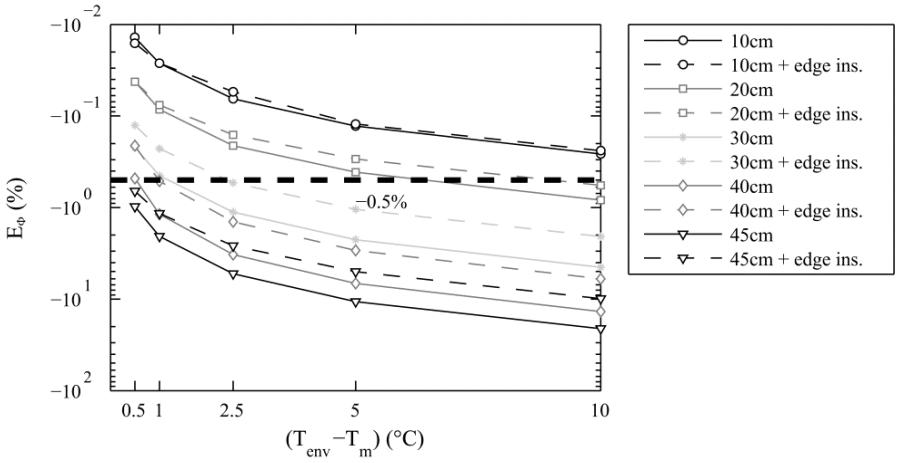

Fig. 14. The sensitivity of intrinsic error on room temperature for different straw bale thicknesses

5.3 Thermal conductivity evaluation of EPS reference sample

Figure 15 shows the graphical results of the three repetitions performed on the reference EPS slab. As expected [20], the thermal conductivity shows a linear progression with mean test temperature. The average value of thermal conductivity for a mean test temperature of 10°C is 33.69 $mW \cdot m^{-1} \cdot K^{-1}$ which is 1.38% lower than measured in the reference laboratory. This difference is in the range of accuracy of the reference apparatus. In consequence, the thermal conductivity given by our device can be considered as accurate for that given sample thickness. If the standard mid-gap measurement area was used, the obtained thermal conductivity would have been: 32.99 $mW \cdot m^{-1} \cdot K^{-1}$ which this time is almost 3.5% lower than the value measured in the reference laboratory. These results confirm the need for measurement area correction and gives additional credit to the thermal numerical simulations.

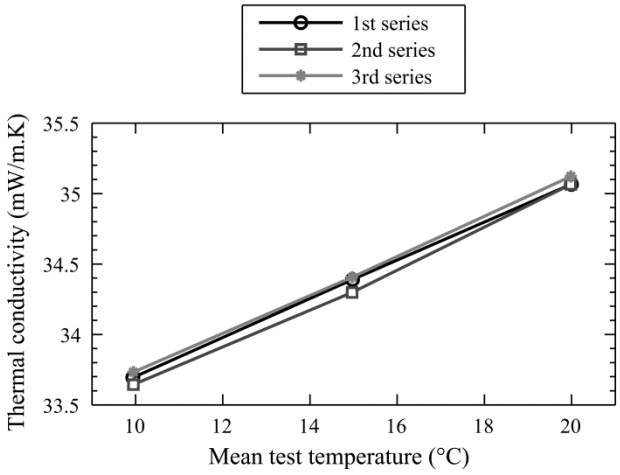

Fig. 15. Measurement repetitions on the reference EPS slab

5.4 Thermal conductivity evaluation of commercial XPS

Extruded polystyrene belongs to cellular foams family whose insulation performances are really good, with thermal conductivity ranging from 25 to 40 $mW \cdot m^{-1} \cdot K^{-1}$. Data concerning the variation of their thermal conductivity with temperature is still missing [20] but it's assumed to be linear, as EPS. **Figure 16** shows measured thermal conductivities for the two commercial XPS as a function of mean test temperature. For a mean temperature of 10°C, the device gives a thermal conductivity of 32.7548 for material A and 35.32 for material B. It gives respectively a difference of -0.74 % and +0.91 % compared to declared values. Of course, there is still a great uncertainty about how the declared values were obtained and how they were rounded during certification procedures. It can be emphasized that XPS has a linear evolution of thermal conductivity as already proven for expanded polystyrene. These first validation tests were conducted mainly to confirm general performance as well as validate the measurement area choice. Other tests should be performed in the future on higher thickness specimens.

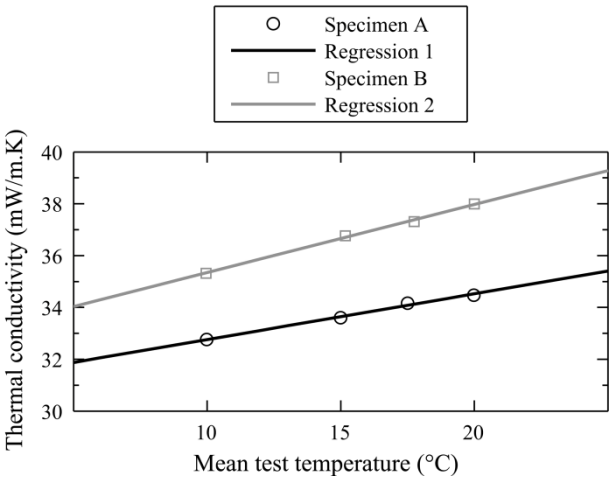

Fig. 16. Thermal conductivity as a function of the mean temperature of the test for commercial XPS slabs

6. CONCLUSION

An original device was presented in this paper, dedicated to the measurement of thermal conductivity of a large number of insulation materials. It can answer the need for performance assessment of non-traditional insulation products, and especially high thickness crops by-products. Straw bales for example can have many configurations of internal fibers organization, which can lead to variations in the resulting thermal conductivity. Standard precision equipment, like commercial GHP, shows insufficient guard size in order to test entire straw bales and forces to perform some material rearrangement.

The entire prototype apparatus was described including the hot and cold plate assemblies, temperature measurement and heat flow-rate measurement. The ISO 8302 criteria were overall

respected and verified for temperature homogeneity/stability and heat flow-rate intrinsic errors. For this last point, numerical simulations have shown the importance of questioning the measurement area value when dealing with a large range of sample thicknesses. Corrections were made in order to limit the systematic errors and different validation tests confirm the performance of the apparatus.

The large plate prototype can give reliable results as long as the room temperature is well controlled. Future research should focus on thermal conductivity measurements on an entire straw bale. This may represent a real progress for this particular material for which proper thermal conductivity comparative studies are still missing.

REFERENCES

[1] Cripps A, Handyside R, Dewar L, Fovargue J (2004) Crops in construction handbook, CIRIA, London

[2] Yates T (2006) The use of non-food crops in the UK construction industry. J Sc Food Agr 86(12):1790–1796

[3] Jones B (2002) Building with straw bales. Green Books, Totnes

[4] King B (2006) Design of straw bale buildings. Green Building Press, San Rafael

[5] Wihan J (2007) Humidity in straw bale walls and its effect on the decomposition of straw. PhD Thesis, University of East London School of Computing and Technology

[6] De Ponte F, Klarsfeld S (2002) Conductivité thermique des isolants. Techniques de l'ingénieur. http://www.techniques-ingenieur.fr/base-documentaire/mesures-analyses-th1/methodes-thermiques-d-analyse-42384210/conductivite-thermique-des-isolants-r2930. Accessed April 4th 2012

[7] Munch-Andersen J (2004) Halmhuse: Udformning og materialeegenskaber: Statens Byggeforskningsinstitut, SBI

[8] FASBA (2009) Thermal performance: strawbale building resarch development, ed. FASBA, Verden.

[9] McCabe J (1998) The thermal insulating value of straw bale for construction. National passive conference. Albuquerque

[10] Goodhew S, Griffiths R (2004) Analysis of thermal-probe measurements using an iterative method to give sample conductivity and diffusivity data. Appl En 77(2):205–223

[11] Shea A, Wall K, Walker P (2012) Evaluation of the thermal performance of an innovative prefabricated natural plant fibre building system. Building Serv Eng Res Technol 34(4):1-12

[12] Beck A, Heinemann U, Reidinger M, Fricke J (2004) Thermal transport in straw insulation. J Th Env Buil Sc 27(3):227–234

[13] Pruteanu M (2010) Investigations Regarding the Thermal Conductivity of Straw.Bulletin Poly Inst Jassy 56(60):9-16 .

[14] Ashour T (2003) The use of renewable agricultural by-products as building materials. PhD Thesis, Benha University

[15] International standard, ISO 8302 (1991) thermal insulation - determination of steady-state thermal resistance and related properties

[16] Leong WH, Hollands K, Brunger A (1998) On a physically-realizable benchmark problem in internal natural convection. Int J Heat Mass Tr 41(23):3817–3828

[17] Reid D (2005) Guarded hot plate apparatus design and construction for thermal conductivity measurements. PhD Thesis, Ryerson University

[18] Zarr R, Healy W, Filliben J, Flynn D (2002) Design concepts for a new guarded hot plate apparatus for use over an extended temperature range. Insulation Materials: Testing and Applications. Vol. 4, ASTM International, West Conshohocken

[19] Leephakpreeda T (2012) Applications of thermoelectric modules on heat flow detection, ISA Transactions 51(2):345–350

[20] Klarsfeld S (2004) Isolation thermique à température ambiante. Techniques Ingénieur. http://www.techniques-ingenieur.fr/base-documentaire/energies-th4/echangeurs-de-chaleur-et-isolation-42376210/isolation-thermique-a-temperature-ambiante-proprietes-be9860. Accessed December 10th 2012

CHAPTER 4

Developing a research BEHAM model

4.1 Introduction

The available BEHAM tools often lack transparency and/or modularity in the underlying mathematical description. In **Chapter 1**, we mentioned that several authors pointed out general computational tools as offering great potentialities for improving the performance of hygrothermal models and increasing the scale of study. They contain a wide range of modelling tools and their user-community is very active, which often ensures the availability of powerful hygrothermal models. Moreover, they allow combining many existing hygrothermal building models in a single computational environment.

In the appended paper, a first version of the research BEHAM model is presented. *COMSOL Multiphysics*[1] is chosen as solving environment because it offers crucial qualities required to go further in the characterization of crop-based materials performance. It is here used to simulate the behaviour of LHC sample during a Moisture Buffer Value test, an experimental protocol used to characterize moisture exchange capacity in the hygroscopic region. This paper also highlights specificities of CBM in terms of latent heat effect. Finally, it introduces efficiency criteria for evaluating model performance, which are essential for tool inter-comparison.

[1] http://www.comsol.com/

4.2 Appended paper

Modeling the Dynamic Hygrothermal Behavior of Biobased Construction Materials

Samuel DUBOIS*[1], Arnaud EVRARD[2], Frédéric LEBEAU[1]

[1]Dept. STE, Gembloux Agro-Bio Tech, University of Liege, Belgium

[2]Architecture et Climat, Université Catholique de Louvain, Belgium

*Corresponding author, supported by a F.R.I.A Grant,
Address: Dept. of environmental sciences and technologies, Gembloux Agro-Bio Tech, 2 Passage des déportés, 5030 Gembloux, Belgium (s.dubois@doct.ulg.ac.be)

KEYWORDS

Ham Modelling, Moisture Buffer Value, Lime Hemp Concrete, Hygroscopic, Latent Heat

STATUS

Published in*:

Journal of Building Physics, 2014

**Minor changes have been made compared to the original version*

ABSTRACT

The construction materials with high moisture exchange capacity may have a strong impact on indoor climate conditions as well as on energy performance of buildings. Crop-based materials, characterized by their high porosity and hygroscopic properties, belong to this category. Modeling their hygrothermal behavior with accuracy is thus particularly relevant for an efficient building design. A transient Building Element Heat Air and Moisture (BEHAM) model is developed in *COMSOL Multiphysics* to simulate the moisture exchange between a Lime-Hemp Concrete bloc and surrounding air during a Moisture Buffer Value (MBV) evaluation test.

The simulation results are compared to well-validated BEHAM software with the help of performance criteria. The proposed model shows a slightly better efficiency in the characterization of both moisture exchange and latent heat effect phenomena. In addition, it offers advantages in terms of flexibility and transparency as well as further evolution potential.

1. INTRODUCTION

Many authors (Padfield, 1999; Peuhkuri et al., 2005; Osanyintola and Simonson, 2006; Rode and Grau, 2008; Abadie and Mendonça, 2009, Li et al., 2012) have studied the capacity of porous hygroscopic materials to dampen the indoor humidity variations through moisture exchange, which is usually referred as the "Moisture buffer effect". The moisture exchange capacity is directly related to their porous structure as the latter will determine the sorption and capillary behavior as well as the transport coefficients. Crop-based insulation materials, which have recently appeared as a serious candidate in the search of sustainable and energy-efficient materials, have typically a strong buffer performance as both their moisture storage and transfer capabilities are high. The impact of such materials on the moisture balance at room or building level is thus typically non-negligible, like often stated for traditional materials. Moreover, ignoring their specific hygric behavior might lead to an incorrect prediction of direct and indirect energy demands for heating/cooling the building because of latent heat effects, comfort conditions modifications, and the dependence of heat transport parameters on moisture content (Osanyintola and Simonson, 2006; Tariku et al., 2010a). Is it thus important to solve with accuracy the transient and coupled balance equations that govern heat and moisture transport in those porous media.

Traditionally, models which deal with detailed Heat, Air and Moisture (HAM) analysis of envelope response have been focusing mainly on one envelope component at a time. For that reason they are called Building Element Heat, Air and Moisture (BEHAM) models. The origin of such tools is found in the Glaser's method (Glaser, 1959), a 1D calculation method for designing moisture-safe walls that is based on the description of steady-state diffusion. Later, in the 90's, the first physical models accounting for complex diphasic water transport in transient conditions were developed (Pedersen, 1991; Künzel, 1995; Häupl et al., 1997). They took profit of the knowledge acquired in the mathematical description of porous media since Philip and De Vries work (Philip and De Vries, 1957) as well as the progress in numerical resolution techniques and power. These models are always based on partial differential equations (PDEs) solved with finite elements or volumes methods on multilayered components of the envelope. Till today, many BEHAM computer software were developed and some commercialized (Hagentoft et al., 2004; Janssens et al., 2008). The description of the moisture flows is often classificatory. It can have several levels of complexity ranging from diffusivity models, where moisture content is used driving potential, to conductivity model with the actual thermodynamic driving potentials (Scheffler and Plagge, 2010). The most complex models incorporate pore space mathematical description which is used to obtain the hygrothermal transport and storage functions.

Lately, several authors (Kalagasidis, 2004; van Schijndel, 2009; Tariku et al., 2010a) have pointed out the possibility of using a single computational environment to combine different

building simulation tools. In this way, a whole building HAM model is more easily achievable, comprising indoor air and of envelope description tools as well as HVAC systems contributions. In the *Matlab/Simulink* popular environment, *COMSOL Multiphysics* (formerly *FemLab*) seems to be particularly interesting to manage the multidimensional PDE-based BEHAM problems (Tariku et al., 2010b; van Schijndel, 2009). It offers evident advantages in terms of modularity, transparency and ease of use. This answers the need for research-oriented modeling where lots of available tools are still opaque with little access to equations or material functions. In Tariku et al. (2010b) a *COMSOL* heat, air and moisture transfer model already passed successfully the standard *HAMSTAD* benchmarks exercises, proving its ability to solve complex transient problems.

The objective of this paper is to test the ability of a *COMSOL Multiphysics* model to simulate the coupled heat and moisture transfer taking place inside a crop-based material. For this purpose, a simple case study at material scale is used, dedicated to the characterization of hygroscopic products: the Moisture Buffer Value (MBV) test. This experimental protocol highlights the moisture exchange capacity of materials in the hygroscopic moisture content region. A material sample is continuously weighed and is subject to a normalized humidity cycle in isothermal conditions. Unlike previous works on MBV experiment modeling, not only the measured mass variation of the sample will be compared to the model output but also its exchange surface temperature which varies trough latent heat effects. In this way, we can validate the complex thermal aspects linked to moisture transfers that are incorporated in the model. All simulated results will be compared to the outputs of *WUFI Pro*, a validated BEHAM analysis software, with the help of objective efficiency criteria providing a clear outlook on model performance.

2. MATHEMATICAL MODEL

2.1 Macroscopic conservation equations

It is assumed that the porous medium $\Omega \subset R^3$ is a multiphase system consisting of the solid matrix, a liquid water phase and a gaseous phase, comprising dry air and water vapor. Two conservation PDEs are developed, one for moisture mass and one for heat, on an averaged representative elementary volume (REV) (Bear, 1988). The following additional hypothesis are taken for the mathematical description : (1) The material is non-deformable and isotropic; for a non isotropic material, standard transfer coefficients have to be replaced by tensors; (2) the fluid phases do not chemically react with the solid matrix; (3) The moisture content of the material as vapor θ_v is considered negligible compared to the correspondent term in liquid phase; (4) The dry air pressure is constant (no air advection) and the total gas pressure gradient are considered negligible; (5) no liquid to ice phase change is considered; (6) there is a local thermodynamic

equilibrium between the different phases; (7) There is no thermal effects due to friction or compression; (8) thermal diffusion (Soret effect) is neglected; (9) no hysteresis phenomena are accounted for.

Equation (1) shows the governing macroscopic equation for moisture flow through a porous medium given those hypotheses.

$$\rho_l \frac{\partial \theta_l}{\partial t} = -\nabla \cdot \left(\boldsymbol{j_c^{M_l}} + \boldsymbol{j_d^{M_v}}\right) + \sigma^{M_{v+l}} \quad (1)$$

With the different moisture flux densities being $\boldsymbol{j_c^{M_l}}$, the capillary transport of liquid water and $\vec{\boldsymbol{j}}_{\boldsymbol{d}}^{\boldsymbol{M_v}}$, the diffusion of vapor. Each of these moisture flux densities can be expressed as a function of a driving potential using constitutive mass transport relations. In an unsaturated porous building material, where gravity plays a negligible role in normal operating conditions, the liquid water is subjected to the suction of the medium through capillary forces. The capillary pressure in a pore p_c represents the difference between gas and liquid pressure around the meniscus:

$$p_c = p_g - p_l \quad (2)$$

Liquid transfers due to capillarity go from low capillary pressure (or high moisture content) to high capillary pressure (low moisture content). Replacing advection of liquid water and diffusion of vapor with Darcy's and Fick's law, respectively, the final expression of moisture balance is presented in **Equation 3**.

$$\rho_l \frac{\partial \theta_l}{\partial t} = -\nabla \cdot (K_l \cdot (\nabla p_c + \rho_l \cdot \vec{g}) - \delta_v \cdot \nabla p_v) + \sigma^{M_{v+l}} \quad (3)$$

Applying the law of conservation of internal energy, the enthalpy change in an averaged volume element is determined by the divergence of heat flux density by conduction, enthalpy transport due to transfer of fluid phases and the presence of heat sink or source. The balance equation does not take into account transfers by radiation and assumes that the local thermal equilibrium hypothesis is valid.

$$\frac{\partial (\rho h)}{\partial t} = -\nabla \cdot \left(\boldsymbol{j_{cond}^{Q}} + \boldsymbol{j_c^{M_l}} \cdot h_l + \boldsymbol{j_d^{M_v}} \cdot h_v\right) + \sigma^{Q} \quad (4)$$

The enthalpies in right-hand side of Equation (4) are related to the temperature through:

$$h_l = c_l \cdot (T - T_0) \quad (5)$$

$$h_v = c_v \cdot (T - T_{sat}) + L + c_l (T_{sat} - T_0) \quad (6)$$

Where L is the latent heat of phase change (J/kg) for pure water at T_{sat} =100°C and 1atm. The total specific enthalpy in the REV in left-hand side of **Equation 4** turns into:

$$\frac{\partial (\rho h)}{\partial t} = (c_0 \rho_0 + \rho_l \theta_l c_l) \cdot \frac{\partial T}{\partial t} \quad (7)$$

Rewriting the heat conservation equation considering all the constitutive assumptions yields the final mathematical formulation implemented in the model:

$$(c_0\rho_0 + \rho_l\theta_l c_l)\cdot\frac{\partial T}{\partial t} = -\nabla\cdot(-\lambda\nabla T + K_l(\nabla p_c + \rho_l\vec{g})h_l - \delta_v\nabla p_v h_v) + \sigma^Q \quad (8)$$

2.2 Additional relations

Equations 3 and **8** form the system to be solved. Two relationships have to be formulated between the different moisture field variables (i.e. the moisture content θ_l, the vapor pressure p_v and the capillary pressure p_c) in order to limit the number of unknowns. As the local thermodynamic equilibrium hypothesis is assumed valid around the meniscus in a pore, the Kelvin's equation relates the capillary pressure to the relative humidity (RH). Relative humidity is of course linked to the vapor pressure through the vapor saturation pressure, which is a function of temperature that can be approximated by different empirical relations. The sorption isotherm of the material, also called moisture storage curve (MSC), provides the second necessary relation, between the moisture content and relative humidity or capillary pressure. For the description of this material function, the most ordinary technique is to gather experimental data and to use fitting curves with adjustable parameters for a continuous description on the whole RH range. These parametric curves can be purely empirical or physically-based. The latter technique supposes to use a pore system description. Here, the pore structure of the material is described by the model of Häupl and Fechner (2003). The pore size distribution analytical function is formulated as a sum of N pore size compartments (the modes of the distribution), each centered on a main value of the pores radius $R_i\ (m)$. The moisture storage process up to the filled radius r is obtained by the integration of the pore size distribution function following the bundle of capillary representation. Ultimately the moisture storage curve $\theta_l(\varphi)$ is given by:

$$\theta_l(\varphi) = \sum_i^N \theta_i \cdot \left(1 - \left(1 + \left(\frac{2\sigma}{\rho_w R_v T\cdot \ln(\varphi)\cdot R_i}\right)^2\right)^{1-n_i}\right) \quad (9)$$

Where $\theta_i\ (m^3/m^3)$ is the partial volume of the ith pore size compartment and n_i its shape factor describing its width. With Kelvin's equation and the MSC, it is possible to re-write the conservation equations system on a unique moisture field variable. This only requires simple mathematical re-formulations.

In addition to the moisture variables connections, the other material properties have to be properly defined. The thermal conductivity, thermal capacity, liquid conductivity and vapor permeability are in reality function of the two dependent variables giving typically non-linear PDEs. In some particular cases they could be considered as constant parameters but when large ranges of moisture content or temperature are met in the material, these simplifications could

lead to incorrect predictions. In consequence, depending on the case study, these functions have to be characterized properly. When needed, the liquid water conductivity dependency on water content can be derived from the porosity model.

3. CASE STUDY

Modeling the hygrothermal behavior of a bio-based material is considered here a case study to evaluate the performance and flexibility of the model solved with *COMSOL Multiphysics* in comparison to a validated model. The output of each model was compared to measurement gathered during a typical dynamic experiment dedicated to the characterization of hygroscopic material: the Moisture Buffer Value determination. This experimental protocol highlights the moisture exchange capacity of materials by massing of a sample subjected to a normalized humidity cycle in isothermal conditions. But unlike previous works on MBV modeling, not only the measured mass variation of the sample will be compared to the model output but also the temperature at the exchange surface, which varies through latent heat effects. In this way, we can validate the complex thermal aspects linked to moisture transfers that are incorporated in the model. The experimental validation will be conducted on a typical bio-based material: the Lime-Hemp Concrete (LHC).

3.1 MBV determination protocol

The need for a standardized parameter to characterize the moisture exchange capacity of materials led to the definition of MBV during the *NORDTEST* project (Peuhkuri et al., 2005) together with the proposal of a dynamic experimental protocol for materials classification. The practical MBV is defined as *:''the amount of water that is transported in or out of a material per open surface area, during a certain period of time, when it is subjected to variations in relative humidity of the surrounding air''* (Peuhkuri et al., 2005). Concretely, the samples are subject to cyclic step changes in relative humidity at a constant temperature of $23\,°C$ and are weighed regularly. The cycle is composed of a moisture uptake phase during 8 hours at 75% RH followed by moisture release during 16 hours at 33% RH (**Figure 1**) and is repeated until constant mass variation between 2 consecutive cycles is reached. This experimental value is a direct measurement of the amount of moisture transported to and from the material for the given exposure cycle.

Another approach might be used to predict the MBV of a material. Indeed, a theoretical value, called the ideal MBV, can be computed analytically using semi-infinite solid theory and Fourier series without transfer resistance at exchange surface (Peuhkuri et al., 2005). There is always a disagreement between measured and analytically calculated MBV due to the dynamic nature of the experimental protocol and film resistance on specimen exchange surface.

3.2 Lime-Hemp Concrete material

LHC are types of innovative concretes made out of the mix of hemp shivs (the woody core of industrial hemp stalk) and lime-based binders. With appropriate mixing proportions, they can be used in various applications like walls, roof insulation or even plasters (Evrard and De Herde, 2010). Many authors worked on LHC characterization and provided a set of physical and hygrothermal parameters for different mixes (Collet et al., 2008; Samri, 2008; Evrard and De Herde, 2010). The pore size distributions of the mixes or individual components were assessed by some of them with mercury porosimetry technique. There seems to be three general classes of pores: the microscopic porosity in the lime matrix (with peaks at ~0.05µm and ~0.5µm), the mesoscopic porosity in the hemp shivs (~10µm) and macroscopic porosity between de shivs in the binder (>1mm). **Figure 1a** shows a slice view of one hemp shiv obtained by X-ray microtomography. The high total porosity of the vegetal particle can be clearly seen with the typical tubular structure of the meso-scopic pores. **Figure 1b** shows a slice of a LHC sample, with mix proportions for wall casting, also obtained by tomography. The arrangement of the particles (appearing in grey due to low density) inside the binder (appearing in black due to high density) is visible with resulting macroporosity.

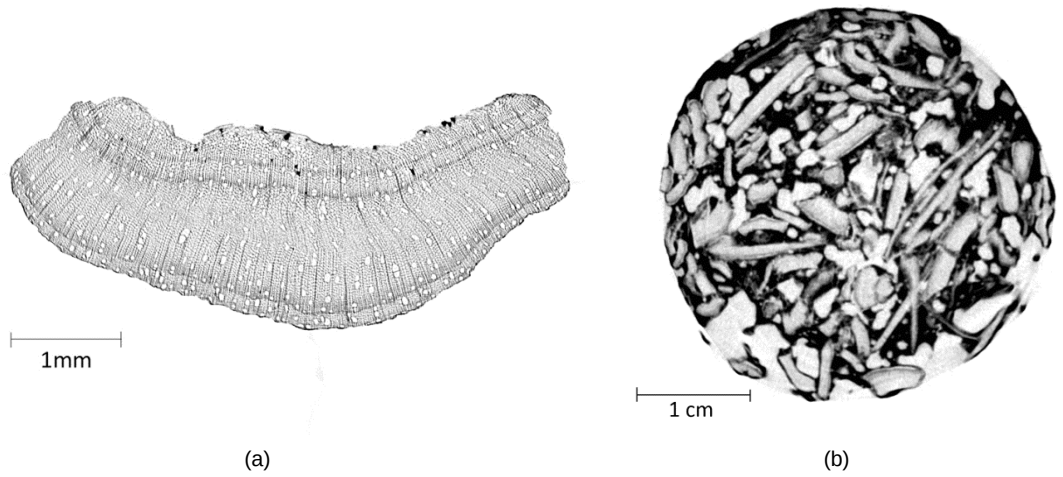

Fig. 1. Microtomography slices: a hemp shiv (a); a Lime-Hemp sample for wall casting application (b)

Table 1 compares the LHC material to some current construction materials with regard to different physical properties. Three main parameters are chosen as hygrothermal performance indicators: the thermal conductivity, the thermal effusivity and the ideal MBV. Thermal conductivity express the tendency of the material to allow heat to pass in steady-state conditions and lower values are thus favorable; thermal effusivity is an indicator of the heat exchange capacity of the material with its environment and high value are desirable to use thermal inertia effects; ideal MBV is an indicator of moisture buffering capacity of the material and high values are desirable to use natural damping of indoor humidity. This ideal MBV is here computed to

express the exchange capacity of the material on a 33/75%RH cycle and, as said before, it is derived from steady state parameters.

Table 1. LHC compared to standard construction materials.

	Density ρ	Total open porosity ε	Therm. conductivity λ	Therm. effusivity b	Ideal MBV 33-75
	kg/m^3	–	$W/(mK)$	$W \cdot s^{0.5}/(m^2K)$	$g/(m^2.\%RH)$
Spruce (parallel to grain)	455	0,73	0,23	396,2	6,694
Oak (parallel to grain)	685	0,72	0,3	555,2	5,565
Pumice concrete	664	0,67	0,14	281,1	5,307
Aerated Clay brick[c]	672	0,67	0,12	261,8	5,307
Straw bale[a]	100	0,9	0,085	130,4	5,247
Wood wool panel	450	0,55	0,08	232,4	4,424
Lime-hemp wall-mix[b]	440	0,73	0,115	281,0	3,783
Expanded clay concrete	700	0,67	0,13	278,1	3,086
Cellulose Insulation[c]	55	0,93	0,036	71,0	2,893
Aerated concrete (500kg/m³)	500	0,77	0,12	225,8	1,963
Extruded brick	1650	0,41	0,6	917,3	1,668
Oak (radial)	685	0,72	0,13	365,5	1,330
Sand-lime blocks	1900	0,29	1	1270,8	1,254
Spruce (radial)	455	0,73	0,09	247,8	1,217
Concrete W/C=.5	2300	0,18	1,6	1768,6	1,064
Manufactured brick	1725	0,38	0,6	937,9	0,402
Mineral wool	60	0,95	0,04	45,2	0,000
Extruded polystyrene (XPS)	40	0,95	0,03	42,4	0,000

Source : ***IBP Institute***
[a] Jakub Wihan, 2007
[b] Evrard and De Herde, 2010
[c] Masea Database

3.3 Test platform

A HPP749 (*Memmert*) climatic chamber was used to carry out the MBV humidity cycles in an isothermal closed environment. This device was upgraded with an additional dehumidification stage consisting of an AD 21-138 (*Aircraft*) refrigerating dryer in order to improve its performance. As the average air velocity in the chamber is necessary to determine the vapor diffusion resistance factor at the surface of the material, it was measured in the horizontal direction with an hot-wire anemometer 8465-300 (*TSI*). It showed an average value of $0.135 \pm 0.03\ m/s$.

The tested material is a LHC wall-mix (Evrard and De Herde, 2010) from the same origin as samples used by Evrard (2008). The binder is the widespread Tradical PF70 mixed with *Chanvribat* hemp particles. The components mix proportions of the bloc are given in **Table 2**.

The LHC sample bloc has a unique moisture exchange surface of 150x150mm and a thickness of 75mm, which is stated sufficient given the theoretical moisture penetration depth during the MBV experiment. Lateral and back faces are isolated from water exchange with polyethylene film and tape (**Fig. 2**). One SHT75 (*Sensirion*) sensor is implemented 15cm above the sample in

order to monitor the evolution of humidity and temperature in the chamber. Finally, a DS18B20 (*Dallas*) temperature sensor is placed on the surface of the material with a small thermal insulation cap on top of it. This sensor is dedicated to the detection of the latent heat effect. The insulation cap was stated necessary to monitor the actual surface temperature, avoiding the influence of the surrounding air. Once instrumented, the sample was placed inside the chamber on an M-Power (*Sartorius*) laboratory scale with a 0-3100g range and 0.01g resolution. This scale was monitored every 5 minutes trough its RS232 output via a *LabVIEW* acquisition program. The whole experimental set-up is shown on **Figure 3**.

Table 2. Composition of the sample bloc

LHC wall mix	(%mass)	kg if 20kg of Chanvribat
Chanvribat	17	20
Tradical PF70	33	40
Water	50	60
Total	100	120

Fig. 2. LHC bloc with sealed lateral faces

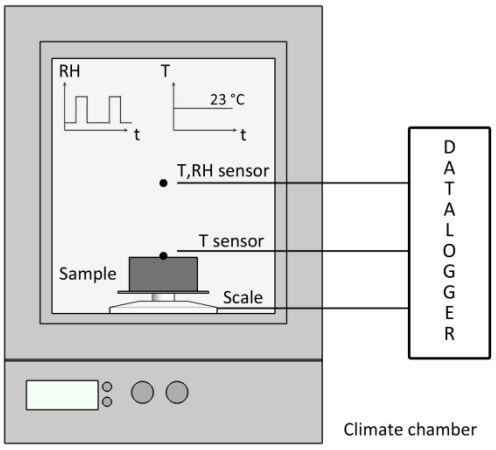

Fig. 3. Experimental set-up

4. MODELING PROCEDURE

4.1 Equations re-formulation

The incorporation of the mathematical model in *COMSOL Multiphysics* offers the advantage of flexibility in the mathematical formulation. Indeed, the user can choose the equations set complexity as well as the mathematical expressions for the moisture retention curve and other material functions. During the MBV solicitation cycle, which lies in the range 33/75%RH, the LHC bloc will be mainly subject to hygroscopic storage and vapor water transport. In consequence, the conservation equations should be simplified in order to minimize the computational time. Even if the MBV determination experiment is conducted in isothermal conditions, the heat balance equation is still necessary to account for latent heat effects in the material. Again, the model used in this paper offers the advantage of being fully modular.

The chosen dependant variables for simulations are temperature and relative humidity. In addition, no liquid water transport is accounted for, enthalpy transport is accounted for, and no source/sink term is necessary. The PDEs will be solved in 1 dimension giving the following final expressions for moisture and heat conservation equations:

$$\xi \cdot \rho_l \cdot \frac{\partial \varphi}{\partial t} = \delta_{v0} \cdot \frac{\partial^2(\varphi \cdot p_{sat}(T))}{\partial x^2} \tag{10}$$

$$(c_0\rho_0 + \rho_l\theta_l c_l)\frac{\partial T}{\partial t} = \frac{\partial}{\partial x}\left(\lambda_0 \frac{\partial T}{\partial x} + \delta_{v0} \cdot \frac{\partial(\varphi \cdot p_{sat}(T))}{\partial x} \cdot h_v\right) \tag{11}$$

Water is consider as pure water with liquid density $\rho_l = 1000\ kg/m^3$, liquid specific heat capacity $c_l = 4187\ J/(kg \cdot K)$, vapor specific heat capacity $c_v = 2000\ J/(kg \cdot K)$ and latent heat of vaporization $L = 2257\ kJ/kg$. The following material parameters are considered constant with values for the material in dry state, taken from previous measurements (Evrard, 2008): $\rho_0 = 440\ kg/m^3$, $\lambda_0 = 0.115\ W/m$, $c_0 = 1560\ J/(kg \cdot K)$ and $\delta_{v0} = 4.12E-11\ kg/(m \cdot s \cdot Pa)$.

4.2 Moisture retention curve calibration

The moisture capacity ξ was obtained by calibrating the Häupl & Fechner's porosity model with experimental data for LHC. Indeed, the multimodal moisture storage function was fitted on experimental points that were previously obtained by Evrard and De Herde (2010) with pressure plate and salt solutions methods. Literature data from mercury intrusion porosimetry on LHC helped to select the main pore radii $R2$ and $R3$ in accordance with the real pore size distribution. The main pore radius $R1$ has no physical meaning and is used as an artificial mean to account for surface adsorption, which can be considered similar to capillary condensation in very small

pores. The selected parameters are given in **Table 3** and the obtained porosity distribution is shown on **Figure 4**. This calibration of the pore space function in the BEHAM model opens large perspectives for further work on LHC that should address their behavior in the overhygroscopic moisture content region.

Table 3. Moisture storage function parameters

Main radius			Partial volume			Shape parameter		
R1	R2	R3	θ_1	θ_2	θ_3	n_1	n_2	n_3
5.6E-4µm	0.08µm	0.5µm	0.11	0.133	0.33	1.09	1.32	1.20

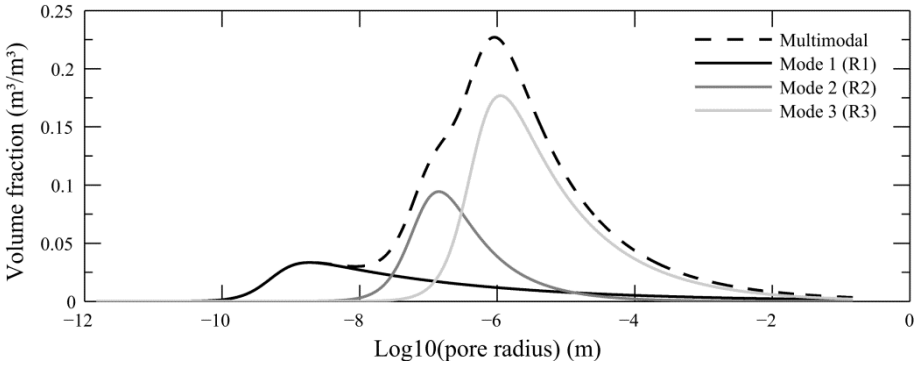

Fig. 4. The LHC multimodal pore size distribution function with highlighting of the different pore space compartments

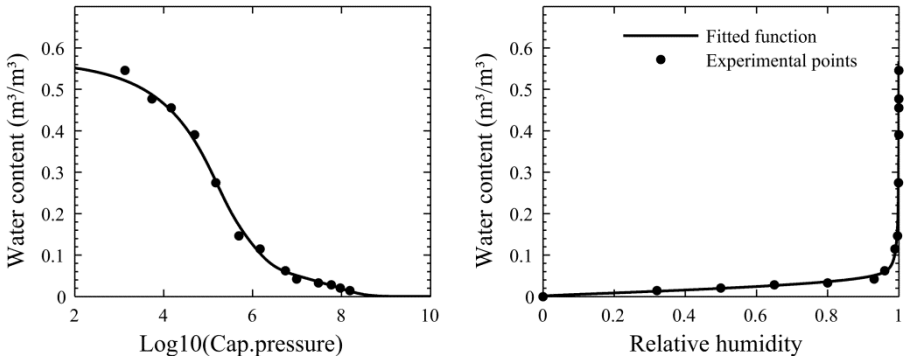

Fig. 5. Fitted moisture content of LHC as a function a capillary pressure and relative humidity

4.3 Boundary and initial conditions

Referring to **Figure 6**, we can write the following boundary and initial conditions for moisture transport:

$$\left(\boldsymbol{j}^{\boldsymbol{M_v}}\right)\cdot\boldsymbol{x} = \frac{\left(\varphi_\infty p_{sat,\infty} - \varphi_s p_{sat,s}\right)}{Z_s} \qquad x = 0 \qquad (12)$$

$$\frac{\partial \varphi}{\partial x} = 0 \qquad x = L \qquad (13)$$

$$\varphi(x, 0) = \varphi_0 \qquad 0 < x < L \qquad (14)$$

where $\boldsymbol{j^{M_v}}$ is the moisture flux density ($kg/m^2\,s$), φ_∞ / $p_{sat,\infty}$ the relative humidity / saturation pressure in the climatic chamber, and φ_s / $p_{sat,s}$ the relative humidity / saturation pressure at the exchange surface.

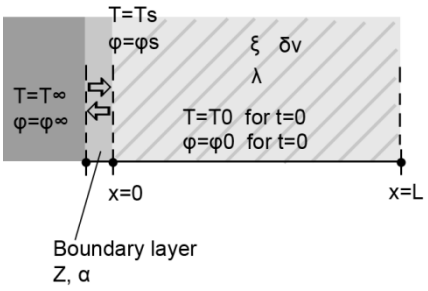

Fig. 6. Domain and boundary conditions

The vapor diffusion resistance factor Z_s ($Pa/(kg \cdot m^2 \cdot s)$) characterizes the moisture transfer resistance that exists on the material surface and slows down the moisture exchange. Its value is fixed to $5 \cdot E7\ Pa/(kg \cdot m^2 \cdot s)$ which is the usually accepted value for environments with an ambient air velocity around $0.1\ m/s$ (Peuhkuri et al., 2005). It's similar to a value of $Z_{s,v} = 360\ s/m$ when the surface flux density is written in terms of absolute humidity:

$$\left(\boldsymbol{j^{M_v}}\right) \cdot \boldsymbol{x} = \frac{(v_\infty - v_s)}{Z_{s,v}} \qquad (15)$$

To calculate the accumulated moisture, Equation (16) is used.

$$G_v = \int_0^t g_v dt \qquad (16)$$

The resulting relative mass of the sample is given by:

$$m(t) - m_0 = G_v(t) * A \qquad (17)$$

where $m(t)$ is the mass of the sample at time t (kg), m_0 is the initial mass of the sample (kg) and A is the exchange surface area of the sample (m^2).

For heat transport, the boundary and initial conditions are given by:

$$\left(\boldsymbol{j^{Q}}\right) \cdot \boldsymbol{x} = \alpha \cdot (T_\infty - T_s) + \left[\left(\varphi_\infty p_{sat,\infty} - \varphi_s p_{sat,s}\right)/Z_s\right] \cdot h_v \qquad x = 0 \qquad (18)$$

$$\left(\boldsymbol{j^{Q}}\right) \cdot \boldsymbol{x} = \alpha \cdot (T_\infty - T_L) \qquad x = L \qquad (19)$$

$$T(x, 0) = T_0 \qquad 0 < x < L \qquad (20)$$

with $\boldsymbol{j^Q}$ the heat flux density (W/m^2), T_∞ the chamber temperature ($°C$), T_s the temperature at exchange surface ($°C$) and T_L the temperature at the bottom of the sample ($°C$). The convective heat transfer coefficient α (W/m^2K) is fixed to $1{,}44E8/Z_{surf}$ according to (Peuhkuri et al., 2005).

The input data T_∞ and φ_∞ for ambient air variations used as boundary solicitation in the model are the measured RH and temperature from the experimental cycles, which might be quite different from the ideal step cycle. The initial conditions inside the bloc are fixed to $\varphi_0 = 55\%RH$ and $T_0 = 23.1°C$ to match real equilibrium conditions before the start of the test.

4.4 Numerical resolution

The two PDEs need to be solved simultaneously in order to obtain the desired temperature and humidity fields across the domain as well as the resulting heat and mass fluxes. *COMSOL Multiphysics* is based on finite-element resolution technique and provides an equation-based modeling module that allows users to encode their own PDEs equations. The latter is referred as "PDE interfaces module" (Tariku et al., 2010b). The two conservation equations were thus encoded in the following general form:

$$a\frac{\partial X}{\partial t} + \nabla \cdot \Gamma = 0 \tag{21}$$

where a is referred as the damping coefficient, X is the dependent variable and Γ is the conservative flux. In order to treat the MBV transient problem, the built-in time dependent explicit solver was used to get the variables fields. The time discretization consists of a free variable time stepping with a maximum time step fixed to 5 minutes, which corresponds to the boundary conditions variation step. Spatially, the domain is meshed with respect to the expected dependent variables gradients. The finite elements distribution density is increased near the exchange surface using a geometric progression.

The outputs of the *COMSOL* model are compared to results from the validated *WUFI Pro* BEHAM software. The simulation in *WUFI* was performed with the same material parameters and a piecewise moisture retention curve. However, boundary conditions were defined on an hourly basis and only the convective heat transfer coefficient can be encoded in the software.

4.5 Efficiency criteria and error indices

Three criteria were used to formulate an objective assessment of the models performance relatively to the MBV test simulations: the Nash-Sutcliffe efficiency coefficient (NSE), the percent bias (PBIAS) and the root mean square error (RMSE). Such indicators also provide a mean of comparison between the *COMSOL* model and the *WUFI Pro* software. The NSE is

defined as one minus the sum of squared differences between simulated and observed values normalized by the variance of observed data:

$$NSE = 1 - \frac{\sum_{i=1}^{n}(X_{model,i} - X_{obs,i})^2}{\sum_{i=1}^{n}(X_{obs,i} - \bar{X}_{obs})^2} \quad (22)$$

where $X_{model,i}$ is the model predicted value for time step i, $X_{obs,i}$ is the experimental observation for the same time step and $\bar{X}_{obs}$ is the mean of all experimental values. A NSE coefficient of 1 means a perfect fit of the model to experimental data. If the indicator falls below zero that would imply that the residual variance is larger than data variance and thereby the mean value of observed data would be a better predictor that the model. The NSE also characterizes how well $(X_{obs,i}, X_{model,i})$ points fit the 1:1 line (identity line). The second indicator, the PBIAS, is defined as:

$$PBIAS = \frac{\sum_{i=1}^{n}(X_{obs,i} - X_{model,i})}{\sum_{i=1}^{n} X_{obs,i}} \cdot 100 \quad (23)$$

It indicates the average tendency of modeled data to systematically under or over-estimate the observed data. Finally, the RMSE is the most commonly used error index and is scale-dependent. A RMSE value of zero indicates a perfect fit to observed data.

Simulations can be judge satisfactory if the indicators stays in a predefined range. These acceptance values can be fixed to NSE > 0.8 and $|PBIAS| < 15\%$ in light of watershed modeling techniques, where accuracy issues were widely discussed (Moriasi et al., 2007). As RMSE is not normalized, it's more difficult to give a clear acceptance range.

5. RESULTS

5.1 Experimental results

Figure 7 shows the MBV humidity cycles and the mass variation of the sample measured experimentally. Numbers were assigned to four of the 24h cycles to facilitate the subsequent analyzes. For each cycle, the climatic chamber is capable of reaching a 33-70% RH transition in 20 minutes and 75-50% RH in 30 minutes. However, the ends of the two transitions are really slow and need further improvement to get closer to a step solicitation. The actual humidity values are also higher than expected, with an average of 40% during the low humidity phase (6.20PM-10.20AM) and 75.3% during the high humidity phase (10.20AM-6.20PM). This is partly due to poor calibration of the humidity sensors regulating the chamber. It is then necessary to take into account these conditions during the computer simulations and MBV determination.

The absorption/desorption dynamics can be seen trough the mass variation of the sample. The test starts with a desorption phase from initial equilibrium humidity, which is close to 55% RH with an average of 55,1% on the hour preceding the start of the test. As expected, the practical buffer value for LHC is lower than the ideal value (**Table 1**), with an average of 2.34 $g/(m^2 \cdot \%RH)$ on the four last cycles. This can be explained by surface resistance effect (boundary layer). **Figure 8** shows measurements details for the cycle number 1, chosen as reference cycle to illustrate LHC behavior. The latent heat effects resulting of the moisture movements can be clearly seen trough the surface temperature monitoring. The surface temperature remains above air temperature during absorption phase, with a mean value of $+0.30°C$ and a maximum of $+0.67°C$, and below air temperature during desorption, with a mean of $-0.07°C$ and a maximum of $-0.21°C$. The amplitude between the minimum and maximum surface temperature is $0.81°C$.

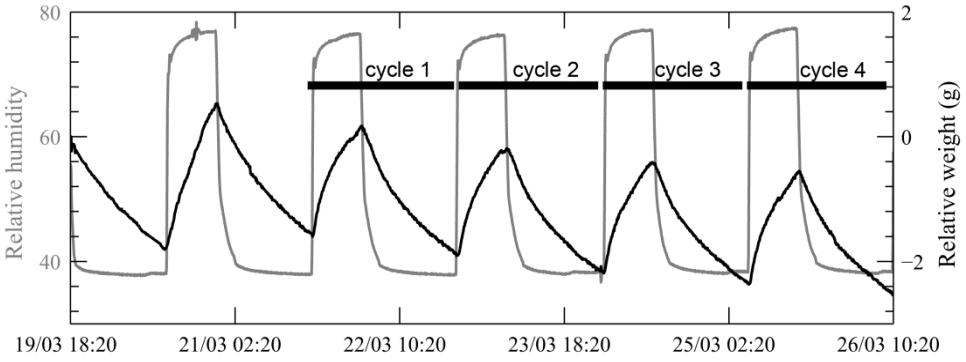

Fig. 7. The *MBV* protocol experimental curves and cycles numbers[2]

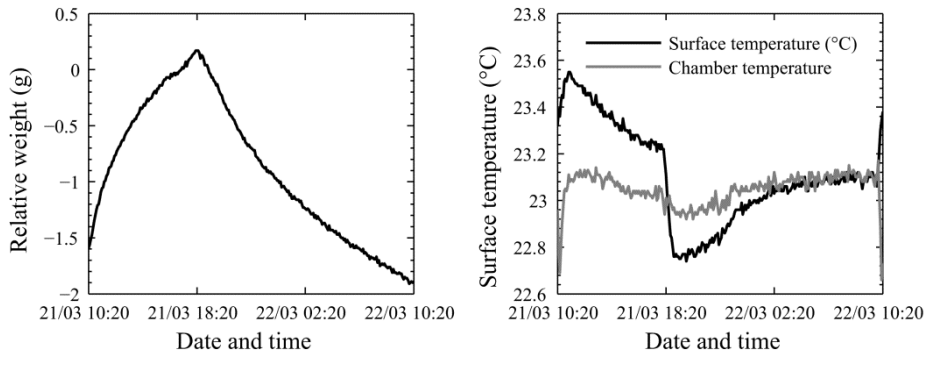

Fig. 8. Cycle number 1: relative mass variation of the sample (a); air temperature in the chamber and temperature at the surface of the bloc (b)

5.2 Mass variation modeling

Figure 9 presents the sample mass variation predicted by *COMSOL Multiphysics* and *WUFI Pro* models compared to measured data. Relative mass is defined in **Equation 17**. In addition,

Table 4 shows results expressed in terms of practical MBV for the four complete cycles with a value for absorption phase, another for desorption phase and the mean of these two phases. Both models provide similar results with a small over-evaluation of moisture exchange, larger in the case of *WUFI Pro* simulation.

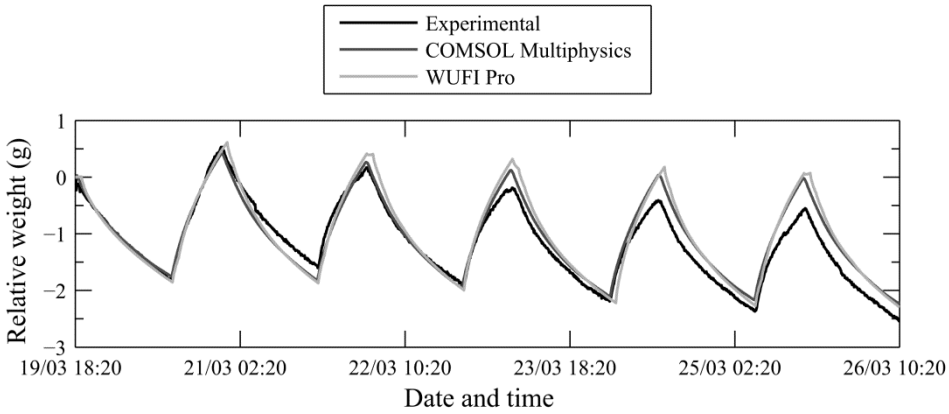

Fig. 9. Relative mass variation of the sample during the MBV determination cycles compared to models outputs

Table 4. $MBV_{practical}$ $(g/(m^2 \cdot \%RH))$ results for the experimental and the simulated data sets

	ΔRH	Cycle 1			Cycle 2			Cycle 3			Cycle 4		
		Abs.	Des.	Mean	Abs.	Des.	Mean	Abs.	Des.	Mean	Abs.	Des.	Mean
Experimental	~35.3%	2.13	2.57	2.35	2.15	2.52	2.34	2.24	2.44	2.34	2.27	2.51	2.39
COMSOL Multiphysics	~35.3%	2.41	2.73	2.57	2.61	2.81	2.71	2.70	2.74	2.72	2.67	2.78	2.72
WUFI PRO	~35.3%	2.67	2.91	2.79	2.91	3.16	3.04	2.88	3.03	2.96	2.94	2.98	2.96

The performance indicators were computed for the two models and are provided in **Table 5**. They give similar values for both modeling environments with a slightly better performance of the proposed model. Nash-Sutcliffe efficiency is above 0.8 in both cases, implying a satisfactory modeling. However, the PBIAS indicates clearly the overestimation tendency of the models, which stays below the 15% limit. Comparison between the PBIAS and RMSE points out a better performance of *COMSOL* simulation. To complete the analysis, correlation plots are represented in **Figure 10** showing scattering of $(X_{obs,i}, X_{model,i})$ points around the identity line. The dashed line represents the best linear regression between modeled and experimental points. A perfect model would of course give a regression line equal to identity line.

Table 5. Efficiency criteria for mass variation modeling

	NSE	PBIAS	RMSE
COMSOL Multiphysics	0.89	-7.51%	0.22g
WUFI PRO	0.84	-9.47%	0.27g

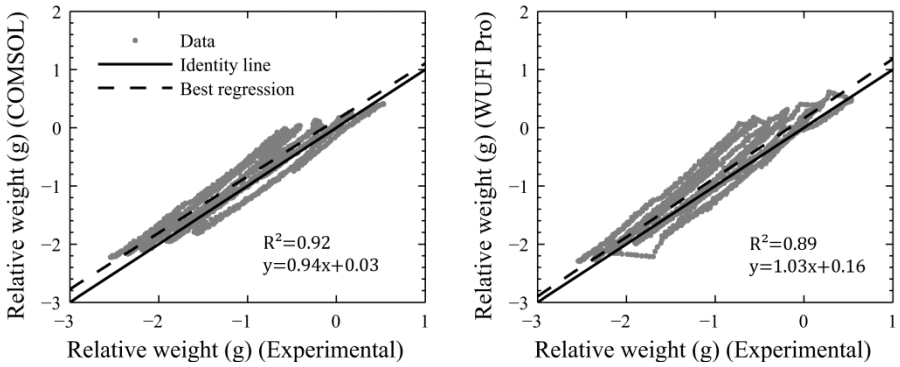

Fig. 10. Correlation plots of relative mass variation modeling

5.3 Surface temperature modeling

Surface temperature results are presented in **Figure 11**. The general shape of the temperature variation seems to be accurately predicted by both models in spite of a clear discrepancy for the amplitude. Temperature is systematically higher than observed during absorption phases and lower during desorption phases for both models. In other words there is an overestimation of surface latent heat effects.

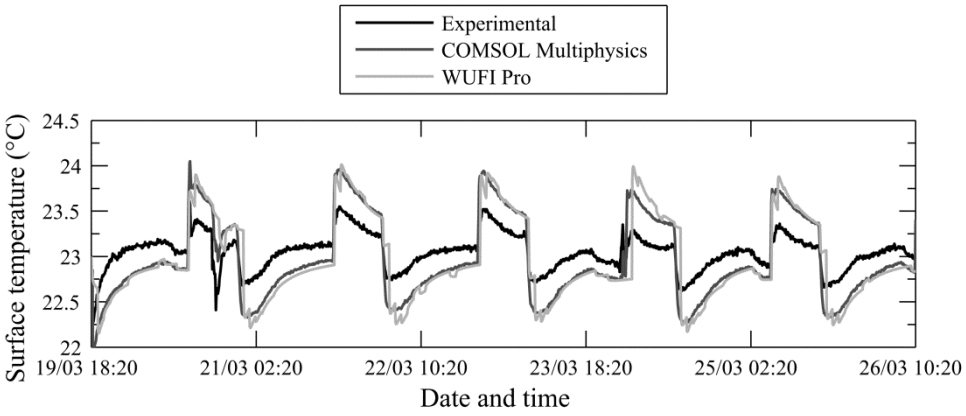

Fig. 11. Surface temperature of the sample during the MBV determination cycles compared to models outputs

Given the performance indicators, which are presented in **Table 6**, it is possible to evaluate quantitatively the accuracy of surface temperature description. The NSE is lower than zero for both models indicating very poor prediction. The PBIAS are really low due to the mathematical nature of this indicator, which only evaluate systematic over or under-prediction.

Table 6. Efficiency criteria for surface temperature modeling

	NSE	PBIAS	RMSE
COMSOL Multiphysics	-1.24	0.36%	0.295°C
WUFI PRO	-2.09	0.38%	0.346°C

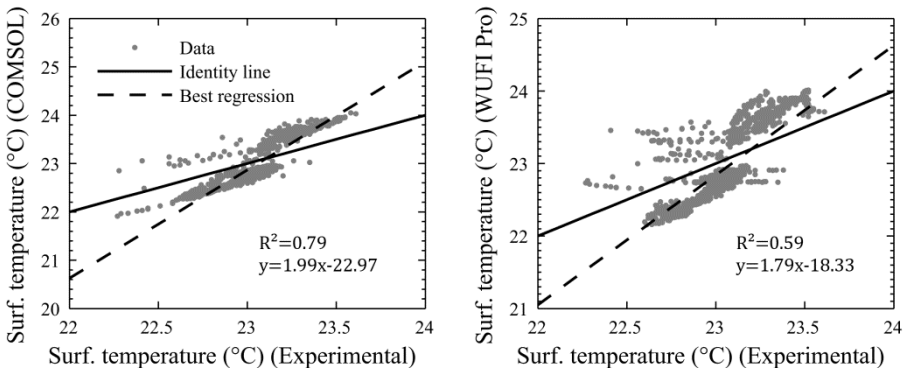

Fig. 12. Correlation plots of surface temperature modeling

The difference between the experimental and simulated data sets could be explained either by experimental bias or improper surface transfer coefficients definition. Anyway it was proved the *COMSOL* BEHAM model performs as well as the validated code. The surface temperature variation is really interesting to observe and its shape is correctly accounted for, translating a good characterization of involved phenomena. One of the remaining challenges is to evaluate correctly the impact of such effects on the thermal efficiency of materials that could bring some additional credit to the crop-based products.

6. CONCLUSIONS AND PERSPECTIVES

Accurate BEHAM models are necessary to account for moisture exchange capacity of hygroscopic materials, which can greatly influence the characterization of building performance. Lately, *COMSOL Multiphysics* was partially benchmarked and presented as a valuable alternative to standard BEHAM tools. It offers advantages in the research field, particularly with regards to its modularity and interoperability. In this paper, a MBV determination experiment was led to gather experimental data that could be compared to the output of a hygrothermal model developed in *COMSOL* computational environment. For this purpose, a complete MBV test platform was developed and improved with a surface temperature monitoring system. The studied material, the Lime-Hemp Concrete, belongs to crop-based materials, which are being widely promoted and have a strong moisture buffer capacity linked to their high porosity and hygroscopicity.

First, the partial differentials equations for heat and moisture transport were presented with associated relations and material functions. The model was then reformulated for the case study and calibrated for LHC characterization. In order to obtain an objective assessment of model performance, an efficiency indicator and two error indices were used as prescribed in watershed modeling field. Output data sets were compared to a validated BEHAM tool showing good agreement between the two software. As a conclusion, the *COMSOL* BEHAM tool is able to solve high MBV material behavior in an adaptable way. On the one hand, moisture exchanges

were predicted accurately by both models, i.e. the computed indicators remain within the limits sets with a slight advantage for *COMSOL*. On the other hand, resulting temperature variations on the surface of the specimen indicate an overestimation of latent heat effect amplitude for both computations. This marks the necessity of further research on crop-based products as well as additional parameters optimization. In this perspective, large opportunities are introduced by using such an HAM tool. It offers the possibility of solving problems in 1D, 2D or 3D with research oriented modularity. The incorporated description of porous space based on Häupl & Fechner (2003) gives the storage and transport function on the whole moisture content, which is promising in solving more complex building physics problems involving crop-based products. Finally, the interoperability of *COMSOL* allows for inverse modeling to optimize material parameters, taking advantage of software package like *DREAM* (ter Braak, 2006) in Matlab.

NOMENCLATURE

c_0	(J/kgK)	Specific heat of the dry material
c_α	(J/kgK)	Specific heat of the α-phase
h	(J/kg)	Total specific enthalpy stored in the porous material
h_α	(J/kg)	Specific enthalpy of the α-phase
$\vec{j}_c^{M_l}$	$(kg/(m^2 s))$	Mass flux density of liquid water through capillary transport
$\vec{j}_d^{M_v}$	$(kg/(m^2 s))$	Mass flux density of vapor through diffusion
$\vec{j}_{cond}^{Q}$	(W/m^2)	Thermal conduction flux density
K_l	(s)	Liquid water conductivity of the porous material
p_c	(Pa)	Capillary pressure
p_{sat}	(Pa)	Saturation vapor pressure
p_α	(Pa)	Pressure of the α-phase
T	(K)	Temperature
v	(kg/m^3)	Absolute humidity
δ_{v0}	$(kg/Pa.m.s)$	Vapor permeability of the dry porous material
δ_v	$(kg/Pa.m.s)$	Vapor permeability of the porous material
ε	$(-)$	Total open porosity of the porous material
θ_α	(m^3/m^3)	Volumetric fraction of the α-phase
λ_0	(W/mK)	Thermal conductivity of the porous material in dry state
λ	(W/mK)	Thermal conductivity of the porous material
ξ	$(m^3/(m^3 \cdot \%RH))$	Moisture capacity
ρ	(kg/m^3)	Total density of the material
ρ_0	(kg/m^3)	Mass density of the dry porous material
ρ_α	(kg/m^3)	Mass density of the α-phase
σ^{M_α}	$(kg/(m^3 s))$	Mass source/sink terms for the α-phase
σ^{Q}	(W/m^3)	Heat source/sink
φ	$(-)$	Relative humidity

Subscripts

l	Related to liquid water
v	Related to water vapor
g	Related to the gaseous mixture of dry air and water vapor
a	Related to dry air

REFERENCES

Abadie, M. O. and Mendonça, K. C. (2009). Moisture performance of building materials: From material characterization to building simulation using the Moisture Buffer Value concept. *Building and Environment, 44*(2), 388-401.

Bear, J. (1988). Dynamics of fluids in porous media. Dover Publications, New York. 784 p.

Collet, F., Bart, M., Serres, L. and Miriel, J. (2008). Porous Structure and Vapour Sorption of Hemp-based Materials. *Constr. Build. Mater.*, 22, 1271–1280.

Evrard, A. and De Herde, A. (2010). Hygrothermal Performance of Lime-Hemp Wall Assemblies. *Journal of Building Physics, 34*(1), 5-25.

Glaser, H. (1959). Graphisches Verfahren zur Untersuchung von Diffusionsvorglinge. *Kalfetechnik, 10, 345-349.*

Hagentoft, C.-E., Kalagasidis, A. S., Adl-Zarrabi, B., Roels, S., Carmeliet, J., Hens, H. and Djebbar, R. (2004). Assessment Method of Numerical Prediction Models for Combined Heat, Air and Moisture Transfer in Building Components: Benchmarks for One-dimensional Cases. *Journal of Thermal Envelope and Building Science, 27*(4), 327-352.

Häupl, P. and Fechner, H. (2003). Hygric Material Properties of Porous Building Materials. *Journal of Thermal Envelope and Building Science, 26*(3), 259-284.

Häupl, P., Grunewald, J., Fechner, H. and Stopp, H. (1997). Coupled heat air and moisture transfer in building structures. *International Journal of Heat and Mass Transfer, 40*(7), 1633-1642.

Janssens, A., Woloszyn, M., Rode, C., Kalagasidis, A. S. and De Paepe, M. (2008). From EMPD to CFD : overview of different approaches for Heat Air and Moisture modeling in IEA Annex 41. Proceedings of the IEA ECBCS Annex 41 Closing Seminar, Conference, Denmark.

Kalagasidis, A. S. (2004). HAM-Tools : an integrated simulation tool for heat, air and moisture transfer analyses in building physics. Ph.D. Thesis, Dept. of Building Technology, Building Physics Division, Chalmers University of Technology, Sweden.

Kalagasidis, A. S., Weitzmann, P., Nielsen, T. R., Peuhkuri, R., Hagentoft, C.-E. and Rode, C. (2007). The International Building Physics Toolbox in Simulink. *Energy and Buildings, 39*(6), 665-674.

Künzel, H. M. (1995). Simultaneous heat and moisture transport in building components : one- and two- dimensional calculation using simple parameters. IRB Verlag.

Li, Y., Fazio, P. and Rao, J. (2012). An investigation of moisture buffering performance of wood paneling at room level and its buffering effect on a test room. *Building and Environment, 47*(1), 205-216.

Moriasi, D. N., Arnold, J. G., Van Liew, M. W., Bingner, R. L., Harmel, R. D. and Veith, T. L. (2007). Model evaluation guidelines for systematic quantification of accuracy in watershed simulations. *Transactions of the ASABE, 50*(3), 885-900.

Osanyintola, O. F. and Simonson, C. J. (2006). Moisture buffering capacity of hygroscopic building materials: Experimental facilities and energy impact. *Energy and Buildings, 38*(10), 1270-1282.

Padfield, T. (1999). The role of absorbent building materials in moderating changes of relative humidity. Ph.D. Thesis, Dept. of Structural Engineering and Materials, Technical University of Denmark, Denmark.

Pedersen, C. R. (1991). A transient model for analyzing the hygrothermal behavior of building constructions. Proceedings of the 3rd IBPSA, Conference, France.

Peuhkuri, R. H., Mortensen, L. H., Hansen, K. K., Time, B., Gustavsen, A., Ojanen, T. and Harderup, L.-E. (2005). Moisture Buffering of Building Materials. In C. Rode (Ed.): Department of Civil Engineering, Technical University of Denmark.

Philip, J. R., De Vries, D. A. (1957). Moisture movement in porous materials under temperature gradients. *Trans. Am. Geophys. Union, 38, 222-232*

Rode, C. and Grau, K. (2008). Moisture Buffering and its Consequence in Whole Building Hygrothermal Modeling. *Journal of Building Physics, 31*(4), 333-360.

Roels, S. and Janssen, H. (2006). A Comparison of the Nordtest and Japanese Test Methods for the Moisture Buffering Performance of Building Materials. *Journal of Building Physics, 30*(2), 137-161.

Samri, D. (2008). Analyse physique et caractérisation hygrothermique des matériaux de construction : approche expérimentale et modélisation numérique. Ph.D. Thesis, Institut National des Sciences Appliquées de Lyon, France

Scheffler, G. A. and Plagge, R. (2010). A whole range hygric material model: Modelling liquid and vapour transport properties in porous media. *International Journal of Heat and Mass Transfer, 53*(1–3), 286-296.

Tariku, F., Kumaran, K. and Fazio, P. (2010a). Integrated analysis of whole building heat, air and moisture transfer. *International Journal of Heat and Mass Transfer, 53*(15–16), 3111-3120.

Tariku, F., Kumaran, K. and Fazio, P. (2010b). Transient model for coupled heat air and moisture transfer through multilayered porous media. *International Journal of Heat and Mass Transfer, 53*(15–16), 3035-0344.

ter Braak, C. J. F. (2006). A Markov Chain Monte Carlo version of the genetic algorithm Differential Evolution: easy Bayesian computing for real parameter spaces. *Statistics and Computing*, 16, 239-249.

van Schijndel, A. W. M. (2009). Integrated modeling of dynamic heat, air and moisture processes in buildings and systems using SimuLink and COMSOL. *Building Simulation, 2*(2), 143-155.

Woloszyn, M. and Rode, C. (2008). Tools for performance simulation of heat, air and moisture conditions of whole buildings. *Building Simulation, 1*(1), 5-24.

CHAPTER 5

Parameter estimation

5.1 Introduction

As shown in **Chapter 3**, some construction materials do not easily conform to the standard measurement techniques dedicated to the determination of steady-state transfer functions. Moreover, there is still some uncertainty in the representativeness of such parameters to study the transient behaviour of materials and some properties are difficult to assess, like the liquid transport function. Parameter optimization techniques offer great perspectives in Building Physics. This is a valuable alternative to time-consuming experimental protocols.

In the appended paper we show how it is possible to use the BEHAM research model (presented in **Chapter 4**) to perform parameter estimation in an inverse modelling approach. The general computational environment in which it was elaborated offers a large integration potential and could interact with many other modelling tools. Here, the BEHAM model is combined to the DREAM parameter sampling algorithm. The latter is based on Bayesian approaches, widely used in scientific domains where there is a large uncertainty in models parameters, *e.g.* in watershed modelling (Vrugt et al., 2009) or crop yield prediction (Dumont et al., 2014).

5.2 Appended paper

An Inverse Modelling Approach to Estimate the Hygric Parameters of Clay-Based Masonry during a Moisture Buffer Value Test

Samuel DUBOIS*[1], Fionn McGREGOR[2], Frédéric LEBEAU[1], Arnaud EVRARD[3], Andrew HEATH[2]

[1]Dept. of environmental sciences and technologies, Gembloux Agro-Bio Tech, University of Liege, Belgium

[2]Dept. of Architecture and Civil engineering, University of Bath, UK

[3]Architecture et Climat, Université Catholique de Louvain, Belgium

*Corresponding author, supported by a F.R.I.A Grant,
Address: Dept. of environmental sciences and technologies, Gembloux Agro-Bio Tech, 2 Passage des déportés, 5030 Gembloux, Belgium (s.dubois@doct.ulg.ac.be)

KEYWORDS

Moisture Buffer Value, Clay, HAM Modelling, Parameter estimation, MCMC, DREAM

STATUS

Published in:

Building & Environment, 2014

ABSTRACT

This paper presents an inverse modelling approach for parameter estimation of a model dedicated to the description of moisture mass transfer in porous hygroscopic building materials. The hygric behaviour of unfired clay-based masonry samples is specifically studied here and the Moisture Buffer Value (MBV) protocol is proposed as a data source from which it is possible to estimate several parameters at once. Those include materials properties and experimental parameters. For this purpose, the mass of two clay samples with different compositions is continuously monitored during several consecutive humidity cycles in isothermal conditions. Independently of these dynamic experimental tests, their moisture storage and transport parameters are measured with standard steady-state methods.

A simple moisture transfer model developed in COMSOL Multiphysics is used to predict the moisture uptake/release behaviour during the MBV tests. The set of model parameters values that minimizes the difference between simulated and experimental results is then automatically estimated using an inverse modelling algorithm based on Bayesian techniques. For materials properties, the optimized parameters values are compared to values that were experimentally measured in steady state. And because a precise understanding of parameters is needed to assess the confidence in the inverse modelling results, a sensitivity analysis of the model is also provided.

1. INTRODUCTION

Clay has been used as a construction material since man has started building. In 2012 UNESCO released an inventory of Earth construction heritage sites [1]. It shows the immense legacy of earth construction and earth architecture around the world. These sites demonstrate how durable this material can be. In modern times earth has to compete with materials such as concrete and due to its natural variability, earth is often considered as a primitive material not fit for modern construction. However, earth based masonry and renders have many qualities that are becoming more and more important in the context of global climate change and the challenge to reduce carbon emissions. The choice of using earth as a construction material varies depending on the economical situation of a country. In developing countries earth is a cheap material that can often be sourced close to the building site making it the first choice for economical reasons. In richer industrialised countries, earth is chosen for its sustainable, highly hygroscopic and aesthetic qualities [2].

Clay-based materials show high moisture storage capacity through surface adsorption and capillary condensation effects in the hygroscopic domain. Such phenomena coupled with moisture transport inside the porous structure are stated to offer a regulation capacity of the indoor air humidity [3], improving comfort for occupants [4-6]. One way to quantify this regulation behaviour is to evaluate the moisture buffer capacity, i.e. the moisture exchange capacity under a dynamic exposure to ambient relative humidity (RH) cycle. The relative humidity variations can be caused either by temperature change of the ambient air or through changing the amount of moisture in it.

The NORDTEST project [7] has been one of the first attempts to find a consensus for an experimental protocol able to adequately characterize the buffer capacity through the definition of a global parameter called the Moisture Buffer Value (MBV). Beside the direct humidity regulation that is evaluated by the MBV at material scale, the buffer performance of hygroscopic materials also causes latent heat effects whose impact on energy balance is only partially assessed [8].

Along with the will to characterize porous hygroscopic and capillary materials experimentally, the modelling of their behaviour has progressed substantially in the last decades [9-12]. Indeed, Heat Air and Moisture (HAM) models which deal with detailed hygrothermal analysis of porous materials have improved in accuracy through the development of computer power and a better knowledge of the involved phenomena. Many HAM computer models and associated software have been developed for building applications and some have been commercialized [13, 14]. The main difference between the models is in the description of the moisture flows that can have several levels of complexity, ranging from diffusivity models using moisture content as driving potential to conductivity models using the actual thermodynamic driving potential and separated liquid and vapour flows [15]. All these models rely on material and boundary

condition parameters, most of them being time consuming to obtain.

The computation of temperature and moisture content fields in building materials, from the known parameters and boundary conditions forms a *direct HAM problem* [16]. This approach is the most common in Building Physics, where the aim is often to predict the behaviour of material assemblies under various climatic solicitations. The validity of such approaches relies on the quality of characterization for the hygrothermal properties of the material. In contrast to direct modelling process, there exist several methods that allow parameter estimation from temperature and moisture content field measurements, which establishes a new kind of *inverse HAM problem*. Among inverse modelling methods, the Bayesian approaches are becoming more and more popular in environmental models. In Bayesian optimization, parameters are not unknowns with a single value to determine, but stochastic variables whose distributions have to be specified. The distribution given before estimation is called 'a priori' and the distribution given after integration of the experimental data is called 'a posteriori'. Historically, the emergence of the Markov Chain Monte Carlo (MCMC) simulations with the Random Walk Metropolis algorithm as first widely used approach [17] have greatly simplified the estimation of posterior distribution of parameters. Recently, Ter Braak [18] developed the Differential Evolution-Markov Chain (DE-MC) method, able to run several Markov chains in parallel with a so called 'genetic' algorithm for the sampling process, improving the parameter space exploration efficiency. The Differential Evolution Adaptive Metropolis (DREAM) algorithm [19, 20] is an evolution of the DE-MC, able to automatically tune the scale and orientation of the proposed parameter distributions (i.e. self-adaptive randomized subspace sampling) during the evolution towards posterior distribution. A good review about Bayesian approaches and inverse modelling algorithms evolution can be found in [21].

The goal of this paper is to illustrate the use of a MCMC sampler to estimate the parameters of a HAM model in an inverse modelling problem. For this purpose, we propose to study the applicability of the MBV protocol as the source of experimental data to estimate hygric properties of porous construction materials. Specifically, the mass variation of different clay-based samples is measured experimentally during a MBV test. In parallel, their moisture storage and transport properties are measured in steady-state conditions. The DREAM algorithm is then coupled to a simplified moisture transfer model which simulates the moisture exchange of samples. The parameters sampling process consists in automatically tuning the HAM model in order to match experimental mass variation by testing various combinations of parameters values and evaluating the resulting model efficiency. Eventually, the inverse modelling approach can propose a 'best parameters set' which minimizes the difference between the simulated and the measured moisture uptake/release of sample. Four parameters are estimated in this paper; two are directly related to the material and two others linked to experimental conditions. For the

first category, the best estimated parameters resulting from the inverse modelling approach can be compared to their corresponding value measured in steady-state.

The questions arising from this study are: (1) how the different model parameters interact during the MBV cycle, with possible correlations; (2) is it reliable to use this single dynamic experiment to retrieve several parameters at once with the inverse modelling method; (3) do the dynamic conditions of the MBV test offer a more 'realistic' configuration for material properties assessment?

2. THE MOISTURE BUFFER VALUE

The need for a standardized parameter to characterize the moisture buffering capacity of materials led to the definition of the Moisture Buffer Value (MBV) during the NORDTEST project [4] together with the proposal of a dynamic experimental protocol for materials classification. The practical MBV is defined as : *"the amount of water that is transported in or out of a material per open surface area, during a certain period of time, when it is subjected to variations in relative humidity of the surrounding air"* [7]. Concretely, the samples are subjected to cyclic step changes in relative humidity (RH) at a constant temperature of $23\ °C$ and are weighted regularly. The cycle is composed by moisture uptake during 8 hours at high RH followed by moisture release 16 hours at low RH and is repeated until constant mass variation between 2 consecutive cycles is reached. The practical MBV in $kg/(m^2 \cdot \%RH)$ is then given by Eq.1.

$$MBV_{practical} = \frac{\Delta m}{A \cdot \Delta RH} \tag{1}$$

where Δm is the mass variation during the 8 hours absorption phase or the 16 hours desorption phase in one complete cycle, A (m^2) is the total exchange surface and ΔRH is the difference between the high and low relative humidity of the cycle. This experimental value is a direct measurement of the amount of moisture transported to and from the material for the given exposure cycle. In the original protocol, the cycle is fixed to a 75/33%RH scheme.

A theoretical value of the MBV, called MBV_{ideal}, can be computed analytically using semi-infinite solid theory and Fourier series without transfer resistance at exchange surface. There is always a disagreement between measured and analytically calculated due to the dynamic nature of the experimental protocol, the film resistance on specimen exchange surface and deviations from the typical step transitions . However is has been shown in McGregor et al. [22] that a good agreement can be found between measured and calculated MBV when reducing the film resistance in the dynamic test and improving the precision of the steady state measured properties.

3. MATERIALS AND METHODS

3.1 Samples

Two different soils were used for the experimental measurement. The *Gr* soil is a natural soil extracted from the Wealden clay group in the UK. The natural soil had high clay content, so 50% by weight of fine builders sand was added. The final particle size distribution consisted of 18% of clay, 24% of silt and 58% of sand. The *Mt* is a manufactured soil; it was prepared with 10% of a commercial bentonite, 15% of kaolin clay, 20% of silt and 55% of sand.

The tested sample blocs have all three a cylindrical shape and a nominal height of 3cm, which is stated sufficient given the theoretical moisture penetration depth during the MBV experiment. Lateral and back faces are sealed from water exchange with aluminium tape providing one-dimensional conditions. **Table 1** gives the general physical properties of the samples including their volume, true exchange surface area and dry density.

Table 1. Properties of the tested samples

	Volume of sample cm^3	Exchange surface area m^2	Dry density kg/m^3
Gr8	21.92	0.0078	2010
Mt9	24.06	0.008	1860

The vapour resistance factors of the two samples were determined by the wet cup method described by the ISO 12572 Standard. Samples are sealed on the top of a cup containing potassium nitrate solution. The cup is placed in a chamber at 50%HR and 23°C, giving typically 94 ± 0.60%HR in the air layer above the salt solution. The processed results give a value of $\mu =$ 8.8 for *Gr8* sample and 8.3 for *Mt9* sample.

The moisture storage curves were determined by a Dynamic Vapour Sorption (DVS) system. The DVS equipment precisely records the mass of a sample of up to 4g in varying RH conditions. The sorption isotherms were precisely recorded up to 95%RH within 10 days. Above 95%RH the samples need much longer to reach Equilibrium Moisture Content (EMC) and therefore the equilibrium was not expected to be reached at these levels but this is not considered a limitation for this study as 95%RH is above the RH level from all tests. Once the adsorption curve measurement is finished, the DVS apparatus initiates the reverse cycle to obtain the experimental points of the desorption curve. All equilibrium moisture content values are expressed as variable u (in kg of water per kg of dry material, noted in figures in a simplified manner as kg/kg). **Figure 1** shows the DVS curves for the two tested materials.

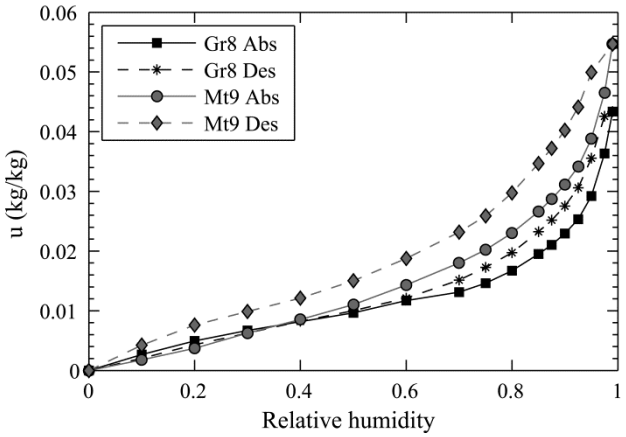

Fig. 1. Moisture storage curves

It can be observed that absorption curves only start to rise steeply from around 80% due to the increase of capillary condensation effects. As a consequence, it is assumed that hysteresis phenomena are negligible during the MBV experiments performed later and only absorption curves will be considered. Indeed, the chosen relative humidity cycle imposed on samples is 16hrs at 50% and 8hrs at 85%. A relative humidity superior to 80% is thus not expected to be found during a prolonged period in the material. . For each material, a continuous moisture storage function $u(\varphi)$ is then fitted on absorption experimental points by minimizing the sum of least squared errors. The Smith [23] model was selected for its easy handling and the good description in the range of humidity considered:

$$u(\varphi) = C_1 + C_2 \ln(1 - \varphi) \tag{2}$$

where C_1 and C_1 are empirical parameters. **Table 2** shows the optimized values for both materials. A major advantage of using Smith function is an expression of the moisture capacity $\xi = \frac{\partial u}{\partial \varphi}$ dependant only on one constant parameter:

$$\xi(\varphi) = \frac{C_2}{\varphi - 1} \tag{3}$$

This is particularly interesting in the inverse modelling approach that we introduce in this paper as it will limit the number of parameters needed to characterize the behaviour of the sample during the MBV experiment. Moreover, the data in **Table 2** shows that *Mt9* material has a greater moisture capacity in comparison to *Gr8* and is thus expected to show a greater practical MBV as its vapour resistance factor is also smaller. **Figure 2** shows the fitted Smith functions and experimental points on the 50-90% range for both samples as well as obtained moisture capacities functions.

Table 2. Smith model empirical parameters fitted on the 50-90%RH range for absorption curves

Parameters	*Gr8* Abs	*Mt9* Abs
C_1	0.0036	0.0029
C_2	-0.0083	-0.0124

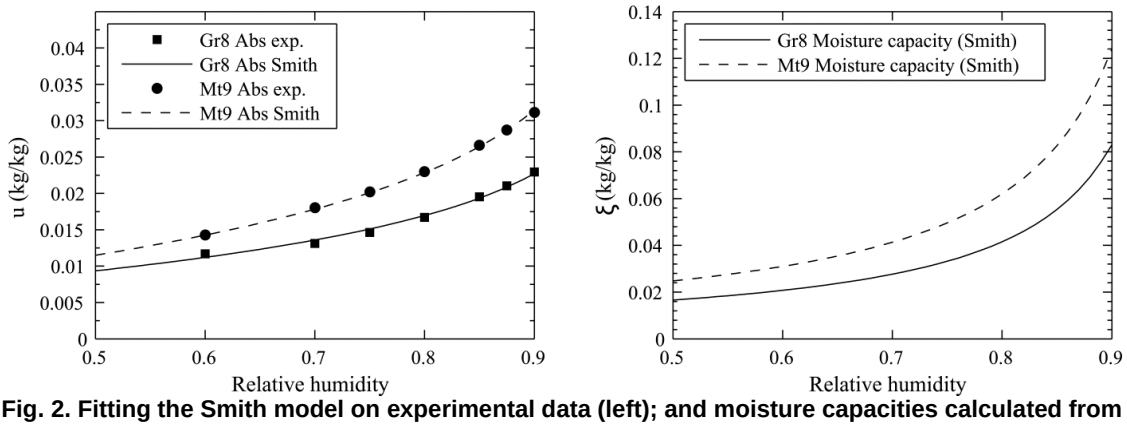

Fig. 2. Fitting the Smith model on experimental data (left); and moisture capacities calculated from Smith model (right)

3.2 MBV Test platform

The MBV was recorded in a climatic chamber (*TAS*) offering a stability of +/- 0.3 to 1.0°C and +/- 3.0 % of RH. As previously said, the test chamber was set to produce cycles of 85%RH during 8 hours and 50%RH during 16 hours with a constant temperature of 23°C. The values used where consistently used at the University of Bath and are better representations of the climate in the UK than the values used for the NORDTEST protocol. The weight of the samples were continuously logged with a reading every minute on a scale (*Ohaus*) with a precision of 0.01g. The scale and the sample were covered with a wind shield to maintain an air velocity as close as possible to 0.1m/s which was recommended by the NORDTEST and is typical of the interior air velocity in a building. The samples were conditioned at 19°C and 55%RH in an environmental controlled room. The tests run for at least 7 consecutive cycles so the behaviour over a longer period can be observed. Relative humidity and temperature sensors (*Tinytag*) recoded the internal conditions above the specimens for control. **Figure 3** shows the complete experimental set-up.

The relative humidity transitions are close to perfect steps with times of 12min for low to high RH transitions and 14min for high to low RH. The control sensors put in the chamber indicate a mean measurement of 85.9%RH during adsorption phase and 49.6%RH during desorption phase. The measured dynamic humidity cycle is used as input for boundary conditions during the modelling phase instead of ideal step transitions with chamber set points. Concerning the temperature, a mean value of 23.21°C was measured during the whole cycle and this constant value was used to determine vapour saturation pressure when needed.

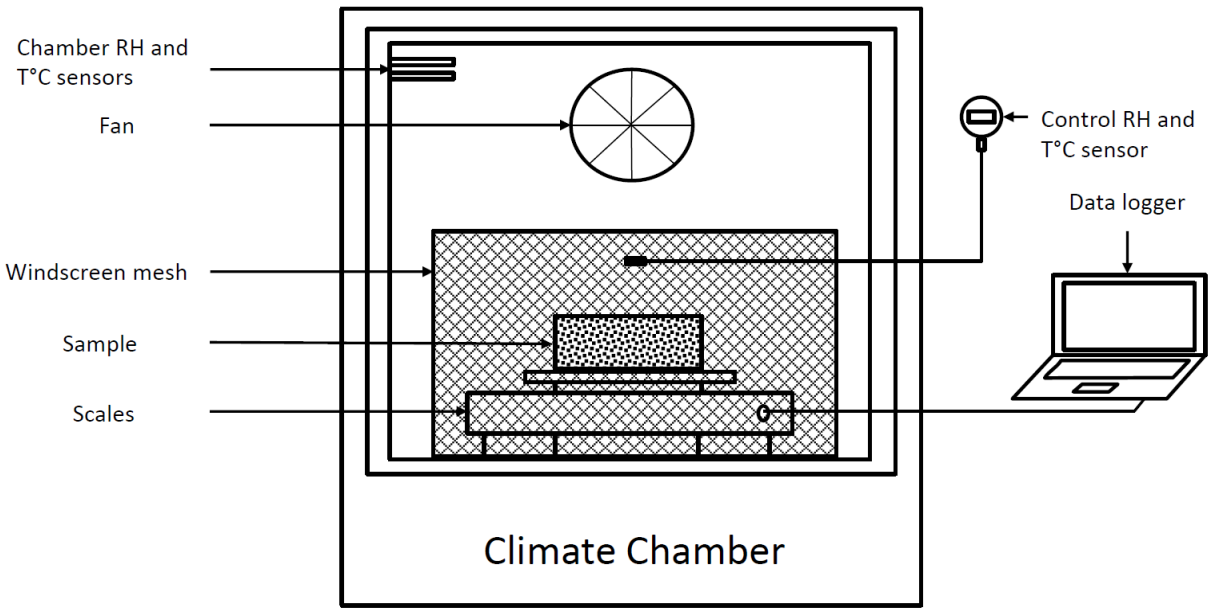

Fig. 3. Experimental set-up

Figure 4 presents the measured ambient relative humidity and temperature in the chamber during a typical 24hrs cycle.

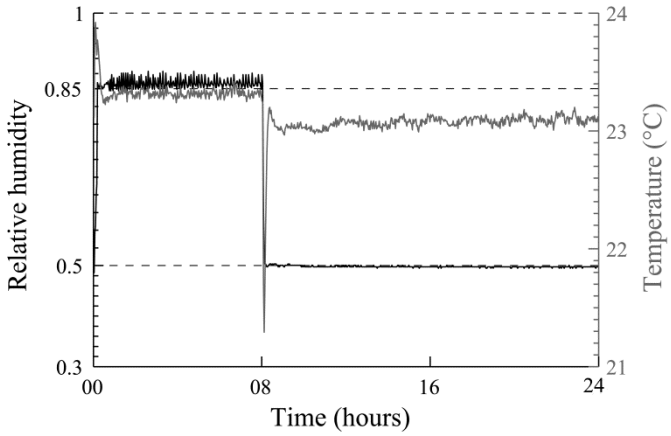

Fig. 4. Ambient conditions in the chamber

3.3 Description of the moisture transfer model

3.3.1 Moisture balance equation

Modelling the hygric behaviour of the clay-based samples during the MBV determination experiment is considered as a tool for parameter estimation through an inverse modelling approach. The moisture transfer model was developed in *COMSOL Multiphysics* and is interoperable with the parameter sampling algorithm that is encoded in Matlab and presented in the next section.

The following hypotheses were taken for the mathematical description of mass transfer:

(1) The soil sample is non-deformable and isotropic; (2) the fluid phases do not chemically react with the solid matrix; (3) The dry air pressure is constant (no air advection) and the total gas pressure gradients are considered negligible; (4) no liquid transport is considered and vapour pressure is the only driving potential for moisture movement; (5) there is a local thermodynamic equilibrium between the different phases; (6) there is no thermal diffusion (Soret effect); (7) no hysteresis phenomena is present as explained before.

The dependent variable chosen for this problem is the relative humidity φ and which was solved in 1D. Since the experiment was conducted under isothermal conditions, the heat balance equation was not considered here, even if some latent effects near the surface of the material might happen. For a material having an ideal MBV similar to the clay samples considered here, Dubois et al. [24] showed that, during a MBV test with 33/75%RH cycles, the amplitude of temperature variation at sample surface was very low (less than 3°C). In consequence, it can be assumed here that temperature does not have a significant impact on the moisture exchange behaviour.

Since the experiment was conducted under isothermal conditions, the heat balance equation is not considered here, even if some latent effects near the surface of the material might alter slightly the moisture transfer [24]. The mass conservation equation was formulated with relative humidity φ as main dependent variable:

$$\rho_0 \cdot \xi(\varphi) \cdot \frac{\partial \varphi}{\partial t} = \frac{\delta_a p_{sat}}{\mu} \cdot \frac{\partial^2 \varphi}{\partial x^2} \tag{4}$$

where $\xi\ (kg_v \cdot kg_0^{-1})$ is the isothermal moisture capacity considered constant for the given RH interval and $p_{sat}\ (Pa)$ is vapour saturation pressure considered constant during the simulation and calculated from mean temperature in the chamber during the test (**Fig. 4**). The vapour permeability of the sample is expressed here in terms of vapour resistance factor $\mu = \frac{\delta_a}{\delta}\ (-)$ where δ and $\delta_a\ (kg \cdot Pa^{-1} \cdot m^{-1} \cdot s^{-1})$ are the vapour permeabilities of the sample and dry air respectively.

3.3.2 Boundary conditions

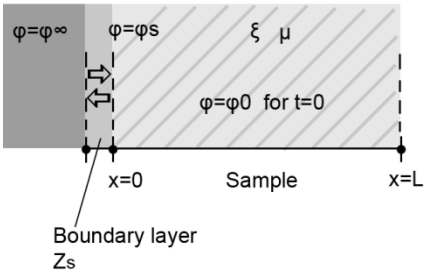

Fig. 5. 1D representation of sample bloc with boundary layer

Referring to **Figure 5**, we can write the following boundary and initial conditions for moisture transport:

$$\left(\boldsymbol{j}_{\boldsymbol{x}}^{\boldsymbol{M_v}}\right)\cdot\boldsymbol{x} = \frac{p_{sat}(\varphi_\infty - \varphi_s)}{Z_s} \qquad x = 0 \qquad (5)$$

$$\left(\boldsymbol{j}_{\boldsymbol{x}}^{\boldsymbol{M_v}}\right)\cdot\boldsymbol{x} = 0 \qquad x = L \qquad (6)$$

$$\varphi(x, t_0) = \varphi_0 \qquad 0 < x < L \qquad (7)$$

where $\boldsymbol{j}_{\boldsymbol{x}}^{\boldsymbol{M_v}}$ $(kg \cdot m^{-2} \cdot s)$ is the vapour flux density, φ_∞ and φ_s are the ambient relative humidity and the relative humidity at the exchange surface respectively, Z_s $(Pa \cdot m^2 \cdot s \cdot kg^{-1})$ the surface resistance, t_0 (s) the initial time and φ_0 the initial relative humidity in the sample. The input data φ_∞ for the ambient air condition used as a boundary in the model were the measured RH from the experimental cycles (**Fig. 4**).

The surface resistance characterizes the moisture transfer resistance that exists on the material surface and slows down the moisture exchange. Its value is generally fixed at $5E7$ $(Pa \cdot m^2 \cdot s)/kg$ which is the usually accepted value for environments with an ambient air velocity around $0.1\ m/s$ [7]. It's similar to a value of $Z_{s,v} = 360\ s/m$ when the surface flux density is written in terms of absolute humidity:

$$\left(\boldsymbol{j}_{\boldsymbol{x}}^{\boldsymbol{M_v}}\right)\cdot\boldsymbol{x} = \frac{(\omega_\infty - \omega_s)}{Z_{s,\omega}} \qquad (8)$$

To calculate $G_v(t)$, the accumulated moisture in the sample at time t, the following integration is performed on material surface:

$$G_v(t) = \int_0^t \boldsymbol{j}_{\boldsymbol{x}}^{\boldsymbol{M_v}} dt \qquad (9)$$

After that, experimental and simulated data is easily compared through the relative weight variation of the sample:

$$\underbrace{m(t) - m_0}_{experimental} = \underbrace{G_v(t)}_{model} * A \qquad (10)$$

where $m(t)$ (kg) is the measured weight of the sample at time t, m_0 (kg) is the measured initial weight of the sample and A (m^2) is its exchange surface area (**Table 1**).

3.4 Inverse modelling approach

3.4.1 Parameter sampling and optimization algorithm

The recently developed DREAM algorithm [19] was used in order to estimate parameters of the moisture transfer model based on the observed moisture uptake/release data sets for both

samples during the MBV cycles. In the process, the *COMSOL* model was run continuously together with the parameter sampling algorithm offered by DREAM until a convergence criterion was respected. It is an optimization process as the parameters set is automatically optimized to reduce the error between simulated and observed mass variation of samples.

First, initial values of parameters were randomly generated in the prior parameter space which consists for each parameter of an uniform distribution limited by chosen probable values. Here, because multiple Markov chains run simultaneously for global parameter space exploration, an initial set of parameters values was assigned to each chain. Then, a so-called likelihood function quantified the model output closeness to experimental data for the initial parameter combination in each chain, using a classical sum of squared residuals (SSR). Only the four last experimental cycles were used to perform this quantitative comparison, although the starting point for the simulation was located at the beginning of cycle number 1.

From initial values of parameters, the differential evolution algorithm generates a new set of parameters for each chain, called a child set, as a combination of current parameters stored in all chains, called a parent set. All chains are thus updated conditionally on other chains. Based on the comparison of resulting likelihood function score between parent and child parameters, children parameters are either accepted or rejected, in which case the parent parameters are kept in the concerned chain for the next iteration step. The acceptance/reject criterion is based on the Metropolis ratio [25]. The process is then repeated until a convergence criterion is respected, i.e. a Gelman-Rubin convergence diagnostic value of 1.2 [26]. This chain updating scheme, specific to DREAM, improves greatly the efficiency of the MCMC sampling process compared to more traditional MCMC methods [20].

The output of the algorithm is a posterior distribution for each parameter, i.e. the probability distribution function of its value after statistical convergence of the MCMC sampler or in other terms, the marginal uncertainty on parameter value given the experimental observations. When the convergence diagnostic is achieved, the posterior distribution is stationary. Afterwards, the resulting possibility of analyzing the uncertainty of parameters and models outputs is a great advantage of the DREAM algorithm. An extensive study including such discussion is found in [21]. **Figure 6** illustrates the operation of the inverse modelling algorithm. It should be noted that experimental data quality plays a crucial role in parametric optimization because measurements intervene both as inputs of the model and the likelihood function. In consequence, a good confidence in the sensors gathering that information is essential.

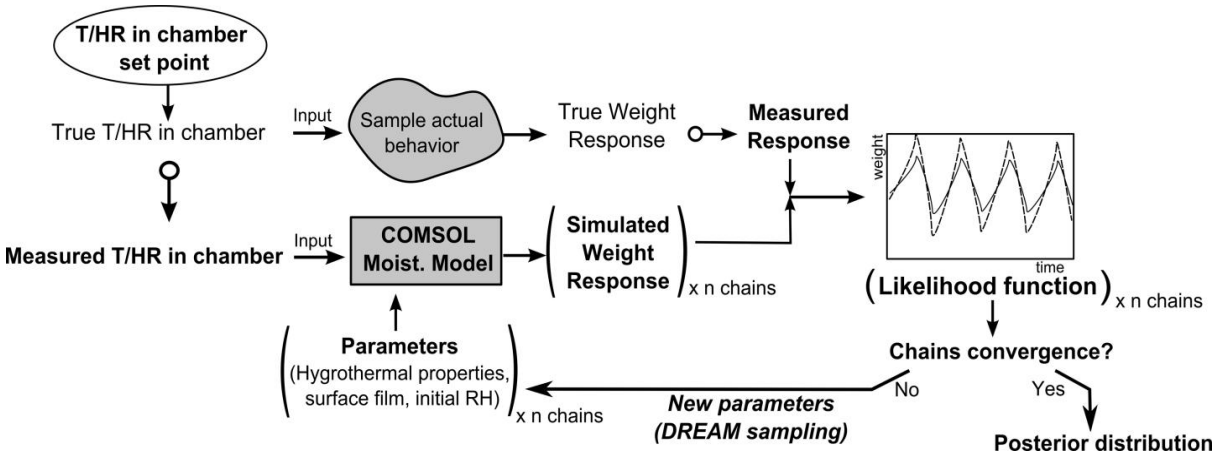

Fig. 6. Operation of the parameter sampling and optimization algorithm

3.4.2 Parameters estimates

On the basis of the posterior distribution of model parameters, one can determine parameter estimates or, in other words, 'best values' of parameters to explain experimental data. This can be done either by taking the parameter combination offering the optimal response in terms of model performance or by computing averaged values among chains which includes information about the marginal distribution.

For the first technique, referring to Dubois, Evrard [24], the Nash-Sutcliffe efficiency coefficient was used as the objective function to optimize:

$$NSE = 1 - \frac{\sum_{i=1}^{N}\left(y_i - \hat{y}_i(X,\theta)\right)^2}{\sum_{i=1}^{N}(y_i - \bar{y}_i)^2} \tag{11}$$

where $\hat{y}_i$ is a element of the $N \times 1$ vector of model outputs, $X = (X_1, X_2, \dots, X_r)$ is an $N \times r$ matrix of input values, $\theta = (\theta_1, \theta_2, \dots, \theta_d)$ is the d parameter vector, y_i is a element of the $N \times 1$ vector of measurements and $\bar{y}_i$ is the mean of all experimental observations. A NSE coefficient of 1 means a perfect fit of the model to experimental data. If the indicator falls below zero that would imply that the residual variance is larger than data variance and thereby the mean value of observed data would be a better predictor that the model. The parameter set that minimizes the NSE is written θ_{opt} and can stem from any of the Markov chains.

When it is better to summarize information about the posterior distribution in the estimates, the following mean parameter set can be computed:

$$\theta_{mean} = \frac{1}{k * 8}\sum_{j}^{8}\sum_{i}^{k}\theta_{i,j} \tag{12}$$

where θ_{mean} is called posterior mean estimate, k is the number of last elements used in each chains to perform the averaging process and $\theta_{i,j}$ is a single parameter combination in one chain

j. The number of elements to use in each chain was fixed here to k=500.

3.4.3 Parameters assumptions

For each observed mass variation data set corresponding to one clay-based material, two types of parameters are optimized. First, materials hygric properties linked to their porous structure, namely the vapour resistance factor of the sample μ and the parameter C_2 for moisture storage function model. The latter determines the moisture capacity function $\xi(\varphi)$ on the interest relative humidity range as shown in **Equation 3**. In addition to this first category, the surface resistance factor Z_s and the initial relative humidity φ_0 constitute boundary and initial conditions parameters whose posterior distributions are also estimated through the DREAM sampling process. Those two experimental parameters are very difficult to measure and the inverse modelling method potentially offers an efficient way to determine them.

All four parameters to optimize constitute the vector $\theta = (\mu, C_2, Z_s, \varphi_0)$. **Table 3** summarizes their prior distribution of probability, i.e. *a priori* knowledge of parameters typical values. It consists of uniform distributions in our case, also called noninformative priors. The boundaries are defined from "realistic values" knowing previous studies on clay and experimental conditions though the range were kept wide enough to analyze the efficiency of the parameter sampling convergence with a somewhat overdispersed parameter space.

Here, one objective is to compare the estimates of μ and C_2 with values measured experimentally in steady-state conditions, for each clay-based sample. The inverse modelling approach potentially offers a more realistic assessment of moisture transfer parameters as they are assessed from a dynamic experiment consisting of a realistic humidity cycle. Of course, such conclusions cannot be inferred if a significant doubt persists concerning the uniqueness of the solution of the optimization process.

Table 3. Prior uniform distribution of parameters

Parameter	Prior distribution	Unit
$\boldsymbol{\mu}$	[4 − 25]	/
$\boldsymbol{C_2}$	[-0.05 − 0]	/
$\boldsymbol{Z_s}$	[1E6 − 1E8]	$(Pa \cdot m^2 \cdot s)/kg$
$\boldsymbol{\varphi_0}$	[0.50 − 0.65]	/

6. RESULTS AND DISCUSSIONS

6.1 Experimental observations

The relative mass variations of both samples during the MBV characterization test, for the first

seven cycles, are shown on **Figure 7**. The last four cycles, used to perform the parameters optimization, are indicated clearly on the figure. The difference between the two materials in terms of moisture exchange capacity is directly observable. According to the measured steady-state hygrothermal properties, we know that *Mt9* material shows both higher vapour permeability and moisture capacity, resulting in a higher theoretical MBV, which is confirmed here. **Figure 8** provides the analysis of these data sets in terms of practical MBV (**Eq. 1**). Two values are provided for each cycle and each material, one for the absorption phase and one for the desorption phase. We recall here that the cycle used is of type 50/85%RH, which must be taken into account when comparing these values with other materials tested according to the 33/75%RH protocol. It should also be observed that after seven cycle repetitions a stable moisture exchange scheme is still not achieved. Indeed, if that were the case, the absorption and desorption practical MBV value would be almost identical. The speed of convergence towards equilibrium cycle is determined mainly by the initial humidity condition in the sample. Cycles stability was not required in this work because the inverse modelling approach allows to work on any dynamic data set and no comparison to ideal MBV values was attended.

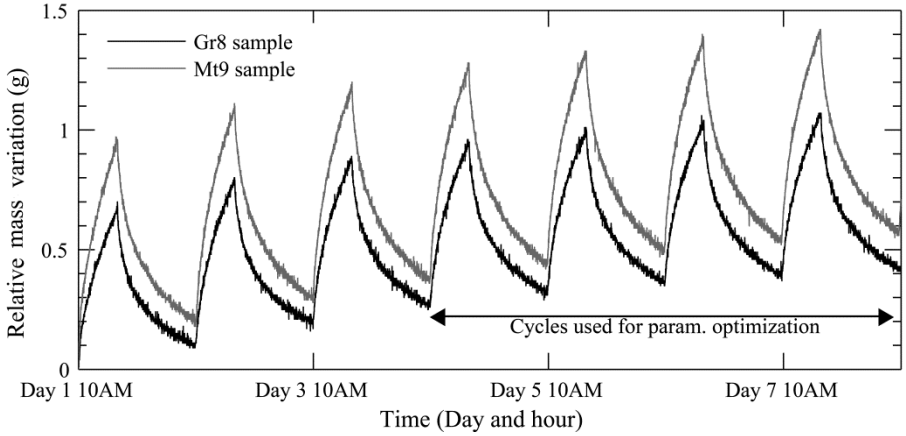

Fig. 7. Relative mass evolution of the samples during the seven first cycles

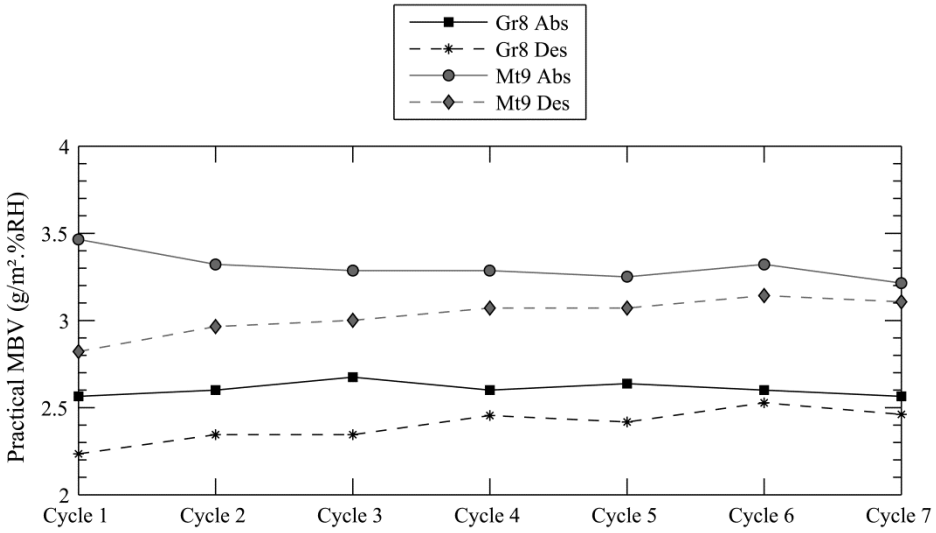

Fig. 8. $MBV_{practical\ 50\text{-}85}$ results for the experimental data sets

6.2 Optimization of model parameters

6.2.1 Parametric sensitivity study

Before going further in the parameter estimation process, it is important to assess the impact of each parameter on the output of the *COMSOL* model. Therefore, a sensitivity analysis was performed on a reference simulated case in which initial values of parameters are fixed arbitrary but close to expected values for clay samples (**Table 4**). The following is a purely theoretical analysis: from the reference scenario, one individual parameter was changed at a time and the resulting mass variation scheme studied in comparison to the reference output. The parameters analyzed correspond to those which were to be optimized with the inverse modelling approach. As input in the reference simulation and each parameter sensitivity study, the boundary conditions of the model consisted of 7 repetitions of the measured RH cycle (**Fig. 4**). Indeed, it is important to observe the impact of parameters modification over multiple repetitions of the RH cycle. The key point is to have confidence in the uniqueness of parameter values to fit a particular cycle. If it is proven that the individual modification of two different parameters produces a similar effect on sample mass variation, the risk exists that a local minimum of the objective function is ignored, although it represents the 'true' value of parameters. Indeed, if several parameter combinations produce a similar effect, a small experimental bias alone can determine the dominance of one or the other in terms of SSR score in the DREAM algorithm.

Table 4. Parameters combination in the reference scenario

ρ_0	μ	C_2	Z_s	A	φ_0
$kg \cdot m^{-3}$	–	–	$(Pa \cdot m^2 \cdot s)/kg$	m^2	–
2000	10	-0.01	5e7	0.08	0.55

For material parameters, i.e. vapour resistance coefficient μ and Smith model parameter C_2, an increase/decrease of +20/-20% of the parameter value (compared to reference case) are considered separately. **Figure 9** shows the effect of these various schemes on the model response in terms of weight variation of the sample.

It can be observed that increasing any of these two parameters will result in a decrease of individual weight cycle amplitude. The inverse is true when decreasing their value. In addition to this daily impact, the overall tendency to move towards an equilibrium cycle is also modified. Regarding this second effect, the Smith parameter seems to have a stronger impact. Given the model assumptions, it can be recalled that the vapour transport coefficient is considered constant whereas moisture capacity changes with relative humidity, through the Smith model (**Eq. 2**). In reality, the vapour diffusion coefficient is also dependent on relative humidity. Moreover, liquid transport in smaller capillaries might add a contribution to moisture transport during the high humidity phase. In addition to the inverse calculation methodology, the goal of this paper is to

test the ability of the chosen mathematical description to accurately represent the sample behaviour.

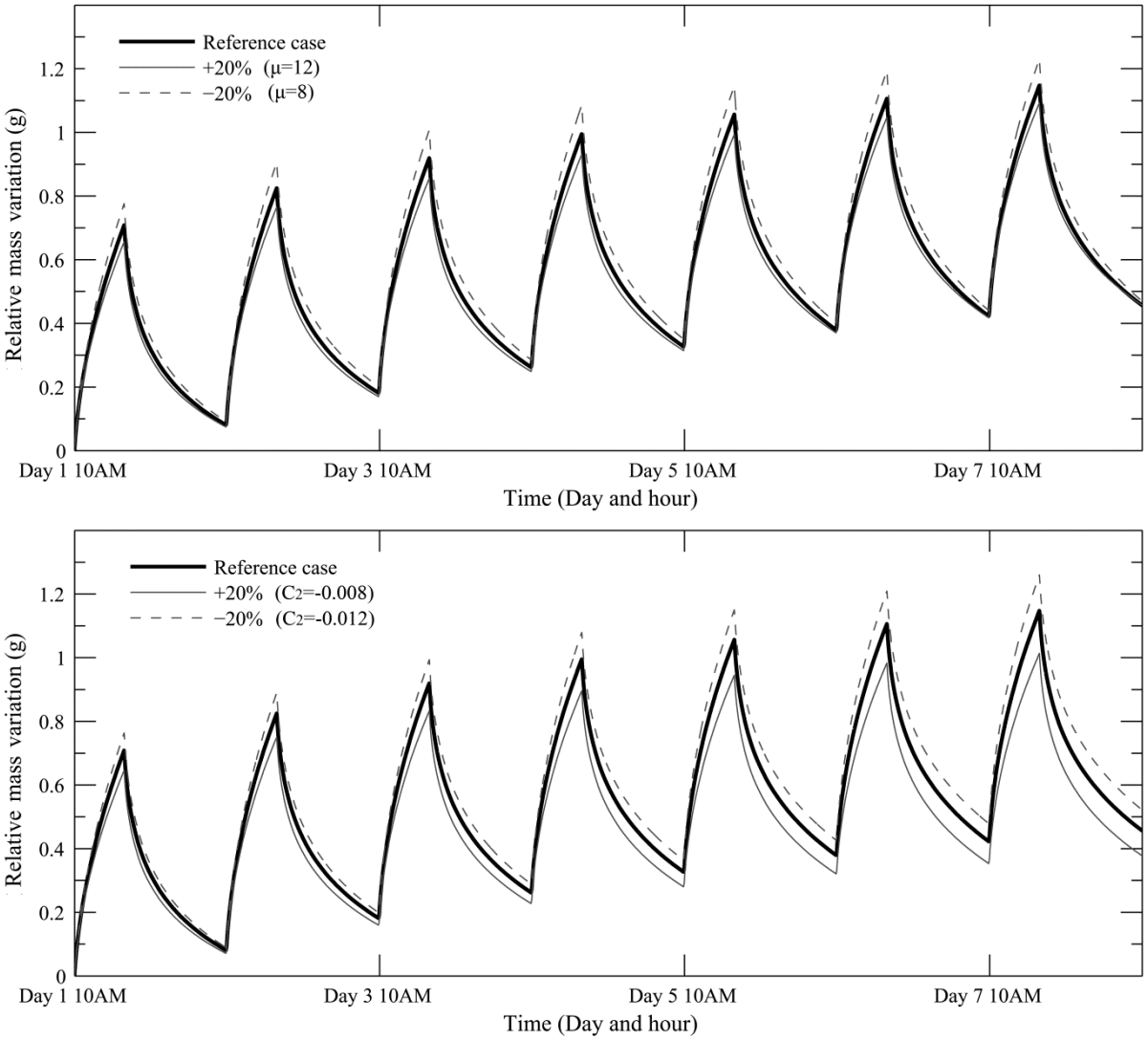

Fig. 9. Sensitivity of moisture uptake/release due to material hygric parameters; (t.) reference case compared to +20 an -20% variation of vapour resistance factor and (b.) compared to +20 an -20% variation of moisture storage parameter C_2

Concerning the boundary and initial conditions parameters, a modification of +50/-50% was imposed to the surface resistance Z_s and a +2.5/-2.5% scheme to initial relative humidity in the sample φ_0. The modification of the initial humidity in the sample had a limited impact because of its large effect on resulting mass variation of the sample. Similarly, surface resistance was modified with +50 and -50% of its value in order to have a noticeable impact on model output. **Figure 10** presents the simulated relative weight variation of the reference sample with each of these parameters varied individually, similarly to **Figure 9**. The effect of surface resistance

appears to be restricted to daily cycles. The major modification in comparison to reference cycle occurs at the transition from high to low humidity in the chamber.

The initial RH in the sample has a clear impact on the transition towards equilibrium cycle. It can be explained easily: if the initial RH corresponds to the average of humidity during the entire day, the cycle would be in perfect equilibrium from the start. We note that the impact on daily cycle is difficult to assess but is supposed to be negligible.

In order to get a more precise overview about model output sensitivity on parameters modifications, results of the study can be expressed in terms of sensitivity residuals, defined as:

$$\varepsilon_i = \left(\hat{y}_i\left(X, \theta_{ref}\right) - \hat{y}_i(X, \theta')\right) \quad (13)$$

where θ_{ref} is the parameter set with reference values (**Table 4**) and θ' is identical to the reference set with the modification of one parameter. **Figure 11** shows the sensitivity residuals for all scenarios with increased values of an individual parameter. Such an approach allows precise identification of the impact on long term equilibrium and daily cycles of each individual parameter in a highly visual and easily comparable form. The specific impact of each parameter on the resulting output is clear.

The initial relative humidity φ_0 plays preferentially on long term evolution, with a moderate impact on daily cycles whereas the exchange surface resistance shows precisely the opposite behaviour. Material parameters denote a more complex combination of effects. Both impact daily cycles in a similar way but the C_2 parameter seems able to modify long term evolution in a more noticeable manner. Also, the long term impact of increasing this moisture storage property appears to be very similar to an increase of initial humidity in the sample. Given these observations, a combination of +20% on μ value and +1% on φ_0 value is illustrated to check if the same effect as an increase of C_2 alone can be produced and results are shown on **Figure 12**. It seems that producing exactly the same residuals is not possible which gives confidence for the subsequent optimization task.

With the results of the sensitivity analysis, we can already draw some conclusions regarding the inverse modelling approach. First, the model assumptions, and in particular the definition of moisture storage and transport functions, will determine the ability of the optimization algorithm to extricate a relevant description of the material. In our case, the inclusion of a RH-dependent moisture capacity potentially reduces the number of local minima in the $SSR(\theta_{1\ldots d})$ space. It can be assumed that the global best score in terms of SSR is far from the score of the closest local minima. To take a contradictory example, if moisture capacity was considered constant in **Equation 4**, the DREAM tool would probably have difficulty in converging towards a single best parameter combination. Of course, the mass variation of a sample during a MBV experiment does not provide enough information to determine both complex transport and storage functions. This would probably require the definition of a new non-isothermal cycle in order to create various vapour pressure and relative humidity gradients in the material.

A second short remark is specific to the use of MBV cycles for parameter evaluation. It appears that the optimization process should not be performed over one unique mass variation cycle because some parameter effects only develop over the repetition of RH cycles.

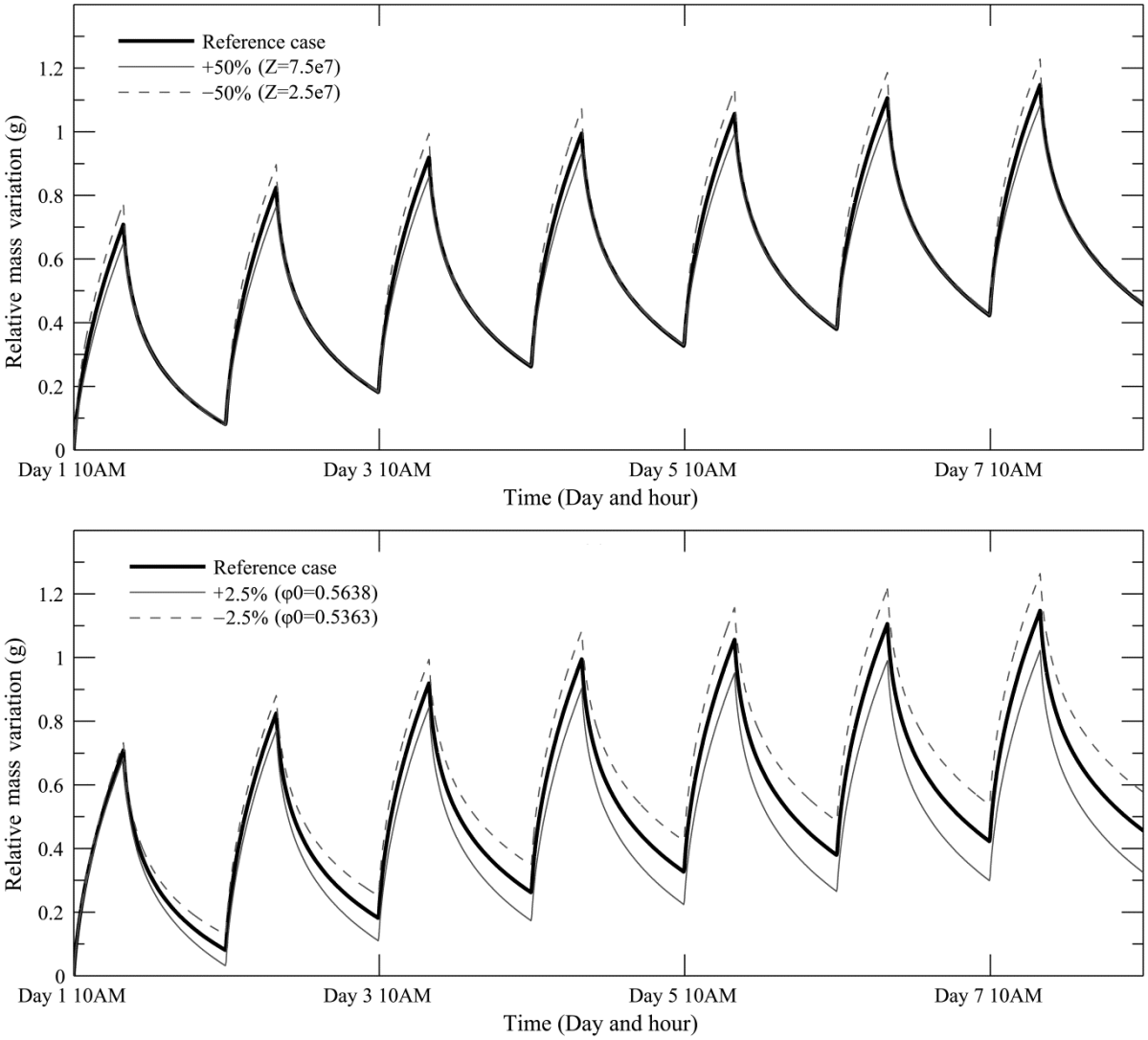

Fig. 10. Sensitivity of moisture uptake/release due to boundary and initial conditions parameters; (t.) reference case compared to +50 an -50% variation of surface resistance factor and (b.) compared to +2.5 an -2.5% variation of initial relative humidity in the sample

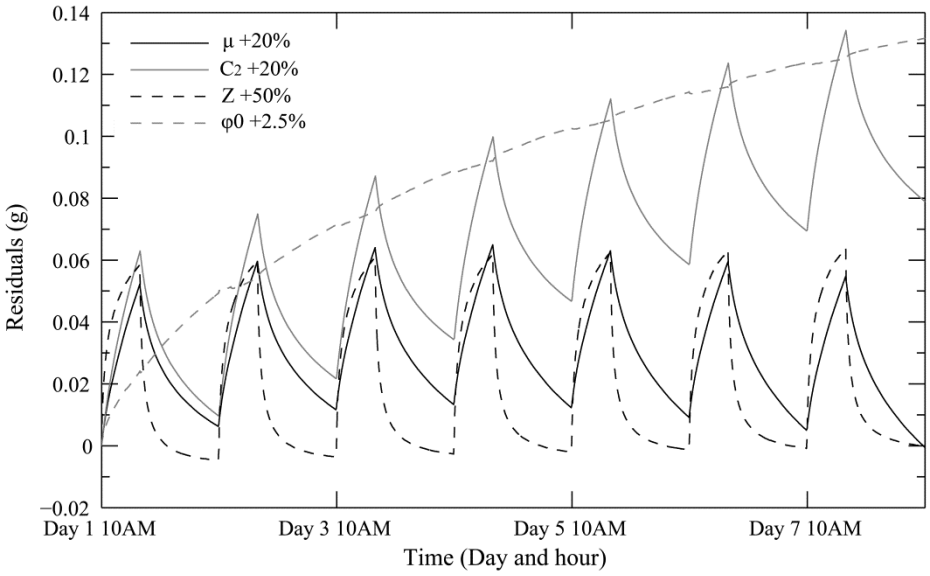

Fig. 11. Sensitivity residuals for parameters increase scenarios

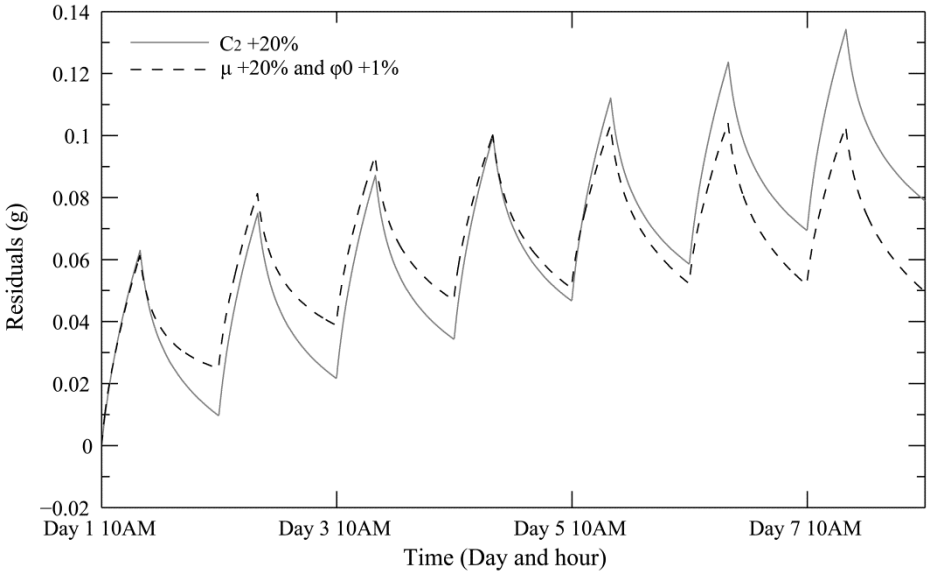

Fig. 12. Sensitivity residuals for materials parameters

6.2.2 DREAM algorithm outputs

The DREAM algorithm was run with 8 Markov chains and a total of 25000 model evaluations for each material. The total number of runs was determined during preliminary studies in order to provide a sufficient number of iterations after the MCMC sampler convergence criterion to compute significant posterior distributions. **Figure 13** presents the marginal probability distributions of the four parameters for the last 500 sampling iterations in each Markov chain. The results are presented in the form of histograms using data from all the chains.

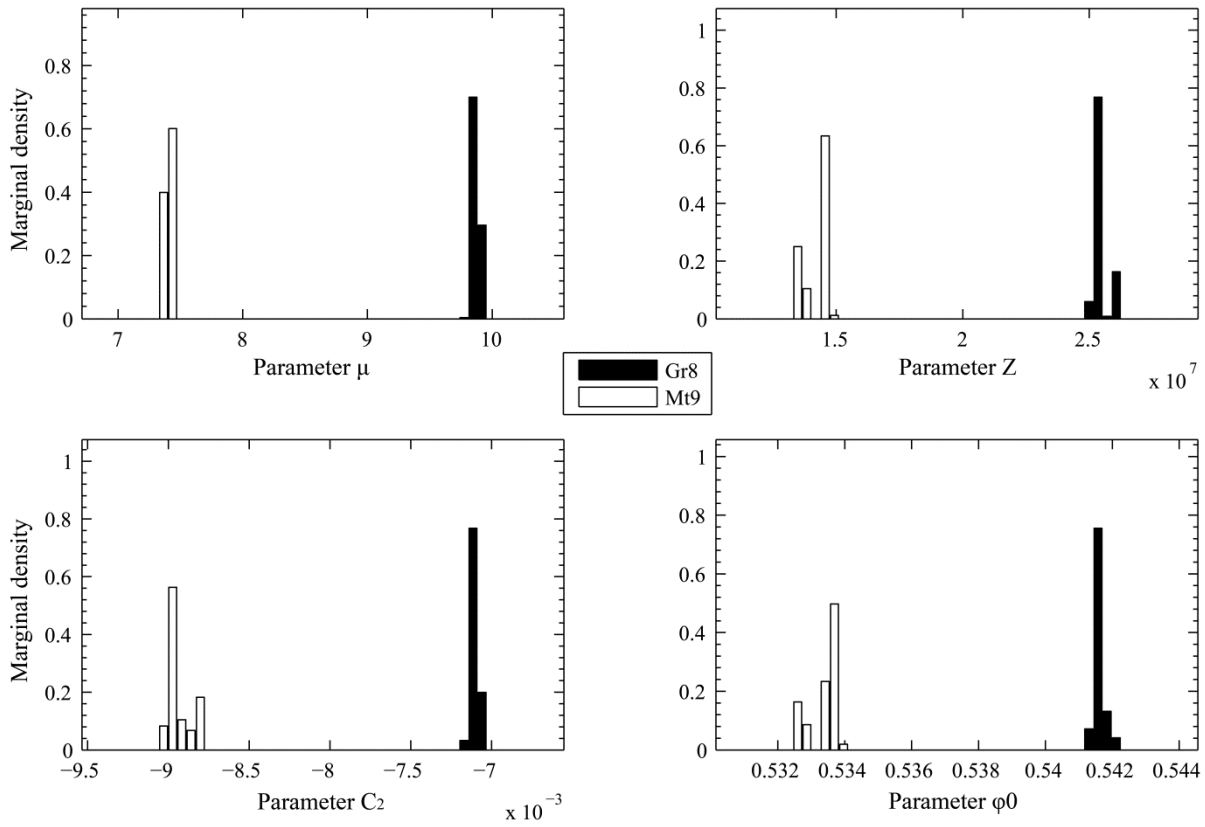

Fig. 13. Marginal posterior probability distributions of the μ, C_2, Z_s and φ_0 parameters constructed using 4000 samples generated after convergence of the DREAM algorithm

Each estimated parameter exhibits a narrow posterior distribution with a highly noticeable dominant mode. This is true for both tested materials. The uncertainty in parameters values given the experimental data seems to be really low. On the basis of posterior distribution data, **Table 5** provides a summary of parameters estimates for *Gr8* material and **Table 6** for *Mt9* material. The tables include parameters estimates vectors defined in section 3.4.2, the coefficient of variation (CV) associated to the mean estimates and steady-state experimental values of parameters for diffusion resistance factor and Smith function parameter.

Table 5. θ_{opt} the vector of optimal parameters estimates, θ_{mean} the vector of mean parameters estimates and associated coefficient of variation, and SS the measured steady-state values of hygric transfer parameters (*Gr8* Material)

Parameter	θ_{mean}	CV (%)	θ_{opt}	SS Value
μ	9.88	0.28	9.90	8.8
C_2	-7.10E-3	0.31	-7.11E-3	-8.30E-3
Z_s	2.55E7	1.00	2.56E7	/
φ_0	5.42E-1	0.03	5.42E-1	/

Table 6. θ_{opt} the vector of optimal parameters estimates, θ_{mean} the vector of mean parameters estimates and associated coefficient of variation, and SS the measured steady-state values of hygric transfer parameters (*Mt9* Material)

Parameter	θ_{mean}	CV (%)	θ_{opt}	SS Value
μ	7.40	0.33	7.41	8.3
C_2	-8.95E-3	0.79	-8.99E-3	-1.24E-2
Z_s	1.42E7	3.41	1.45E7	/
φ_0	5.33E-1	0.08	5.34E-1	/

Optimal and mean estimates are very close for each parameter in both materials, as it could be expected given the narrow posterior distributions. The low parameters uncertainty is also confirmed with the fact that the coefficient of variation is ≤1% for all parameters posterior distributions other than the surface resistance factor Z_s of the *Mt9* material. The latter shows a 3.4% CV but it should be reminded that the sensitivity of model on this parameter is quite low in comparison to other parameters. In consequence, optimal estimates or mean estimates could be used equivalently to represent the behaviour of clay samples.

For both samples, **Figure 14** shows the *COMSOL* model output with all four optimized parameters compared to: (1) the experimental mass variation, and (2) the model output when using measured steady-state values to describe the vapour permeability and the sorption isotherm of the clay and optimized values for surface resistance and initial relative humidity in the sample. In consequence, the two model outputs illustrated only differ in the values of hygric properties for *Gr8* and *Mt9* samples.

The optimal parameter set results in a NSE of 0.997 for *Gr8* material and a NSE of 0.996 for *Mt9* material reflecting a very high efficiency of the model in the description of clay samples mass variation after the optimization process. In contrast, the measured steady-state properties result in a *NSE* of 0.875 for *Gr8* material and 0.7513 for *Mt9* material. The efficiency found for *Gr8* sample is very similar to the one found in a previous direct MBV modelling approach [24] and can already be considered as a good modelling efficiency. Globally, the optimization process can improve further the fitting to experimental data and potentially reduce the uncertainty on material and experimental parameters. In particular, when dealing with complex hygrothermal models, it can be used as a precious tool for reducing the experimental uncertainty linked to material characterization. As improving the precision in experimental material characterizing can be expensive and time-consuming, the inverse modelling techniques offers an alternative to consider.

It is certainly interesting to analyze the parameters values obtained after the inverse modelling process. The exchange surface resistance Z_s depends on the boundary layer which in turn is linked to the airflow configuration around the sample exchange surface. Its value was theoretically limited to the range 1E6 $(Pa \cdot m^2 \cdot s)/kg$ (a very low resistance corresponding to

hardly any effect of the boundary layer on moisture transfer) to 1E8 $(Pa \cdot m^2 \cdot s)/kg$ (a very high resistance corresponding to a negligible air flow) before the parameter estimation phase (**Table 3**). Those limit values were inspired by values found in [27]. A value of Z_s =5E7 $(Pa \cdot m^2 \cdot s)/kg$ is often presented as a standard value in test chambers corresponding to an averaged airflow velocity of 0.1 m/s above the sample. However, this experimental parameter is often poorly controllable in climate chamber experiments and it seems that there is still no accurate way to determine it. Inverse modelling estimation can thus provide a solution to this issue although the quality of the estimation should be confirmed in complementary studies. Here, the estimated values for surface resistance are close to the reference value but differ between the two experimental tests. It is difficult to assess the origin of this difference although it can supposedly be caused by airflow variations from one test to the other, which could result from small difference of sample location in the chamber. Especially when one knows that the mass variation sensitivity on that parameter is low around 1E7 $(Pa \cdot m^2 \cdot s)/kg$ according to [27].

Concerning the initial relative humidity φ_0 in the material, although its value is supposed to be identical for both clay samples, the difference is so small it could be imputed to sample manipulation before the test. The estimated values are close to expected provided the sample conditioning before the test.

The most interesting part in results analysis is of course to discuss the values estimated for the hygric properties of the materials. Compared to values measured in steady-state, the optimal estimate of vapour resistance factor μ is 12.5% higher for *Gr8* material and 11% lower for *Mt9* material. The difference between the two clay materials is thus more pronounced under the inverse modelling results. Whereas the steady-state μ parameter is assessed on the basis of a constant mean relative humidity of 72%RH (wet-cup test), the estimated parameter represents in fact the vapour transport in the active depth of the material, averaged over various RH conditions met during the 24 hours cycle. Resulting identical values for the two methods would be particularly astonishing as they not characterize exactly the same behaviour. Still, it is confirmed that *Gr8* material has a higher resistance to vapour transport. For moisture storage parameter C_2, characterizing the moisture capacity evolution with relative humidity, the estimated value is respectively 14% higher for *Gr8* material and 28% higher for *Mt9* material compared to steady-state measurement. It corresponds to less moisture storage capacity for both materials (**Eq. 3**). The higher moisture storage capacity observed with the DVS method for *Mt9* material compared to *Gr8* is confirmed by the inverse modelling approach but less pronounced. Again, the dynamic nature of inverse modelling estimation must be highlighted. The DVS provides equilibrium sorption isotherms whereas the values obtained from posterior distributions characterize a dynamic behaviour where equilibrium values are not perfectly representative. Indeed, a lower moisture capacity for both materials (compared to DVS results) can mean a kind of 'latency' in moisture sorption.

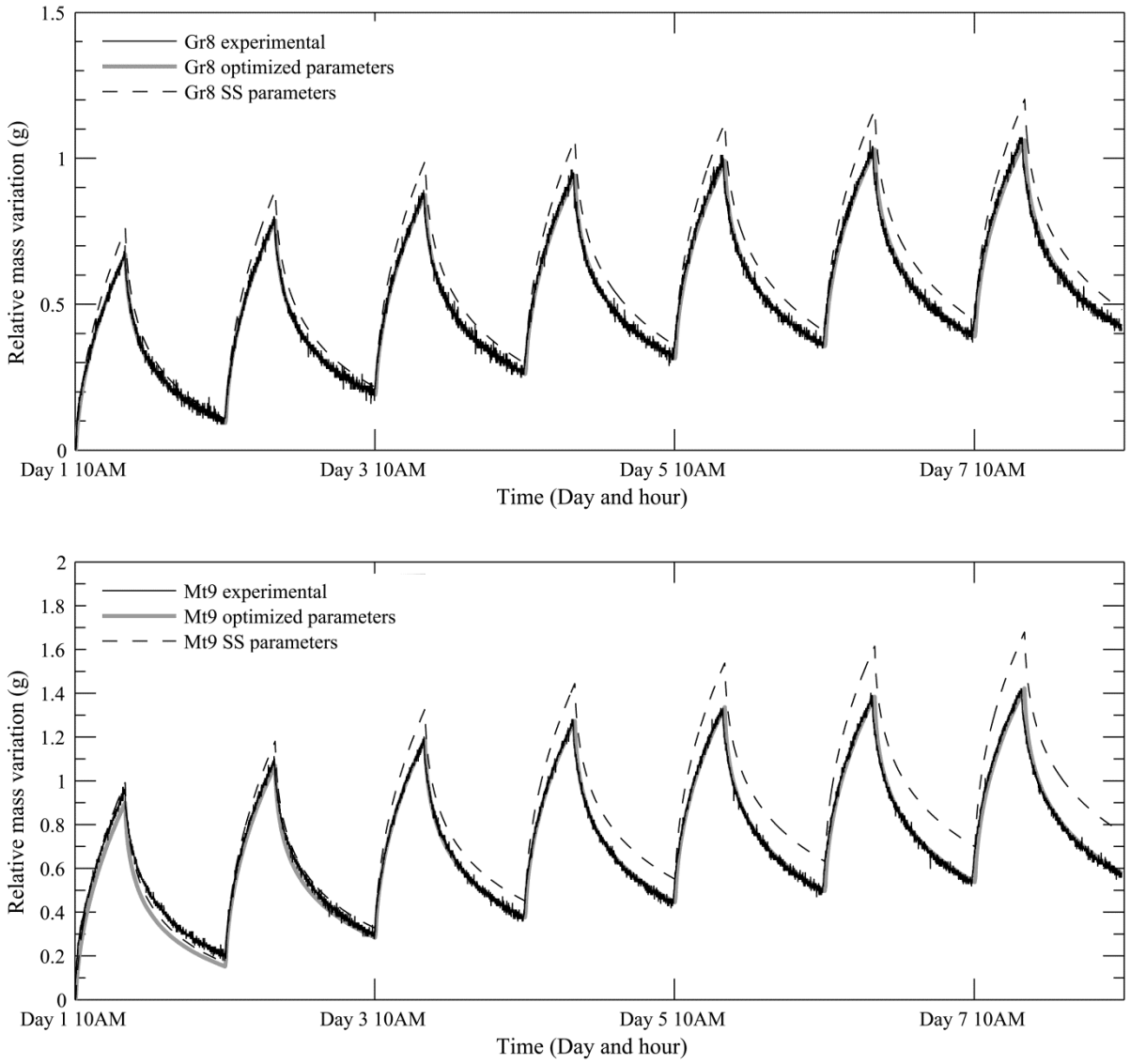

Fig. 14. Model output with optimized or steady-state parameters used to describe the hygric properties of clay samples compared to experimental cycles

7. CONCLUSION

An inverse modelling method based on Bayesian techniques and MCMC simulations was tested for parameter estimation for a moisture transfer model applied to the study of construction materials. The MBV protocol, dedicated originally to assess the moisture exchange capacity of hygroscopic materials, was proposed here as an experimental data source from which it is possible to infer information concerning the moisture storage function and the vapour transport coefficient. But the approach can be applied theoretically to all kind of HAM models and case studies as long as the HAM model can be combined numerically to a parameter optimization algorithm.

Two different clay masonry materials were first subjected to repeated 50/85%HR cycles in a 16hrs/8hrs scheme, similar to the NORDTEST protocol. The monitoring of their weight during this test constitutes the measurement data intended to be compared with the output of a hygric model. Relevant material properties involved in moisture uptake/release behaviour were also measured precisely for both samples. This step included a wet-cup test for vapour permeability determination and a DVS test to assess their moisture storage at different RH levels.

The numerical model used to describe the moisture transfer in the clay samples during the MBV cycles was developed in *COMSOL* and uses a simplified mass balance equation, without liquid transport. Four parameters were chosen to be optimized in order to fit experimental data. They form two categories: (1) The materials properties which include the vapour resistance factor and a coefficient characterizing the evolution of moisture capacity with relative humidity in the porous structure; (2) Experimental parameters composed of the surface resistance and initial humidity in the sample. A sensitivity analysis showed that each parameter had a different impact on simulated moisture exchange giving confidence in the optimization process. The latter was performed with the recently developed DREAM algorithm combined with the hygric model in the Matlab environment. Compared to other inverse modelling tools, DREAM offers the advantages of Bayesian techniques and MCMC sampling, i.e. the determination of parameters posterior distribution with a possible evaluation of the uncertainty of parameters values and model outputs given the experimental data.

This study showed that the MBV test provides a relevant ground for the estimation of moisture transfer properties, in the analysis of highly hygroscopic clay-based material in dynamic conditions. This experimental protocol provides important information about the material behaviour which can be extracted with an inverse modelling approach. Inverse modelling is still not very common in Building Physics but can be very powerful provided the model accurately represents the hygrothermal behaviour. The DREAM MCMC sampler converged and provided very little dispersed posterior distributions for all parameters. On this basis, the computed estimates for vapour transport and moisture storage parameters were compared to their values measured under steady-state conditions. Based on the sensitivity analysis of model output, there is good confidence in optimized values of parameters and in their representativeness under dynamic moisture exchange conditions. There is no reason to believe that steady-state parameters provide a 'better' description of the material behaviour. The differences between steady-state and estimated values could be partly explained by the dynamic nature of the MBV test which causes complex interactions between moisture storage and transport phenomena. The estimated parameters through inverse modelling are potentially more representative of the actual conditions met in a building where steady-state conditions almost never happen.

Despite these interesting results, the inverse modelling approach requires some precautions as indicated throughout in the text. First, the experimental acquisition system should be highly reliable as the observed data uncertainty plays a major role in the optimization process and final

parameter estimates. Moreover, a precise understanding of the model parameters and their effect on model output is required and will help to determine the ideal number of measurement points to use in the MCMC sampler, in order to maximize posterior distribution quality and minimize computational time. When appropriate, the model itself has to be modified through definition of new parameters whose effects on model output can be clearly distinguished. Nevertheless, if these conditions are respected, the technique is very promising. Numerous new test protocols could be created to highlight various behaviours of construction materials and continue the improvement of mathematical models. The inverse modelling approach could also be applied to larger scale studies where having experimental data for all needed parameters can be tricky or at least a time-consuming task.

NOMENCLATURE

$\boldsymbol{\delta}$	$(kg \cdot m^{-1} \cdot s^{-1} \cdot Pa^{-1})$	Vapour permeability
$\boldsymbol{\mu}$	$(-)$	Vapour diffusion resistance factor
$\boldsymbol{\xi}$	$(kg_v \cdot kg_0^{-1})$	Isothermal moisture capacity
$\boldsymbol{\rho}$	$(kg \cdot m^{-3})$	Density
$\boldsymbol{\varphi}$	$(-)$	Relative humidity
$\boldsymbol{\omega}$	$(kg \cdot kg^{-1})$	Absolute humidity
$\boldsymbol{j_x^{M_v}}$	$(kg \cdot m^2 \cdot s^{-1})$	Vapour flux density
$\boldsymbol{p_{sat}}$	(Pa)	Vapour saturation pressure
$\boldsymbol{p_v}$	(Pa)	Vapour partial pressure
$\boldsymbol{t}$	(s)	Time
$\boldsymbol{u}$	$(kg_v \cdot kg_0^{-1})$	Moisture content
$\boldsymbol{x}$	(m)	Position in the sample
$\boldsymbol{Z_s}$	$(Pa \cdot m^2 \cdot s \cdot kg^{-1})$	Vapour diffusion resistance factor at material surface

Subscripts

∞	Related to the climate of the chamber
$\boldsymbol{a}$	Related to dry air
$\boldsymbol{s}$	Related to the exchange surface of the material
$\boldsymbol{v}$	Related to the water vapour
$\boldsymbol{0}$	Related to the dry state of the material or to the initial condition

REFERENCES

[1] Gandreau D, Delboy L. Inventory of earthen architecture. UNESCO;2012.

[2] Minke G. Building with Earth: Design and Technology of a Sustainable Architecture. Basel: Birkhäuser; 2006.

[3] Padfield T. The role of absorbent building materials in moderating changes of relative humidity [PhD Thesis]. [Lyngby (DK)]: Technical Univ. of Denmark; 1998.

[4] Toftum J, Fanger PO. Air humidity requirements for human comfort. ASHRAE Transactions. 1999;99.

[5] Fang L, Clausen G, Fanger PO. Impact of temperature and humidity on the perception of indoor air quality. Indoor Air. 1998;8:80-90.

[6] Simonson CJ, Salonvaara M, Ojanen T. The effect of structures on indoor humidity–possibility to improve comfort and perceived air quality.

Indoor Air. 2002;12:243-51.

[7] Peuhkuri RH, Mortensen LH, Hansen KK, Time B, Gustavsen A, Ojanen T, et al. Moisture Buffering of Building Materials. Lyngby (DK): Technical Univ. of Denmark; 2005 Dec. 78p. Report No: BYG·DTU R-126.

[8] Osanyintola OF, Simonson CJ. Moisture buffering capacity of hygroscopic building materials: Experimental facilities and energy impact. Energy and Buildings. 2006;38:1270-82.

[9] Künzel HM, Kiessl K. Calculation of heat and moisture transfer in exposed building components. International Journal of Heat and Mass Transfer. 1996;40:159-67.

[10] Häupl P, Grunewald J, Fechner H, Stopp H. Coupled heat air and moisture transfer in building structures. International Journal of Heat and Mass Transfer. 1997;40:1633-42.

[11] Rode Pedersen C. Combined heat and moisture transfer in building constructions [PhD Thesis]. [Lyngby (DK)]: Technical Univ. of Denmark; 1990.

[12] Dos Santos GH, Mendes N. Combined Heat, Air and Moisture (HAM) Transfer Model for Porous Building Materials. Journal of Building Physics. 2009;32:203-20.

[13] Hagentoft C-E, Kalagasidis AS, Adl-Zarrabi B, Roels S, Carmeliet J, Hens H, et al. Assessment Method of Numerical Prediction Models for Combined Heat, Air and Moisture Transfer in Building Components: Benchmarks for One-dimensional Cases. Journal of Thermal Envelope and Building Science. 2004;27:327-52.

[14] Janssens A, Woloszyn M, Rode C, Sasic-Kalagasidis A, De Paepe M. From EMPD to CFD–overview of different approaches for Heat Air and Moisture modeling in IEA Annex 41. IEA ECBS Annex 41 Closing seminar; 2008 Jun 19; Lyngby, Denmark.

[15] Scheffler GA, Plagge R. A whole range hygric material model: Modelling liquid and vapour transport properties in porous media. International Journal of Heat and Mass Transfer. 2010;53:286-96.

[16] Dantas L, Orlande H, Cotta R. An inverse problem of parameter estimation for heat and mass transfer in capillary porous media. International Journal of Heat and Mass Transfer. 2003;46:1587-98.

[17] Metropolis N, Rosenbluth AW, Rosenbluth MN, Teller AH, Teller E. Equation of state calculations by fast computing machines. The journal of chemical physics. 1953;21:1087.

[18] Ter Braak CJ. A Markov Chain Monte Carlo version of the genetic algorithm Differential Evolution: easy Bayesian computing for real parameter spaces. Statistics and Computing. 2006;16:239-49.

[19] Vrugt JA, Ter Braak C, Diks C, Robinson BA, Hyman JM, Higdon D. Accelerating Markov chain Monte Carlo simulation by differential evolution with self-adaptive randomized subspace sampling. International Journal of Nonlinear Sciences and Numerical Simulation. 2009;10:273-90.

[20] Vrugt JA, Ter Braak CJ, Clark MP, Hyman JM, Robinson BA. Treatment of input uncertainty in hydrologic modeling: Doing hydrology backward with Markov chain Monte Carlo simulation. Water Resources Research. 2008;44.

[21] Dumont B, Leemans V, Mansouri M, Bodson B, Destain J-P, Destain M-F. Parameter identification of the STICS crop model, using an accelerated formal MCMC approach. Environmental Modelling & Software. 2014;52:121-35.

[22] McGregor F, Heath A, Fodde E, Shea A. Conditions affecting the moisture buffering measurement performed on Compressed Earth Blocks. Building and Environment. 2014.

[23] Smith SE. The sorption of water vapor by high polymers. Journal of the American Chemical Society. 1947;69:646-51.

[24] Dubois S, Evrard A, Lebeau F. Modeling the hygrothermal behavior of biobased construction materials. Journal of Building Physics. 2013.

[25] Chib S, Greenberg E. Understanding the metropolis-hastings algorithm. The American Statistician. 1995;49:327-35.

[26] Gelman A, Rubin DB. Inference from iterative simulation using multiple sequences. Statistical science. 1992:457-72.

[27] Roels, S, Janssen, H. Is the moisture buffer value a reliable material property to characterize the hygric buffering capacities of building materials. Working paper A41-T2-B-05-7 for IEA Annex 41 project. 2005.

CHAPTER 6

Improving the BEHAM description of CBM in nonisothermal conditions

6.1 Introduction

In **Chapter 4** and **Chapter 5** the hygrothermal behaviour of hygroscopic material blocs was characterized in a well-controlled environment and nearly isothermal conditions. A model designed to predict the behaviour of CBM should be able to evolve progressively to incorporate descriptions for all hygrothermal conditions potentially occurring in a building element, including extreme solicitations. A frequent assumption in commercial BEHAM tools is that the moisture storage of materials is independent of temperature. This chapter studies the appropriateness of this particular assumption for CBM and proposes a simple mathematical description to construct a temperature-dependent moisture storage curve, based on theories from the Drying Technologies scientific domain.

In the appended paper, a thermal shock on a straw bale wall is carried out in a bi-climatic chamber. The internal conditions of straw bales are monitored with specific hygrothermal sensors. Several versions of the resarch BEHAM model are then compared in their ability to predict the resulting evolution of temperature and relative humidity, with the efficiency criteria defined in **Chapter 4**. Each model version differs in the representation of moisture storage; the first version incorporates an empirical description of temperature effect on moisture storage; the second one incorporates a physically-based theory to describe the same phenomena; the last version assumes a sorption curve independent of temperature.

6.2 Appended paper

The Effect of Temperature on Moisture Storage in Crop-Based Materials: Modelling a Straw Bale Wall Subject to a Thermal Shock

Samuel DUBOIS*[1], Cristophe Blecker[2], Arnaud EVRARD[3], Frédéric LEBEAU[1]

[1]Dept. STE, Gembloux Agro-Bio Tech, University of Liege, Belgium

[2]Dept. CBI, Gembloux Agro-Bio Tech, University of Liege, Belgium

[3]Architecture et Climat, Université Catholique de Louvain, Belgium

*Corresponding author, supported by a F.R.I.A Grant,
Address: Dept. of environmental sciences and technologies, Gembloux Agro-Bio Tech, 2 Passage des déportés, 5030 Gembloux, Belgium (s.dubois@doct.ulg.ac.be)

KEYWORDS

Ham Modelling, Crop-based materials, Hygroscopicity, Thermal shock, Adsorption

STATUS

Submitted to:

Journal of Building Physics

ABSTRACT

Among insulation products, crop-based materials present a high moisture storage capacity associated with dynamic phase change phenomena occurring in their porous structure. Modelling their hygrothermal behaviour is essential in order to assess how they impact the energy performance of the building and the indoor climate. It is also needed to prevent any risk of unexpected degradation from mould growth. Traditionally, transient numerical models that predict internal conditions of construction materials consider that the variation of moisture storage with temperature is negligible although the sorption behaviour is known to be temperature-dependent. This paper investigates this particular effect for crop-based materials and offers a refinement of standard mathematical representations. For this purpose, the evolution of internal conditions of a straw-bale wall subject to a thermal shock is compared to variations of a flexible research model. The latter is capable of incorporating the temperature-dependency of the sorption curve alternately with a physically-based and an empirical description.

Results show that when large temperature gradients occur in a crop-based material, a model that considers the temperature impact on moisture storage greatly enhances the prediction of internal relative humidity. A one-parameter description of this particular effect succeeds in drastically improving the model efficiency and a complex physically-based approach only offers little additional improvement. This analysis also illustrates the upgrading potential of a heat and moisture transfer model that is developed in a general computational tool.

1. INTRODUCTION

Straw bales have been successfully used as building materials in the last century, either in load-bearing or infill techniques [1]. Interest in this atypical product has recently resurfaced mainly due to sustainability and health related qualities [2] associated with good thermal and acoustic performance [3, 4]. Moreover, such crop-based materials are characterized by a passive ability to buffer the indoor humidity, defined rigorously through the Moisture Buffer Value concept [5], which has a direct impact in terms of energy consumption of the building [6, 7]. The extent of this moisture exchange capacity is related to the porous structure of the material because the latter will determine the sorption and capillary behaviour as well as the heat and moisture transfer functions. An accurate prediction of the underlying physical phenomena is thus critical to assess the specific advantages arising there from.

Building Element Heat, Air and Moisture (BEHAM) models were developed in order to predict coupled heat and mass transfers in porous media. The use of non-linear partial differential equations (PDE's) with numerical solvers is the more accurate technique to account for the complexity of highly hygroscopic products behaviour. Many available models are able to perform such computations and were compared in previous studies [8-10]. From the mathematical point of view, they differ mainly in the underlying assumptions and resulting simplifications in the mathematical expressions. Additionally, some authors [11, 12] showed that models developed in general computational software are attractive in terms of evolution potential and interoperability with other computational tools. Recently, Dubois et al. [13, 14] illustrated how a heat and moisture transfer model developed in the *COMSOL Multiphysics* software can be used to accurately simulate highly hygroscopic materials during a moisture buffer value evaluation test. Now, the numerical tool needs to be confronted to strongly non-isothermal conditions. In fact, there are still very few validation studies in which hygroscopic materials are subjected to significant temperature gradients in literature related to BEHAM models.

One of the most frequent hypothesis in BEHAM models is to neglect the effect of temperature on moisture storage [15]. In most of the available tools, a unique moisture storage curve (MSC) is used to express the relationship between equilibrium moisture content (EMC) and relative humidity (RH) in hygroscopic materials; a function needed to solve the moisture balance equation. Exhaustive studies related to moisture storage in wood and plant fibres can be found [16-18] and it is yet widely accepted that the variation of equilibrium moisture content with temperature exists in the hygroscopic domain and is linked to the thermodynamics of sorption. Rode & Clorius [19] tested a BEHAM model that was modified to incorporate both the temperature-dependency of moisture storage and the hysteresis effect. In a numerical analysis, the tool was used to predict internal conditions in solid wood elements subject to natural climatic solicitations over ten consecutive years. A comparison of various model versions showed that the temperature can play a significant role in the moisture storage behaviour and in

the resulting RH variations inside the construction element. However, in the same paper, a confrontation of the refined model output to measurement data exhibited some discrepancy that the authors explained partly by problems in the definition of sensors locations and active sensing area. So far, there is still a lack of direct confrontation between measured and modelled data that would allow validating the descriptions for temperature-dependency of the moisture storage. For that purpose, it seems that simple case studies still need to be examined before trying to simulate complex climatic operations involving both high temperature and high moisture content variations.

In this paper, the modelling of a straw bale panel subjected to a thermal shock is investigated. It is a short time-scale experiment that allows controlling precisely the climatic solicitations on the wall in order to avoid exploring a too large hygrothermal domain. In particular, we ensure that hysteresis and liquid moisture transport phenomena in the materials are small during the test. The objective is to test different moisture storage descriptions including temperature-dependency in their ability to give a efficient prediction of the RH field inside the straw. Indeed, RH sensors are common to assess the humidity condition in porous structure due to the local thermodynamic equilibrium assumption.

The first part of the study describes the experimental set-up involving a large scale climatic chamber and specific sensors that are used to produce the validation data. In a second step, a research BEHAM model is refined with two distinct methods for characterizing the sorption curve dependence on temperature. Among those, an original empirical approach which relies on a single parameter definition is proposed. Ultimately, the experimental results are compared to the outputs of three variations of the model; one model version for each approach described for the temperature-dependent sorption characteristics and one simplified version with a single sorption isotherm. In order to supplement available literature, a clear evaluation of the prediction efficiency is offered for model inter-comparison purpose.

2. MATERIALS AND METHODS

2.1 Test wall and hygrothermal sensors

The tested straw bale panel assembly was produced by the Belgian company *Paille-Tech* [20]. Straw bales are used as infill in a wood frame made of 45x175mm lumbers. Vertical studs are spaced at 345mm on centre with bales stacked vertically between them. The resulting preferential orientation of straws is parallel to wall depth. To complete the structure, the frame is braced on the external side with breathable wood particle boards. On the internal side the straw bales are covered with a 40mm earth plaster. The details of construction are shown on **Figure 1a**.

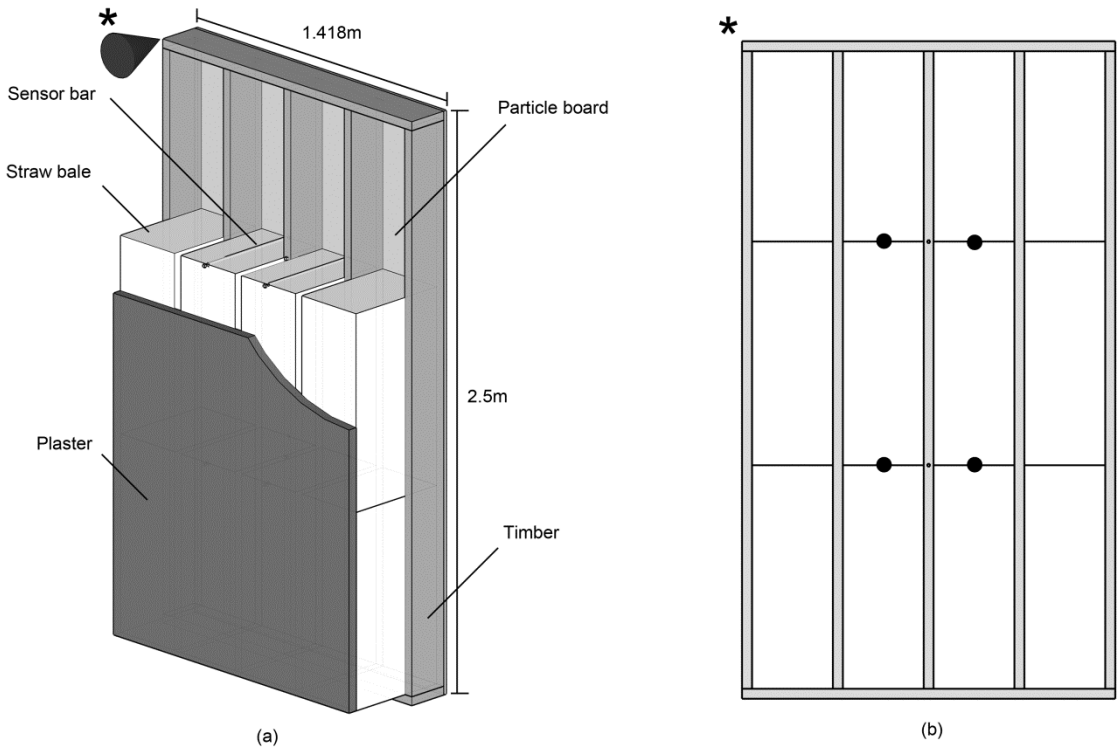

Fig. 1. Straw bales panel assembly (a) with sensor bars location (b)

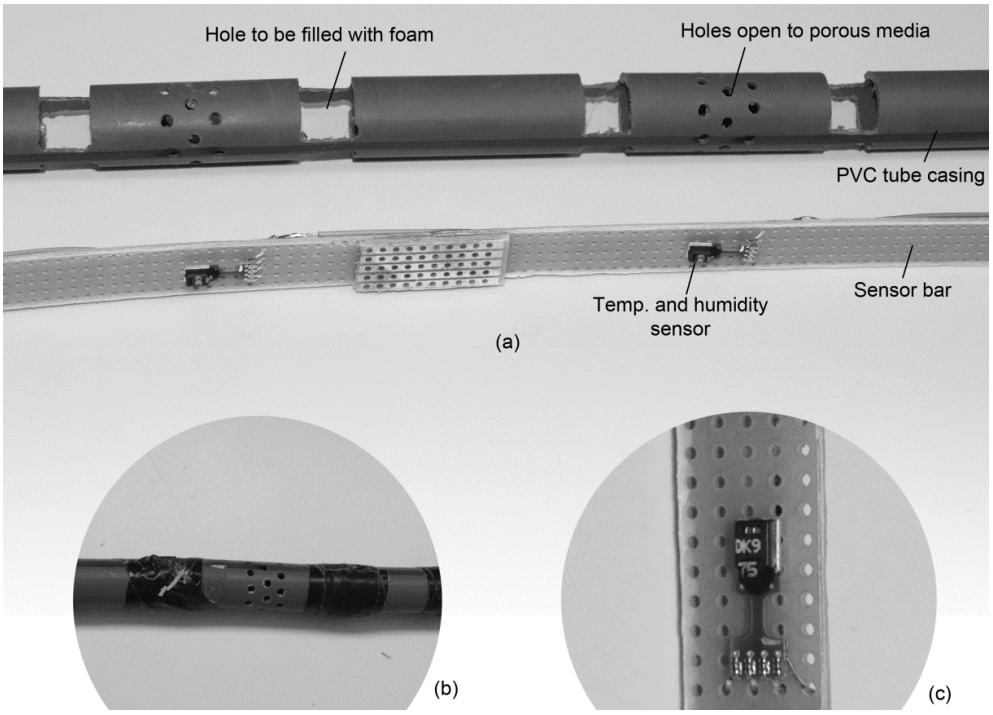

Fig. 2. (a) Sensor bar description; (b) final aspect before insertion into the wall; and (c) close-up of the temperature/relative humidity sensor

A common issue in measuring hygrothermal conditions inside high thickness materials is the assessment of the exact sensors locations along the wall depth. Individual sensors are generally chosen for straw bales monitoring [21, 22], which requires a particular attention during

assembly and doesn't provide a guarantee of equal sensor interspacing. In order to limit this source of error, rigid sensor bars were created instead, made from several sensing elements fixed on a rigid support.

Each bar is composed of four SHT75 (*Sensirion*) digital temperature and relative humidity (RH) sensors welded on a support board (**Fig. 2c**). Each sensor is factory-calibrated and offers an accuracy of 1.8%RH on relative humidity and 0.3°C on temperature measurements in the typical ranges met in building materials. First the sensors were welded on a Bakelite strip board with conductive copper bands (**Fig. 2c**). This long plate was then protected in a PVC tube of 15mm diameter (**Fig. 2a**). Perforations at the location of the sensors enable the measurement. Finally, thermal insulation foam was injected between sensors through large holes provided for this purpose. The filled holes are then protected with plastic tape (**Fig. 2b)**

Four sensors bars were used to gather hygrothermal conditions in the straw bales along the wall depth (**Fig. 1b**). In complement, individual SHT75 elements were incorporated in the plaster in the alignments of sensor bars. They are protected with a small concrete rawlplug. **Figure 3** shows typical sensors alignment with resulting measurement points relative to wall depth.

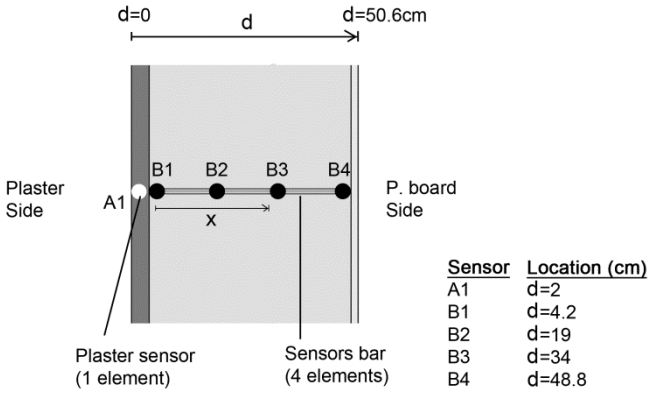

Fig. 3. Final location of individual sensors

2.2 Thermal shock in a controlled climate chamber

Various sizes of walls were planned to be tested with the device, therefore the climatic chamber was made modular with a fixed base and some movable parts. A diagram illustrating the operation of a test wall is shown in **Figure 4**. The positions of the floor and the front chamber panels can be adjusted to fit the desired dimensions. Each structural panel composing the chamber is made from 100x38mm timbers wood-frame closed with 18mm OSB bracing. Extruded polystyrene provides thermal insulation and the surfaces facing the indoor air volumes are covered with a moisture barrier layer to avoid moisture penetration in the chamber structure. The chamber panels were firmly fixed around the test wall with multiple bolts and compressible air-tight joints on contact area.

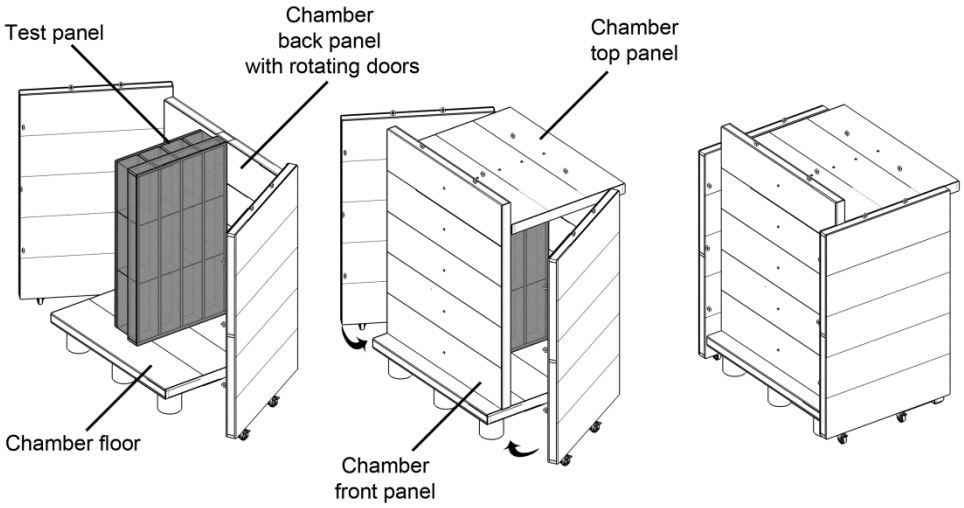

Fig. 4. Modular climate chamber design

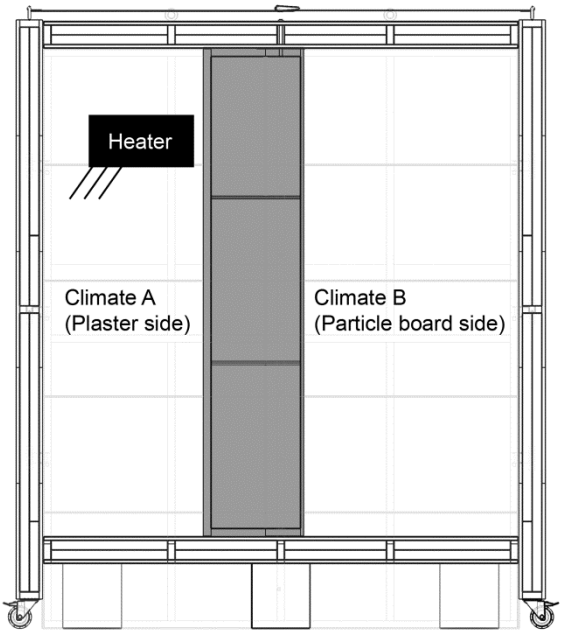

Fig. 5. Bi-climatic system with heater on plaster side

Once the back panel rotating doors are closed, two climates can be controlled and monitored on each side of the test wall. That is why the testing device can be referred to as a 'Bi-climatic chamber' (**Fig. 5**). It offers opportunities for one-dimensional analysis of the wall assembly and was designed to impose various climatic schemes: realistic conditions or more artificial solicitations among which hydric or thermal shocks. Here, a 2kW pulsed air heater was placed in the 'Climate A' volume together with a PID control system. At the beginning of the experiment, a temperature step was applied on the plaster side of the wall (from room

temperature ≈20°C to 35°C). After 54h, the heating system was switched off and the two doors of the climate chamber were opened to the hall climate. The entire monitoring system continued to log data for another 20 days. During the entire test, Climate B was not controlled. In addition to panel sensors, four temperature/RH sensors were placed in each sub-chamber at various height levels to get an averaged measurement of climates A and B hygrothermal conditions. The sampling rate of every sensor is one measurement per minute. It should be stressed that the entire test chamber lies itself in a workshop hall were temperature and humidity fluctuations are low.

2.3 Hygrothermal model

2.3.1 General assumptions and macroscopic balance equations

A combined heat and moisture transfer model was previously developed in *COMSOL Multiphysics* to simulate a case study in which temperature gradients are expected to be low [13, 14]. The model was upgraded here to confront the thermal shock study by incorporating a temperature dependence of moisture content.

The simulated straw bales are considered as a 1D multiphase system and the developed conservation PDEs are based on volume averaging theory [23]. For the present research, the balance equation system was solved for relative humidity and temperature as main dependent variables. **Equation 1** shows the moisture mass conservation equation:

$$\rho_0 \xi_\varphi \frac{\partial \varphi}{\partial t} + \rho_0 \xi_T \frac{\partial T}{\partial t} = -\frac{\partial}{\partial x}\left[\underbrace{-\frac{\delta_a \varphi}{\mu}\frac{\partial p_{sat}}{\partial T}\frac{\partial T}{\partial x} - \frac{\delta_a p_{sat}}{\mu}\frac{\partial \varphi}{\partial x}}_{j_x^{M_v}}\right] \quad (1)$$

where $\boldsymbol{j_x^{M_v}}(kg \cdot m^{-2} \cdot s^{-1})$ is the vapour diffusion flux density, $\rho_0(kg \cdot m^3)$ is the bulk density of the material, $u\ (kg_v \cdot kg_0^{-1})$ is the material moisture content, $\delta_a\ (kg \cdot m^{-1} \cdot s^{-1} \cdot Pa^{-1})$ the vapor permeability of dry air and $\mu\,(-)$ is the vapour resistance factor of the material, considered constant during the thermal shock. This parameter does not strictly account for vapour transport but also handle other moisture transport modes occurring in the hygroscopic moisture content range, namely capillary water transport in very small pores and multilayered adsorbed water diffusion. The hypothesis of a constant value only holds if the moisture content of the material does not vary too much. On the left hand side, the moisture capacities terms $\xi_\varphi\ (kg_v \cdot kg_0^{-1})$ and $\xi_T(kg_v \cdot kg_0^{-1} \cdot K^{-1})$ represent the variation of moisture content with RH at constant temperature $\left(\frac{\partial u}{\partial \varphi}\Big|_T\right)$ and the variation of moisture content with temperature at constant RH $\left(\frac{\partial u}{\partial T}\Big|_\varphi\right)$ respectively. The second term only exists if temperature is assumed to have an influence on moisture storage. On the right hand side of the equation it is observed that

neither liquid transfer nor advective vapour fluxes are accounted for as they are assumed to play only little role during the simulated heat shock. Finally, it should be oberved that the hysteresis phenomenon is not considered as it is expected to be of little influence provided: (1) the initial condition of the straw bales, in equilibrium with an atmosphere of 50%RH and (2) the variation of moisture content that is not expected to reach values where hysteresis plays a significant role.

Applying the law of conservation of heat, the enthalpy change in an averaged volume element is determined by the divergence of heat conduction flux density, by sensible heat transport and by latent heat involved in the phase change process:

$$\frac{\partial H}{\partial t} = \frac{\partial}{\partial x}\underbrace{\left[\lambda_{eff}\frac{\partial T}{\partial x}\right]}_{Conduction} - \underbrace{\boldsymbol{j}_{\boldsymbol{x}}^{\boldsymbol{M_v}} \cdot c_v \frac{\partial T}{\partial x}}_{Sensible\ heat} - \underbrace{\dot{m}(Q_{st})}_{latent\ heat} \tag{2}$$

Where $H\ (J \cdot m^{-3})$ is the enthalpy, $\dot{m}\ (kg \cdot m^{-3} \cdot s^{-1})$ the phase change rate, λ_{eff} is the effective thermal conductivity of the material and $Q_{st}\ (J \cdot kg^{-1})$ is the amount of energy involved in the sorption process, known as the isosteric heat of sorption. Under the assumption that moisture storage in vapour phase is negligible compared to liquid phase, the phase change rate term is equal to the vapour flux divergence. The effective thermal conductivity is considered constant during the thermal shock and its value was chosen to account for an average value met during the thermal shock. By developing the enthalpy term, the heat balance equation becomes:

$$\frac{\partial\left(\rho_0 c_0 (T - T_0) + \rho_0 u c_l (T - T_0)\right)}{\partial t} = \frac{\partial}{\partial x}\left[\lambda_{eff}\frac{\partial T}{\partial x}\right] - \boldsymbol{j}_{\boldsymbol{x}}^{\boldsymbol{M_v}} \cdot c_v \frac{\partial T}{\partial x} - \frac{\partial \boldsymbol{j}_{\boldsymbol{x}}^{\boldsymbol{M_v}}}{\partial x} \cdot (Q_{st}) \tag{3}$$

Finally, with additional transformations and the assumption that sensible heat transport is negligible in comparison to latent heat, the heat balance equation becomes:

$$\rho_0(c_0 + u c_l + \xi_T c_l (T - T_0))\frac{\partial T}{\partial t} + \rho_0 \xi_\varphi \frac{\partial \varphi}{\partial t} c_l (T - T_0) = \frac{\partial}{\partial x}\left[\lambda_{eff}\frac{\partial T}{\partial x}\right] - \frac{\partial \boldsymbol{j}_{\boldsymbol{x}}^{\boldsymbol{M_v}}}{\partial x}(Q_{st}) \tag{4}$$

2.3.2 Temperature effect on moisture storage

When water molecules are absorbed on the inner porous structure some heat of sorption is released, and a corresponding amount of energy is required to desorb it. This enthalpy change is greater than the heat of vaporization of free water $L\ (J \cdot kg^{-1})$ and the difference is expressed as the differential heat of sorption or net isosteric heat $q_{st}\ (J \cdot kg^{-1}) = Q_{st} - L$. This quantity depends on the moisture content because successive water molecules layers show different bonding energy to the solid matrix of the material. One of the methods to determine this function is based on the Clausius-Clapeyron (CC) formula [24]. With a minimum of two sorption curves data sets, measured at different temperatures, we have:

$$q_{st}(u) = R_v \ln\left(\frac{\varphi_{T1}(u)}{\varphi_{T2}(u)}\right)\left(\frac{T_1 T_2}{T_1 - T_2}\right) \quad (5)$$

Where R_v $(J \cdot kg^{-1} \cdot K^{-1})$ is the water vapour specific gas constant and $\varphi_{T1}(u)$ and $\varphi_{T2}(u)$ respectively the sorption isotherms at temperature T_1 and T_2. From this equation, it is easily deduced that the equilibrium moisture content increases with decreasing temperature with a maximum at 0°C [25].

Sorption curves of straw bales were measured on the 0-90%RH range at 23°C and 35°C with a dynamic vapour sorption (DVS) apparatus. This device was precisely parameterized to account for the specific equilibrium time observed for the straw material for each temperature. The Oswin moisture storage function [26] was then fitted on resulting (φ_i, u_i) experimental points. It offers a continuous expression of moisture content in dependence with relative humidity:

$$u(\varphi) = C * \left(\frac{\varphi}{1-\varphi}\right)^n \quad (6)$$

Where C and n are constant parameters, estimated independently for the two temperatures by minimizing the sum of squared residuals. Best parameters are C=0.0793 and n=0.48 to fit the sorption isotherm at 23°C and C=0.0730 and n=0.49 for sorption isotherm at 35°C. **Figure 6a** shows the two measured sorption isotherms together with the fitted Oswin storage functions and **Figure 6b** shows the net isosteric heat computed for straw using **Equation 5**.

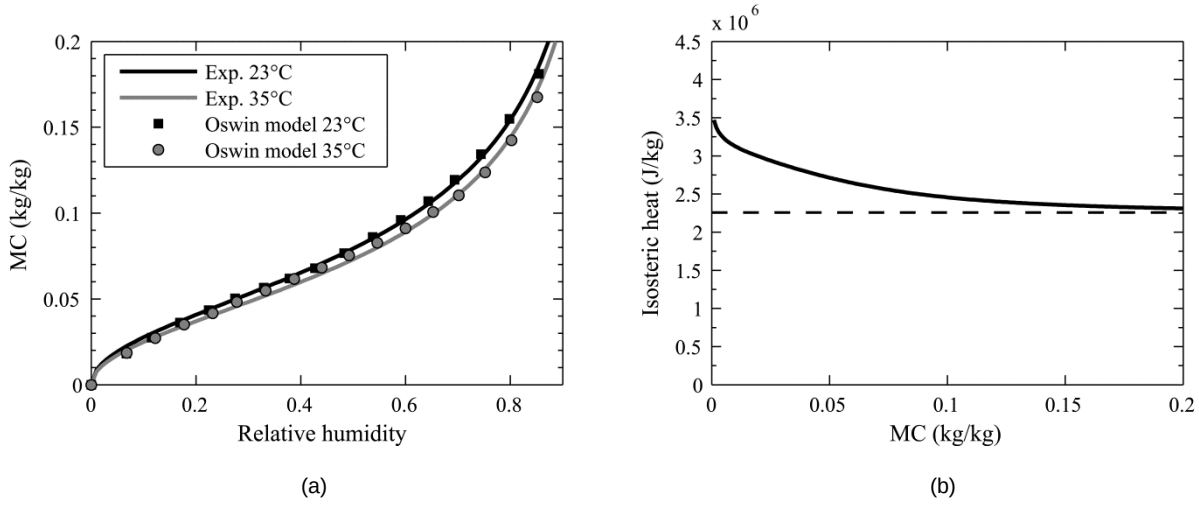

Fig. 6. Measured sorption isotherms of straw at 23 and 35°C fitted with Oswin model (a); net isosteric heat (b)

Once the net isosteric heat function is known or determined on the basis of two sorption isotherms, Poyet & Charles [27] showed that the CC equation can be arranged to construct a temperature-dependent expression of the moisture storage by expressing the equilibrium relative humidity as:

$$\varphi(u,T) = \varphi_{Tref}(u) \cdot \exp\left[\frac{q_{st}(u)}{R_v}\left(\frac{T-T_{ref}}{TT_{ref}}\right)\right] \quad (7)$$

Where $\varphi_{Tref}(u)$ is a reference sorption curve at temperature T_{ref}, which in our study can be either 23 or 35°C. One of the big advantages of this method is that any model can be used to describe this reference isotherm. However, in order to solve the heat shock case study a continuous expression in the form $u(\varphi,T)$ is desirable. Indeed, such '3D' representation of the moisture content u would provide values for moisture capacities in all combinations of temperature and humidity conditions that are potentially met in the material. Unfortunately, **Equation 7** is not directly reversible and two different approaches were undertaken to overcome this issue. These approaches result in two different descriptions of the moisture storage function $u(\varphi,T)$, one is physically based and the other is purely empirical.

The most physically-accurate method is to create an arbitrary number of moisture storage curves $\varphi(u,T_i)$ at different temperatures T_i using **Equation 7**. Then, it is possible to obtain the continuous $u(\varphi,T)$ expression by linear interpolation between the reciprocal of these individuals isotherms. This operation requires that 3D interpolation is available in the numerical environment.

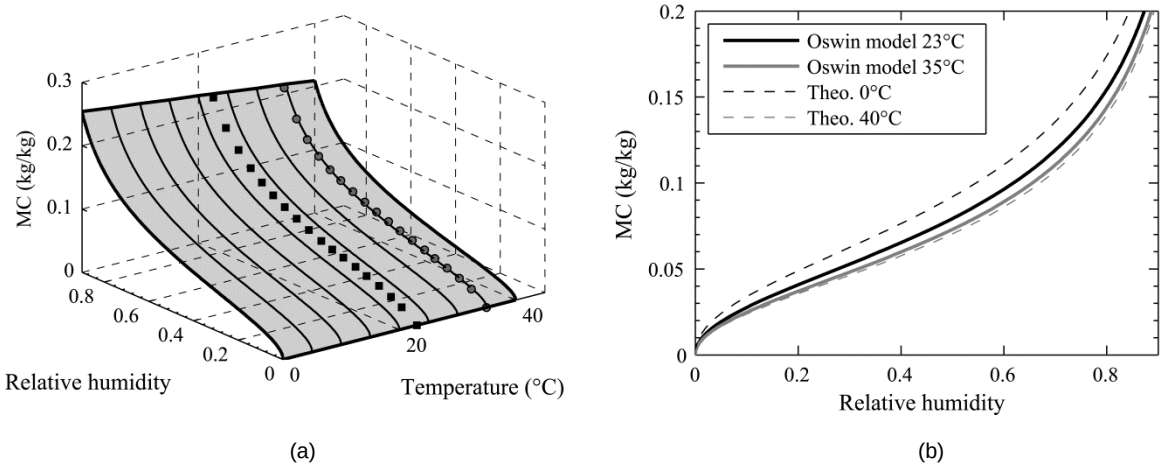

Fig. 7. Temperature-dependent MSC constructed by linearization between 9 isotherms (a); theoretical MSCs of straw at 0 and 40°C with physically based model and the two experimental curves used to determine them (b)

An interpolated 'surface', based on nine individual curves is shown in **Figure 7a**. As an illustration purpose, the two boundary isotherms, which correspond to 0°C and 40°C, are shown on **Figure 7b**. We recall that only the adsorption curve is considered in this work as hysteresis phenomena are assumed to be negligible in the heat shock working range.

The second modelling technique studied here is characterized by a simpler representation of temperature effect on moisture storage. In contrast to the physically based method embodied in

Equation 7, Keey [28] proposed an empirical expression of thermal moisture capacity assuming a linear dependence on moisture content:

$$\left.\frac{\partial u}{\partial T}\right|_{\varphi} = -A \cdot u \tag{8}$$

According to Keey, the parameter A (K^{-1}) lies between 0.005 and 0.01 for wood, for RH values in the 10-90%RH range. On the basis of this simplified assumption, we propose to write the following expression for the temperature-dependent MSC:

$$u(\varphi, T) = u_{Tref}(\varphi) \cdot \left(1 - A\left(T - T_{ref}\right)\right) \tag{9}$$

Where $u_{Tref}(\varphi)$ is the Oswin storage function whose parameters are fitted on experimental points measured at temperature T_{ref}. Here the 23°C experimental sorption isotherm is chosen arbitrarily as reference. The value of parameter A was optimized to minimize the difference between the computed curve and experimental measurements for a temperature of 35°C. This optimization led to a value of $A = 0.0058$ with a residual error given in **Figure 8**.

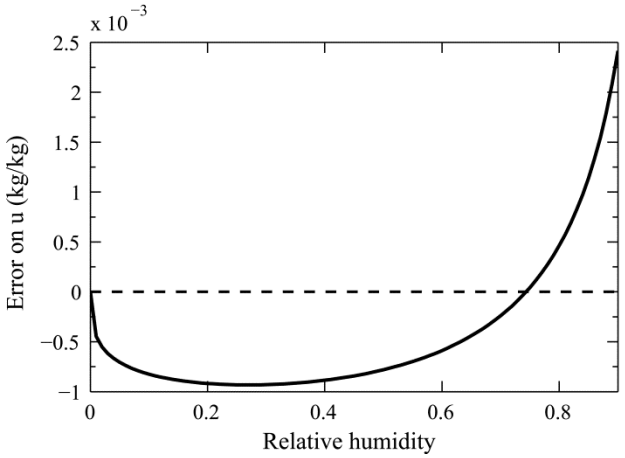

Fig.8. Error of the second method to obtain the temperature dependent MSC, for A=0.0058

2.4 Modelling procedure

2.4.1 Variations of the model

The chosen computing environment provides direct access to mathematical expressions, which allows high modularity depending on the case study and potential efficiency enhancement. Three distinct versions of the *COMSOL* model were prepared in order to analyze the impact of the moisture storage description on output error, given the results from the thermal shock experiment. **Table 1** provides the balance equations and moisture content description for all three versions.

The *PB-Version* of the BEHAM model represents the most complex description; the MSC is constructed on the basis of the physically based description of EMC dependence on temperature (**Eq. 7**). It results that the net isosteric heat function is also included in the heat balance. In E1-version, the model is simplified with the one-parameter description of moisture storage dependence on temperature (**Eq. 9**). The isosteric heat is equal to the heat of vaporization of free water because no direct characterization of the differential heat of sorption can be obtained from this approach. Finally, the *ISO-version* is characterized by the standard description found in most BEHAM software, which is a single sorption isotherm. Similarly to the *E1-version*, the heat of sorption shows a simplified representation. It should be noted that all versions are similar with regard to the description of heat and moisture transport.

Table 1. The three variations of the model

PB-Version **- Temperature effect on MSC: Physically based**	
Balance equations	Moisture storage
$\rho_0 \xi_\varphi \frac{\partial \varphi}{\partial t} + \rho_0 \xi_T \frac{\partial T}{\partial t} = -\frac{\partial}{\partial x}\left[-\boldsymbol{j_x^{M_v}}\right]$	$u(\varphi, T)$ Interpolated from 9 isotherms individually computed from:
$\rho_0(c_0 + uc_l + \xi_T c_l(T - T_0))\frac{\partial T}{\partial t} + \rho_0 \xi_\varphi \frac{\partial \varphi}{\partial t} c_l (T - T_0) = \frac{\partial}{\partial x}\left[\lambda_{eff} \frac{\partial T}{\partial x}\right] - \frac{\partial \boldsymbol{j_x^{M_v}}}{\partial x}(L + q_{st}(u))$	$\varphi(u, T_i) = \varphi_{Tref}(u) \cdot \exp\left[\frac{q_{st}(u)}{R_v}\left(\frac{T_i - T_{ref}}{T_i T_{ref}}\right)\right]$
E1-Version **- Temperature effect on MSC: One-parameter empirical description**	
Balance equations	Moisture storage
$\rho_0 \xi_\varphi \frac{\partial \varphi}{\partial t} + \rho_0 \xi_T \frac{\partial T}{\partial t} = -\frac{\partial}{\partial x}\left[-\boldsymbol{j_x^{M_v}}\right]$	
$\rho_0(c_0 + uc_l + \xi_T c_l(T - T_0))\frac{\partial T}{\partial t} + \rho_0 \xi_\varphi \frac{\partial \varphi}{\partial t} c_l (T - T_0) = \frac{\partial}{\partial x}\left[\lambda_{eff} \frac{\partial T}{\partial x}\right] - \frac{\partial \boldsymbol{j_x^{M_v}}}{\partial x}(L)$	$u(\varphi, T) = u_{Tref}(\varphi) \cdot \left(1 - A\left(T - T_{ref}\right)\right)$
ISO-Version **- No temperature effect on MSC**	
Balance equations	Moisture storage
$\rho_0 \xi_\varphi \frac{\partial \varphi}{\partial t} = -\frac{\partial}{\partial x}\left[-\boldsymbol{j_x^{M_v}}\right]$	
$\rho_0(c_0 + uc_l)\frac{\partial T}{\partial t} + \rho_0 \xi_\varphi \frac{\partial \varphi}{\partial t} c_l (T - T_0) = \frac{\partial}{\partial x}\left[\lambda_{eff} \frac{\partial T}{\partial x}\right] - \frac{\partial \boldsymbol{j_x^{M_v}}}{\partial x}(L)$	$u(\varphi) = C * \left(\frac{\varphi}{1 - \varphi}\right)^n$

2.4.2 Boundary and initial conditions

In order to reduce the number of parameters needed to solve the problem, it was decided to limit the study domain to the straw bales material. The behaviours of the particle board and the plaster are not simulated. Dirichlet boundary conditions are thus applied to both extremities of the domain with temperature and relative humidity values measured just behind the plaster (sensor B1) and just behind the particle board (sensor B4). Referring to **Figure 3**, we can write the following expressions for boundary and initial conditions:

$$\begin{cases} \varphi(t) = \varphi_{B1}(t) \\ T(t) = T_{B1}(t) \end{cases} \quad x = 0m \text{ (B1)} \tag{10}$$

$$\begin{cases} \varphi(t) = \varphi_{B4}(t) \\ T(t) = T_{B4}(t) \end{cases} \quad x = 0.45m \ (B4) \tag{11}$$

$$\begin{cases} \varphi(x,0) = \varphi_0(x) \\ T(x,0) = T_0(x) \end{cases} \quad 0 < x < 0.45m \tag{12}$$

Where $\varphi_\alpha(t)$ and $T_\alpha(t)$ are the actual RH and temperature time series measured at sensor α, $\varphi_0(x)$ is the initial relative humidity vector and $T_0(x)$ the initial temperature vector. The last two vectors are determined from initial temperature and RH measured at sensors B1, B2, B3 and B4.

2.4.3 Straw bale properties

For the version 1 of the model, a total of 8 material parameters values $(\rho_0, c_0, \lambda_{eff}, C_{T1}, n_{T1}, C_{T2}, n_{T1}, \mu)$ are needed in order to solve the heat and moisture balance equations (**Eq. 1** and **4**) in the straw bale material, knowing the conditions imposed on its limits with B1 and B4 sensors. In order to solve the *E1-version* of the model, the value of parameter *A* is needed instead of two Oswin parameters needed in the *PB-version* to define a second isotherm. Finally the third version (*ISO*) requires nor the definition of a second isotherm neither the value of parameter *A*.

Measuring all those parameters can be particularly tricky because of the size of straw bales and the intrinsic variability they show. The parameters used during the direct modelling approach are given in **Table 2**.

First the bulk density is expected to be included in the 80-120 $kg \cdot m^{-3}$ range but it is impossible to know the actual value for the straw bales incorporated in the panel. In consequence, the median and most probable value was implemented in simulations. The dry thermal capacity was determined by differential thermal analysis on a crushed sample previously dried. A guarded hot plate (GHP) apparatus designed for high thickness specimens [29] was used to determine the dry thermal conductivity of an entire straw bale at 20°C. With

thermal flow parallel to fibres the value obtained was $\lambda_0 = 0.0682\, W \cdot m^{-1} \cdot K^{-1}$. In subsequent simulations a constant effective thermal conductivity is used, λ_{eff}, which represents an averaged value over conditions met during the test. In consequence, it should be expect to be higher than the measured conductivity.

Table 2. Straw bales parameters used in simulations

Parameter	Unit	Value	Method
$\boldsymbol{\rho_0}$	$(kg \cdot m^{-3})$	100	Estimated from standard values
$\boldsymbol{c_0}$	$(J \cdot kg^{-1} \cdot K^{-1})$	2426	DTA
$\boldsymbol{\lambda_{eff}}$	$(W \cdot m^{-1} \cdot K^{-1})$	0.08	Estimated from dry value (GHP)
$\boldsymbol{C_{23°C}}$	$(-)$	0.0793	DVS
$\boldsymbol{n_{23°C}}$	$(-)$	0.48	DVS
$\boldsymbol{C_{35°C}}$	$(-)$	0.0730	DVS
$\boldsymbol{n_{35°C}}$	$(-)$	0.49	DVS
$\boldsymbol{A}$	(K^{-1})	0.0058	Estimated from DVS
$\boldsymbol{\mu}$	$(-)$	2	Estimated from literature

In section 2.3.2 the values for the Oswin model parameters were presented, on the basis of DVS measurements analysis. It was also described how parameter $\boldsymbol{A}$ value could be obtained. With one or the other technique retained for the description of the temperature effect on moisture storage, the isothermal and non isothermal moisture capacities functions, $\boldsymbol{\xi_{\varphi}(\varphi, T)}$ and $\boldsymbol{\xi_T(\varphi, T)}$ are then easily determined. A large uncertainty remains concerning the actual moisture content modification with temperature and the 'representativeness' of the chosen mathematical description which has to be confirmed in this research. Finally, the vapour resistance factor of straw is quite difficult to measure with standard dry or wet-cup methods. At first approximation, its value was fixed based on the work of Wihan [30]. As for effective thermal conductivity, a constant vapour transport is assumed given the lack of available data in literature and the difficulties in assessing the vapour transport variation with dependent variables. However, it can be expected to be negligible based on measurements performed on other materials and expected conditions in the straw bales during the thermal shock [31].

3. RESULTS AND DISCUSSIONS

3.1 Sub-chambers sensors data

The temperature measured in sub-chambers A and B are shown in **Figure 9**. The temperature is maintained around 34°C in the A-part volume during the 54 first hours of the test. Then, as the doors of the chamber are opened on both end sides, its value drops rapidly to meet the hall temperature. Thereafter, the temperature measured in both sub-chambers corresponds to the

variations occurring in the large test hall where the device was placed. Values oscillated around 20°C following a natural daily cycle with higher temperature during the day.

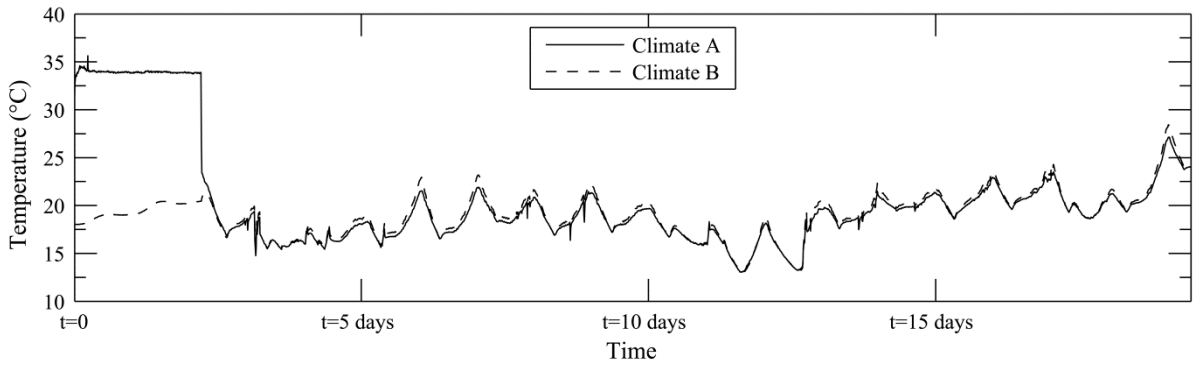

Fig.9. Temperature measured in sub-chambers A and B

3.2 Numerical results

Figure 10 presents the temperature and RH simulated at B2 sensor location by the three versions of the model compared to measured data. **Figure 11** provides the same information at B3 sensor location, a bit further in the straw depth relatively to the thermal shock progression. No distinction can be made visually between models concerning the temperature field modelling. The output of all model variations seems to compare quite well to experimental temperature in the case of sensor B2. A small delay can be observed between experimental and numerical temperature peaks for sensor B3. This could be explained most likely by small errors in the definition of the straw inertia through density and heat capacity parameters. Concerning the RH field, the *ISO-version* of the model clearly underscored in modelling performance. For both sensors, it seems that *ISO-version* only accounts for the general humidity decreases which can be observed throughout the entire test period. All the higher frequencies of humidity variation, apparently linked to the temperature variation, are not modelled by this simplest description.

To enlarge the discussion, some efficiency criteria were computed for all simulations and summarized in **Table 3**. We used the Nash-Sutcliffe efficiency coefficient (NSE), the percent bias (PBIAS) and the root mean square error (RMSE) as defined in [14]. Results are presented for temperature and relative humidity data sets separately but both sensors locations are considered together.

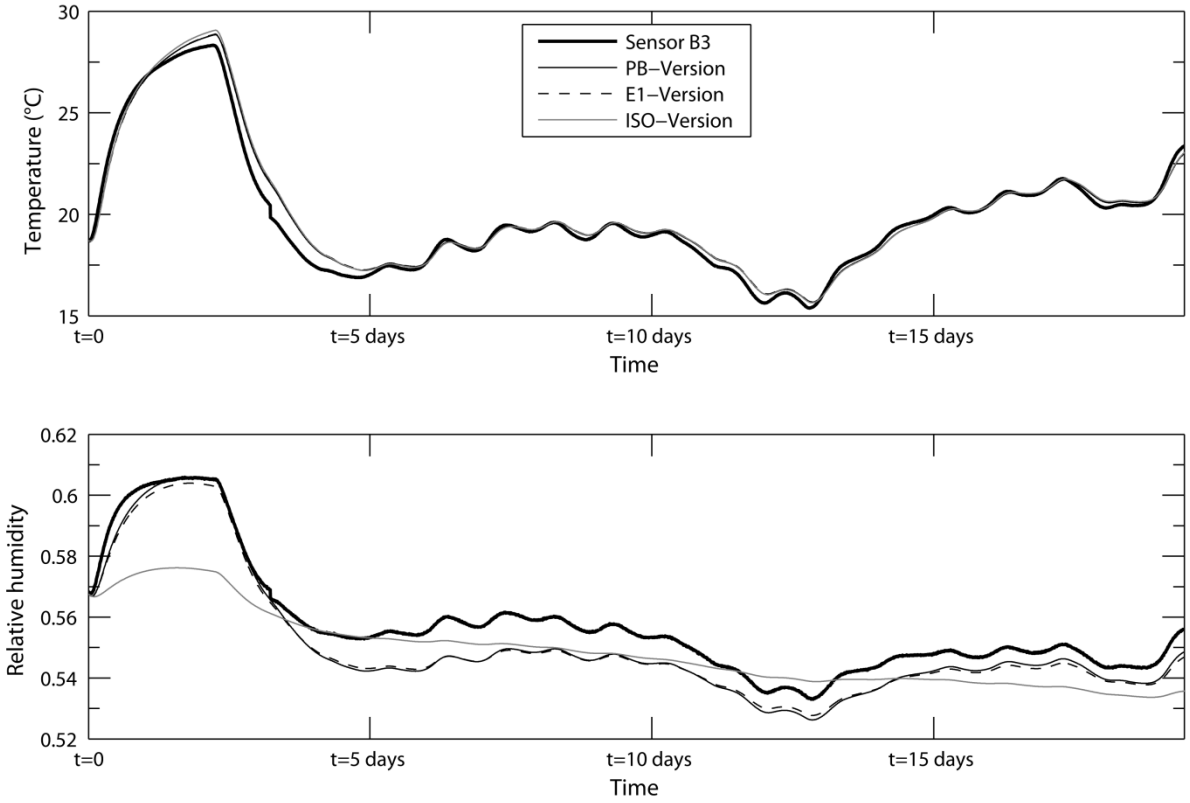

Fig.10. Simulation results for the three model versions compared to experimental data (B2)

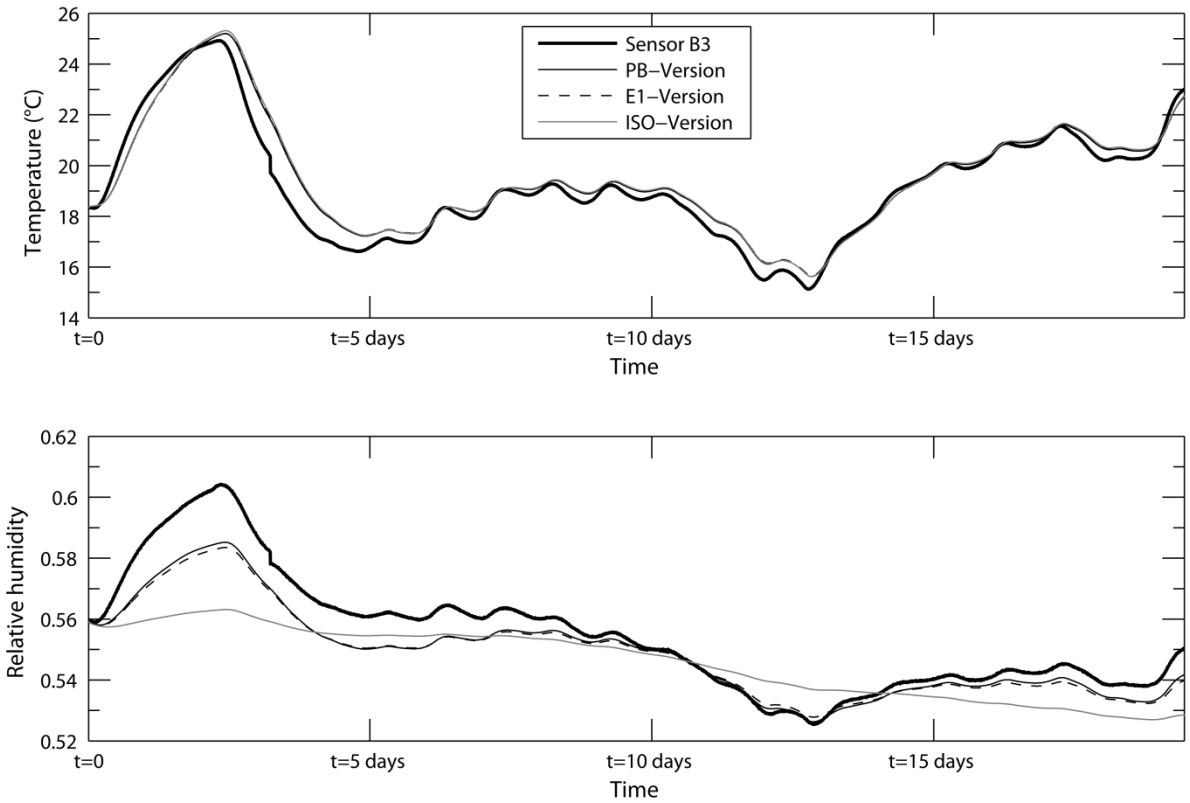

Fig.11. Simulation results for the three model versions compared to experimental data (B3)

Table 3. Efficiency criteria computed for all model versions, distinctly presented for the temperature and relative humidity fields

	Temperature			Relative humidity		
	NSE	**PBIAS**	**RMSE**	**NSE**	**PBIAS**	**RMSE**
PB-Version	0.966	-0.07%	0.502	0.834	1.13%	0.0077
E1-Version	0.962	-0.08%	0.530	0.819	1.19%	0.0080
ISO-Version	0.958	-0.09%	0.553	0.504	1.57%	0.0133

For the temperature field modelling, all model versions show a similar efficiency with NSE>0.95. The improvement of efficiency respects the simplification magnitude in the mathematical description as *PB-version* performs slightly better than *E1-version* that shows itself a better NSE and RMSE than ISO-version. They all show a little tendency to overestimate temperature as PBIAS is around -0.1%. The internal relative humidity modelling is clearly less accurate with the standard HAM description corresponding to *ISO-version*. The NSE rises spectacularly when the effect of a variable isotherm is included.

It is observed that the formulation proposed by Keey (**Eq. 12**) and the corresponding proposal for continuous expression of MSC gives a good representation of straw behaviour, which is only slightly improved by the physically-based approach. This formulation offers advantages in terms of model coding and computational time. In specific application where temperature gradients are high it offers a simple way to account for temperature dependence of moisture content. The temperature effect on moisture storage is then characterized with only one parameter whereas the physically-based method requires at least two parameters, i.e. to characterize a second complete isotherm in order to define the net isosteric heat function.

In section 2.3.5, we showed that much uncertainty remains in the characterization of the straw bale material. Moreover, a lot of simplification hypotheses were assumed during these simulations: absence of liquid transport, constant transport coefficients and no hysteresis phenomena. It seems clear that considering these different effects could improve further the efficiency but it might require an unnecessary amount of efforts compared to the additional efficiency obtained. Concerning the material parameters, some large obstacles remain in determining their values for such unusual construction product. In that context, inverse modelling techniques, as presented in [13] could offer an original way of improving simulations.

4. CONCLUSION

In this paper, a flexible numerical model for heat and moisture transfer in building materials is used to simulate the behaviour of a hygroscopic wall assembly under non isothermal

solicitations. A prefabricated straw bale panel was first subjected to a 35°C thermal shock in a climate chamber. Specific T/RH sensors were created to answer the need for proper sensing location. The monitoring of internal conditions in straw bales during this test constitutes the measurement data intended to be compared with the output of the model. The test was chosen so that the hysteresis effect and explicit liquid moisture transport can be neglected given the expected resulting RH in the materials.

The numerical model used to describe the heat and moisture transfer in the straw during the heat shock is developed in *COMSOL* and uses a mass balance equation in which moisture content variation with temperature can be considered. Two approaches were illustrated to characterize a continuous 'sorption surface' with relative humidity and temperature dependencies. This study shows that choosing a one-parameter empirical approach can greatly enhance the efficiency of a BEHAM model for the prediction of the internal relative humidity field, in comparison to the frequent isothermal sorption characteristic assumption. This technique is easy to implement and offers a true continuous description of moisture capacities. The physically-based method needs to be constructed from multiple individual isotherms and only offers slight further improvement. It should be specified that those refinements might become insignificant when temperature gradients are moderate, as often in normal use conditions of a building. A better definition of other material and experimental parameters should then provide a better source for prediction optimization. The combination of the temperature effect on moisture storage with other physical phenomena which are not perfectly understood, i.e. hysteresis and liquid transport, should also be discussed more extensively. Still, this paper proves that in some particular conditions the single isotherm assumption does not transpose adequately the actual behaviour of crop-based materials. A possible consequence is the misinterpretation of RH sensors readings when the latter are used for internal conditions monitoring.

NOMENCLATURE

$\boldsymbol{\delta}$	$(kg \cdot m^{-1} \cdot s^{-1} \cdot Pa^{-1})$	Vapour permeability
$\boldsymbol{\lambda_{eff}}$	$(W \cdot m^{-1} \cdot K^{-1})$	Effective thermal conductivity
$\boldsymbol{\mu}$	$(-)$	Vapour diffusion resistance factor
$\boldsymbol{\xi_{\varphi}}$	$(kg_v \cdot kg_0^{-1})$	Isothermal moisture capacity
$\boldsymbol{\xi_T}$	$(kg_v \cdot kg_0^{-1} \cdot K^{-1})$	Thermal moisture capacity
$\boldsymbol{\rho}$	$(kg \cdot m^{-3})$	Density
$\boldsymbol{\varphi}$	$(-)$	Relative humidity
$\boldsymbol{c}$	$(J \cdot kg^{-1} \cdot K^{-1})$	Heat capacity
$\boldsymbol{H}$	$(J \cdot m^{-3})$	Enthalpy
$\boldsymbol{j_x^{M_v}}$	$(kg \cdot m^2 \cdot s^{-1})$	Vapour flux density
$\boldsymbol{L}$	$(J \cdot kg^{-1})$	Heat of vaporization of free water
$\boldsymbol{\dot{m}}$	$(kg \cdot m^{-3} \cdot s)$	Phase change rate
$\boldsymbol{T}$	(K)	Temperature
$\boldsymbol{T_0}$	(K)	Reference temperature (273 K)
$\boldsymbol{p_{sat}}$	(Pa)	Vapour saturation pressure
$\boldsymbol{p_v}$	(Pa)	Vapour partial pressure
$\boldsymbol{q_{st}}$	$(J \cdot kg^{-1})$	Net isosteric heat of sorption
$\boldsymbol{Q_{st}}$	$(J \cdot kg^{-1})$	Isosteric heat of sorption
$\boldsymbol{R_v}$	$(J \cdot kg^{-1} \cdot K^{-1})$	Specific gas constant of vapour
$\boldsymbol{t}$	(s)	Time
$\boldsymbol{u}$	$(kg_v \cdot kg_0^{-1})$	Moisture content
$\boldsymbol{x}$	(m)	Position in the wall

Subscripts

$\boldsymbol{a}$	Related to dry air
$\boldsymbol{l/v}$	Related to the liquid/gaseous phase of water
$\boldsymbol{0}$	Related to the dry state or initial condition

REFERENCES

[1] B. King, Design of straw bale buildings, Green Building Press, San Rafael 2006.

[2] A. Cripps, R. Handyside, L. Dewar, J. Fovargue, Crops in construction handbook, Report:CIRIA, London, UK, 2004.

[3] A. Shea, K. Wall, P. Walker, Evaluation of the thermal performance of an innovative prefabricated natural plant fibre building system, Building Services Engineering Research and Technology, 34 (4) (2013) 369-380. DOI: **10.1177/0143624412450023**

[4] S. Fuchs, O. Krumm, E. Cauderay, La construction en botte de paille, Report:ATBA, Lausanne, Switzerland, 2009.

[5] R.H. Peuhkuri, L.H. Mortensen, K.K. Hansen, B. Time, A. Gustavsen, T. Ojanen, J. Ahonen, K. Svennberg, J. Arfvidsson, L.-E. Harderup, Moisture Buffering of Building Materials, in: C. Rode (Ed.), Department of Civil Engineering, Technical University of Denmark, 2005.

[6] O.F. Osanyintola, C.J. Simonson, Moisture buffering capacity of hygroscopic building materials: Experimental facilities and energy impact, Energy and Buildings, 38 (10) (2006) 1270-1282.
DOI: **10.1016/j.enbuild.2006.03.026**

[7] M.V. Madurwar, R.V. Ralegaonkar, S.A. Mandavgane, Application of agro-waste for sustainable construction materials: A review, Construction and building materials, 38 (2013) 872-878.
DOI: **10.1016/j.conbuildmat.2012.09.011**

[8] C.-E. Hagentoft, A.S. Kalagasidis, B. Adl-Zarrabi, S. Roels, J. Carmeliet, H. Hens, J. Grunewald, M. Funk, R. Becker, D. Shamir, O. Adan, H. Brocken, K. Kumaran, R. Djebbar, Assessment Method of Numerical Prediction Models for Combined Heat, Air and Moisture Transfer in Building Components: Benchmarks for One-dimensional Cases, Journal of Thermal Envelope and Building Science, 27 (4) (2004) 327-352.
DOI: **10.1177/1097196304042436**

[9] A. Janssens, M. Woloszyn, C. Rode, A. Sasic-Kalagasidis, M. De Paepe, From EMPD to CFD–overview of different approaches for Heat

Air and Moisture modeling in IEA Annex 41, in: Proceedings of the IEA ECBCS Annex 41 Closing Seminar (2008), Lyngby, Denmark, 2008.

[10] J.M. Delgado, E. Barreira, N.M. Ramos, Hygrothermal Numerical Simulation Tools Applied to Building Physics, Springer, 2013.

[11] A.W.M. van Schijndel, Integrated modeling of dynamic heat, air and moisture processes in buildings and systems using SimuLink and COMSOL, Building Simulation, 2 (2) (2009) 143-155.
DOI: **10.1007/s12273-009-9411-x**

[12] F. Tariku, K. Kumaran, P. Fazio, Integrated analysis of whole building heat, air and moisture transfer, International Journal of Heat and Mass Transfer, 53 (15–16) (2010) 3111-3120.
DOI: **10.1016/j.ijheatmasstransfer.2010.03.016**

[13] S. Dubois, F. McGregor, F. Lebeau, A. Evrard, A. Heath, An inverse modelling approach to estimate the hygric parameters of clay-based masonry during a moisture buffer value test, submitted to Building and Environment (2014).

[14] S. Dubois, A. Evrard, F. Lebeau, Modeling the hygrothermal behavior of biobased construction materials, Journal of Building Physics, Published online (2013).
DOI: **10.1177/1744259113489810**

[15] H.S.L.C. Hens, Building Physics - Heat, Air and Moisture: Fundamentals and Engineering Methods with Examples and Exercises, John Wiley & Sons, 2008.

[16] K. Strømdahl, Water sorption in wood and plant fibres, Ph.D Thesis, Technical University of Denmark Danmarks Tekniske Universitet, 2000.

[17] B. Time, Hygroscopic moisture transport in wood, Ph.D Thesis, Norwegian University of Science and Technology, 1998.

[18] W. Simpson, Sorption theories applied to wood, Wood and Fiber Science, 12 (3) (1980) 183-195.

[19] C. Rode, C.-O. Clorius, Modeling of moisture transport in wood with hysteresis and temperature-dependent sorption characteristics, in: Proceedings of the Performance of Exterior Envelopes of Whole Buildings IX (2004), Oak Ridge, USA, 2004.

[20] A. Evrard, A. Louis, B. Biot, S. Dubois, Moisture equilibrium in straw bales walls, 28th Conference, Opportunities, Limits & Needs Towards an environmentally responsible architecture (PLEA 2012), Lima, Perú, 7-9 November 2012.

[21] R. Jolly, Straw bale moisture monitoring report, CMHC, Ottawa, Canada, 2002.

[22] J. Carfrae, P. De Wilde, J. Littlewood, S. Goodhew, P. Walker, Long term evaluation of the performance of a straw bale house built in a temperate maritime climate, in: Proceedings of the 11th International Conference on Non-conventional Materials and Technologies (NOCMAT 2009), Bath, UK, 2009.

[23] S. Whitaker, A Theory of drying, Advances in heat transfer, 13 (1977) 119-203.

[24] C. Skaar, Water in wood, Syracuse University Press, 1972.

[25] B. Cudinov, M. Andreev, Hygroscopicity of wood at temperatures below zero degrees centigrade. 2. The condition of the hygroscopic moisture and the equilibrium moisture content, Leipzig, VEB Fachbuchverlag, Holztechnologie, 19 (3) (1978) 147-151.

[26] C. Oswin, The kinetics of package life. III. The isotherm, Journal of the Society of Chemical Industry, 65 (12) (1946) 419-421.

[27] S. Poyet, S. Charles, Temperature dependence of the sorption isotherms of cement-based materials: Heat of sorption and Clausius–Clapeyron formula, Cement and Concrete Research, 39 (11) (2009) 1060-1067.
DOI: **10.1016/j.cemconres.2009.07.018**

[28] R.B. Keey, Introduction to Industrial Drying Operations, Pergamon Press, 1978.

[29] S. Dubois, F. Lebeau, Design, construction and validation of a guarded hot plate apparatus for thermal conductivity measurement of high thickness crop-based specimens, Materials and Structures, Published online (2013).
DOI: **10.1617/s11527-013-0192-4**

[30] J. Wihan, Humidity in straw bale walls and its effect on the decomposition of straw, Ph.D Thesis, University of East London School of computing and Technology, 2007.

[31] G. Galbraith, J. Guo, R. McLean, The effect of temperature on the moisture permeability of building materials, Building Research & Information, 28 (4) (2000) 245-259.
DOI: **10.1080/09613210050073706**

CHAPTER 7

Coupling the BEHAM model with zone balance to assess materials performance

7.1 Introduction

The first step in assessing CBM performance is to understand the specific dynamics of heat and mass transfers occurring within them. We showed how a research BEHAM model can be designed to accurately predict internal conditions encountered in materials, based on partial differential equations (PDE). Furthermore, the proposed model was upgraded to give a better conceptualization of the response of straw bale wall subject to transient climatic conditions with high temperature gradients. However, those approaches, based on the study of individual materials or envelope parts, required an a priori determination of the interior and exterior climatic conditions which are imposed to the studied element. Therefore, it prevents any detailed assessment of the impact of chosen materials on the indoor environment and prohibits any conclusion concerning the overall envelope performance in the context of an operating building. For example, in the case of a heat shock presented in the precedent chapter, we might be interested in evaluating how CBM participate in the indoor air balance. Does it offer some improvement of indoor conditions for occupants?

In response to this problematic, the development of whole-building hygrothermal models has recently attracted much attention among researches in Building Physics (Hens, 2005; Rode and Grau, 2008; Woloszyn and Rode, 2008; van Schijndel, 2009). Such models are obtained by combining a description of hygrothermal transfers in indoor air volumes with a description of the hygrothermal response of the envelope. By integrating these two model categories, it becomes possible to characterize the

evolution of the indoor climate of a zone or a building while considering the actual participation of envelope materials.

The Annex 41 of the International Energy Agency (IEA) emerged in 2005 as a cooperative project on the whole-building heat, air and moisture response. It is part of the Energy Conservation in Buildings and Community Systems program (ECBCS). Seventeen tools were then already identified to perform some common modelling exercises where the indoor air of a room had to dynamically interact with the heat, air and moisture response of the envelope (Rode and Woloszyn, 2007). In fact, these simulation tools differ in the level of spatial discretization they offer for the description of indoor air and envelope domains, sometimes referred to as the 'granularity' (Janssens et al., 2008). The highest granularity for indoor air volume is the CFD modelling whereas the coarser one consists of a perfectly-mixed air assumption for the whole building. For envelope modelling, very fine models can provide a 3D description of coupled heat, air and moisture transfers in construction materials assemblies. The coarser level uses some simple model to characterize the envelope response, like lumped approaches, which do not provide an actual computation of temperature and moisture fields in the whole depth of porous walls (Janssens et al., 2008). Various combination of granularity for envelope and indoor air modelling are observed among models capable of whole-building hygrothermal modelling, often depending on their origin. Indeed, some originate from BES models, and are generally characterized by a coarser granularity for envelope modelling, while others originate from BEHAM tools, and the air volume modelling is often really simplified. An extensive review of available tools can be found in (Woloszyn and Rode, 2008).

Recently, some authors showed that general scientific computational tools like *Matlab* (Sasic Kalagasidis, 2004; van Schijndel, 2009; Tariku et al., 2010) or *SPARK* (Tran Le et al., 2010) can be used to develop whole building hygrothermal models that meet important requirements for research-oriented modelling. However, there is still very few validation studies in real full-scale environments (Salonvaara et al., 2004).

In this chapter, a room-scale hygrothermal model is constructed by combining the research BEHAM model developed in *COMSOL Multiphysics* with a description of heat and moisture balance for indoor air volumes. Our research BEHAM model can be in-

tegrated in the *Matlab* environment, as done before during the inverse modelling approach, and can be handled in the *Simulink* interface which is adaptable to the description of indoor air balance equations. A thermal shock test on a straw bale wall, with an experimental set-up similar to the one presented in **Chapter 6**, will serve as the basis for a preliminary validation. This simple test should pave the way to a deeper understanding of the specificity of CBM materials, in particular to assess the impact of moisture buffering and latent heat phenomena on energy consumption and indoor conditions. Although many publications describe the development of similar models, it is the confrontation with experimental data involving CBM that is central here.

7.2 Experimental test

The experimental set-up is identical to the one described in **Chapter 6**. Once the straw wall is anchored in the climate chamber, two air zones ensued, one on each of its sides (**Fig. 7.1**). The first air volume on the side of plaster is 2.84 m^3 (zone-1) and was provided with a 2kW pulsed air heater that was continuously monitored by a wattmeter. The heat shock took place in that zone through injection of hot air. The second zone, on the side of the particle board, has a volume of 4.01 m^3 (zone-2) and its climate was not controlled during the test. Six temperature/RH sensors were added to sensors dedicated to internal conditions monitoring, which were detailed in **Chapter 6**. Those new sensors are dedicated to the measurement of hygrothermal conditions in the interior and exterior air domains. The first two sensors were used to measure the hygrothermal conditions in zone-1, two other were placed in zone-2 and the last two for measuring the external environment, *i.e.* the climate in the hangar that houses the climate chamber (**Fig. 7.2**).

At the beginning of the test, the control circuit of the heater was activated. The latter is composed of a PID controller adjusted to maintain the temperature at 35°CC during six days. After this period, the heating system was switched off but the hygrothermal monitoring system was maintained for a further six days while the room was naturally returning to equilibrium. the output of the wattmeter connected to the heater is shown on **Figure 7.3**, for the entire test period.

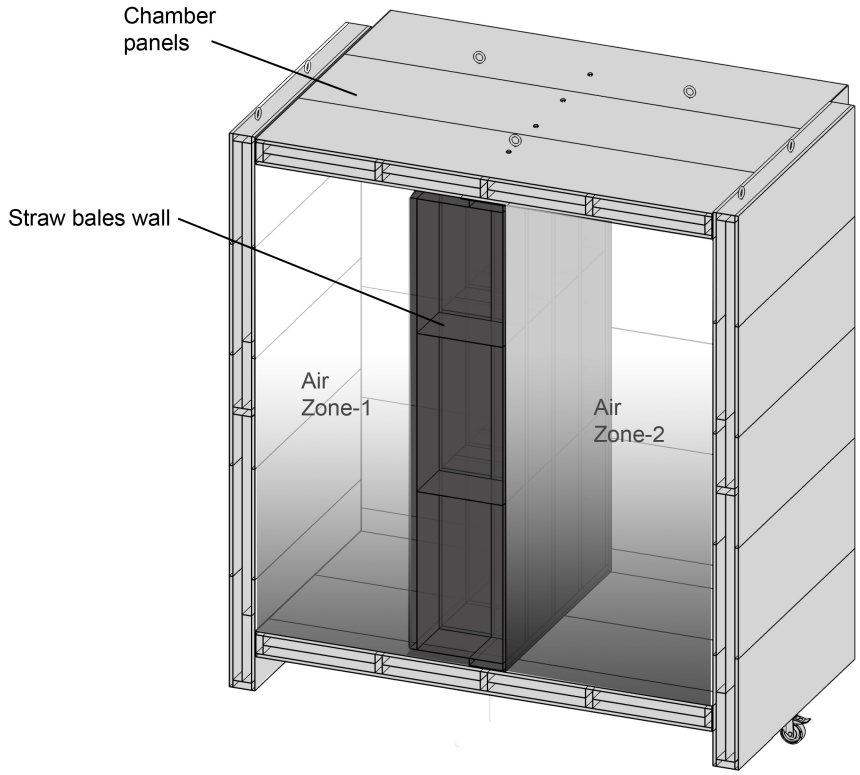

Figure 7.1: Modelled air zones and envelope elements

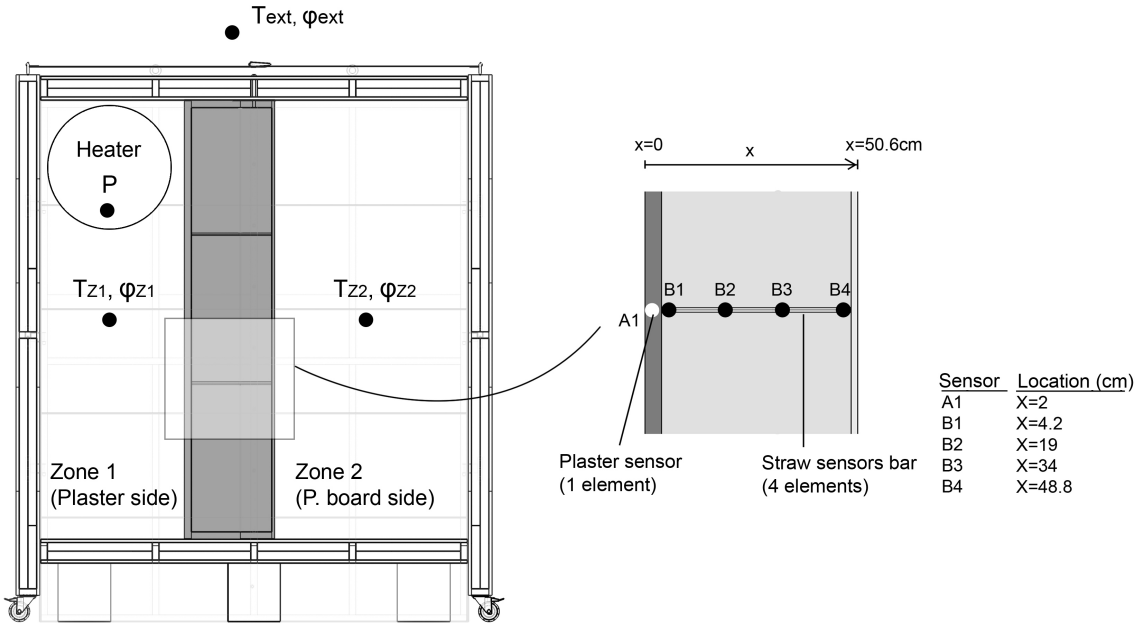

Figure 7.2: Climate chamber and hygrothermal sensors

Intended for the following analyzes, the test period is divided into a 'heating period' (from $t = 0$ up to $t = 6days$) and a 'return-to-equilibrium period' ($t = 6days$ up to $t = 12days$). During the first day, the injected power in zone-1 shows high values in order

to counter the chamber inertia. It stabilizes afterwards at around 120W, with small fluctuations due to the fluctuations of temperature in the exterior environment. After six days, the heating circuit was switched off and the wattmeter output stabilizes at around 20W which corresponds to the power injected for running the heater ventilator. The latter was kept active in order to ensure a good air circulation in zone-1.

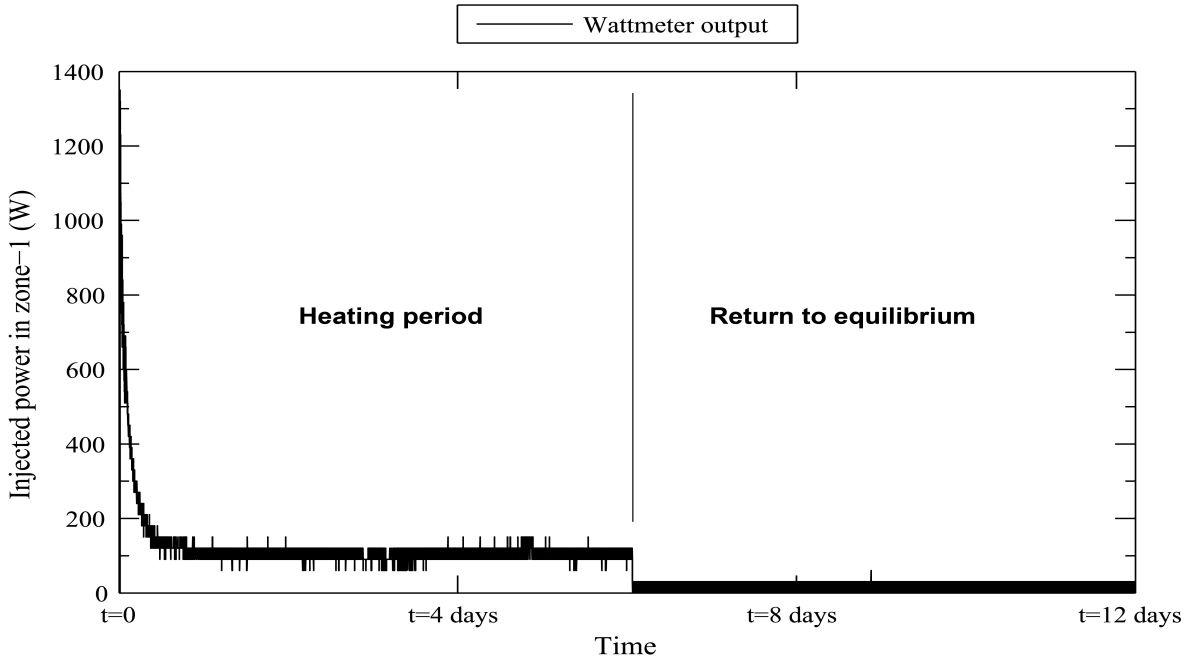

Figure 7.3: Heating power in zone-1

7.3 Architecture of the hygrothermal model

In this modelling exercise, the unknowns were the temperature T_{Zi} and the absolute humidity ω_{Zi} in each air zone$_i$ of the bi-climatic chamber. The air humidity can also be expressed in terms of vapour partial pressure. The unknown quantities must be determined from balance equations performed on each zone, while considering the hygrothermal interaction with the straw bale wall and the panels of the chamber, the loads from air infiltration, and the internal heat gains caused by the heater in zone-1. The model is divided into two distinct sub-parts which are coupled to obtain the overall response of interior air domain.

7.3.1 BEHAM model

The first model sub-part is dedicated to the description of the coupled heat and moisture transfers in the envelope, *i.e.* the straw bale wall and the constitutive panels of the chamber. It was developed using the *COMSOL Multiphysics* software (see **Chapter 4** and **Chapter 6**) directly transposed into *Matlab*. As illustrated above, this general computational tool provides a powerful solution for solving partial differential equations by the finite element method. Furthermore, its flexibility allows modifying at will the physical phenomena considered in the different envelope elements.

Balance equations and models versions

The REV modelling assumptions are identical to the ones applied in **Chapter 6**; two PDE balance equations are solved simultaneously in one dimension:

Humidity balance (PDE)

$$\rho_0 \xi_\phi \frac{\partial \phi}{\partial t} + \rho_0 \xi_T \frac{\partial T}{\partial t} = -\frac{\partial}{\partial x}[\underbrace{-\frac{\delta_{air}\phi}{\mu}\frac{\partial p_{sat}}{\partial T}\frac{\partial T}{\partial x} - \frac{\delta_{air} p_{sat}}{\mu}\frac{\partial \phi}{\partial x}}_{\mathbf{j^{M_v}}}] \tag{7.1}$$

Heat balance (PDE)

$$\rho_0(c_0 + u c_l + \xi_T c_l (T - T_0))\frac{\partial T}{\partial t} + \rho_0 \xi_\phi \frac{\partial \phi}{\partial t} c_l (T - T_0) = \frac{\partial}{\partial x}[\lambda_{eff}\frac{\partial T}{\partial x}] - \frac{\partial \mathbf{j^{M_v}}}{\partial x}(L) \tag{7.2}$$

Three versions of the BEHAM model were prepared to assess how the various physical phenomena taking place in the straw bales impact the predicted climate in zone-1. In other terms, using successively various versions of the BEHAM tool, with an increasing simplification level, allows evaluating which assumptions can be reasonably undertaken in the description of the behaviour of envelope elements. The first version (**BEHAM-HM1**) considers the following function for the moisture storage of materials:

$$u(\phi, T) = u_{Tref}(\phi) \cdot (1 - A(T - T_{ref})) \tag{7.3}$$

Where A (K^{-1}) is a constant coefficient determined from sorption isotherms

measured at different temperatures for straw (see **Chapter 6**). Due to a lack of data, this parameter was estimated for the plaster material on the basis of numerical optimization tests. It was neglected for the particle board, which is expected to confront only to little temperature gradients. The second version of the BEHAM module (referred to as **BEHAM-HM2**) simulates the moisture mass transfer in the wall straw but not the effect of temperature on the sorption characteristics (A = 0); finally, version 3 (referred to as **BEHAM-H**) does not take into account the moisture transfer into the wall straw; this last version corresponds to a scenario where the straw bale wall is not permeable to water transfer. The different scenarii used for the description of hygrothermal transfers in the straw bale wall are a perfect illustration of the flexibility of the software, which is highly desirable in a research perspective.

In contrast to the straw bale wall where different versions of moisture storage equations were compared, only the heat transfer was taken into account in the structural panels of the climatic chamber (justified by the presence of a vapour barrier). The properties of the various constitutive materials are listed in **Table 7.1**. Because this is a preliminary study, the transport coefficients were considered constant during the test. Note that the fraction of wood was taken into account in the values of thermal conductivity for the straw and polystyrene.

Table 7.1: Hygrothermal properties of materials

Materials	ρ_0 (kg/m^3)	λ $(W/(m\cdot K))$	c_0 $(J/(kg\cdot K))$	μ (-)	C (-)	n (-)	A (K^{-1})
XPS + wood fr.	30	0.048	1500	-	-	-	-
OSB	620	0.13	1500	-	-	-	-
Straw + wood fr.	100	0.07	2420	1.5	0.08	0.42	0.0058
Clay plaster	2051	1	750	18.5	0.0029	0.445	0.002
P. board	570	0.09	2100	22.5	0.13	0.29	0

Boundary and initial conditions

Referring to **Figure 7.4**, the boundary conditions (BC) for the chamber panels in contact with zone-i are written:

$$\mathbf{j^Q}(t)\cdot\mathbf{x} = \frac{T_{Zi}(t) - T^{ch}_{surf,Zi}(t)}{R_{surf,Zi}} \qquad x{=}0 \text{ (heat BC)} \tag{7.4}$$

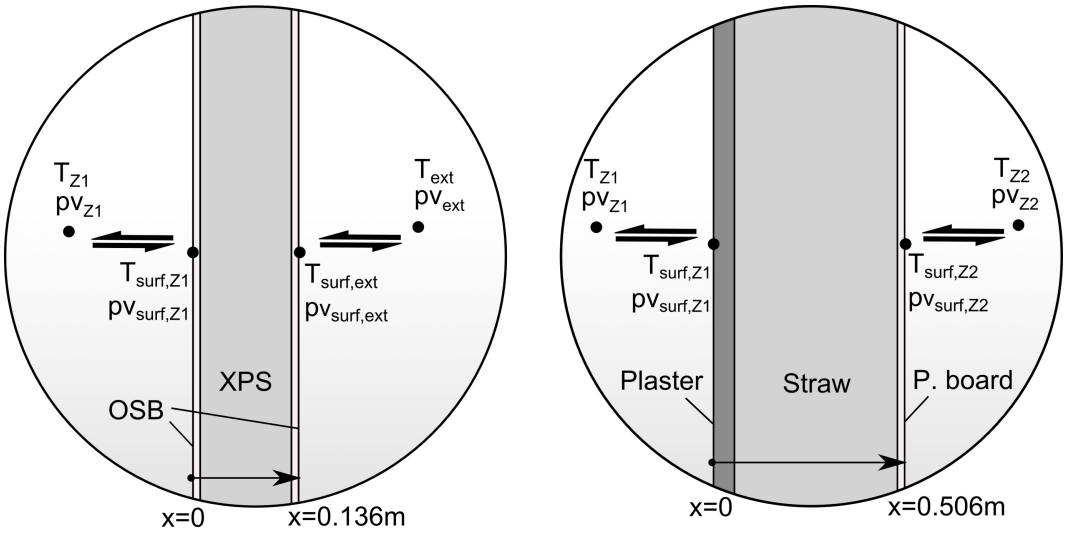

Figure 7.4: Boundary conditions applied on the chamber panels and on the straw bale wall

$$\mathbf{j^Q}(t)\cdot\mathbf{x} = \frac{T_{ext}(t) - T^{ch}_{surf,ext}(t)}{R_{surf,ext}} \qquad x\text{=}0.136m \text{ (heat BC)} \tag{7.5}$$

Where $\mathbf{j^Q}\cdot\mathbf{x}$ $(W\cdot m^{-2})$ is the heat flux density at the surface of the panel, $T^{ch}_{surf,Zi}$ (K) is the surface temperature of the chamber panel in contact with zone-i side, $T^{ch}_{surf,ext}$ (K) is the surface temperature of the chamber panel on the exterior domain side, $R_{surf,Zi}$ and $R_{surf,ext}$ $(m^2\cdot K^{-1}\cdot W^{-1})$ are the surface heat transfer resistances for zone-i and for the exterior domain respectively . The initial conditions in the chambers panels are constructed on the basis of initial temperature and RH readings in the adjacent domains.

For the straw bale wall, the boundary conditions are defined as (**Fig. 7.4**):

$$\mathbf{j^Q}(t)\cdot\mathbf{x} = \frac{T_{Z1}(t) - T^{st}_{surf,Z1}(t)}{R_{surf,Z1}} \qquad x\text{=}0 \text{ (heat BC)} \tag{7.6}$$

$$\mathbf{j^Q}(t)\cdot\mathbf{x} = \frac{T_{Z2}(t) - T^{st}_{surf,Z2}(t)}{R_{surf,Z2}} \qquad x\text{=}0.506m \text{ (heat BC)} \tag{7.7}$$

Where $T^{st}_{surf,Zi}$ (K) is the surface temperature of the straw bale wall on the zone-i side.

$$\mathbf{j^{M_v}}(t)\cdot\mathbf{x} = \frac{p_{v,Z1}(t) - p^{st}_{v,surf,Z1}(t)}{Z_{surf,Z1}} \qquad x\text{=}0 \text{ (humidity BC)} \tag{7.8}$$

$$\mathbf{j}^{\mathbf{M_v}}(t)\cdot\mathbf{x} = \frac{p_{v,Z2}(t) - p^{st}_{v,surf,Z2}(t)}{Z_{surf,Z2}} \qquad x{=}0.506m\ (humidity\ BC) \tag{7.9}$$

Where $\mathbf{j}^{\mathbf{M_v}}\cdot\mathbf{x}$ $(kg\cdot m^{-2}\cdot s^{-1})$ is the vapour flux density at material surface, $p^{st}_{v,surf,Zi}$ (Pa) is the vapour pressure at the surface of the straw bale wall on the zone-i side, $Z_{surf,Zi}$ $(Pa\cdot m^2\cdot s\cdot kg^{-1})$ is the surface vapour transfer resistance for zone-i interior domain.

One big issue in building hygrothermal models is the definition of surface resistance coefficients. In this study, due to the lack of a precise measurement, all room interior surfaces, were assigned with the following values: $R_{surf,Zi} = 0.20\ m^2\cdot K^{-1}\cdot W^{-1}$ and $Z_{surf,Zi} = 1E8\ Pa\cdot m^2\cdot s\cdot kg^{-1}$. The heat transfer resistance of the exterior surface was assigned with a value of $R_{surf,ext} = 0.13\ m^2\cdot K^{-1}\cdot W^{-1}$.

7.3.2 Air zone model

The second module performs the heat and moisture balances on the air volumes corresponding to zone-1 and zone-2. This sub-model is built on the assumption that the indoor air is perfectly-mixed, implying that the unknown variables do not depend on spatial coordinates inside the air volumes. Therefore, the balance equations for indoor air volumes are accounted for by *Ordinary Differential Equations* (ODE).

Zone humidity balance (ODE)

The following loads are involved in the moisture balance of each zone: $\dot{Q}^m_{e,st}$ $(kg\cdot s^{-1})$, the moisture exchange with the straw bale wall and $\dot{Q}^m_v$ $(kg\cdot s^{-1})$, the moisture exchange with the exterior domain by air infiltration in the zone. The humidity ODE for zone-i is written:

$$\rho_a V\frac{d\omega_{Zi}}{dt} = \underbrace{\dot{Q}^m_{e,st}}_{straw\ bale\ wall} + \underbrace{\dot{Q}^m_v}_{air\ infiltration} \tag{7.10}$$

Where

$$\dot{Q}^m_{e,st} = A_{st}\frac{(p^{st}_{v,surf,Zi} - p_{v,Zi})}{Z_{surf,Zi}} \tag{7.11}$$

$$\dot{Q}_v^m = \dot{m}(\omega_{ext} - \omega_{Zi}) \tag{7.12}$$

with ρ_a $(kg \cdot m^{-3})$ the density of dry air, V (m^3) the volume of the zone, A_{st} (m^2) the exchange area of the straw bale wall , $p_{v,Zi}$ (Pa) the vapour pressure in zone-i, $\dot{m}$ $(kg \cdot s^{-1})$ the air infiltration rate and ω_{ext} $(kg \cdot kg^{-1})$ the exterior absolute humidity. The infiltration rates in zone-1 and zone-2 were not measured in this study and their values were roughly estimated during preliminary simulations. The parameter was assigned with $\dot{m} = 0.0005\ kg \cdot s^{-1}$ for both zones.

Zone heat balance (ODE)

The following loads are involved in the heat balance of each zone: $\dot{Q}_{e,st}^h$ (W), the heat exchange with the straw bale wall, $\dot{Q}_{e,ch}^h$ (W), the heat exchange with the chamber panels, $\dot{Q}_v^h$ (W), the heat exchange with the exterior domain by air infiltration in the zone, and $\dot{Q}_{heater}^h$ (W) the heat load from the heating system. The heat ODE for zone-i is written:

$$\rho_a V(c_a + \omega_{Zi} c_v)\frac{dT_{Zi}}{dt} = \underbrace{\dot{Q}_{e,st}^h}_{straw\,bale\,wall} + \underbrace{\dot{Q}_{e,ch}^h}_{chamber\,panels} + \underbrace{\dot{Q}_v^h}_{air\,infiltration} + \underbrace{\dot{Q}_{heater}^h}_{Heater\,load} \tag{7.13}$$

Where

$$\dot{Q}_{e,st}^h = A_{st}\frac{(T_{surf,Zi}^{st} - T_{Zi})}{R_{surf,Zi}} \tag{7.14}$$

$$\dot{Q}_{e,ch}^h = A_{chtot,Zi}\frac{(T_{surf,Zi}^{ch} - T_{Zi})}{R_{surf,Zi}} \tag{7.15}$$

$$\dot{Q}_v^h = \dot{m} c_a (T_{ext} - T_{Zi}) \tag{7.16}$$

Where c_a $(J \cdot kg^{-1} \cdot K^{-1})$ is the specific heat of dry air, $A_{chtot,Zi}$ (m^2) is the total surface of chamber panels in contact with zone-i. The heater load is obtained directly by the

power measurement circuit connected to the heater. Attention is drawn to the fact that all the chamber panels in contact with a zone were considered as resulting in a single heat load.

7.3.3 The integration of models

The two subparts of the room-scale hygrothermal model were combined within *Simulink*[1] modelling tool, which is included in *Matlab* GCT. *Simulink* is a block diagram environment dedicated to the resolution of dynamical systems and fully integrated with *Matlab* standard tools and functions. Combining ODE and PDE-based models requires the use of a particular block called an S-Function (system-function).

For a better understanding, we must recall that each block within a *Simulink* model diagram describes a particular system and is defined by the following characteristics: a vector of inputs, u, a vector of outputs, y, and a vector of states, x as shown in **Figure 7.5** (MathWorks, 2014).

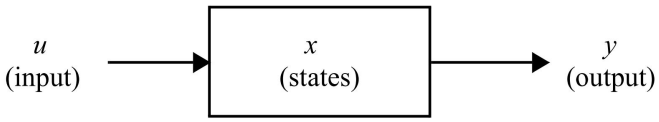

Figure 7.5: Simulink block

The state vector may consist of continuous states, discrete states or a hybrid combination of both. The evolution of the system is described by mathematical relationships between the inputs, the outputs, and the states:

$$y = f_0(t, x, u)$$

$$\dot{x}_c = f_d(t, x, u)$$

$$x_{d_{k+1}} = f_u(t, x, u)$$

Where t is the simulation time value, x_c is the continuous states vector and x_d is the discrete states vector with $x = x_c + x_d$. If the block has no states, the x vector is empty.

In a model, various blocks, or sub-systems, can be combined to describe a general system. The transmission of data between the inputs and outputs of the different blocks is

[1] http://www.mathworks.com/products/simulink/

materialized by directional lines. The software includes libraries of predefined blocks which allow solving many continuous, discrete or hybrid states problems.

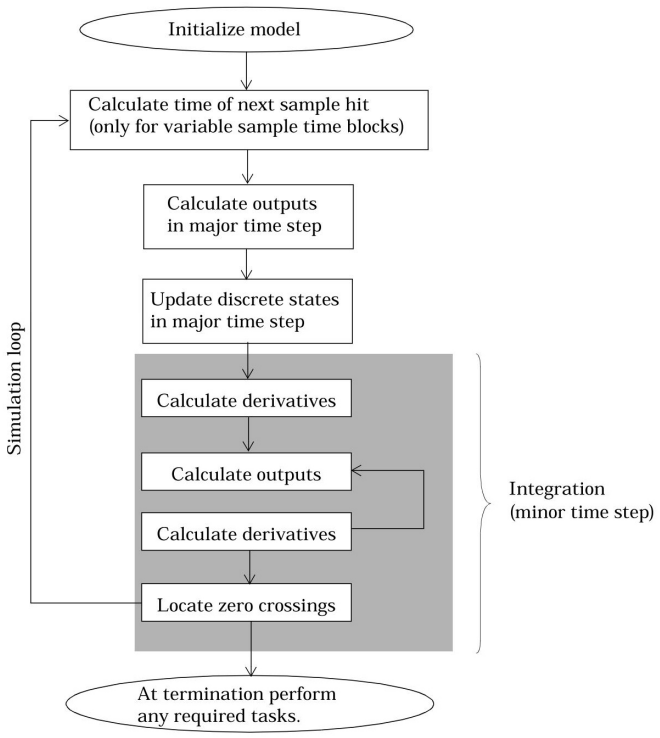

Figure 7.6: Simulation stages in Simulink

During the simulation, *Simulink* makes repeated calls to each block according to a specific scheme. The first stage of the simulation is an initialization of the model. It includes initializing each block. It is followed by the simulation loop consisting of a series of steps. At each step *Simulink* executes the code that defined the behaviour of all individual blocks and updates their states and outputs. **Figure 7.6** shows the *Simulink* simulation stages (MathWorks, 2014).

An S-Function is nothing more than a customizable code that describes the behaviour of a dynamical system and allows the user to create new blocks in order to enhance *Simulink* capabilities. Designing an S-Function means defining the state(s) of the system, the derivative function of continuous state(s), the update function of discrete state(s), and the relationships that link the outputs to the inputs and states of the system. Solving the room balance-equations with a PDE model for envelope elements requires the use of such custom S-Function associated with standard blocks available in the default *Simulink* library.

Three S-Functions were created here: one for describing the transient behaviour of the

straw bale wall, another for describing the transient behaviour of the chamber panels in contact with zone-1, and a last S-Function for the chamber panels in contact with zone-2. The outputs of those S-Functions are the hygrothermal conditions at wall surface on the interior side, which make the bridge between the BEHAM and the zone balance equations. Their inputs are the hygrothermal conditions in exterior and interior air volumes, needed to define the boundary conditions on all chamber envelope elements. Each of the S-functions is characterized by hybrid states: The hygrothermal conditions inside envelope materials are updated at a regular time interval, using conditions in air zones and the external climate for the computation of boundary conditions; wall surface conditions are thus updated on a discrete time basis, with a regular major time step ($\sim 15 min$). Between those major time intervals, the wall surface conditions are maintained constant and still intervene in room balance equations. The latter are based on a continuous state description. The two zone balance ODEs (Equations (7.10) and(7.13)) are solved with standard blocks included in the library of *Simulink* and follow a minor time stepping ($\sim 1 s$). As an illustration purpose, **Figure 7.7** schematically presents the behaviour of the straw bale wall S-Function. **Figure 7.8** shows the general architecture of the model for the heat shock case study.

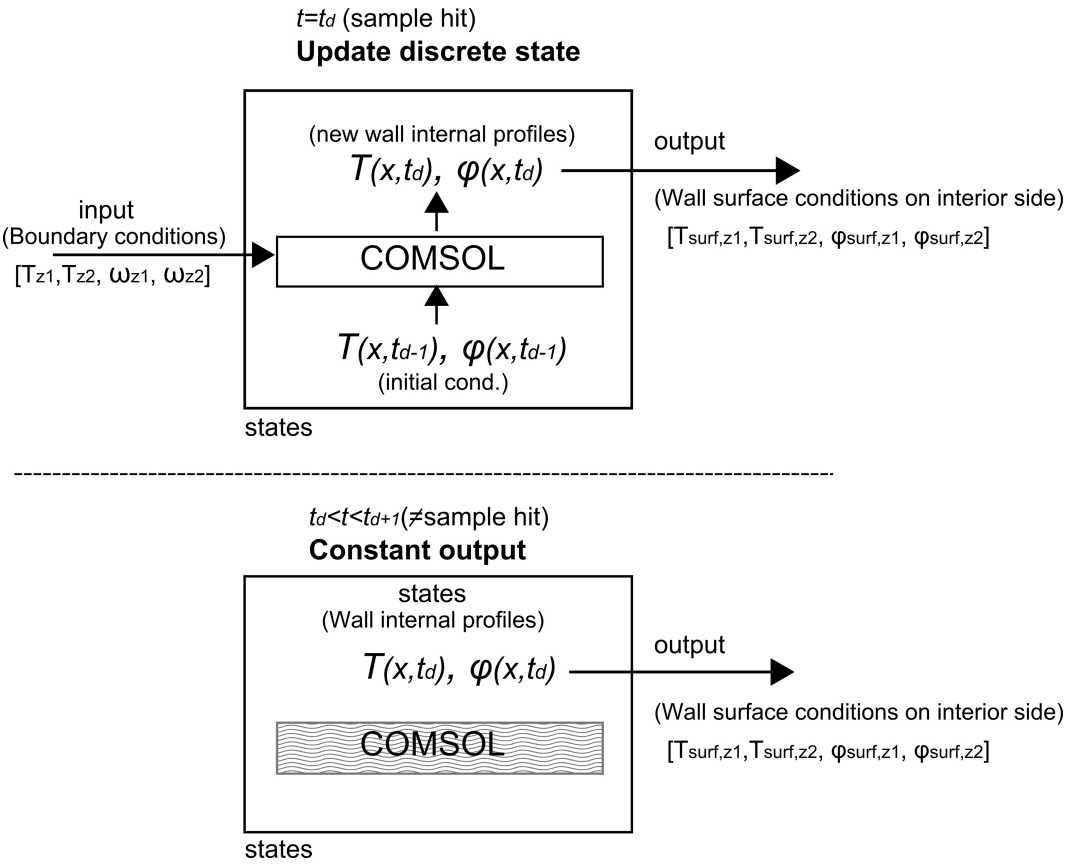

Figure 7.7: The S-Function for straw bale wall description; x stands for the position inside the wall

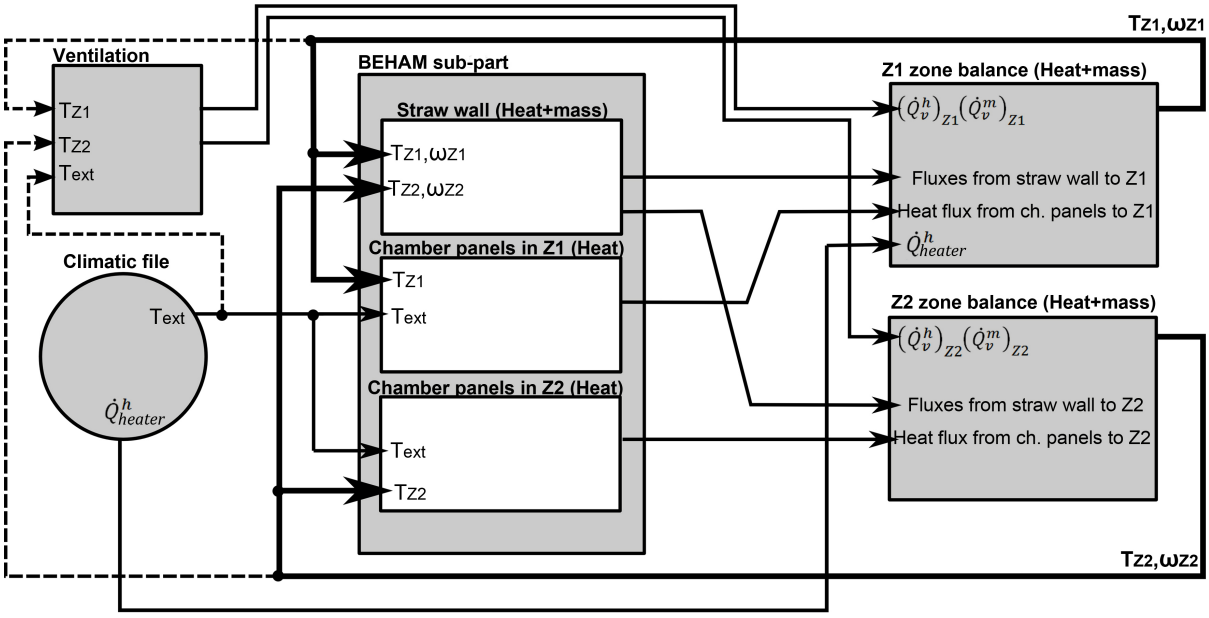

Figure 7.8: Architecture of the room-scale hygrothermal model

7.4 Results and discussions

Figure 7.9 shows the experimental evolution of temperature and vapour partial pressure in zone-1 as well as the room-scale model outputs. The latter are given for the different versions of the BEHAM sub-part used in the room-scale model to characterize the straw bale wall. Regarding indoor humidity conditions, we observe that both versions of the hygrothermal model which consider moisture transfer in the straw bale wall (BEHAM-HM1 and BEHAM-HM2) provide a curve appearence consistent with the experimental measurement. The effect of considering the temperature-dependency of moisture storage is also directly observable. The model with the BEHAM-H module results in a poor characterization of the indoor humidity; the vapour pressure in zone-1 follows exterior solicitations due to air infiltration which is the only humidity load accounted for. The distinction between BEHAM versions is more difficult to observe for indoor temperature simulation. It is stressed that accounting for moisture transport in the straw bale wall translates into a better fit of experimental data. The BEHAM-H model results in a simulated room temperature higher than experimentally observed. This can be explained by the latent heat effect. When the temperature rises in zone-1, the water saturation pressure rises consequently and the RH of the room has a tendency to decrease. Due to the moisture buffer effect, the plaster immediately reacts by releasing some vapour towards the indoor air volume. The water molecules that desorb from the plaster inner matrix require some heat to perform this phase change. In consequence, the hygroscopic wall also indirectly acts as a temperature buffer. The BEHAM module which does not account for moisture transfer in the straw bale wall naturally predicts a higher temperature in zone-1.

In order to illustrate more clearly the moisture buffer effect, **Figure 7.10** shows the RH evolution in zone-1 according to the BEHAM-HM1 and BEHAM-H model versions compared to experimental data. One can note that without the moisture exchange in the straw bale wall (a scenario corresponding to BEHAM-H), the heat shock will cause a drop of RH in zone-1 followed by a stabilization around 20%RH during the entire heating period. In contrast, the measurement data shows that the initial RH drop is rapidly compensated by a moisture release from the wall that causes the RH to rise again. At the beginning of the test, the measured RH in the room was 48%RH. After

the initial drop that brings the RH to 22%, the straw bale wall reaction is observable in the form of a slow rise of RH which reaches 34% in approximately 10 hours. This response of the breathable wall is thus directly noticeable by analysis of the indoor RH. The BEHAM-HM1 model, which corresponds to the lower level of simplification in the description of the straw bale wall behaviour, demonstrates a good fit to experimental data.

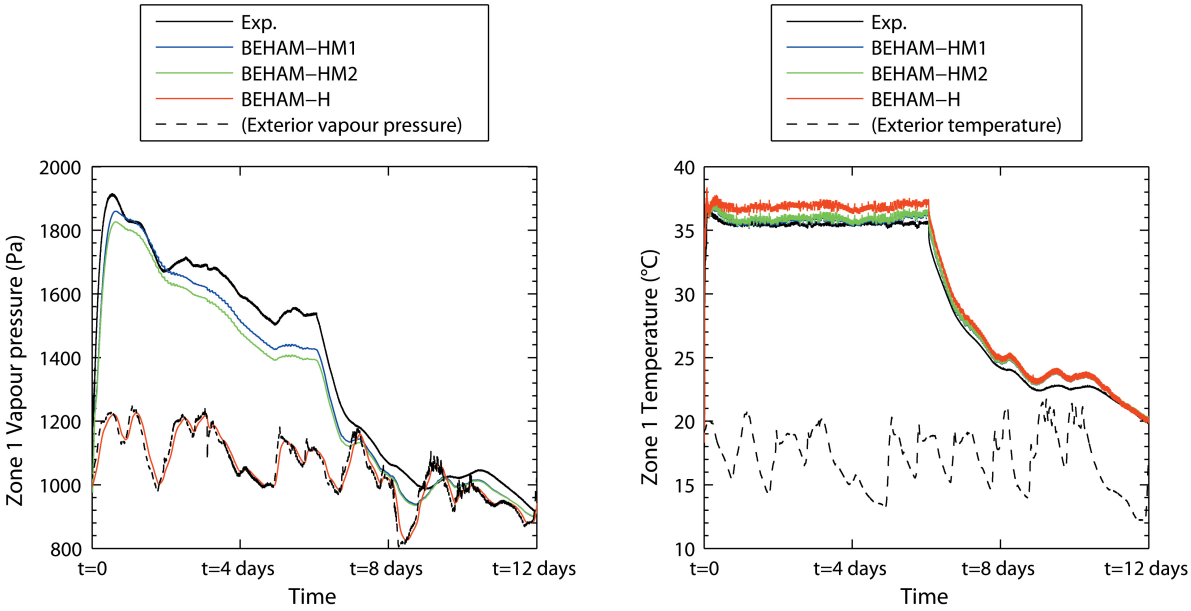

Figure 7.9: Model outputs compared to experimental results; Zone-1 vapour pressure and temperature

The great advantage of the hygrothermal model at zone-scale lies in the fact that it allows analyzing the real heat and mass flows occurring at the various interior surfaces of the envelope. By real, we mean that the mutual exchanges between the envelope and the indoor air are accounted for; not only the transfers from the indoor air towards the envelope as it is the case when BEHAM models are used alone. For example, one can estimate the impact of the different moisture transfer mechanisms included in the BEHAM model on the heat flow occuring between the heated indoor environment and the straw bales wall. This could lead to the identification of potential benefits for the occupant in terms of comfort or energy consumption. In particular, many interrogations persist in the evaluation of the latent heat effect on building energy performance (BRE, 2002; Osanyintola and Simonson, 2006). During a 35°C thermal shock, energy performance benefits would principally lie in the reduction of cooling loads and comfort benefits in keeping the *Predicted Percentage of Dissatisfied* (PPD) value as low as

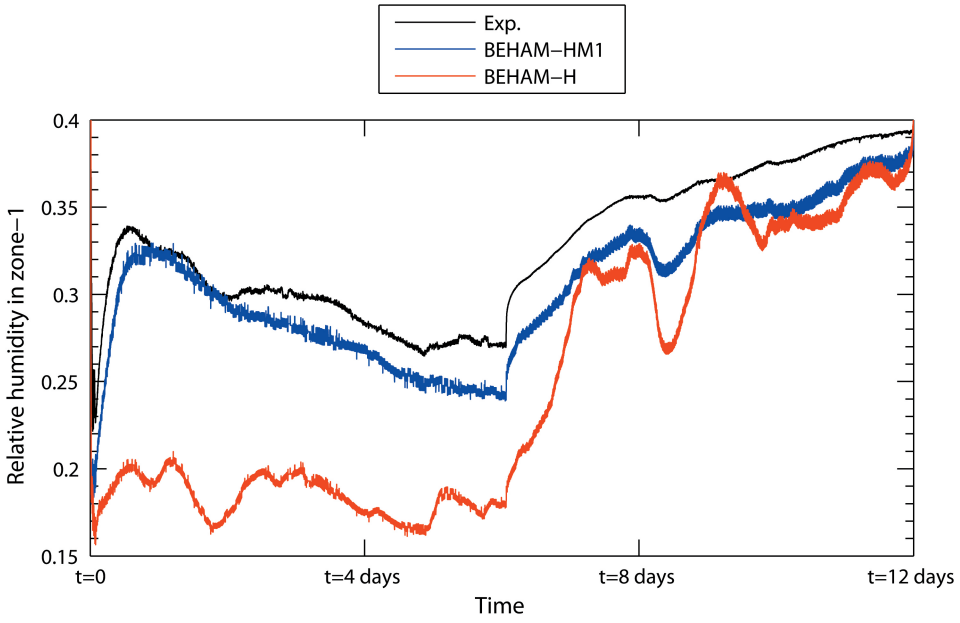

Figure 7.10: BEHAM-HM1 and BEHAM-H model versions outputs compared to experimental results; RH in zone-1

possible as defined in ISO 7730 (2005). The PPD value will determine how many occupants will fall outside the limits of comfort by feeling to cold or to warm. This indicator depends on the metabolic level of occupants as well as on their clothing. However, the full analysis of PPD values is beyond the scope of this chapter. Some simple criteria were chosen as indoor comfort and energy performance indicators for zone-1 under the heat shock scenario. Those indicators are the zone temperature, the zone relative humidity, the surface temperature of the straw bales wall and the thermal flux from zone air towards the straw bales wall. The criteria were computed for each version of the envelope model used for the study of the straw bales wall. Results are presented in **Table 7.2** for the heating period (see **Fig. 7.3**).

It can be observed that the moisture transfers happening in the straw bales wall play a significant role in indoor climate regulation. During the heating period, both indoor air and surface temperature are lower when hygroscopic effects are considered. In addition, the RH level is maintained closer to the initial room value while it drops more severely if the straw bale wall is considered as impermeable to water transfer. Globally, BEHAM-HM1 and BEHAM-HM2 provide very similar results. Under BEHAM-HM1 assumptions, the heat flux going from the room to the straw bale wall is increased by 17.3% in comparison to the no-moisture-transfer model (BEHAM-H). This result is

particularly significant in reducing the cooling load and improving the energy storage during an overheated period. The difference between BEHAM-HM1 and BEHAM-HM2 models for the same flow is really small (1.1%). It means that integrating the effect of temperature on sorption behaviour only plays little when assessing room-scale effects. When analyzing the results presented in Table 7.2, it should be remembered that only one wall is hygroscopically active in zone-1; the straw bale wall only represents an area of 3.66 m^2 on the total interior surface of 10.43 m^2 in zone-1. The benefits of hygroscopic walls on all interior surface could really be noticeable; and this time also in terms of indoor temperature.

Table 7.2: Averaged indoor comfort criteria during heating period

		BEHAM-HM1	**BEHAM-HM2**	**BEHAM-H**
T_{Z1}	(K)	309.019	309.089	309.962
ϕ_{Z1}	(-)	0.278	0.271	0.185
$T^{st}_{surf,Z1}$	(K)	307.293	307.382	308.490
$(\dot{Q}^{h}_{e,st})_{Z1}$	(W)	-31.617	-31.267	-26.9628

7.5 Chapter conclusions

A hygrothermal model at building-scale was developed by combining the BEHAM research model with balance equations performed on indoor air volumes. This was carried out in the *Simulink* environment. A preliminary confrontation of this model with experimental data from a heat shock on a straw bales panel allows to:

1. Illustrate the use of a hygrothermal model at room-scale that considers the coupled heat and moisture transfers in hygroscopic envelopes;

2. Confirm the capabilities of hygroscopic materials on improving the energy performance of the building under the considered scenario;

3. Quantify this effect during the proposed scenario with some simple indicators. In particular, we show how one can benefit from the assessment of the mutual exchanges between the envelope and the indoor air zone in order to characterize the performance of atypical materials;

4. Address the weaknesses of the proposed simulation, namely the lack of a precise determination of the convective transfer coefficients at envelope surfaces, the rates of ventilation in zones and all the materials properties. Because the estimation of those parameters is difficult to measure experimentally, it is worth noticing that *Matlab* provides the ability to easily use inverse modelling modules that can facilitate the process (see **Chapter 5**).

The experimental test used here for the purpose of model validation is really simple. For example, the ventilation rates have a major effect on indoor climate in real environments whereas they were kept really low during the presented heat shock test. However, we showed that hygrothermal models are getting more and more powerful and seem ready for the confrontation to a large range of experimental case studies, eventually with more realistic solicitations.

CHAPTER 8

Conclusions and Recommendations

8.1 Concluding remarks

The first main objective of this thesis was to develop a modular BEHAM model in a general computational tool. The second one was to improve the prediction efficiency of heat and moisture transfers inside CBM, investigated both relatively to the mathematical description of the involved physical phenomena and in terms of assigned values for materials properties. The last objective was to study the impact of 'breathable walls' containing CBM on indoor climate and building energy performance.

It should be observed that each objective is in fact bound to a particular aspect of the BEHAM model. The need to enlarge the scope of mathematical descriptions is linked to the formalism at the core of the model and is answered with balance equations refinement. The definition of materials properties falls into the domain of models inputs. Finally, the impact on indoor climate is related to boundary conditions of the model and their combination to room scale balance representation. Moreover, the raised issues cover multiple scales of study, from theoretical considerations about the modelling of pores-related phenomena up to building-scale exchanges between a wall assembly and a large indoor air volume.

As a starting point, a review of mathematical formulations for the moisture balance equation on the representative elementary volume of a porous material was proposed in **Chapter 2**. This step aimed to draw a map of the mathematical representations found in the current literature, in the light of a physically-based description and knowing that moisture balance description is an important source of differentiation between models. The obtained inventory of moisture balance equations, including

possible simplifications depending on the case study, offers a rich source to develop flexible BEHAM models and interpret experimental results. It was also important to identify how Building Physics can benefit from other scientific domains like Soil Sciences or Drying Technologies in order to explore non-typical solicitations of the envelope. Soil Sciences offer an important source of knowledge concerning the description of the over-hygroscopic region while drying technologies can answer the need for a better characterization of non-isothermal moisture transfer. Another important data that arose from this section is the definition of various secondary transport coefficients in dependence to primary transport functions. This result is of great interest to develop specific experimental set-ups dedicated to the determination of material properties.

Once the mathematical background well-defined, came the question of choosing a numerical solving environment for the development of a BEHAM tool, in order to meet the first objective of the thesis. Although available BEHAM programs are becoming more and more powerful, the *COMSOL Multiphysics* general computational tool seems to offer a very interesting alternative for addressing the various challenges related to CBM study. Indeed, it presents the required qualities of transparency and modularity but also a facilitated integration potential with existing and validated tools as shown in **Chapter 5** and **Chapter 7**. The modularity of the proposed model was highlighted across the chapters where many forms of the model were tested. In **Chapter 4**, a first version was presented and validated at material-scale using a Moisture Buffer Value test. This chapter also illustrated the benefits of using clear efficiency criteria for model comparison. It was shown that the proposed model can perform as well as a commercial BEHAM tool, with clear transparency benefits.

Another objective was to improve BEHAM models effeciency through innovative methods for the determination of material properties. In the experimental point of view, **Chapter 3** illustrates how prototype devices can be developed to cope with specificities of CBM. A guarded hot plate apparatus was designed and validated, allowing to measure precisely the thermal conductivity of entire straw bales. Although the measurement of thermal conductivity of straw bales can be performed with other methods, a precise assessment of anisotropy effects caused by fibres orientation is now achievable, at the highest accuracy. It is clear that developing specific

experimental devices dedicated to hygrothermal properties measurement represents a time-consuming task. **Chapter 5** presents a numerical alternative found in inverse modelling tools. The DREAM algorithm, integrated with the *COMSOL* model in *Matlab*, was used to estimate the hygric transfer parameters of some clay plasters during a Moisture Buffer Value test. Results show that dynamic experiments at material scale can be used to recover materials properties.

The wall scale study proposed in **Chapter 6** addresses the refinement of the mathematical formalism at the core of BEHAM models. Although the temperature effect on moisture storage is often neglected, due to is minor effect in standard operating conditions, it was judged important to evaluate its role in details for CBM, and propose a simple way of describing it mathematically. Several versions of the *COMSOL* model were compared to simulate the internal conditions of a straw bale wall subject to a thermal shock in a bi-climatic chamber. Again, the modularity of the proposed model was therefore highlighted. The efficiency in predicting internal relative humidity variations caused by the thermal shock is greatly improved by a single-parameter empirical representation of temperature effect on moisture storage. Alternately, a physically-based approach can bring some additional efficiency.

The last objective was to study the effect of CBM on indoor air volumes. In this purpose, **Chapter 7** illustrates the combination of the research model with a zone balance representation. This coupled approach showed a good accuracy in predicting the indoor air conditions of a bi-climatic chamber used to impose a thermal shock on a straw bale wall, during an experiment similar to the one presented in **Chapter 6**. This upscaling in the analysis of CBM hygrothermal behaviour allows estimating the actual benefits of hygroscopic materials.

All validation procedures found in this work to support the modelling approaches rely on experimental data. It was important to develop a series of experimental set-up able to highlight the specific behaviour of highly hygroscopic materials. All along the thesis, some new techniques were proposed for this purpose. The most significant one is the creation of an efficient sensors bar to monitor the internal conditions of straw bales, presented in **Chapter 5**.

8.2 Recommendations and guidelines for further work

Faced to the results presented in this thesis, many perspectives are opened for further work.

First, it was shown in **Chapter 6** that BEHAM models can be further improved to account for specific environmental solicitations that diverge from an ideal and averaged scheme. We applied a simple representation for temperature dependence of sorption characteristics and showed that it can improve the efficiency of the model for predicting CBM behaviour when large temperature gradients are met. While this improvement might not be relevant for studies with a long time scale, it might have a significant impact in specific applications and avoid any misinterpretation of sensors readings. Similarly, many issues persist when modelling CBM or any capillary material subject to large moisture content gradients. Hysteresis and liquid transport were not modelled here but they are certainly going to be better assessed in the future. Again, flexible research models, like the one used here, are able to easily incorporate new mathematical descriptions and activate them when needed. Moreover, such models can deal with several temporal and spatial discretization and offer a complete transparency which accommodates with the needs of scientific research.

In parallel to the BEHAM models refinement, scientists should continue to propose innovative test programs designed to highlight the hygrothermal phenomena related to the porous structure that are less efficiently described. Associated with those experimental considerations, the monitoring systems dedicated to the observation of internal conditions still need to evolve to reduce the uncertainty in validation data.

An essential conclusion of the work presented here is the benefits stemming from the combination of individual numerical models and algorithms as it is allowed by general computational tools. In this respect, the inverse modelling approach used in **Chapter 5** to estimate materials parameters offers many great perspectives for future work. The application of this technique could now be extended to a large range of experiments, starting at material-scale. We saw that the MBV protocol is promising for the estimation of materials hygric properties; other standardized protocols could be developed which would allow the estimation of other material properties. Of course, as

mentioned in **Chapter 5**, the efficiency of inverse modelling technique is related to the capacity of BEHAM models to predict reality. In consequence, preliminary researches should focus on the study of hygrothermal conditions that are accurately understood. Then, together with the improvement of BEHAM models the range of estimated properties could be enlarged progressively. If such methods are further validated it may offer a substantial gain of time for the characterization of materials, which might sometimes be a difficult task as shown in **Chapter 3**.

In addition to the application of inverse modelling for the estimation of material properties at material-scale, it is also possible to consider applying this method at larger scale and for any particular model parameter. **Chapter 7**, it was shown that some parameters are difficult to determine experimentally for whole building hygrothermal models, like the surface convective coefficients or ventilation rates. The numerical algorithms for parameter estimation might offer a good solution to overcome this issue. Additional work should be considered for validating the approach with other hygrothermal models and case studies.

Another aspect of tools combination illustrated in **Chapter 7** is the combination of individual hygrothermal models to reach larger scale representations. It seems to be a major guideline to improve the understanding of the impact of hygroscopic materials on indoor climate. Indeed, as repeated along the text, the main drawback of BEHAM tools in assessing how CBM interact with indoor air is that such models rely on an a priori definition of the indoor climate. However, we showed that coupling such a model with ordinary differential equations for the description of zone balance, allows to properly characterize the mutual exchange between envelope and indoor air. In order to illustrate this modelling approach for a particular scenario, a thermal shock was performed on a plastered straw bale wall. Now that whole-building hygrothermal models are becoming more usual and easily available, such confrontation to large-scale experimental data sets should be a priority. The operation of a building covers many different realities and the behaviour of CBM, or other hygroscopic materials, should be analyzed accordingly. Even if whole-building hygrothermal models are still in an early development process, it seems that the efficiency of the HAM description will notably improve in the future, through the combination of high efficiency models for each building domain. We put a lot of hope in future coupling of BEHAM tools with

computational fluid dynamics, which offers the higher level of granularity for indoor air movement description.

Concerning the real advantages of CBM materials in terms of indoor comfort and building energy performance, this thesis only provides a brief introduction to the methods that will certainly allow a better comprehension in the future. The chosen heat shock scenario, which was accurately simulated by the proposed model, already confirmed that there is a real potential of hygroscopic structure in improving energy usage in buildings. This improvement mainly relies on the latent heat effect that needs to be further studied. In particular, it seems that a better synergy should be created between expectations of professionals in the construction sector and scientific research lines. Now that a lot of effort has been devoted to models development, the time has come to work towards a precise characterization of breathable structure benefits and drawbacks, using realistic numerical and experimental case studies.

Bibliography

ASHRAE (2009). *ASHRAE Handbook: Fundamentals*. American Society of Heating, Refrigerating and Air-Conditioning Engineers, Atlanta.

ASTM (2003). ASTM D5084: Standard test methods for measurement of hydraulic conductivity of saturated porous materials using a flexible wall permeameter. Standard, American Society for Testing and Materials.

ASTM (2006). ASTM D2434: Standard test method for permeability of granular soils (constant head). Standard, American Society for Testing and Materials.

ASTM (2009). ASTM C1699: Standard test method for moisture retention curves of porous building materials using pressure plates. Standard, American Society for Testing and Materials.

ASTM (2011a). ASTM E1269: Standard test method for determining specific heat capacity by differential scanning calorimetry. Standard, American Society for Testing and Materials.

ASTM (2011b). ASTM E2396: Standard test method for saturated water permeability of granular drainage media [falling-head method] for vegetative (green) roof systems. Standard, American Society for Testing and Materials.

Baggio, P., Bonacina, C., and Schrefler, B. (1997). Some considerations on modeling heat and mass transfer in porous media. *Transport in porous media*, 28(3):233–251.

Bear, J. (1988). *Dynamics of fluids in porous media*. Dover Publications, Dover.

Bevan, R. and Woolley, T. (2008). *Hemp lime construction: a guide to building with Hemp Lime composites*. BRE Press, Garston.

BPIE (2011). Europe's buildings under the microscope. Technical report, Buildings Performance Institute Europe.

BRE (2002). Final report on the construction of the hemp houses at haverhill, suffolk. Technical report, Building Research Establishment.

Bronsema, N. (2010). Moisture movement and mould management in straw bale walls for a cold climate. Master's thesis, University of Waterloo, Waterloo, Canada.

Brun, M., Lallemand, A., Quinson, J.-F., and Eyraud, C. (1977). A new method for the simultaneous determination of the size and shape of pores: the thermoporometry. *Thermochimica acta*, 21(1):59–88.

Burge, P. (2004). Sick building syndrome. *Occupational and Environmental Medicine*, 61(2):185–190.

Carmeliet, J., De Wit, M., and Janssen, H. (2005). Hysteresis and moisture buffering of wood. In *Symposium of Building Physics in the Nordic Countries*, pages 55–62.

Cerezo, V. (2005). *Propriétés mécaniques, thermiques et acoustiques d'un matériau à base de particules végétales: approche expérimentale et modélisation théorique*. PhD thesis, INSA Lyon & Ecole Nationale des Travaux Publiques, Lyon, France.

Collet, F. (2004). *Caractérisation hydrique et thermique de matériaux de génie civil à faibles impacts environnementaux*. PhD thesis, INSA Rennes, Rennes, France.

Collet, F., Bart, M., Serres, L., and Miriel, J. (2008). Porous structure and water vapour sorption of hemp-based materials. *Construction and building materials*, 22(6):1271–1280.

Collet, F., Chamoin, J., Pretot, S., and Lanos, C. (2013). Comparison of the hygric behaviour of three hemp concretes. *Energy and Buildings*, 62:294–303.

Costola, D. (2011). *External coupling of building energy simulation and building element heat, air and moisture simulation*. PhD thesis, Technical University Eindhoven, Eindhoven, Netherlands.

Crawley, D. B., Hand, J. W., Kummert, M., and Griffith, B. T. (2008). Contrasting the capabilities of building energy performance simulation programs. *Building and Environment*, 43(4):661–673.

Cripps, A., Handyside, R., Dewar, L., and Fovargue, J. (2004). *Crops in construction handbook*. CIRIA, London.

De Ponte, F. and Klarsfeld, S. (2002). Conductivité thermique des isolants. Technical report, Techniques de l'ingénieur.

Duggal, A. and Muir, W. (1981). Adsorption equilibrium moisture content of wheat straw. *Journal of agricultural engineering research*, 26(4):315–320.

Dumont, B., Leemans, V., Mansouri, M., Bodson, B., Destain, J.-P., and Destain, M.-F. (2014). Parameter identification of the stics crop model, using an accelerated formal mcmc approach. *Environmental Modelling & Software*, 52:121–135.

EC (2011). Energy efficiency plan 2001, communication from the commission to the european parliament, the council, the european economic and social committee and the committee of the regions. Technical report, European Commission.

EEA (2010). The european environment state and outlook 2010. material resources and waste. Technical report, European Environment Agency.

EIO (2011). Resource-efficient construction: the role of eco-innovation for the construction sector in europe. Technical report, Eco-Innovation Observatory.

Emmerich, S. J. (2001). Validation of multizone iaq modeling of residential-scale buildings: A review. *Transactions American Society of Heating Refrigerating and Air Conditioning Engineers*, 107(2):619–628.

Evrard, A. (2008). *Transient hygrothermal behaviour of lime–hemp materials*. PhD thesis, Université Catholique de Louvain, Louvain-La-Neuve, Belgium.

Fang, L., Clausen, G., and Fanger, P. O. (1998). Impact of temperature and humidity on the perception of indoor air quality. *Indoor Air*, 8(2):80–90.

Feustel, H. E. (1999). Comis—an international multizone air-flow and contaminant transport model. *Energy and Buildings*, 30(1):3–18.

Finkbeiner, M., Inaba, A., Tan, R., Christiansen, K., and Klüppel, H.-J. (2006). The new international standards for life cycle assessment: Iso 14040 and iso 14044. *The international journal of life cycle assessment*, 11(2):80–85.

Glaser, H. (1959). Graphisches verfahren zur untersuchung von diffusionsvorgängen. *Kältetechnik*, 11(10):345–349.

Hameury, S. (2005). Moisture buffering capacity of heavy timber structures directly exposed to an indoor climate: a numerical study. *Building and Environment*, 40(10):1400–1412.

Hansen, K., Rode, C., Hansen, E., Padfield, T., and Kristiansen, F. (2001). Experimental investigation of the hygrothermal performance of insulation materials. In *Performance of exterior envelopes of whole buildings VIII*.

Hedlin, C. (1967). Sorption isotherms of five types of grain straw at 70°f. *Canadian Agricultural Engineering*, 9(1).

Hens, H. (1996). Heat, air and moisture transfer in insulated envelope parts. Technical report, International Energy Agency.

Hens, H. (2005). Annex 41 - whole building heat, air and moisture response.

Hill, R. C. and Bowen, P. A. (1997). Sustainable construction: principles and a framework for attainment. *Construction Management and Economics*, 15(3):223–239.

Huntzinger, D. N. and Eatmon, T. D. (2009). A life-cycle assessment of portland cement manufacturing: comparing the traditional process with alternative technologies. *Journal of Cleaner Production*, 17(7):668–675.

IEA (1991). Annex-xiv: Condensation and energy, source book. Technical report, International Energy Agency.

Imbabi, M. S.-E. (2006). Modular breathing panels for energy efficient, healthy building construction. *Renewable Energy*, 31(5):729–738.

ISO (1991a). ISO 8301: Thermal insulation - determination of steady-state thermal resistance and related properties - heat flow meter apparatus. Standard, International Organization for Standardization.

ISO (1991b). ISO 8302: Thermal insulation - determination of steady-state thermal resistance and related properties - guarded hot plate apparatus. Standard, International Organization for Standardization.

ISO (2000). ISO 12571: Hygrothermal performance of building materials and products - determination of hygroscopic sorption properties. Standard, International Organization for Standardization.

ISO (2001). ISO 12572: Hygrothermal performance of building materials and products - determination of water vapour properties. Standard, International Organization for Standardization.

ISO (2005). ISO 7730: Ergonomics of the thermal environment - analytical determination and interpretation of thermal comfort using calculation of the pmv and ppd indices and local thermal comfort criteria. Standard, International Organization for Standardization.

ISO (2013). ISO 11357-4: Plastics. differential scanning calorimetry (dsc) determination of specific heat capacity. Standard, International Organization for Standardization.

Janssens, A., Woloszyn, M., Rode, C., Sasic-Kalagasidis, A., and De Paepe, M. (2008). From empd to cfd–overview of different approaches for heat air and moisture modeling in iea annex 41.

Jones, B. (2002). *Building with straw bales.* Green Books, Totnes.

JTI (1985). Equilibrium moisture content (emc) of straw. Technical report, Jordbrukstekniska Institutet.

Kibert, C. J. (2003). Green buildings: an overview of progress. *Journal of Land Use*, 19:491.

King, B. (1996). *Buildings of earth and straw: structural design for rammed earth and straw-bale architecture.* Ecological Design Press, Sausalito.

King, B. and Aschheim, M. (2006). *Design of straw bale buildings: the state of the art.* Green Building Press, San Rafael.

Lacinski, P. and Bergeron, M. (2000). *Serious straw bale: a home construction guide for all climates.* Chelsea Green Publishing Co., White River Junction.

Landry, M. R. (2005). Thermoporometry by differential scanning calorimetry: experimental considerations and applications. *Thermochimica acta*, 433(1):27–50.

Li, Y., Fazio, P., and Rao, J. (2012). An investigation of moisture buffering performance of wood paneling at room level and its buffering effect on a test room. *Building and Environment*, 47(1):205–216.

Maalouf, C., Lachi, M., Mai, T., and Wurtz, E. (2013). Numerical and experimental study of the hygric inertia of a hemp-lime concrete. *International Journal of Mathematical Models and Methods in Applied Sciences*, 7(2):8.

Madurwar, M. V., Ralegaonkar, R. V., and Mandavgane, S. A. (2013). Application of agro-waste for sustainable construction materials: a review. *Construction and building materials*, 38:872–878.

Malkawi, A. and Augenbroe, G. (2004). *Advanced building simulation*. Routledge, New York.

MathWorks (2014). Simulink: Developing s-functions. online, http://www.mathworks.com/help/pdf_doc/simulink/sfunctions.pdf.

Moro, F. and Böhni, H. (2002). Ink-bottle effect in mercury intrusion porosimetry of cement-based materials. *Journal of colloid and interface science*, 246(1):135–149.

Mortensen, L. H., Peuhkuri, R., and Rode, C. (2005). Full scale tests of moisture buffer capacity of wall materials. In *7 th Nordic Symposium on Building Physics, Reykjavík*, pages 662–669.

Moschandreas, D. (1981). Exposure to pollutants and daily time budgets of people. *Bulletin of the New York Academy of Medicine*, 57(10):845.

Nilsson, D., Svennerstedt, B., and Wretfors, C. (2005). Adsorption equilibrium moisture contents of flax straw, hemp stalks and reed canary grass. *Biosystems engineering*, 91(1):35–43.

Osanyintola, O. F. and Simonson, C. J. (2006). Moisture buffering capacity of hygroscopic building materials: Experimental facilities and energy impact. *Energy and Buildings*, 38(10):1270–1282.

Padfield, T. (1998). *The role of absorbent building materials in moderating changes of relative humidity*. PhD thesis, Technical University of Denmark, Lyngby, Denmark.

Peuhkuri, R. H., Mortensen, L. H., Hansen, K. K., Time, B., Gustavsen, A., Ojanen, T., Ahonen, J., Svennberg, K., Arfvidsson, J., and Harderup, L.-E. (2005). Moisture buffering of building materials. Technical Report 87-7877-195-1, Department of Civil Engineering, Technical University of Denmark.

Redlich, C. A., Sparer, J., and Cullen, M. R. (1997). Sick-building syndrome. *The Lancet*, 349(9057):1013–1016.

Rhydwen, R. (2006). *A model for UK hemp cultivation and processing to supply the building industry with hurds for hemp and lime concrete and fibres for insulation bats, with the ethos of environmental protection as a priority*. PhD thesis, University Of East London, London, UK.

Ritter, H. and Drake, L. (1945). Pressure porosimeter and determination of complete macropore-size distributions. pressure porosimeter and determination of complete macropore-size distributions. *Industrial & Engineering Chemistry Analytical Edition*, 17(12):782–786.

Rode, C. and Clorius, C. O. (2004). Modeling of moisture transport in wood with hysteresis and temperature dependent sorption characteristics. In *Performance of Exterior Envelopes of Whole Buildings IX: International Conference*.

Rode, C. and Grau, K. (2008). Moisture buffering and its consequence in whole building hygrothermal modeling. *Journal of Building Physics*, 31(4):333–360.

Rode, C. and Woloszyn, M. (2007). Whole-building hygrothermal modeling in iea annex 41. *Thermal Performance of Exterior Envelopes of Whole Buildings X, Clearwater, USA*.

Ronchetti, P. (2007). The barriers to the mainstreaming of lime-hemp: A systemic approach. Master's thesis, Dublin Insitute of Technology, Dublin, Ireland.

Roodman, D. M., Lenssen, N., and Peterson, J. A. (1995). *A building revolution: how ecology and health concerns are transforming construction*. Worldwatch Institute Washington, DC.

Salonvaara, M., Ojanen, T., Holm, A., Künzel, H. M., and Karagiozis, A. N. (2004). Moisture buffering effects on indoor air quality-experimental and simulation results. In *Proceedings of Buildings IX, Clearwater, Florida*.

Samri, D. (2008). *Analyse physique et caractérisation hygrothermique des matériaux de construction : approche expérimentale et modélisation numérique*. PhD thesis, INSA Lyon, Lyon, France.

Sasic Kalagasidis, A. (2004). *HAM-Tools - An integrated simulation tool for heat, air and moisture transfer analyses in Building Physics*. Chalmers University of Technology.

Scheffler, G. A. (2008). *Validation of hygrothermal material modelling under consideration of the hysteresis of moisture storage*. PhD thesis, Dresden University of Technology, Dresden, Germany.

Shea, A., Lawrence, M., and Walker, P. (2012). Hygrothermal performance of an experimental hemp–lime building. *Construction and building materials*, 36:270–275.

Shea, A., Wall, K., and Walker, P. (2013). Evaluation of the thermal performance of an innovative prefabricated natural plant fibre building system. *Building Services Engineering Research and Technology*, 34(4):369–380.

Steeman, H. J. (2009). *Modelling local hygrothermal Interaction between airflow and porous materials for building applications*. PhD thesis, University of Gent, Gent, Belgium.

Strømdahl, K. (2000). *Water sorption in wood and plant fibres*. PhD thesis, Technical University of Denmark, Lyngby, Denmark.

Struck, C., de Wilde, P. J., Hopfe, C. J., and Hensen, J. L. (2009). An investigation of the option space in conceptual building design for advanced building simulation. *Advanced Engineering Informatics*, 23(4):386–395.

Svennberg, K. (2003). *Determination of moisture properties for materials exposed to the indoor air*. PhD thesis, Lund Institute of Technology, Lund, Sweden.

Svennberg, K., Hedegaard, L., and Rode, C. (2004). Moisture buffer performance of a fully furnished room. In *Proceedings of Buildings IX, Clearwater, Florida*.

Tariku, F., Kumaran, K., and Fazio, P. (2010). Integrated analysis of whole building heat, air and moisture transfer. *International Journal of Heat and Mass Transfer*, 53(15–16):3111–3120.

Time, B. (1998). *Hygroscopic moisture transport in wood*. PhD thesis, Norwegian University of Science and Technology, Trondheim, Norway.

Time, B. (2002). Studies on hygroscopic moisture transport in norway spruce (picea abies) part 2: Modelling of transient moisture transport and hysteresis in wood. *European Journal of Wood and Wood Products*, 60(6):405–410.

Toftum, J. and Fanger, P. O. (1999). Air humidity requirements for human comfort. *ASHRAE Transactions*, 99.

Tran Le, A., Maalouf, C., Mai, T., Wurtz, E., and Collet, F. (2010). Transient hygrothermal behaviour of a hemp concrete building envelope. *Energy and Buildings*, 42(10):1797–1806.

van Schijndel, A. W. M. (2009). Integrated modeling of dynamic heat, air and moisture processes in buildings and systems using simulink and comsol. *Building Simulation*, 2(2):143–155.

Viitanen, H., Vinha, J., Salminen, K., Ojanen, T., Peuhkuri, R., Paajanen, L., and Lähdesmäki, K. (2010). Moisture and bio-deterioration risk of building materials and structures. *Journal of Building Physics*, 33(3):201–224.

Vrugt, J. A., Ter Braak, C. J., Gupta, H. V., and Robinson, B. A. (2009). Equifinality of formal (dream) and informal (glue) bayesian approaches in hydrologic modeling? *Stochastic Environmental Research and Risk Assessment*, 23(7):1011–1026.

Washburn, E. W. (1921). Note on a method of determining the distribution of pore sizes in a porous material. pages 115–116.

Wihan, J. (2007). *Humidity in straw bale walls and its effect on the decomposition of straw*. PhD thesis, University of East London, London, UK.

Woloszyn, M. and Rode, C. (2008). Tools for performance simulation of heat, air and moisture conditions of whole buildings. *Building Simulation*, 1(1):5–24.

Yates, T. (2006). The use of non-food crops in the uk construction industry. *Journal of the Science of Food and Agriculture*, 86(12):1790–1796.